VYSOKÉ UČENÍ TECHNICKÉ V BRNĚ

Fakulta chemická

Habilitační práce v oboru

Chemie a technologie ochrany životního prostředí

SPECIACE RTUTI V ŽIVOTNÍM PROSTŘEDÍ

RNDr. Pavel Coufalík, Ph.D.

Brno 2020

Poděkování

Chtěl bych tímto poděkovat všem svým kolegům a spolupracovníkům, se kterými jsem mohl pracovat na společném výzkumu.

Obsah

Seznam komentovaných publikací 4

1 Úvod 6

2 Cíle habilitační práce 8

3 Stanovení celkového obsahu rtuti 9

4 Extrakce rtuti a jejích forem 10

4.1 Sekvenční extrakce 10

4.2 Vyvinutý postup sekvenční extrakce 12

4.3 Selektivní extrakce forem rtuti 14

5 Termická desorpční analýza 16

6 Biogeochemický cyklus rtuti 19

6.1 Rtuť v polárním ekosystému 20

6.2 Antropogenní kontaminace 25

7 Perspektiva vývoje kontaminace životního prostředí rtutí 27

Reference 29

Přílohy I – XI 33

Seznam komentovaných publikací

I. **Coufalík, P.**, Krmíček, L., Zvěřina, O., Meszarosová, N., Hladil, J., Komárek, J., 2018. Model of mercury flux associated with volcanic activity. *Bulletin of Environmental Contamination and Toxicology* 93, 503–508.

II. **Coufalík, P.**, Zvěřina, O., Komárek, J., 2016. The direct determination of HgS by thermal desorption coupled with atomic absorption spectrometry. *Spectrochimica Acta Part B* 118, 1–5.

III. Zvěřina, O., **Coufalík, P.**, Barták, M., Petrov, M., Komárek, J., 2018. The contents and distribution of cadmium, mercury and lead in *Usnea antarctica* lichens from Solorina Valley, James Ross Island (Antarctica). *Environmental Monitoring and Assessment* 190, 13, 1–9.

IV. Száková, J., Havlíčková, J., Šípková, A., Gabriel, J., Švec, K., Baldrian, P., Sysalová, J., **Coufalík, P.**, Červenka, R., Zvěřina, O., Komárek, J., Tlustoš, P., 2016. Effect of the soil microbial community on mobile proportions and speciation of mercury (Hg) in contaminated soil. *Journal of Environmental Science and Health, Part A* 51, 4, 364–370.

V. Šípková, A., Száková, J., **Coufalík, P.**, Zvěřina, O., Kacálková, L., Tlustoš, P., 2014. Mercury distribution and mobility in contaminated soils from vicinity of waste incineration plant. *Plant, Soil and Environment* 60, 2, 87–92.

VI. **Coufalík, P.**, Zvěřina, O., Krmíček, L., Pokorný, R., Komárek, J., 2015. Ultra-trace analysis of mercury in alkaline lavas and regolith from James Ross Island. *Antarctic Science* 27, 3, 281–290.

VII. **Coufalík, P.**, Zvěřina, O., Mikuška, P., Komárek, J., 2014. Seasonal variability of mercury contents in street dust in Brno, Czech Republic. *Bulletin of Environmental Contamination and Toxicology* 93, 4, 503–508.

VIII. Zvěřina, O., **Coufalík, P.**, Brat, K., Červenka, R., Kuta, J., Mikeš, O., Komárek, J., 2017. Leaching of mercury from seal carcasses into Antarctic soils. *Environmental Science and Pollution Research* 24, 2, 1424–1431.

IX. Zvěřina, O., Láska, K., Červenka, R., Kuta, J., **Coufalík, P.**, Komárek, J., 2014. Analysis of mercury and other heavy metals accumulated in lichen *Usnea antarctica* from James Ross Island, Antarctica. *Environmental Monitoring and Assessment* 186, 12, 9089–9100.

X. **Coufalík, P.**, Meszarosová, N., Coufalíková, K., Zvěřina, O., Komárek, J., 2018. Determination of methylmercury in cryptogams by means of GC-AFS using enzymatic hydrolysis. *Microchemical Journal* 140, 8–13.

XI. Kuboušková, S., Krmíček, L., **Coufalík, P.**, Pokorný, R., 2016. Petrological and geochemical characteristics of Palaeogene low-rank coal on the Faroe Islands: Restricted effects of alteration by basaltic lava flows. *International Journal of Coal Geology* 165, 157–172.

1 Úvod

Kontaminace životního prostředí toxickými prvky je globálním problémem, který se projevuje i ve zdánlivě nedotknutých oblastech Země[1]. Těžba a zpracování nerostných surovin, průmyslová výroba, spalování fosilních paliv a výroba elektrické energie jsou dnes hlavní antropogenní zdroje kontaminantů, které vstupují do ekosystému. Formy kovů se schopností bioakumulace a jejich osud v životním prostředí jsou předmětem zájmu širokého okruhu vědních oborů, které se zabývají interakcí toxických látek s živými organismy, a to často s odlišným úhlem pohledu. Cílem těchto studií tak může být sledování zdrojů znečištění, transport (lokální či dálkový), depozice, přeměny jednotlivých forem kovů, schopnost vstupovat do potravního řetězce, toxicita pro živé organismy i kontaminace potravin. Zde je vhodné definovat rozdíl mezi formou kovu a konkrétní specií. Pod pojmem specie kovu chápejme definovanou chemickou sloučeninu, oxidační stav nebo izotop prvku, kdežto formu prvku lze chápat jako okruh specií s podobnými chemickými či fyzikálními vlastnostmi. Toxicita specií/forem kovů závisí nejen na jejich biologickém působení, ale i na jejich rozpustnosti za daných podmínek, mobilitě v prostředí či přítomnosti látek, které mají schopnost retence pro tyto formy. Při sledování osudu zkoumaného prvku v životním prostředí se tak musíme zaměřit na matečné horniny v dané lokalitě, anorganické i organické komponenty půd či sedimentů, mikroorganismy, rostlinné i živočišné druhy.

Mezi nejčastěji sledované kovy patří zejména specie olova, kadmia, rtuti a arsenu, které představují zdravotní riziko pro lidskou populaci. Z hlediska toxicity a bioakumulační schopnosti[2] je rtuť a její specie nejvíce rizikovým polutantem z této skupiny látek. Rtuť je globální polutant[3], který má poměrně složitý koloběh v ekosystému[4]. Kvůli vysoké tenzi atomárních par je její koncentrace v atmosféře vysoká – přibližně 1,5 – 1,7 ng m^{-3} na Severní polokouli a 1 – 1,3 ng m^{-3} na Jižní polokouli[5,6]. Současná emise rtuti do atmosféry (cca 7200 t za rok) je tvořena ze 70 % z přírodních zdrojů (včetně re-emise již deponované rtuti); antropogenní emise rtuti pochází nejvíce ze spalování uhlí[7,8]. Hlavní specií rtuti v atmosféře je Hg^0 (90 – 99 %)[5]; část rtuti je vázána na pevné částice jako tzv. částicová rtuť („particulate mercury“) a část se vždy vyskytuje ve vysoce reaktivní oxidované formě. Částicová a dvojmocná rtuť velmi rychle podléhají suché i mokré depozici na povrch[4].

Emise rtuti do atmosféry, její depozice na povrch a následné re-emise, způsobují zkoncentrování tohoto polutantu v nejchladnějších oblastech Země. Polární oblasti tak fungují jako tzv. „studená past“[1]. Koncentrace rtuti v Arktidě prudce rostou posledních 150 let a dnes dosahují kritických hodnot. Vysoká bioakumulace rtuti v potravním řetězci se svými toxickými účinky projevuje nejen u živočichů, ale i u lidské populace závislé na konzumaci ryb a mořských savců[9-11]. Antarktický cirkumpolární oceánský proud i proudění vzduchu nad kontinentem (centrální tlaková výše obklopená četnými tlakovými nížemi) částečně izolují Antarktidu před kontaminací polutanty z nižších zeměpisných šířek. Ačkoli je koncentrace rtuti v atmosféře Jižní hemisféry o 30 % nižší, lze předpokládat, že rozvoj průmyslové výroby i nárůst populace na Jižní polokouli budou mít negativní vliv na rostoucí kontaminaci oblasti Jižního oceánu i Antarktidy[1,12].

Vývoj emise rtuti antropogenního původu i emise rtuti z přírodních zdrojů[13] je otazníkem nejbližší budoucnosti. Klimatické změny s sebou mohou přinést tání permafrostu, který představuje mnohem větší depozit rtuti, než je celkové množství rtuti v ostatních půdách, oceánech i atmosféře[14]. Vliv antropogenní činnosti na vývoj koncentrace rtuti v atmosféře tak může být mnohem vyšší, než přísluší spalování fosilních paliv a průmyslové výrobě.

2 Cíle habilitační práce

Ústředním tématem této habilitační práce je studium speciačního vývoje rtuti v ekosystému, která pochází z přírodních i antropogenních zdrojů. Mezi hlavní cíle práce patří:

- Vývoj analytických metod pro stanovení stopových a ultrastopových obsahů rtuti ve vzorcích životního prostředí se zaměřením na:
  I) vývoj sekvenční extrakce pro ultrastopové obsahy rtuti
  II) rozvoj instrumentace, metodiky a vyhodnocení dat pro termickou desorpční analýzu rtuti
  III) vývoj metody pro stanovení ultrastopových obsahů methylrtuti v rostlinné matrici
- Definování vstupu rtuti do pevninského ekosystému vlivem sopečné činnosti a zvětrávání vyvřelých hornin – stanovení přirozeného pozadí.
- Studium vlivu dálkového transportu a depozice specií rtuti na kontaminaci Antarktidy.
- Posouzení environmentálních rizik kontaminovaných půd a sedimentů nakládáním s nebezpečnými odpady, průmyslovou a zemědělskou činností člověka.

Přiložené původní vědecké práce (Příloha I – XI) tvoří ucelený koncept studia koloběhu rtuti v přírodě. V rámci této habilitační práce byly vyvinuty potřebné analytické postupy, které jsou založeny na kapalných extrakcích s komplementárním stanovením vybraných specií rtuti termickou cestou. Vyvinutá metodika byla aplikována na jednotlivé případové studie, které zahrnovaly studium speciace rtuti v horninách, sopečném popelu, regolitu, půdách, sedimentech, pouličním prachu, uhlí, půdní mikrobiotě, lišejnících a v koloniích řas a sinic.

V následujících kapitolách bude nejprve popsán vyvinutý analytický aparát, a následně budou rozebrány přírodní i antropogenní zdroje rtuti s ohledem na mobilitu jednotlivých forem, bioakumulaci a transformaci specií. (Číslování přiložených publikací autora je podle pořadí výskytu v textu.)

3 Stanovení celkového obsahu rtuti

U stanovení celkového obsahu rtuti ve vzorcích hornin, půd a sedimentů, narážíme na obecný problém kvantitativního stanovení kovů v anorganických matricích, totiž velmi obtížný rozklad silikátové matrice vzorku. Z analytického hlediska je tak pro stanovení rtuti mnohem výhodnější použití jednoúčelových analyzátorů rtuti s termooxidačním rozkladem vzorku, např. AMA-254 (Altec, ČR) nebo spektrometr obdobné konstrukce DMA-80 (Milestone, Itálie), které mohou pracovat přímo s pevným vzorkem i kapalnými roztoky. Pro stanovení celkového obsahu rtuti v pevných vzorcích, extraktech i mineralizátech byl v rámci přiložených publikací autora použit především atomový absorpční spektrometr AMA-254 (Altec, ČR).

Princip stanovení rtuti pomocí analyzátoru AMA-254 spočívá v termickém uvolnění rtuti ze vzorku v proudu kyslíku se záchytem atomů Hg na amalgamátoru, po kterém následuje pulzní ohřev s vypuzením atomů Hg do optické části spektrometru. Zdrojem záření je nízkotlaká rtuťová výbojka o vlnové délce 253,65 nm. Vzorek na dávkovací lodičce (Ni) se zahřeje ve spalovací trubici na 750 °C. Kyslík odnáší produkty oxidačního rozkladu spolu s analytem do katalytické části spalovací pece. Zde, při 550 °C, dochází k dokončení oxidace a záchytu interferentů (např. halogeny, síra). Amalgamace Hg probíhá na pozlacené křemelině v křemenné trubičce s odporovým ohřevem. Po ohřevu amalgamátoru prochází atomy Hg přes dvě vyhřívané kyvety (120 °C) v optické ose spektrometru; v celém systému tak nedochází ke kondenzaci vodních par. Kyvety mají rozdílnou délku, tj. rozdílnou citlivost. Mezi kyvetami je zpožďovací nádobka zařazená mimo optickou osu spektrometru. Atomy prochází nejprve delší kyvetou, poté kratší. Různá citlivost kyvet tak umožňuje měření ve dvou kalibračních rozsazích. Stanovení rtuti pomocí tohoto spektrometru navíc umožňuje mnohonásobnou amalgamaci analytu s opakovaným dávkováním vzorku. Absolutní limit detekce rtuti je velmi nízký – 0,01 ng Hg. Spektrometr má relativně velký lineární rozsah (až do cca 200 ng Hg v absolutním množství).

Parametry metody pro stanovení rtuti pomocí analyzátoru AMA-254 závisí na charakteru vzorku a jeho hmotnosti/objemu, např. publikace I nebo práce Coufalík a kol.[15]. Pro analýzu pevných vzorků je vhodné použít navážku v rozmezí 10 – 250 mg. V případě vysokého obsahu rtuti v materiálu je navážka vzorku omezena měřicím rozsahem analyzátoru. Pro stanovení rtuti v kontaminovaných vzorcích lze využít ředění

pevného vzorku křemenným pískem (publikace II). V případě nízké homogenity vzorku nebo nízkého obsahu analytu je vhodné použít vyšších navážek vzorku s odpovídajícím prodloužením doby dekompozice (pro úplné uvolnění atomů z matrice). Stanovení celkové rtuti ve vzorku přímo z pevného materiálu má nižší přesnost u kontaminovaných materiálů průmyslovou činností (např. Hg^0) nebo např. u půd s roztroušenými krystaly cinabaritu (HgS). Tyto vzorky lze homogenizovat mletím.

Pro stanovení rtuti v roztocích je nutné dokonale vysušit nadávkovaný objem v lodičce v rámci pracovního programu analyzátoru – nebezpečí ztráty části analytu během pulzního ohřevu při dekompozici. Do lodičky se běžně dávkuje 100 µl vzorku (s dobou sušení min 60 s); pro roztoky s nízkým obsahem analytu lze doporučit maximálně 400 µl vzorku. Vysoce korozivní roztoky (např. konc. HNO_3) je vhodné před stanovením rtuti naředit deionizovanou vodou přímo v dávkovací lodičce. Do analyzátoru dále nelze dávkovat látky s vysokým obsahem síry – zanesení transportní cesty i optické části spektrometru.

Stanovení celkové rtuti pomocí roztokové analýzy je vhodné v případě extrémně nízké homogenity pevného vzorku nebo u materiálů, které lze snadno převést do roztoku. U většiny organických matric lze pro stanovení rtuti použít uzavřený rozklad za zvýšeného tlaku, např. v mikrovlnných mineralizátorech. Mineralizace se provádí nejčastěji pomocí konc. HNO_3 nebo směs HNO_3 a H_2O_2. Stanovení celkové rtuti ve vzorku s využitím mineralizace bylo použito pro analýzu segmentů stélky lišejníků *Usnea antarctica* (publikace III). V tomto případě byl stanoven průměrný obsah rtuti ve vybrané části stélky.

4 Extrakce rtuti a jejích forem

4.1 Sekvenční extrakce

Převedení analytu z pevného vzorku do roztoku pomocí extrakčního/rozkladného činidla představuje základní přístup v chemické analýze látek. Zde je nutné rozlišit, zda je cílem analýzy kvantitativní stanovení celkového obsahu analytu ve vzorku nebo stanovení vybraných specií/forem. Nemobilní specie kovů většinou nepředstavují ekologické riziko, ovšem za předpokladu dostatečné stability za daných podmínek. Naopak, vysoce mobilní specie mohou chemickými i fyzikálními procesy přecházet na méně rizikové formy. Pro objektivní vyhodnocení ekologických

rizik je proto nutné zjistit speciaci sledovaného kovu v materiálu, ideálně spolu s chemicko-fyzikální charakteristikou matrice daného vzorku.

Pro účely speciační analýzy kovů v sedimentech byl již na konci sedmdesátých let navržen postup sekvenční extrakce podle Tessiera a kol.[16], který je základem mnoha dosud publikovaných extrakčních schémat pro kovy v environmentálních matricích. Co jsou hlavní principy a současně úskalí této metody? Principem sekvenční extrakce je postupná extrakce jednotlivých specií/forem analytu extrakčními činidly s rostoucí extrakční účinností. Jako extrakční činidla se používají deionizovaná voda, zředěné roztoky anorganických solí, zředěné i koncentrované roztoky kyselin i hydroxidů, směsné roztoky solí s definovaným pH, i organická činidla. Podle chemické povahy extrakčního činidla dochází během extrakce k vyvázání určité chemické nebo fyzikální formy analytu z matrice vzorku. Velmi obsáhlý výčet extrakčních činidel i schémat sekvenční extrakce pro speciační analýzu rtuti v půdách a sedimentech lze nalézt např. v přehledové práci Issaro a kol.[17]. Podmínka rostoucí extrakční účinnosti činidla vzhledem k charakteru specie i její vazby v matrici vzorku je zároveň nejkritičtějším parametrem ovlivňujícím výsledek analýzy. Extrakce probíhá v následných krocích, tj. po extrakci jedné formy z navážky vzorku dochází k opětovné extrakci téhož vzorku dalšími činidly. V ideálním případě by v jednotlivých krocích extrakce nemělo docházet k uvolňování jiné, než cílové formy, respektive extrakční činidla i podmínky extrakce by měly tomuto nežádoucímu jevu zamezit.

Laboratorní provedení tohoto postupu spočívá v extrakci pevného vzorku v extrakčních zkumavkách či vialkách dostatečným přebytkem extrakčního činidla. Extrakce dané formy by měla být kvantitativní. Přílišné naředění analytu do velkého objemu roztoku ovšem znemožňuje stanovení stopových koncentrací. (Autorem doporučený poměr fází je 100 mg pevné matrice na 10 ml extrakčního činidla.) Vzorek je vhodné před extrakcí mlít na analytickou jemnost, pokud není cílem analýzy určení mobilních forem za přirozených podmínek. (Zrnitost materiálu ovlivňuje výtěžek extrakce.) Extrakce probíhá řadu hodin třepáním na třepačce nebo pomocí ultrazvuku za laboratorní nebo zvýšené teploty. Extrakt je poté oddělen centrifugací nebo filtrací; extrakční zbytek promyt deionizovanou vodou, a následně zalit novým činidlem – další extrakční krok. Extrakce tak trvá i několik dní v kontinuálním režimu s pevnými časovými intervaly. Je zřejmé, že tento postup analýzy je nejen pracný, ale do značné míry závislý na zkušenosti operátora. Extrakci je nutné provádět v několika opakováních. Stanovená koncentrace analytu v jednotlivých frakcích bývá průměrem

z paralelních analýz. Do výsledné chyby stanovení obsahu jednotlivých forem analytu tak vstupuje homogenita vzorku (paralelní navážky vzorku) a nepatrné rozdíly v extrakční účinnosti činidla v každém opakování extrakce. Výtěžek sekvenční extrakce, tj. suma obsahů analytu ve všech frakcích, by se měl co nejvíce blížit 100 % celkového obsahu analytu ve vzorku, který je stanoven po jeho úplném rozkladu nebo přímo z pevného materiálu. Za správné provedení extrakce beze ztrát i kontaminací lze reálně považovat extrakci s výtěžkem mezi 90 – 110 %.

4.2 Vyvinutý postup sekvenční extrakce

Speciační/frakcionační analýza rtuti vyžaduje pro každou komplexní matrici specifický pracovní postup, který minimalizuje ztráty jednotlivých forem rtuti, a zároveň odděluje jednotlivé frakce s minimální chybou. Pro potřeby stanovení ultrastopových obsahů rtuti v půdách a sedimentech byla vyvinuta metoda sekvenční extrakce s využitím původního pracovního postupu autora[15].

Navržená sekvenční extrakce rozděluje formy rtuti ve vzorku na rtuť rozpustnou v deionizované vodě (F1), rtuť uvolnitelnou v kyselém prostředí (F2, 0,5 mol l^{-1} HCl), rtuť vázanou na organickou hmotu (F3, 0,2 mol l^{-1} KOH), elementární rtuť a amalgámy (F4, 50 % HNO_3), HgS (F5, nasycený roztok Na_2S) a reziduální podíl (F6, pevný zbytek) – např. publikace IV. Toto obecné schéma lze dále upravovat podle materiálu a cílů analýzy. Frakce F1 a F2 lze považovat za mobilní rtuť, frakce F3 a F4 zahrnuje semimobilní specie, zbylé frakce lze považovat za nemobilní formy rtuti. Zejména u semimobilních specií rtuti závisí intenzita vazby rtuti na matrici vzorku na chemicko-fyzikálních podmínkách.

Ke stanovení rtuti v extraktech F1-F4 i pevném zbytku lze použít analyzátor rtuti AMA-254. Extrakce HgS (F5) ze vzorku pomocí nasyceného roztoku Na_2S je kvantitativní, nicméně neumožňuje přímé stanovení rtuti v extraktu. Při použití analyzátoru rtuti narážíme na problém kondenzace síry v celém systému vedoucí atomy rtuti včetně optických kyvet. K zanesení dávkovacích i optických prvků dochází velmi rychle, což znemožňuje jakoukoli další analýzu. (Extrémní množství síry zabraňuje uvolnění rtuti z roztoku i při stanovení pomocí atomové absorpční spektrometrie s generováním studených par, CV-AAS[18].) Jednou z možností stanovení obsahu HgS je jeho výpočet z rozdílu mezi sumou ostatních frakcí a celkovým obsahem rtuti, což ovšem zabraňuje určení výtěžku extrakce.

V publikaci V byla extrakce pomocí nasyceného roztoku Na_2S vynechána a nahrazena stanovením obsahu rtuti v pevném zbytku po extrakčním kroku F4. Stanovený reziduální podíl tak odpovídá nemobilním speciím rtuti, tj. HgS, Hg_2Cl_2 a rtuti vázané v silikátové matrici vzorku. Stanovení obsahu rtuti v pevném zbytku po kroku F4 navíc umožňuje vypočítat výtěžek extrakce. Druhou možností jak určit výtěžek extrakce a zároveň nepřímo stanovit obsah HgS ve vzorku je použití paralelní extrakce (publikace II). V jedné větvi extrakce stanovíme reziduální podíl rtuti ve vzorku přímo po extrakci pomocí HNO_3 (F4); v druhé větvi provedeme extrakci pomocí Na_2S, extrakt opět neměříme a stanovíme reziduální podíl (F6). Obsah HgS (F5) lze dopočítat z rozdílu mezi obsahy rtuti v reziduálním podílu obou větví. (V každé větvi je nutné provést minimálně dvě paralelní extrakce, tj. pro každý vzorek analyzujeme alespoň 4 alikvoty vzorku.) Tento postup analýzy byl také použit u kontaminovaných půd po těžbě polymetalických rud a pro vzorky půd kontaminovaných mořením obilí pomocí fenylrtuti (publikace IV).

V publikaci VI je popsán modifikovaný postup extrakce pro stanovení ultrastopových obsahů forem rtuti v pevné matrici. Rtuť je zde frakcionována na mobilní podíl uvolnitelný pomocí 0,5 mol l^{-1} HCl, dále na rtuť vázanou na organickou hmotu (extrakce pomocí 0,2 mol l^{-1} KOH), Hg^0 a amalgámy (extrakce 50 % HNO_3) a reziduální podíl. Pro správné a přesné stanovení obsahů forem rtuti ve vzorku okolo 1 µg kg^{-1} je z analytického hlediska výhodnější stanovit obsah v pevném materiálu, nikoli v extraktu, jak je běžně prováděno během sekvenční extrakce. V tomto případě bylo provedeno stanovení celkové rtuti ve vzorku po každém kroku extrakce (samostatná navážka pro každý krok extrakce). Každá extrakce byla provedena ve třech opakováních; pro provedení frakcionační analýzy tak bylo použito celkem 9 alikvotů vzorku.

Hlavním rizikem sekvenční extrakce je potenciální přesah extrakční účinnosti činidla na jinou, než cílenou formu. Tento problém se týká především semimobilních forem rtuti, které jsou vázány na matrici vzorku (vazba na minerální částice nebo organické látky), a nemobilních forem rtuti. Vyvinutý postup extrakce pracující s 50 % HNO_3 (F4) odděluje semimobilní rtuť od nemobilních forem, přičemž předchozí extrakce v deionizované vodě a hydroxidu snižují riziko potenciálního rozpouštění HgS v HNO_3[19]. Velký rozdíl v extrakční účinnosti 0,5 mol l^{-1} HCl a 50 % HNO_3 zabraňuje předčasnému vyvázání semimobilních forem rtuti ze vzorku. Pro správné provedení extrakce je nezbytné provést oplach pevného vzorku deionizovanou vodou po každém

kroku extrakce. Odebrání uvolněných forem rtuti od centrifugovaného zbytku je tímto kvantitativní a zároveň nedochází k nežádoucím chemickým reakcím činidel.

Extrakce mobilních forem rtuti pomocí 0,5 mol l^{-1} HCl ovšem může uvolnit organokovové sloučeniny rtuti ze vzorku. (Extrakce organokovových specií rtuti pomocí 0,5 mol l^{-1} HCl není kvantitativní). V půdách je obsah methylrtuti ($MeHg^+$) obecně velmi nízký[17]. Výskyt organokovových specií, zejména methylrtuti, ethylrtuti a fenylrtuti, lze očekávat u sedimentů (biomethylace) a kontaminovaných půd (např. použitím fenylrtuti v zemědělství). Pro stanovení organických forem rtuti je vhodné provést samostatnou extrakci vzorku, jejíž postup je vhodný pro danou matrici (viz následující kapitola).

4.3 Selektivní extrakce forem rtuti

Pro posouzení míry kontaminace půd, sedimentů, hlušiny nebo čistírenským kalů, a s tím spojených rizik, je rozhodující mobilní podíl rtuti v materiálu. Mobilitu forem rtuti v ekosystému lze posuzovat jednak z hlediska rozpustnosti/uvolnění rtuti za okolních podmínek nebo z hlediska bioakumulační schopnosti v živých organizmech. Je zřejmé, že určení mobility na základě samotné rozpustnosti dané formy např. v deionizované vodě je především chemickým modelem. Nicméně, přítomnost ve vodě rozpustných forem v půdním roztoku je již dostatečným indikátorem potenciálního příjmu rtuti rostlinami. Selektivní extrakce mobilních forem rtuti se často zaměřují na organokovové sloučeniny, ve vodě rozpustný podíl, či podíl uvolnitelný ve zředěných roztocích solí či kyselin (např. $CaCl_2$, NH_4NO_3, EDTA, CH_3COOH).

Methylrtuť ($MeHg^+$) patří k nejčastěji sledovaným speciím rtuti kvůli své toxicitě a vysoké bioakumulační schopnosti v potravním řetězci[20,21]. O stanovení $MeHg^+$ v půdách, sedimentech, rybách a mořských plodech bylo publikováno hojné množství vědecké literatury[17,22-24]. Obecně se $MeHg^+$ extrahuje ze vzorku pomocí kyselé nebo alkalické extrakce v kombinaci s extrakcí organickým rozpouštědlem či dalšími vysolovacími činidly[23,25]; některé analytické postupy pracují s destilací.

Stanovení mobilních forem rtuti v materiálu chemickou cestou určuje potenciálně biodostupný podíl, který by mohl být přijat okolními organismy. Srovnání extrakční účinnosti několika činidel pro extrakci mobilních forem rtuti v půdách bylo provedeno v publikaci V. V publikaci IV byla pro určení biodostupného podílu rtuti v kontaminovaných půdách použita extrakce pomocí zředěné CH_3COOH jako

simulantu přirozených podmínek v půdním roztoku. U vzorků pouličního prachu (publikace VII) byl proveden jednoduchý test biodostupnosti rtuti pro člověka. V práci byla provedena extrakce vzorků pouličního prachu v deionizované vodě a extrakce SBET[26], která je charakterizována jako extrakce podílu rtuti uvolnitelného působením žaludeční kyseliny. (Extrakce je prováděna při 37 °C zředěným roztokem glycinu okyseleným pomocí HCl na pH = 1,5.)

V publikaci V byla provedena sekvenční extrakce vyvinutá autorem, která navíc zahrnovala extrakci organokovových forem rtuti do chloroformu (frakce F0). Extrakci lze provést samostatně nebo na ni navázat sekvenční extrakci. Extrahovaná frakce ovšem obsahuje všechny organokovové specie, což neumožňuje rozlišení vysoce toxické methylrtuti od fenylrtuti ve vzorku bez použití separační techniky. (U některých vzorků navíc může dojít ke špatnému smáčení částic v samotném chloroformu[15].) Pro speciační analýzu organokovových sloučenin rtuti je výhodné použití separační techniky – plynové (GC) nebo vysoce účinné kapalinové chromatografie (HPLC) s dostatečně citlivou detekcí, např. pomocí atomové fluorescenční spektrometrie (AFS) nebo hmotnostní spektrometrie s indukčně vázaným plazmatem (ICP-MS)[25].

Methylrtuť v sedimentech i živočišných tkáních lze stanovit i bez chromatografické separace s využitím instrumentace atomové absorpční spektrometrie[24] (AAS), ovšem za důsledného přečištění od anorganické rtuti v extraktu. Extrakční účinnost použitého činidla musí být dostatečná pro kvantitativní extrakci. Velmi často používaným postupem extrakce $MeHg^+$ ze vzorku je extrakce pomocí 6 mol l^{-1} HCl následovaná extrakcí do toluenu a zpětnou extrakcí $MeHg^+$ do vodné fáze s L-cysteinem (publikace VIII). Cílem této metody je kvantitativní extrakce $MeHg^+$ z materiálu následovaná přečištěním extraktu od anorganické rtuti i složek matrice, což umožňuje stanovení ultrastopových koncentrací $MeHg^+$. Je zřejmé, že klíčovým momentem tohoto postupu je kvantitativní výtěžek extrakce a zpětné extrakce do vodné fáze. Jednou z možností ověření výtěžku extrakce je použití vnitřního standardu – v publikaci VIII je to metoda izotopového zřeďování pro vysoce účinnou kapalinovou chromatografii ve spojení s hmotnostní spektrometrií s indukčně vázaným plazmatem (HPLC-ICP-MS). V případě použití analyzátoru rtuti nebo instrumentace atomové absorpční spektrometrie s elektrotermickou atomizací (ET-AAS) by měl být výtěžek extrakce $MeHg^+$ ověřen nezávislou analýzou (při vývoji metody), např. pomocí plynové chromatografie ve spojení s atomovou fluorescenční spektrometrií (GC-AFS). Tento

postup extrakce pro stanovení $MeHg^+$ pomocí instrumentace AAS byl ověřen na vzorcích kontaminovaných půd – nepublikované výsledky.

U stanovení $MeHg^+$ v biologických vzorcích narážíme během extrakce na výrazné matricové efekty, zejména vznik koloidních roztoků a sraženin složek matrice. Extrakty vzorků získané kyselou či alkalickou hydrolýzou je poté nutné dostatečně zředit. Pro stanovení $MeHg^+$ v lišejnících (publikace IX) i půdách (publikace IV) byla rovněž použita extrakce pomocí 6 mol l^{-1} HCl. Extrakt byl po naředění octanovým pufrem podroben derivatizaci a extrakci do hexanu. Stanovení organokovových specií rtuti bylo provedeno pomocí GC-AFS. Relativně málo prací se věnuje stanovení $MeHg^+$ v rostlinné matrici. Základní přístup zůstává stejný – tj. kvantitativní extrakce do vhodného činidla následovaná prekoncentrací a stanovením pomocí tandemových technik, které zahrnují separaci pomocí GC nebo HPLC a detekci, nejčastěji pomocí AFS pro atomární páry rtuti. Extrakční postupy použité pro stanovení $MeHg^+$ v mikroorganismech nebo lišejnících (publikace IV a IX) pracují se zředěním vzorku pufrem a s větším objemem výsledné organické fáze. Obsah $MeHg^+$ ve vzorku tak musí být dostatečný pro toto zředění. Pro nízké koncentrace analytu je ovšem nutné použít co nejvyšší objem extraktu vzorku a provést prekoncentraci do malého objemu organické fáze, což téměř znemožňuje analýzu kvůli matricovým efektům – vznik sraženiny nebo zákalu během extrakce $MeHg^+$ do organické fáze. Z tohoto důvodu byl vyvinut postup extrakce $MeHg^+$ (publikace X) pracující s enzymatickou hydrolýzou rostlinné matrice. Postup byl vyvíjen na certifikovaném referenčním materiálu (CRM) lišejníku a aplikován na vzorky cyanobakteriálních povlaků (kolonie sinic a řas). Výsledný postup stanovení zahrnuje hydrolýzu matrice pomocí celulázy, extrakci $MeHg^+$ pomocí 6 mol l^{-1} HCl, derivatizaci, extrakci do hexanu a stanovení pomocí GC-AFS.

5 Termická desorpční analýza

Vysoká tenze par elementární rtuti i nízká termická stabilita jejích sloučenin umožňuje stanovení některých specií/forem rtuti termickou cestou, na základě rozdílné teploty rozkladu látek. (Tenze atomárních par Hg při 20 °C činí 0,16 Pa, což odpovídá 14 mg m^{-3} v nasycené plynné fázi.) Za teplot nad 600 °C dochází k uvolnění rtuti ze všech sloučenin[27]. Metoda tzv. termické desorpční analýzy rtuti je vhodná zejména pro stanovení Hg^0, matricově vázané rtuti a HgS[28]. Podrobný popis této metody lze nalézt např. v dřívější publikaci autora[29]. Obecně se jedná o termické uvolnění forem rtuti

nebo termický rozklad konkrétních specií za kontinuálního ohřevu nebo za ohřevu na diskrétní teploty. Vlastní obsah specie/formy se poté stanoví nepřímo, tj. z rozdílu mezi celkovým obsahem rtuti před a po termické úpravě vzorku, nebo přímo z atomárních par rtuti pomocí spektrometrických metod. Nejčastěji používanou detekční analytickou metodou je AAS, ICP-MS nebo optická emisní spektrometrie s indukčně vázaným plazmatem (ICP-OES).

Nepřímé stanovení těkavých specií rtuti (nejčastěji Hg^0) se provádí v sušárně nebo peci s řízeným ohřevem. Vzorek určený k analýze je rovnoměrně rozložen na podložním skle a podroben termické úpravě po určitou dobu. Rozdíl v obsahu rtuti před a po desorpci pak odpovídá sledované formě. Pro stanovení Hg^0 se používá ohřev na 105 °C po dobu 48 hod, který byl aplikován na vzorky půd[30]. Tato jednoduchá metoda byla použita pro stanovení elementární rtuti v sedimentech (publikace VI) i lišejnících (publikace IX).

Nabízí se otázka, zda je tento přístup dostatečně korektní. V případě výskytu organokovových specií rtuti ve vzorku by došlo k záměně za elementární formu. U půd či sedimentů s vysokými obsahy rtuti nebo u vzorků se známou historií (např. kontaminace půd mořením obilí pomocí fenylrtuti) je nutné provést selektivní extrakci organických forem – viz kapitola 4.3. V publikaci VI bylo provedeno ověření metody stanovení Hg^0 termickou cestou pomocí referenční analýzy s využitím vyvinutého postupu sekvenční extrakce. Stanovený obsah Hg^0 vykazoval dostatečnou shodu výsledků, resp. obsah Hg^0 stanovený pomocí sekvenční extrakce byl u některých vzorků nepatrně vyšší. (Frakce F4, tj. podíl extrahovatelný pomocí 50 % HNO_3, je definována jako Hg^0 a rtuť vázaná v amalgámech či komplexních sloučeninách.) Termicky stanovený obsah Hg^0 tak nepřesáhl celkový obsah specií stanovených ve frakci F4.

V publikaci VI byla dále provedena termická desorpce rtuti po teplotních krocích 50 °C v rozmezí teplot 50 – 250 °C. Vzorky byly zahřívány v sušárně po dobu 2 hod, po nichž následovalo stanovení celkové rtuti v alikvotním podílu vzorku. K maximálnímu uvolnění rtuti došlo v rozmezí 150 – 200 °C, tj. došlo uvolnění dvojmocné formy, která není vázána na organickou hmotu. Tento přístup je vhodný především pro studium termické stability forem rtuti ve vzorku, je poměrně zdlouhavý a přináší podstatně méně informací o speciačním vývoji rtuti v materiálu ve srovnání se sekvenční extrakcí.

Praktického využití pro speciační analýzu rtuti ovšem doznala termická desorpční analýza pracující s vyhodnocením křivky termického uvolnění rtuti. Vzorek

je při analýze podroben ohřevu s rychlým nárůstem teploty, od laboratorních podmínek po teplotu cca 500 °C, při níž dochází k uvolnění rtuti z většiny specií. Při ohřevu vzorku je zaznamenáván analytický signál pro desorbovanou rtuť vhodnou detekční technikou, např. pomocí AAS. Na rozdíl od jednoduché termické desorpce se zde pracuje v inertní atmosféře (nejčastěji N_2 nebo Ar); jedná se tedy o pyrolýzu vzorku. Pyrolýzní jednotka (často prototyp) se vždy skládá z vsádkové patrony, do které se navažuje vzorek, pícky nebo reaktoru pro ohřev vzorku a systému pro vedení par analytu do analytické cely. Klíčovým parametrem reprodukovatelnosti měření je vždy termická stabilita celé aparatury za kontinuálního nárůstu teploty. Konstrukčně bývá tato problematika řešena topnými bloky z kovu v kombinaci s vyhřívanou cestou z křemenných trubic pro zamezení kondenzace všech produktů pyrolýzy. Systém pro termickou desorpční analýzu ve spojení s AAS lze pochopitelně využít i pro stanovení celkového obsahu rtuti v materiálu (publikace II). Aparatura tak může nahradit komerční analyzátory rtuti s výjimkou vzorků s ultrastopovými obsahy rtuti, které lze stanovit pouze pomocí prekoncentrace atomů na amalgamátoru.

Termické chování rtuti v materiálu závisí nejen na chemické povaze sloučeniny, ale i na intenzitě vazby dané specie v matrici vzorku. Teplotní intervaly pro desorpci jednotlivých specií se tak mohou lišit v závislosti na komplexním složení matrice a původu vzorku. Uměle připravované materiály (kalibrační standardy aj.) mohou mít nižší termickou stabilitu než přírodní vzorky. Charakteristické teplotní intervaly desorpce čistých specií rtuti závisí také na struktuře a zrnitosti použitých chemikálií. V případě laboratorně připravovaných forem rtuti, např. Hg^{2+} vázané na huminové kyseliny, závisí výsledný interval desorpce i na metodě přípravy. Teplotní intervaly se rozšiřují s nárůstem obsahu specie ve vzorku, přičemž může dojít k překryvu jednotlivých píků a případně i ke změně tvaru charakteristické desorpční křivky daného analytu. Z tohoto důvodu je výhodné pracovat v oblasti nízkých absorbancí do A = 0,1. (K případnému ředění vysoce kontaminovaných vzorků lze doporučit křemenný písek.) Výsledné limity detekce (LOD) a stanovitelnosti (LOQ) specií/forem rtuti závisí na průběhu charakteristické desorpční křivky. Specie s širokým intervalem desorpce mají výrazně zhoršený limit stanovitelnosti např. ve srovnání s úzkým píkem HgS.

V publikaci II je prezentováno vyvinuté zařízení pro termickou desorpční analýzu rtuti ve spojení s AAS spolu s metodikou vyhodnocení termické desorpční křivky. Zařízení pro termickou desorpci se skládá z kontrolní jednotky řídící teplotní program a vlastního pyrolyzéru s křemennou kyvetou ve vyhřívaném bloku (obr. 1,

publikace II). Pro kontinuální detekci atomů rtuti byl použit atomový absorpční spektrometr Perkin Elmer 3030 (USA) s převodníkem digitalizující analytický signál. Pyrolyzér se vyznačuje vysokou termickou stabilitou díky vysokému průtoku Ar, který slouží pro ohřev vzorku i vyhřívání cesty pro transport par analytu. K dalším výhodám tohoto technického uspořádání patří velmi rychlá odezva výkonu topného tělesa pro ohřev Ar vůči aktuální teplotě ve vzorku. Průběh termické desorpce je tudíž vysoce reprodukovatelný. Tento systém umožňuje dávkování relativně velké hmotnosti pevného vzorku, který lze podrobit analýze. Zde se dostáváme k problému analýzy vzorků s vysokým obsahem organické hmoty, která podléhá termickému rozkladu. Tento pyrolyzér byl úspěšně použit i pro analýzu vzorků rašeliny, aniž by došlo ke kondenzaci produktů pyrolýzy v systému[29].

Vyvinuté zařízení bylo použito pro speciační analýzu rtuti ve vzorcích půd, které byly kontaminovány těžbou rumělky (publikace II). Citlivost metody lze ovlivnit průtokem nosného plynu přes analytickou celu. (S klesajícím průtokem Ar roste doba setrvání volných atomů v kyvetě.) U čistého HgS nedochází s poklesem průtoku plynu k rozšiřování píku (při stejné výšce píku). Snížení průtoku plynu tak umožňuje stanovení stopových koncentrací HgS v materiálu. U vzorků půd a sedimentů ovšem dochází k rozšiřování píku matricově vázané rtuti a ztrátě rozlišení. Z termické desorpční křivky vzorků půd (obr. 2, publikace II) lze při optimalizovaném průtoku plynu (500 ml min^{-1}) vyhodnotit pík matricově vázané rtuti a charakteristický pík pro červenou formu cinabaritu. Podle navrženého vyhodnocení signálu byl stanoven obsah HgS ve vzorku ve shodě s výsledky sekvenční extrakce. Metoda termické desorpční analýzy v tomto případě umožnila velmi rychlé stanovení mobilních a semimobilních forem rtuti (pík matricově vázané rtuti) a nemobilního cinabaritu. V kapitole 4.2. byla popsána problematika stanovení HgS pomocí sekvenční extrakce. V lokalitách zatížených těžbou cinabaritu je obsah HgS v půdách (a sedimentech) velmi vysoký a jeho stanovení vůči nesulfidickým formám rtuti je rozhodující pro vyhodnocení environmentálního rizika. Z tohoto hlediska je stanovení HgS pomocí termické desorpční analýzy velmi elegantním a rychlým řešením.

6 Biogeochemický cyklus rtuti

Hovoříme-li o zdrojích rtuti v životním prostředí, máme dnes na mysli většinou sekundární zdroje rtuti. Jedná se o rtuť uvolňovanou do atmosféry z antropogenních

zdrojů i zdrojů přírodních. Skutečně primárními zdroji rtuti na povrchu Země je vulkanická a geotermální činnost[3,13,31], která uvolňuje rtuť do atmosféry ze zemského pláště a zejména ze zemské kůry. Ostatní přírodní zdroje rtuti (vypařování z půdy, oceánů a moří, uvolnění z biomasy…) představují především deponovanou rtuť podléhající re-emisi.

Přiložené práce autora se zabývají problematikou speciačních změn rtuti pocházející z přírodních i antropogenních zdrojů. Cílem těchto studií bylo popsání speciačního vývoje rtuti v materiálu s ohledem na původ rtuti ve vzorku – přirozené zvětrávání hornin, antropogenní kontaminace z těžby nerostných surovin, zemědělství a dopravy, bioakumulace z okolního prostředí. V rámci těchto prací jsou studovány hlavní otázky biogeochemického cyklu rtuti v životním prostředí, tj. definování přirozeného pozadí rtuti, vliv dálkového transportu a depozice z atmosféry na kontaminaci ekosystému a biomethylace rtuti v ekosystému. Tyto přirozené procesy lze nejlépe studovat v prostředí s minimální antropogenní činností. Hlavní podíl studovaných vzorků tak tvoří horniny, sedimenty, regolit, řasy, sinice a lišejníky z ostrova Jamese Rosse (Antarktida), vzorky hornin z Grónska a vzorky hornin a uhlí z Faerských ostrovů.

6.1 Rtuť v polárním ekosystému

Ostrov Jamese Rosse se nachází v severovýchodní části Antarktického poloostrova (64° 10' S, 57° 45' W). Stručná charakteristika severní odledněné části ostrova je uvedena v přiložených publikacích (publikace III, VI, VIII, IX, X) včetně popisu vzorkovaných lokalit. Na obr. 1 jsou vyznačena odběrová místa studovaných vzorků hornin, regolitu, sedimentů, lišejníků a cyanobakteriálních povlaků. Podrobný popis lokalit pro odběr vzorků cyanobakteriálních povlaků (publikace X) včetně kompletního druhového zastoupení je uveden v publikaci Skácelová a kol.[32]. Shrnutí dosavadních poznatků o ostrově Jamese Rosse získaných mnohaletým výzkumem lze nalézt v monografii Prošek a kol.[33] (geologický vývoj, glaciologie, klimatologie, biodiverzita aj.).

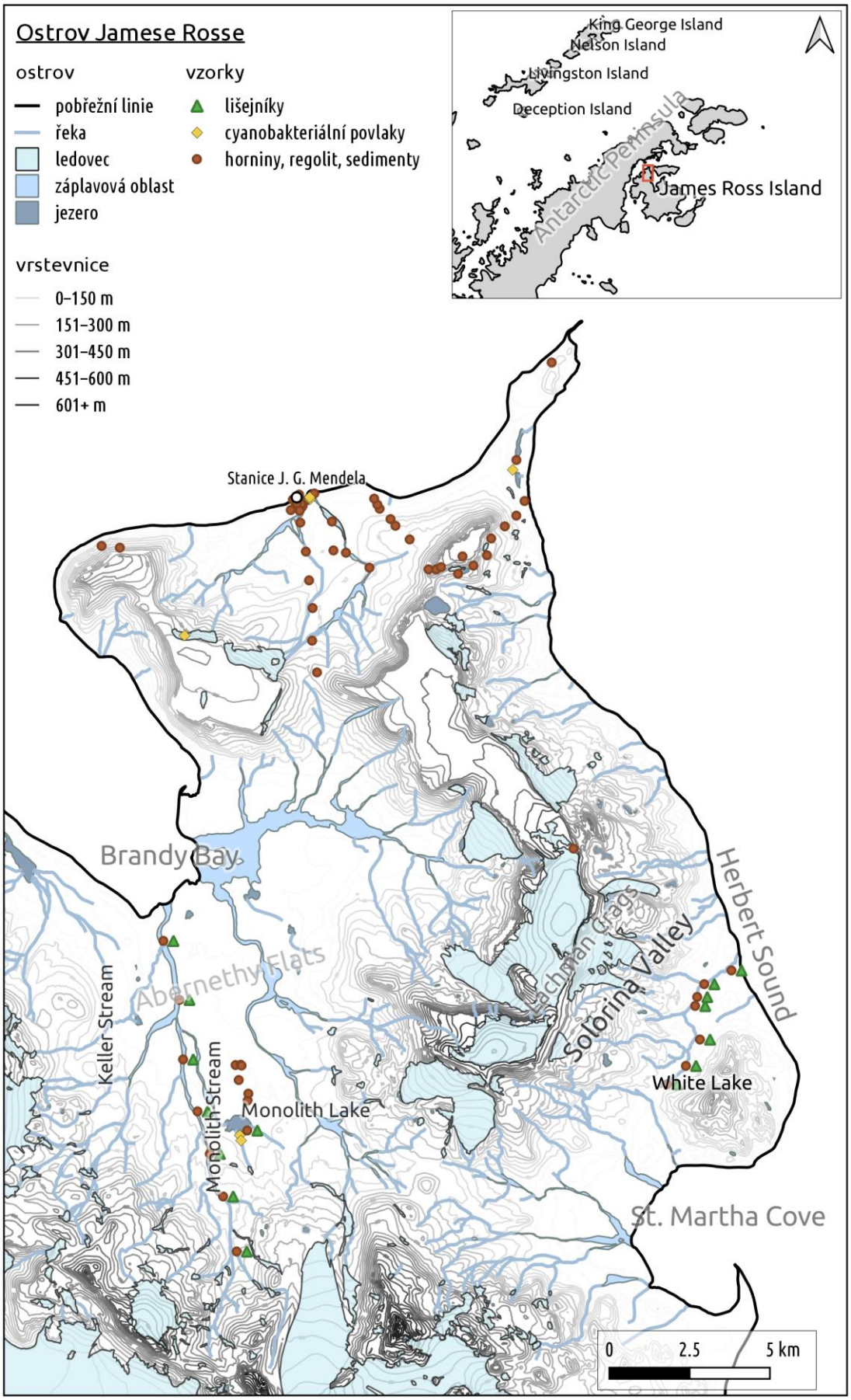

Obr. 1 Severní část ostrova Jamese Rosse[34] s vyznačením odběrových míst

Pro studium chemismu rtuti v ekosystému polárních oblastí je základním krokem definování vstupu rtuti z podloží. Nízký stupeň chemického zvětrávání vyvřelých hornin v polárních oblastech umožňuje studium složení primitivního zemského pláště i kůry. Obsah rtuti v alkalických bazaltech ostrova Jamese Rosse (publikace VI) byl o dva řády nižší, než dříve předpokládané obsahy rtuti zjištěné v bazaltických horninách variabilního geochemického složení. Toto zjištění bylo dále potvrzeno analýzou bazaltů z Grónska. Stanovené obsahy rtuti ve studovaných vzorcích indikují velmi nízký obsah tohoto prvku v zemském plášti. Hodnoty obsahů rtuti v bazaltech s korovými xenolity, které jsou dokladem kontaminace bazaltové taveniny korovým materiálem, byly o něco vyšší (do 8 $\mu g\ kg^{-1}$), tj. přibližně srovnatelné s obsahy rtuti v regolitu (do 11,3 $\mu g\ kg^{-1}$). Kvůli velmi nízké retenční kapacitě regolitu pro rtuť deponovanou z atmosféry (nízký obsah organické hmoty i minerálních částic) lze stanovené obsahy rtuti v regolitu považovat za přirozené pozadí v této části Antarktidy, které je dáno především zvětráváním matečných hornin.

Extrémně nízký obsah rtuti v alkalických bazaltech z Antarktidy i tholeiitických bazaltech z Grónska podnítil navazující studii (publikace I) zabývající se vstupem rtuti do ekosystému vulkanickou činností, tj. primárním přírodním zdrojem rtuti. K analýze byly vybrány vzorky pyroklastického materiálu z širšího okolí Bruntálu a vzorky sopečných popelů z Islandu, Japonska a Aljašky, tedy ze čtyř geotektonicky odlišných lokalit. Analýza vzorků potvrdila předchozí odhad extrémně nízkých obsahů rtuti u vulkanitů derivovaných parciálním tavením plášťových hornin. Na základě studia vyvřelých hornin a sopečných popelů z Antarktidy, Grónska, Islandu, Japonska, Aljašky a České republiky byl po srovnání s dostupnou literaturou[5,35,36] vytvořen model vstupu rtuti vulkanického původu do jejího koloběhu. Tavenina z primitivního pláště je obohacována o rtuť při průchodu zemskou kůrou. Průměrný obsah rtuti v celé zemské kůře je odhadován na přibližně 30 $\mu g\ kg^{-1}$ [36]. Obsah rtuti v tavenině je závislý jak na délce setrvání v zemské kůře (kontaminace taveniny), tak na chemismu vulkanické horniny a její geotektonické pozici. Obsah Hg v primitivním plášti je odhadován na 0,5 $\mu g\ kg^{-1}$ [35]. K této hodnotě by se tedy měly blížit nejnižší obsahy rtuti v geochemicky primitivních bazických lávách. Sopečný materiál ovšem odráží složení magmatu pouze částečně. V případě výlevu lávy na povrch dochází k odplynění vyvrženého materiálu. Během rozpínání plynné fáze je rtuť adsorbována na kondenzující částice pouze v minimální míře[37]. Hlavní specií rtuti uvolňující se do atmosféry představuje Hg^0. V případě minimální re-kondenzace na vyvržený materiál tak může dojít k poklesu

obsahu rtuti i pod tuto hodnotu, což bylo zaznamenáno u vzorků sopečného popela z Islandu.

Na ostrově Jamese Rosse byly zaznamenány relativně vysoké obsahy rtuti a methylrtuti v lišejnících a koloniích mikroorganismů v povrchových vodách. Na základě analýzy regolitu z ostrova Jamese Rosse (publikace VI) nelze rozhodnout, zda vysoké obsahy rtuti a methylrtuti stanovené v lišejnících druhu *Usnea antarctica* (publikace IX) i cyanobakteriálních povlacích (publikace X) jsou výsledkem kontaminace z atmosféry nebo bioakumulace rtuti z lokálních zdrojů. Odledněná území Antarktidy jsou chudá na organickou hmotu, která váže rtuť z okolního prostředí. Z hlediska vysoké bioakumulační schopnosti rtuti[6] může rozklad živočichů stojících na vrcholu potravního řetězce znamenat významný zdroj rtuti i methylrtuti v pevninském ekosystému Antarktidy, jakož i organického uhlíku. V publikaci VIII byl sledován vliv rozkládajících se těl tuleňů na ostrově Jamese Rosse na obsahy Hg a $MeHg^+$ v okolním regolitu. Regolit v bezprostředním okolí uhynulých tuleňů měl několikanásobně vyšší obsah rtuti než přirozené pozadí v dané lokalitě (publikace VI). V těchto vzorcích byla rovněž stanovena $MeHg^+$, která korelovala s celkovým obsahem rtuti. Retenční kapacita regolitu pro Hg a $MeHg^+$ z uhynulých tuleňů byla v tomto případě zvýšena díky vysokému obsahu organického uhlíku. Rozkládající se těla tuleňů tak představují lokální zdroj rtuti i organického uhlíku pro její retenci. Mobilita specií rtuti do širšího okolí tuleně byla ovšem velmi nízká.

Potenciálním lokálním zdrojem polutantů by mohla být stanice Johanna Gregora Mendela. Pro posouzení vlivu provozu stanice na své bezprostřední okolí byly sledovány vybrané kovy regolitu v blízkosti budov stanice i jejího technického zázemí (nepublikované výsledky). Stanovený obsah rtuti v mělkých profilech se pohyboval v rozmezí 5,7 – 12,6 $\mu g\ kg^{-1}$; obsah rtuti v hloubkovém profilu (do 50 cm) se pohyboval v rozmezí 5,8 – 9,2 $\mu g\ kg^{-1}$. Stanovené obsahy Hg, As, Cd, Pb, Co, Cr, Cu, Ni, Sn, Zn v regolitu korespondovaly s obsahy kovů v matečných horninách.

Hlavním zdrojem rtuti v této lokalitě je pravděpodobně depozice z atmosféry (publikace IX). Lišejníky mají obecně vysokou schopnost záchytu polutantů z okolního prostředí. Jedná se nejen o příjem plynných polutantů, ale i záchyt pevných částic ulpělých na povrchu lišejníku i příjem látek ze srážek i tavné vody[38]. (Mechanismus příjmu látek z ovzduší zahrnuje vymražení vzdušné vlhkosti na povrchu stélky, tání námrazy na slunci, příjem vody stélkou lišejníku a její vysušení působením slunečního záření.) Koncentrace rtuti stanovené ve vzorcích lišejníků druhu *Usnea antarctica*

z ostrova Jamese Rosse (publikace IX) byly o dva až tři řády vyšší než koncentrace rtuti v okolním regolitu. Relativně vysoký procentuální podíl $MeHg^+$ ve vzorcích je výsledkem vysoké bioakumulační schopnosti lišejníku pro tutu specii a probíhajících methylačních procesů v polárním ekosystému[6]. Bioakumulace specií rtuti v lišejnících druhu *Usnea antarctica* je také ovlivněna strukturou stélky (publikace III). V publikaci III byl sledován obsah Hg, Cd a Pb v segmentech stélky lišejníků *Usnea antarctica*. Nejvyšší koncentrace rtuti byly zaznamenány v koncových částech stélky, která přirůstá, v přisedlé části byly obsahy nejnižší. Koncové části stélky jsou více vystaveny mokré i suché depozici látek z atmosféry a mají relativně velký povrch vůči své malé hmotnosti. Koncové části stélky tak přijímají větší množství rozpuštěných iontů ve vodě díky záchytu srážek. Obsah rtuti v lišejnících byl o dva řády vyšší než obsah rtuti v regolitu (publikace VI), avšak nižší než stanovené obsahy v jiné lokalitě ostrova Jamese Rosse (publikace IX). Výsledné obsahy rtuti ve stélce jsou závislé i na klimatických podmínkách lokality, zejména proudění větru. Použití lišejníků pro biomonitoring atmosférické depozice rtuti tak může být ovlivněno podmínkami konkrétního stanoviště.

Kontaminace polárních oblastí rtutí je způsobena především dálkovým transportem z nižších zeměpisných šířek[11,39-41]. Během krátkého polárního léta dochází k odtávání sněžníků kumulující polutanty z atmosféry během polární zimy a jara[6]. Mobilní formy rtuti transportované tavnou vodou jsou poté zachycovány pevnými částicemi a především koloniemi mikroorganismů povrchových vod[6]. Pro posouzení akumulace rtuti v jezerech ostrova Jamese Rosse byly studovány mělké profily sedimentů (do 14 cm hloubky). Obsahy celkové rtuti v jezerních sedimentech se pohybovaly do 14 $\mu g\ kg^{-1}$ (nepublikované výsledky) a výrazně se nelišily od okolního regolitu.

Zdrojem methylrtuti v pevninském ekosystému může být probíhající methylace anorganických forem rtuti[42]. Problematika methylace rtuti v pevninském ekosystému byla řešena v publikaci X. Relativně vysoké koncentrace $MeHg^+$ v antarktických lišejnících (publikace IX) i cyanobakteriálních povlacích (publikace X) by mohly být způsobeny methylační schopností některých druhů mikroorganismů, nikoli vstupem z okolního prostředí. Publikace X se zaměřuje na kolonie mikroorganismů tvořící cyanobakteriální povlaky. Cílem tohoto výzkumu bylo rozřešení otázky, zda je $MeHg^+$ ve vodním prostředí pouze bioakumulována nebo se tvoří methylací anorganické rtuti. Poměr $MeHg^+$ vůči celkovému obsahu rtuti ve vzorcích byl extrémně vysoký (až 75 %),

což indikuje aktivní proces methylace v povrchových vodách ostrova i zamokřeném regolitu v místech pokrytých cyanobakteriálními povlaky. (Ovlivnění studovaných lokalit mořským sprejem nebylo prokázáno[43].) Některé druhy mikroorganismů ve studovaných vzorcích[43] se běžně vyskytují jako fotobiont ve stélce druhu *Usnea antarctica*[44]. Je ovšem otázkou, jestli $MeHg^+$ ve lišejnících (publikace IX) pochází pouze z atmosféry nebo je methylována např. působením sinic druhu *Nostoc commune*. Výsledky analýzy vzorků povlaků (publikace X) a jejich druhové určení[43] nasvědčují probíhající methylaci.

6.2 Antropogenní kontaminace

Koncentrace rtuti v životním prostředí v oblastech zatížených činností člověka jsou nesrovnatelné s přirozeným pozadím. Od doby průmyslové revoluce koncentrace rtuti v prostředí neustále roste[6] a lze jen stěží popsat možný vývoj bez antropogenního vlivu. Určení hodnoty přirozeného pozadí rtuti v osídlených oblastech je dosti problematické. O kontaminaci se tak hovoří, vezmeme-li v úvahu běžné (tj. často průměrné) hodnoty obsahů tohoto prvku v environmentálních vzorcích v dané geografické oblasti či státu.

V rámci charakteristiky antropogenních zdrojů rtuti byl stanoven obsah Hg ve vzorcích uhlí z Faerských ostrovů (publikace XI). Obsahy rtuti v bazaltech z Faerských ostrovů (nepublikované výsledky) korespondovaly s obsahy rtuti v lávách ostrova Jamese Rosse (publikace VI). Výzkum tak potvrdil předchozí zjištění o extrémně nízkých obsazích rtuti v plášťovém zdroji. Chemické složení uhlí se značně liší mezi jednotlivými oblastmi světa[7,45]. Obsahy rtuti ve studovaných vzorcích uhlí byly relativně nízké vzhledem k běžným obsahům v uhlí z různých částí Země[7]. Všechny vzorky uhlí měly dále nízký obsah síry. Rtuť obsažená ve vzorcích tak byla pravděpodobně vázána na huminové látky a sulfidy[46]. Jedním z cílů této studie bylo studium vlivu bazaltického výlevu, překrývající souvrství s uhelnými slojemi, na chemické složení uhlí. Z obsahů rtuti ve vzorcích uhlí byla vypočítána hodnota velikosti indexu CAI_{Hg}[46] (Coal Affinity Index), který nepřímo ukazuje na efektivitu uhlí kumulovat Hg. U části vzorků byly zaznamenány velmi nízké hodnoty CAI_{Hg}, což je dáno do souvislosti se sekundárním ochuzení uhlí o Hg v důsledku jeho alterace působením hydrotermálních roztoků, které doprovázely sopečné výlevy. Na základě

analýzy vzorků lze říci, že spalování uhlí z Faerských ostrovů má relativně nízký dopad na kontaminaci okolního prostředí rtutí.

Vývoj speciace rtuti byl sledován na vzorcích půd a sedimentů kontaminovaných průmyslovou činností, těžbou rud i při práci v zemědělství. V předcházející kapitole byl diskutován vliv kolonií mikroorganismů na methylaci rtuti ve vodním prostředí. V publikaci IV byl proveden experiment studující vliv půdních mikroorganismů na speciaci rtuti s důrazem na mobilní a vysoce toxické organokovové specie. V práci byla prokázána bioakumulační schopnost některých druhů mikroorganismů pro methyl a fenylrtuť v kontaminovaných půdách (kontaminace mořením obilí) i jejich schopnost ovlivňovat speciaci (vznik těkavých forem rtuti). Hlavní podíl v kontaminovaných půdách po těžbě polymetalických rud tvořila Hg^0, rtuť vázaná na huminové látky a HgS. Na rozdíl od organokovových specií rtutiF se však jejich obsah v půdách po dobu trvání experimentu nezměnil (90 dní).

Kontaminované vzorky půd z areálu spalovny odpadů (publikace V) měly extrémně vysoký obsah Hg^0 ukazující na jednoznačnou kontaminaci kovovou rtutí. Část elementární rtuti byla přeměněna na sulfidickou rtuť a část oxidované rtuti byla navázána na huminové látky v půdách. Podíl mobilních forem rtuti byl relativně nízký.

V případě zdrojové specie HgS pocházející z těžby a zpracování cinabaritu (publikace II) tvořil HgS ve vzorcích půd a sedimentů majoritní podíl; část celkového obsahu tvořila rtuť vázaná na matrici vzorku (výsledky termické desorpční analýzy). Během zpracování rudy dochází k částečnému uvolnění Hg^0 do okolí, která následně kondenzuje na pevné částice. Matricově vázanou rtuť poté tvoří elementární i dvojmocná rtuť. (Elementární rtuť může za zvýšených teplot penetrovat do částic hornin a vázat se na vnitřní vazebná místa, čímž dojde ke zvýšení její termické stability.) Pomocí sekvenční extrakce byl u těchto vzorků stanoven obsah semimobilních i mobilních forem rtuti (nepublikované výsledky).

V publikaci VII byla provedena studie kontaminace pouličního prachu rtutí v Brně během jednoho roku. Pouliční prach je velmi specifický materiál. Jedná se vždy o směsný vzorek obsahující půdní částice, částice vzniklé otěrem stavebních materiálů vyskytujících se na okolních budovách, částice vzniklé kondenzací ze spalovacích procesů (např. z dopravy) aj. Složení pouličního prachu dále závisí na roční době, aktuálních meteorologických podmínkách, míře re-emise rtuti, antropogenní činnosti a charakteru urbanistické zástavby. Ke kumulaci rtuti v pouličním prachu dochází zejména v místech s nízkou re-suspenzací materiálu. Z tohoto důvodu je kvalita ovzduší

v zastavěném území velmi proměnlivá. Z výsledků vyplývá, že výsledný obsah rtuti v městském ovzduší závisí na intenzitě dopravy v konkrétní lokalitě pouze částečně. Hlavním faktorem ovlivňujícím obsah rtuti v pouličním prachu je pravděpodobně míra re-suspenzace materiálu, která závisí na intenzitě proudění vzduchu v urbanistické zástavbě[47]. Nejnižší obsahy rtuti byly zaznamenány v rezidenčních čtvrtích s minimální dopravou, maximální hodnoty poté ve středu města v tzv. pouličním kaňonu[47], kde dochází ke kumulaci polutantů spolu s částicemi aerosolu.

7 Perspektiva vývoje kontaminace životního prostředí rtutí

V rámci provedeného výzkumu, který je předmětem této habilitační práce, byly zkoumány environmentální vzorky z různých částí Země. Nelze říci, že dnes existuje místo, které by nebylo ovlivněno lidskou činností. Oblasti s rozvinutou průmyslovou výrobou se stávají zdrojem rtuti pro rozsáhlá území kvůli dálkovému transportu rtuti v atmosféře i mořským proudům. Cyklus depozice a re-emise činí z rtuti globální polutant, jehož koncentrace neustále rostou.

Publikace, jež jsou přílohou této habilitační práce, obsahují potřebný analytický aparát pro studium speciace rtuti v ekosystému a zároveň poskytují široký obraz speciačních změn rtuti za různých podmínek. Z metodických prací autora lze zdůraznit především publikaci VI, II a X. Publikace VI popisuje vyvinutý postup sekvenční extrakce pro ultra-stopové obsahy rtuti, který umožňuje stanovit jednotlivé formy v řádu desetin $\mu g\ kg^{-1}$. Originální postup extrakce methylrtuti z rostlinné matrice zahrnující enzymatickou hydrolýzu popsaný v publikaci X představuje univerzální metodu pro vyvázání tohoto analytu z komplexní matrice. Hlavním přínosem publikace II je vývoj zařízení i metodiky vyhodnocení dat pro termickou desorpční analýzu rtuti, která umožňuje velmi rychlá měření a může v řadě případů sekvenční extrakci nahradit.

Studium vzorků z ostrova Jamese Rosse (Antarktida) umožnilo posoudit vliv dálkového transportu rtuti na její koncentrace v tamním ekosystému a zároveň definovat její přirozené pozadí. Na základě analýzy vyvřelých hornin a sopečných popelů z Antarktidy, Grónska, Islandu, Japonska, Aljašky a České republiky (publikace I) byl navržen model toku rtuti do životního prostředí vulkanickou činností. Obsah rtuti v geochemicky primitivním svrchním zemském plášti byl odhadnut $< 0{,}5\ \mu g\ kg^{-1}$. V publikaci III a IX byly popsány vysoké koncentrace rtuti i methylrtuti v antarktických lišejnících ukazující na značnou bioakumulaci atmosféricky deponované rtuti

v pevninském prostředí odledněných oblastí Antarktidy. Jako lokální zdroj kontaminace byl dále potvrzen biotransport prostřednictvím uhynulých tuleňů (publikace VIII). Autorem provedený výzkum tak potvrdil pronikání rtuti z nižších zeměpisných šířek do prostoru Antarktického poloostrova.

Omezení používání kovové rtuti v běžném životě (např. teploměry, manometry, baterie a el. přístroje), legislativa omezující nakládání se sloučeninami rtuti, i postupné upouštění od amalgámové výroby hydroxidu sodného (či modernizace stávajících výrobních zařízení) je jistě dobrým krokem ke snížení znečištění životního prostředí. Prognóza budoucího vývoje antropogenní emise rtuti je spíše pozitivní[8]. Motorem tohoto vývoje by mohlo být masivní omezení spalování fosilních paliv (uhlí), a to zejména pro výrobu elektrické energie.

Důležitým faktorem ovlivňujícím emisi rtuti do atmosféry i její depozici je teplota na Zemi[6,48]. V současné době se hovoří o problematice globálního oteplování především v souvislosti s rostoucí koncentrací skleníkových plynů v atmosféře. Hovoříme-li o tom, co přinese tání permafrostu, máme na zřeteli potenciální emisi oxidu uhličitého a methanu do atmosféry[49]. Věčně zmrzlá půda je ovšem také depozitem rtuti, což může zásadně ovlivnit celkové množství cirkulující rtuti v ekosystému[14].

Reference

(1) Bargagli, R. *Antarctic Ecosystems. Environmental Contamination, Climate Change, and Human Impact*, Springer: Berlin, 2005.

(2) Boening, D.W. *Chemosphere* **2000**, 40, 1335-1351.

(3) Pirrone, N.; Mason, R.; Eds. *Mercury Fate and Transport in the Global Atmosphere*, Springer: New York, 2009.

(4) Selin, N.E. *Annual Review of Environment and Resources* **2009**, 34, 43-63.

(5) Sprovieri, F.; Pirrone, N.; Bencardino, M.; D'Amore, F.; Carbone, F.; Cinnirella, S.; Mannarino, V.; Landis, M.; Ebinghaus, R.; Weigelt, A.; Brunke, E.G.; Labuschagne, C.; Martin, L.; Munthe, J.; Wängberg, I.; Artaxo, P.; Morais, F.; Barbosa, H.M.J.; Brito, J.; Cairns, W.; Barbante, C.; Diéguez, M.C.; Garcia, P.E.; Dommergue, A.; Angot, H.; Magand, O.; Skov, H.; Horvat, M.; Kotnik, J.; Read, K.A.; Neves, L.M.; Gawlik, B.M.; Sena, F.; Mashyanov, N.; Obolkin, V.; Wip, D.; Feng, X.B.; Zhang, H.; Fu, X.; Ramachandran, R.; Cossa, D.; Knoery, J.; Marusczak, N.; Nerentorp, M.; Norstrom, C. *Atmospheric Chemistry and Physic* **2016**, 16, 11915-11935.

(6) Steffen, A.; Douglas, T.; Amyot, A.; Ariya, P.; Aspmo, K.; Berg, T.; Bottenheim, J.; Brooks, S.; Cobbett, F.; Dastoor, A.; Dommergue, A.; Ebinghaus, R.; Ferrari, C.; Gardfeldt, K.; Goodsite, M.E.; Lean, D.; Poulain, A.J.; Scherz, C.; Skov, H.; Sommar, J.; Temme, C. *Atmospheric Chemistry and Physic* **2008**, 8, 1445-1482.

(7) Mukherjee, A.B.; Zevenhoven, R.; Bhattacharya, P.; Sajwan, K.S.; Kikuchi, R. *Resources, Conservation and Recycling* **2008**, 52, 571-591.

(8) Pacyna, J.M.; Travnikov, O.; De Simone, F.; Hedgecock, I.M.; Sundseth, K.; Pacyna, E.G.; Steenhuisen, F.; Pirrone, N.; Munthe, J.; Kindbom, K. *Atmospheric Chemistry and Physics* **2016**, 16, 12495-12511.

(9) AMAP. *Mercury in the Arctic*, Arctic Monitoring and Assessment Programme: Oslo, 2011.

(10) Lehnherr, I. *Environmental Reviews* **2014**, 22, 229-243.

(11) Poissant, L.; Zhang, H.H.; Canário, J.; Constant, P. *Science of the Total Environment* **2008**, 400, 173-211.

(12) Bargagli, R. *Science of the Total Environment* **2008**, 400, 212-226.

(13) Pirrone, N.; Cinnirella, S.; Feng, X.; Finkelman, R.B.; Friedli, H.R.; Leaner, J.; Mason, R.; Mukherjee, A.B.; Stracher, G.B.; Streets, D.G.; Telmer, K. *Atmospheric Chemistry and Physics* **2010**, 10, 5951-5964.

(14) Schuster, P.F.; Schaefer, K.M.; Aiken, G.R.; Antweiler, R.C.; Dewild, J.F.; Gryziec, J.D.; Gusmeroli, A.; Hugelius, G.; Jafarov, E.; Krabbenhoft, D.P.; Liu, L.; Herman-Mercer, N.; Mu, C.; Roth, D.A.; Schaefer, T.; Striegl, R.G.; Wickland, K.P.; Zhang, T. *Geophysical Research Letters* **2018**, 45, 1463-1471.

(15) Coufalík, P.; Červenka, R.; Komárek, J. *Environmental Earth Sciences* **2011**, 62, 421-427.

(16) Tessier, A.; Campbell, P.G.C.; Bisson, M. *Analytical Chemistry* **1979**, 51, 7, 844-851.

(17) Issaro, N.; Abi-Ghanem, C.; Bermond, A. *Analytica Chimica Acta* **2009**, 631, 1-12.

(18) Welz, B.; Sperling, M.; *Atomic Absorption Spectrometry*. Wiley-VCH: Weinheim, 2005.

(19) Mikac, N.; Foucher, D.; Niessen, S.; Lojen, S.; Fischer, J.C. *Analytical and Bioanalytical Chemistry* **2003**, 377, 1196-1201.

(20) Hintelmann, H. In: *Organometallics in Environment and Toxicology: Metal Ions in Life Sciences*, Sigel, A.; Sigel, H.; Sigel, R.K.O.; Eds.; RSC Publishing: Cambridge, 2010.

(21) Morel, F.M.M.; Kraepiel, A.M.L.; Amyot, M. *Annual Review of Ecology and Systematics* **1998**, 29, 543-566.

(22) Carrasco, L.; Vassileva, E. *Talanta* **2014**, 122, 106-114.

(23) Jagtap, R.; Maher, W. *Microchemical Journal* **2015**, 121, 65-98.

(24) Maggi, C.; Berducci, M.T.; Bianchi, J.; Giani, M.; Campanella, L. *Analytica Chimica Acta* **2009**, 641, 32-36.

(25) Uría, J.E.S.; Sanz-Medel, A. *Talanta* **1998**, 47, 509-524.

(26) Hu, X.; Zhang, Y.; Luo, J.; Wang, T.; Lian, H.; Ding, Z. *Environmental Pollution* **2011**, 159, 1215-1221.

(27) Coufalík, P.; Komárek, J. *Journal of Analytical Chemistry* **2014**, 69, 12, 1123-1129.

(28) Biester, H.; Scholz, C. *Environmental Science & Technology* **1997**, 31, 233-239.

(29) Coufalík, P.; Zvěřina, O.; Komárek, J. *Chemical Papers* **2014**, 68, 4, 427-434.

(30) Nóvoa-Muñoz, J.C.; Pontevedra-Pombal, X.; Martínez-Cortizas, A.; Gayoso, E.G.R. *Science of the Total Environment* **2008**, 394, 303-312.

(31) Bagnato, E.; Aiuppa, A.; Parello, F.; Allard, P.; Shinohara, H.; Liuzzo, M.; Giudice, G. *Bulletin of Volcanology* **2011**, 73, 497-510.

(32) Skácelová, K.; Barták, M.; Coufalík, P.; Nývlt, D.; Trnková, K. *Czech Polar Reports* **2013**, 3, 2, 93-106.

(33) Prošek, P.; Barták, M.; Gloser,J.; Láska, K.; Stachoň, Z.; Engel, Z.; Nedbalová, L.; Elster, J.; Komárek, J.; Pavel, V.; Weidinger, K.; Janko, K.; Fischer, S.; Janoušek, V.; Kopačková, V.; Mixa, P.; Mlčoch, B.; Nývlt, D.; Venera, Z.; Vodrážka, R.; Sladký, P.; Suchánek, A.; Jamný, D.; Šandikov, G. *Antarktida*, Academia: Praha, 2013.

(34) CGS. *James Ross Island – northern part*. Czech Geological Survey: Praha, 2009.

(35) Canil, D.; Crockford, P.W.; Rossin, R.; Telmer, K. *Chemical Geology* **2015**, 396, 134-142.

(36) Rudnick, R.L.; Gao, S. In: *Treatise on Geochemistry*, Holland, H.; Turekian, K.; Eds.; Elsevier: Amsterdam, 2014.

(37) Henley, R.W.; Berger, B.R. *Earth-Science Reviews* **2013**, 125, 146-170.

(38) Bargagli, R.; Sanchez-Hernandez, J.C.; Martella, L.; Monaci, F. *Polar Biology* **1998**, 19, 316-322.

(39) Bard, S.M. *Marine Pollution Bulletin* **1999**, 38, 5, 356-379.

(40) Caroli, S.; Cescon, P.; Walton, D.W.H.; Eds. *Environmental Contamination in Antarctica. A Challenge to Analytical Chemistry*, Elsevier: Amsterdam, 2001.

(41) Lindberg, S.E.; Brooks, S.; Lin, C.J.; Scott, K.J.; Landis, M.S.; Stevens, R.K.; Goodsite, M.; Richter, A. *Environmental Science & Technology* **2002**, 36, 1245-1256.

(42) Vandal, G.M.; Mason, R.P.; McKnight, D.; Fitzgerald, W. *Science of the Total Environment* **1998**, 213, 229-237.

(43) Coufalík, P.; Prochazková, P.; Zvěřina, O.; Trnková, K.; Skácelová, K.; Nývlt, D.; Komárek, J. *Polish Polar Research* **2016**, 37, 4, 477-491.

(44) Podterob, A.P. *Pharmaceutical Chemistry Journal* **2008**, 42, 10, 582-588.

(45) Xu, M.; Yan, R.; Zheng, C.; Qiao, Y.; Han, J.; Sheng, C. *Fuel Processing Technology* **2003**, 85, 215-237.

(46) Yudovich, Y.E.; Ketris, M.P. *International Journal of Coal Geology* **2005**, 62, 107-134.

(47) Pospíšil, J.; Jícha, M. In: *Transport, Health and Environment*. Adamec, V., Jandová, V.; Eds.; Transport research Centre: Brno, 2010.

(48) Martínez-Cortizas, A.; Pontevedra-Pombal, X.; García-Rodeja, E.; Nóvoa- Muñoz, J.C.; Shotyk, W. *Science* **1999**, 284, 939-942.

(49) Lawrence, D.M.; Koven, C.D.; Swenson, S.C.; Riley, W.J.; Slater, A.G. *Environmental Research Letters* **2015**, 10, 094011.

Přílohy I – XI

Příloha I

Bulletin of Environmental Contamination and Toxicology (2018) 101:549–553
https://doi.org/10.1007/s00128-018-2430-5

Model of Mercury Flux Associated with Volcanic Activity

Pavel Coufalík[1,2] · Lukáš Krmíček[3,4,5] · Ondřej Zvěřina[1,6] · Natália Meszarosová[1] · Jindřich Hladil[4] · Josef Komárek[1]

Received: 23 April 2018 / Accepted: 27 August 2018 / Published online: 30 August 2018
© Springer Science+Business Media, LLC, part of Springer Nature 2018, Corrected publication September/2018

Abstract
Volcanic activity is one of the primary sources of mercury in the earth's ecosystem. In this work, volcanic rocks from four geotectonically distinct localities (the Czech Republic – intraplate, rift-related alkaline basaltic rocks; Iceland – hotspot/rift-related tholeiitic basaltic rocks; Japan – island arc calc-alkaline andesites; and Alaska – continental arc calc-alkaline dacites) were studied. Ultra-trace Hg contents in all samples ranged from 0.3 up to 6 µg/kg. The highest Hg content was determined for volcanic ash from Mount Redoubt (Alaska, USA). In the case of basaltic volcanic rocks, the obtained results are about two orders of magnitude smaller than values formerly assumed for primary mercury contents in basaltic lavas. They are close to predicted Hg contents in the mantle source, i.e. below 0.5 µg/kg. Hg degassing is probably a key process for the resulting Hg contents in material ejected during volcanic eruption, which is previously enriched by Hg in the shallow-crust.

Keywords Mercury content · Basalt · Andesite · Dacite

Mercury is one of the most important global pollutants circulating in the earth's ecosystem (Selin 2009). Mercury biogeochemical cycle includes mobility of mercury species as well as speciation changes of which methylation processes (biotic and abiotic) stand in focus (Hintelmann 2010). Toxicity of mercury compounds increases with their bioaccumulative potential. Inorganic Hg compounds are less toxic than organometallic compounds which have high bioaccumulation ability in the food chain. The most toxic forms of mercury for humans are the vapours of Hg^0 and methylated Hg species. Inhaled Hg^0 is transported into the brain (and kidneys). This form can pass through the blood–brain and placental barriers. Methylmercury (MeHg) is highly neurotoxic, damages the central nervous system, and is highly dangerous for its development (WHO 2007). MeHg is forming mainly in marine and freshwater sediments from deposited inorganic Hg forms. In the aquatic environment, MeHg accumulates in the food chain from microorganisms, via invertebrates, to fish (and marine mammals, and birds) (Boening 2000). Fish and seafood are the main source of MeHg exposure because almost all MeHg from the food is absorbed in the gastrointestinal tract (WHO 2007).

Mercury emissions into the atmosphere from natural sources include both primary sources and the re-emission of previously deposited Hg (Schroeder and Munthe 1998). The amount of Hg from natural sources is probably close to anthropogenic levels (Bagnato et al. 2011). On the basis of estimates, current volcanic activity and geothermal activity produce approximately 2% of the annual Hg emission into the atmosphere (Pirrone et al. 2010). However, the amount of Hg released by the degassing of active volcanoes can be much higher (Bagnato et al. 2011, 2014; Martín et al. 2013). Estimates of emissions vary due to the evaluation of point measurements of several volcanoes which differ in their character of volcanic activity and composition of magma (Bagnato et al. 2007; Mather et al. 2003). In addition, estimates of Hg emission from volcanoes (Bagnato

✉ Lukáš Krmíček
lukas.krmicek@gmail.com

1 Department of Chemistry, Faculty of Science, Masaryk University, Kotlářská 2, 61137 Brno, Czech Republic

2 Institute of Analytical Chemistry of the Czech Academy of Sciences, Veveří 97, 60200 Brno, Czech Republic

3 Faculty of Civil Engineering, Brno University of Technology, Veveří 95, 60200 Brno, Czech Republic

4 Institute of Geology of the Czech Academy of Sciences, Rozvojová 269, 16500 Prague 6, Czech Republic

5 Department of Geological Sciences, Faculty of Science, Masaryk University, Kotlářská 2, 611 37 Brno, Czech Republic

6 Department of Public Health, Faculty of Medicine, Masaryk University, Kamenice 5, 62500 Brno, Czech Republic

et al. 2014) are based on measurements of active volcanoes in non-eruptive periods.

Primary emissions of Hg occur mainly in mercuryferous belt, which has the highest Hg bedrock enrichment and the highest rate of Hg degassing. These zones occur in areas with increased seismic activity along subduction zones (Rytuba 2003; Schlüter 2000; Selin 2009). However, major amounts of volcanic emissions come into the atmosphere during eruptive periods of active volcanoes (Mather et al. 2003). Generally, aerosol in the eruption column can be composed of pyroclastics, volcanic gas condensates released from the magma, and other transformed particles. The Hg content in volcanic emissions is greatly enriched compared to Hg content in the magma (Mather et al. 2003); however, Hg concentrations in the eruption column are dependent on air dilution (Bagnato et al. 2014). The main Hg species in the eruption column is Hg^0, but gaseous $Hg^{(II)}$ and particulate Hg are released as well (Bagnato et al. 2007). Hg speciation in the eruption column varies among volcanoes. The eruption column of Mount Erebus (Antarctica) contains only 20%–40% Hg^0. Particulate Hg can comprise about 2% of Hg in the dilute eruption column of Mount St. Helens (USA) (Pyle and Mather 2003). The proportion of particulate Hg released during degassing of Etna was estimated at about 1% (Bagnato et al. 2007).

The formation of particulate material ejected during volcanic eruption involves the fragmentation of magma and the erosion of rocks from vent walls. The solubility of volatile components in the melt is controlled by temperature, pressure, and melt composition. The formation of bubbles of CO_2 and water vapor leads to the transition of trace elements from magma to the gaseous phase (Mather et al. 2003). Another source of trace elements in the eruption column can be the dissolution of andesite caused by the mixing of volcanic gases with boiling meteoric water saturated by anions from the gas phase (Symonds et al. 1992). Thus, the composition of magma can be greatly influenced by the time spent in the shallow-crust before eruption (Schmincke 2004). Most trace elements condense during the cooling of volcanic gases, most often in the form of chlorides. Mercury is an exception in this respect. When the gas phase temperature decreases to 100°C the amount of Hg halides is negligible in relation to the Hg^0 concentration (Symonds and Reed 1993).

The question is whether the Hg content in volcanic rocks reflects their chemical composition, and whether it can characterize the Hg content in the earth's crust. It appears that Hg correlation with any chemical differentiation index or degree of secondary alteration is not necessary (Canil et al. 2015). Pilot studies in the 1970s showed that both alkaline and tholeiitic basaltic rocks had noticeably higher Hg contents (hundreds of µg/kg) compared to other geochemical types of volcanic rocks (Fleischer 1970; Dissanayake and Vincent 1975). However, recent measurements have shown substantially lower Hg contents (see Zintwana et al. 2012). In fact, published Hg contents in volcanic rocks were often affected by contamination during the analytical procedure or by the heterogeneity of low Hg levels in samples (Canil et al. 2015; Coufalík et al. 2015; Zintwana et al. 2012). The aim of this work is to propose a model of Hg flux from volcanic activity into the mercury cycle based on the evaluation of Hg contents in volcanic rocks from different geotectonic areas.

Materials and Methods

The volcanic rocks studied in this work came from four geotectonically distinct localities (see Fig. 1). The locality in the Bruntál Volcanic Field (BVF, Czech Republic) was selected for the collection of lapilli (12 samples, marked as BVF) and lava (three samples, marked as BVF lava). The volcanism of the Uhlířský vrch Volcano (49.972 N, 17.440 E) and the Venušina sopka Volcano (49.951 N, 17.477 E) falls into the Plio-Pleistocene basanitic series of the NE part of the Czech Republic (Cajz et al. 2012; Ulrych et al. 2013). These monogenetic Strombolian volcanoes with preserved volcanic cones are products of the Calabrian phase (1.8–1.1 Ma) of Cenozoic volcanism. The respective volcanic rocks represent intraplate, rift-related alkaline basaltic magmas with a composition between olivine nephelinite and nepheline basanite (Cajz et al. 2012). Six samples of volcanic ash and dust were also studied. The samples were obtained from dust collection of the Institute of Geology of the Czech Academy of Sciences. Four samples originated from hotspot/rift-related tholeiitic basaltic rocks from Iceland (Eyjafjallajökull, Mælifellsandur plain), one sample represented island arc andesite of calc-alkaline composition from Japan (Sakurajima), and one sample was from continental arc calc-alkaline dacite from Alaska (Mount Redoubt). Three samples of

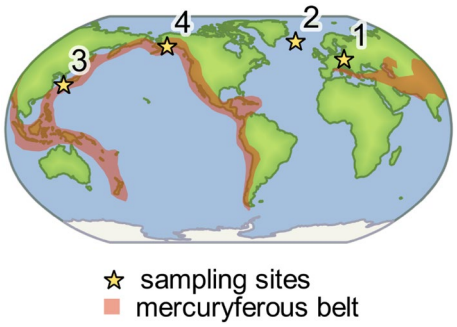

Fig. 1 Sampling areas of studied volcanic rocks: 1 – the Uhlířský vrch and Venušina sopka volcanoes (the Czech Republic), 2 – Eyjafjallajökull and the Mælifellsandur plain (Iceland), 3 – Sakurajima (Japan), 4 – Mount Redoubt (Alaska, USA). The mercuryferous belt is highlighted according to Schlüter (2000)

volcanic ash from Eyjafjallajökull (63.515 N, 18.485 W; 63.682 N, 19.636 W; 63.562 N, 19.619 W) originated from the eruption in 2010. These ashes had an overall macroelement geochemistry varying between basalts and andesites. Chemistry and mineralogy results related to the basaltic sample from the Mælifellssandur plain (63.816 N, 19.124 W) were presented by Dagsson-Waldhauserova et al. (2014). The chemical composition of the ash sample from the Sakurajima volcano (31.555 N, 130.679 E) corresponded to andesite. The collected ash from Mount Redoubt (59.842 N, 151.811 W) originated from the eruption in 2009. The chemical composition of major and trace elements is similar to rocks of dacitic composition, which were thrown or extruded at this event; see Coombs et al. (2013).

In addition, certified reference material (CRM) *Trace Metals – Taiwan Clay 1* (RTC, USA) with an Hg content of 0.865 ± 0.0331 mg/kg and quality control material (QCM) *Metranal 1* (Analytica, Czech Republic) with an Hg content of 1.55 ± 0.14 mg/kg were used to verify the determination of Hg in solid samples.

Samples from the BVF were dried to the constant weight at 30°C. Samples of lapilli were crushed in a mortar, samples of lava in a mechanical press with PTFE lining. Thereafter, the samples were homogenized in *Pulverisette 7* mill (Fritsch, Germany). Samples of volcanic ashes were homogenized in an agate mortar immediately before the analysis.

The determination of Hg in all samples was performed by means of an AMA-254 mercury analyzer (Altec, Czech Republic). This single-purpose atomic absorption spectrometer enables the direct measurement of solid and liquid samples using an thermo-oxidative digestion. The source of radiation was mercury hollow lamp at 253.65 nm. The analytical program of the measurement follows: 20 s drying, 150 s decomposition, 45 s delay. Six analyses of each sample were performed.

Mercury determination by the AMA-254 analyzer was verified by means of CRMs. The Hg content of CRM *Trace Metals – Taiwan Clay 1* was determined to 0.89 ± 0.032 mg/kg; the Hg content of QCM *Metranal 1* was 1.57 ± 0.04 mg/kg. The limit of quantification of total Hg in solid samples was 0.3 µg/kg. The limit of quantification was defined as ten times the standard deviation of the blank.

Results and Discussion

Extremely low Hg contents were determined in the majority of the studied volcanic rocks. The results for basic rocks from the Czech Republic, Iceland, and Japan, and more acidic dacite from Alaska are presented in Fig. 2. The lowest Hg levels (0.3 µg/kg) were observed for ash samples from the Eyjafjallajökull (Iceland) and lapilli from the BVF (0.5 µg/kg) in the Czech Republic. Such low concentrations are approaching the estimation of Hg content in the primitive upper mantle (0.4–0.6 µg/kg) published by Canil et al. (2015). Sakurajima (Japan) and Mount Redoubt (Alaska, USA) are located in the circum-pacific mercury mineral belt (Gray et al. 1998; Rytuba 2003). However, the sample of volcanic ash from Sakurajima had a very low Hg content. Extremely low Hg levels in the studied ash samples are likely the result of Hg release from magmatic rocks during volcanic eruption accompanied by a minimal re-condensation on cooling ejected material.

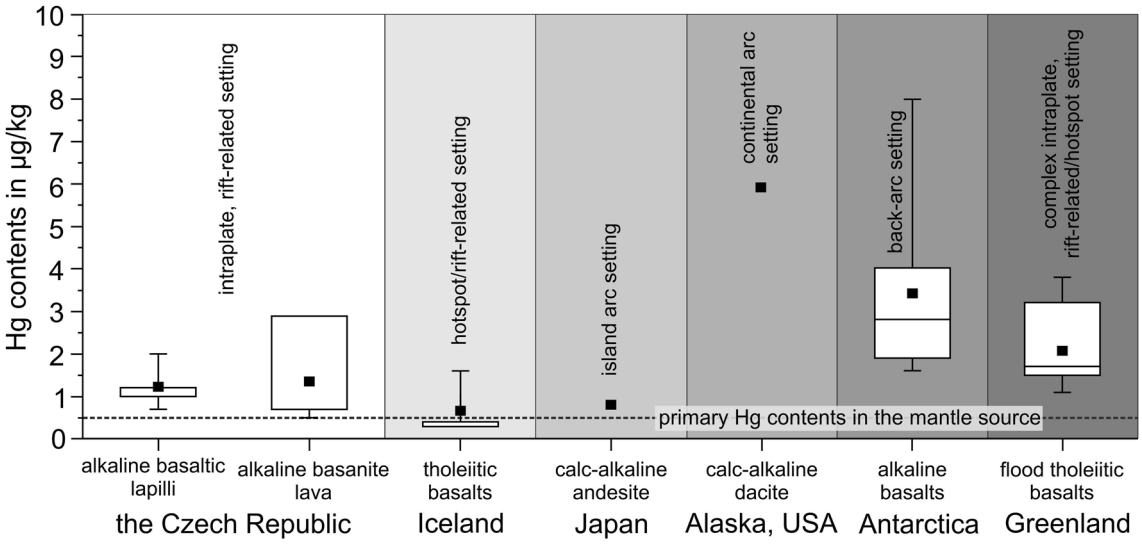

Fig. 2 Hg contents in volcanic rocks from different geotectonic settings. Data for Antarctica and Greenland were taken from Coufalík et al. (2015)

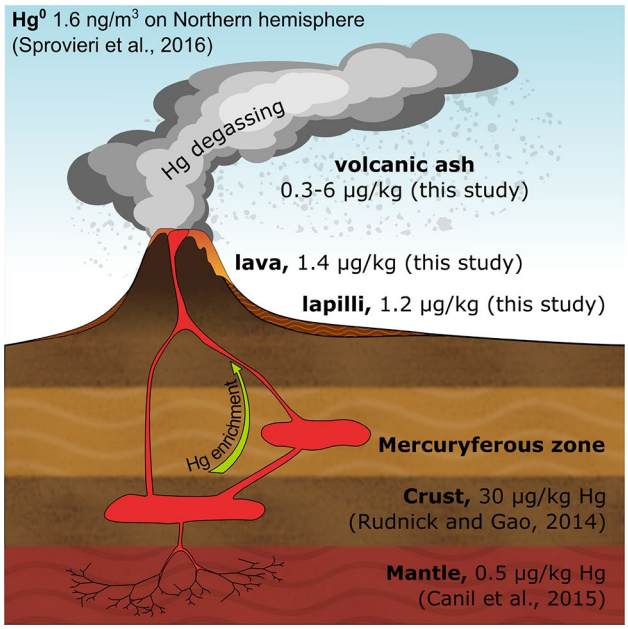

Fig. 3 Model of Hg flux associated with volcanic activity

The idea that Hg concentrations in volcanic rocks of up to 10 µg/kg are the result of degassing processes during rock formation has already been proposed by Gotoh et al. (1978). It can be assumed that the extent of Hg release caused by degassing processes is also dependent on the content of Hg in the ejected magma. Estimates of Hg contents in volcanic magmas are relatively high for some volcanoes. Hg content in the magma of Etna is estimated to tens of µg/kg according to the contents of other elements (Ferrara and Maserti 1990; Pyle and Mather 2003). In contrast, significantly lower Hg contents were observed for basaltic lavas with minimal contamination by crustal material. The mantle peridotites studied by Canil et al. (2015) exhibited Hg contents of between 0.2 and 5 µg/kg. Peridotites with higher Hg contents are often affected by secondary processes or contamination. Very low concentrations of Hg were also determined for back-arc alkaline lavas from James Ross Island, Antarctica, as well as for flood tholeiitic basalts from Greenland (Fig. 2; Coufalík et al. 2015).

The model of Hg flux into the mercury cycle was designed according to our measurements and data from the literature (Canil et al. 2015; Rudnick and Gao 2014; Sprovieri et al. 2016), (Fig. 3). The process of Hg release from primitive mantle and the earth's crust into the atmosphere can be described as follows. The melt of primitive mantle is enriched in Hg in the course of its passage through the earth's crust due to the melting of crustal minerals. The Hg content in primitive mantle is estimated to be 0.5 µg/kg (Canil et al. 2015); the Hg content in bulk continental crust is estimated to be 30 µg/kg (Rudnick and Gao 2014). Ejected material reflects the composition of magma only partially due to the considerable expansion of gases in the eruption column. The expansion of the gaseous phase to atmospheric pressure causes the nucleation of particles (especially SiO_2), which adsorb trace elements, but the adsorption is minimal for Hg (Henley and Berger 2013).

It is generally assumed that basaltic rocks with minimal contamination reflect the composition of primitive mantle magma. On the basis of the low Hg contents found in basic volcanic rocks, relatively low average Hg contents in the earth's crust are also assumed, which are explained by the heterogeneous distribution of Hg (Canil et al. 2015). Hg contents in volcanic rocks from mercuryferous belts should be higher, which was not confirmed in this study. The contents may be somewhat higher in the case of magma existing for long periods in shallow-crust. However, the Hg content in volcanic rocks reflects, in particular, the degree of degassing during volcanic eruption. Hg contents up to 10 µg/kg can be assumed even for more acidic volcanic rocks due to minimal Hg re-condensation in the eruption column, regardless of whether or not they occur in the mercuryferous belt in subduction zones.

Extremely low Hg contents in the studied volcanic rocks indicate a high level of Hg release into the atmosphere during an eruption, accompanied by minimal re-condensation on the ejected material. Thus, Hg contents are not dependent on the geotectonic position of volcanoes (mercuryferous versus non-mercuryferous zones). In the case of basic volcanic rocks, the Hg content may be as low as the assumed content in the mantle source, but only in the case of quantitative degassing.

This principle suggests a different view on natural sources of the mercury. Very low determined contents of Hg in volcanic rocks of basaltic to dacitic composition from various geotectonic positions (up to 6 µg/kg) indicate an effective Hg transport from the bedrock to the atmosphere, thus, the amount of Hg released into the environment by weathering processes is probably not so significant. Concentrations of mercury in terrestrial ecosystem may be more dependent on Hg deposition from the atmosphere than on the composition of the bedrock. This way, the re-emission of deposited mercury as well as Hg speciation changes forming highly toxic species are much faster than in the case of the weathering processes.

Acknowledgements The research was supported by the Grant Agency of the Czech Republic under project P503/12/0682, by Masaryk University under the project MUNI/A/0886/2016, by the Institute of Analytical Chemistry of the CAS under RVO 68081715, by the Institute of Geology of the CAS under RVO 67985831, and by the BUT project LO1408 "AdMaS UP – Advanced Materials, Structures and Technologies", supported by the Ministry of Education, Youth and Sports CR under the "National Sustainability Programme I".

References

Bagnato E, Aiuppa A, Parello F, Calabrese S, D'Alessandro W, Mather TA, McGonigle AJS, Pyle DM, Wängberg I (2007) Degassing of gaseous (elemental and reactive) and particulate mercury from Mount Etna volcano (Southern Italy). Atmos Environ 41:7377–7388. https://doi.org/10.1016/j.atmosenv.2007.05.060

Bagnato E, Aiuppa A, Parello F, Allard P, Shinohara H, Liuzzo M, Giudice G (2011) New clues on the contribution of earth's volcanism to the global mercury cycle. Bull Volcanol 73:497–510. https://doi.org/10.1007/s00445-010-0419-y

Bagnato E, Tamburello G, Avard G, Martinez-Cruz M, Enrico M, Fu X, Sprovieri M, Sonke JE (2014) Mercury fluxes from volcanic and geothermal sources: an update. In: Zellmer GF, Edmonds GF, Straub SM (eds) The role of volatiles in the genesis, evolution and eruption of arc magmas, special publications 410. Geological Society, London, pp 263–285. https://doi.org/10.1144/SP410.2

Boening DW (2000) Ecological effects, transport, and fate of mercury: a general review. Chemosphere 40:1335–1351. https://doi.org/10.1016/S0045-6535(99)00283-0

Cajz V, Schnabl P, Pécskay Z, Skácelová Z, Venhodová D, Šlechta S, Čížková K (2012) Chronological implications of the paleomagnetic record of the Late Cenozoic volcanic activity along the Moravia-Silesia border (NE Bohemian Massif). Geol Carpath 63:423–435. https://doi.org/10.2478/v10096-012-0033-3

Canil D, Crockford PW, Rossin R, Telmer K (2015) Mercury in some arc crustal rocks and mantle peridotites and relevance to the moderately volatile element budget of the earth. Chem Geol 396:134–142. https://doi.org/10.1016/j.chemgeo.2014.12.029

Coombs ML, Sisson TW, Bleick HA, Henton SM, Nye CJ, Payne AL, Cameron CE, Larsen JF, Wallace KL, Bull KF (2013) Andesites of the 2009 eruption of Redoubt Volcano, Alaska. J Volcanol Geotherm Res 259:349–372. https://doi.org/10.1016/j.jvolgeores.2012.01.002

Coufalík P, Zvěřina O, Krmíček L, Pokorný R, Komárek J (2015) Ultratrace analysis of Hg in alkaline lavas and regolith from James Ross Island. Antarct Sci 27:281–290. https://doi.org/10.1017/S0954102014000819

Dagsson-Waldhauserova P, Arnalds O, Olafsson H, Skrabalova L, Sigurdardottir GM, Branis M, Hladil J, Skala R, Navratil T, Chadimova L von Lowis of Menar S, Thorsteinsson T, Carlsen HK, Jonsdottir I (2014) Physical properties of suspended dust during moist and low wind conditions in Iceland. Icel Agric Sci 27:25–39

Dissanayake CB, Vincent EA (1975) Mercury in rocks and minerals of the Skaergaard intrusion, East Greenland. Mineral Mag 40:33–42. https://doi.org/10.1180/minmag.1975.040.309.05

Ferrara R, Maserti BE (1990) Atmospheric mercury levels in the Mount Etna volcanic area after an eruptive phase. Environ Technol 11:51–56. https://doi.org/10.1080/09593339009384838

Fleischer M (1970) Summary of the literature on the inorganic geochemistry of mercury. In: Mercury in the environment, vol 713. U.S. Goverment Printing Office, Geological Survey Professional Paper, Washington, DC, pp 6–13

Gotoh S, Tokudome S, Koga H (1978) Mercury in soil derived from igneous rock in Northern Kyushu, Japan. Soil Sci Plant Nutr 24:391–406. https://doi.org/10.1080/00380768.1978.10433118

Gray JE, Gent CA, Snee W (1998) The southwestern Alaska mercury belt and its relationship to the circum-pacific metallogenic mercury province. Polarforschung 68:187–196

Henley RW, Berger BR (2013) Nature's refineries—metals and metalloids in arc volcanoes. Earth Sci Rev 125:146–170. https://doi.org/10.1016/j.earscirev.2013.07.007

Hintelmann H (2010) Organomercurials. Their formation and pathways in the environment. In: Sigel A, Sigel H, Sigel RKO (eds) Organometallics in environment and toxicology: metal ions in life sciences. RSC Publishing, Cambridge, pp 365–401. https://doi.org/10.1039/9781849730822-00365

Martín JAR, Nanos N, Miranda JC, Carbonell G, Gil L (2013) Volcanic mercury in Pinus canariensis. Naturwissenschaften 100:739–747. https://doi.org/10.1007/s00114-013-1070-1

Mather TA, Pyle DM, Oppenheimer C (2003) Tropospheric volcanic aerosol. In: Robock A, Oppenheimer C (eds) Volcanism and the earth's atmosphere, geophysical monograph, American Geophysical Union, Washington, DC 139:189–2012. https://doi.org/10.1029/139GM12

Pirrone N, Cinnirella S, Feng X, Finkelman RB, Friedli HR, Leaner J, Mason R, Mukherjee AB, Stracher GB, Streets DG, Telmer K (2010) Global mercury emissions to the atmosphere from anthropogenic and natural sources. Atmos Chem Phys 10:5951–5964. https://doi.org/10.5194/acp-10-5951-2010

Pyle DM, Mather TA (2003) The importance of volcanic emissions for the global atmospheric mercury cycle. Atmos Environ 37:5115–5124. https://doi.org/10.1016/j.atmosenv.2003.07.011

Rudnick RL, Gao S (2014) Composition of the continental crust. In: Holland H, Turekian K (eds) Treatise on geochemistry. Elsevier Science, Amsterdam, pp 1–51. https://doi.org/10.1016/B978-0-08-095975-7.00301-6

Rytuba JJ (2003) Mercury from mineral deposits and potential environmental impact. Environ Geol 43:326–338. https://doi.org/10.1007/s00254-002-0629-5

Schlüter K (2000) Review: evaporation of mercury from soils. An integration and synthesis of current knowledge. Environ Geol 39:249–271. https://doi.org/10.1007/s002540050005

Schmincke HU (2004) Volcanism. Springer, Berlin, p 324

Schroeder WH, Munthe J (1998) Atmospheric mercury—an overview. Atmos Environ 32:809–822. https://doi.org/10.1016/S1352-2310(97)00293-8

Selin NE (2009) Global biogeochemical cycling of mercury: a review. Annu Rev Environ Resour 34:43–63

Sprovieri F, Pirrone N, Bencardino M, D'Amore F, Carbone F, Cinnirella S, Mannarino V, Landis M, Ebinghaus R, Weigelt A, Brunke EG, Labuschagne C, Martin L, Munthe J, Wängberg I, Artaxo P, Morais F, Barbosa HMJ, Brito J, Cairns W, Barbante C, Diéguez MC, Garcia PE, Dommergue A, Angot H, Magand O, Skov H, Horvat M, Kotnik J, Read KA, Neves LM, Gawlik BM, Sena F, Mashyanov N, Obolkin V, Wip D, Feng XB, Zhang H, Fu X, Ramachandran R, Cossa D, Knoery J, Marusczak N, Nerentorp M, Norstrom C (2016) Atmospheric mercury concentrations observed at ground-based monitoring sites globally distributed in the framework of the GMOS network. Atmos Chem Phys 16:11915–11935. https://doi.org/10.5194/acp-16-11915-2016

Symonds RB, Reed MH (1993) Calculation of multicomponent chemical equilibria in gas-solid-liquid systems: calculation methods, thermochemical data, and applications to studies of high temperature volcanic gases with examples from Mount St. Helens. Am J Sci 293:758–864. https://doi.org/10.2475/ajs.293.8.758

Symonds RB, Reed MH, Rose WI (1992) Origin, speciation, and fluxes of trace-element gases at Augustine volcano, Alaska: insights into magma degassing and fumarolic processes. Geochim Cosmochim Acta 56:633–657. https://doi.org/10.1016/0016-7037(92)90087-Y

Ulrych J, Ackerman L, Balogh K, Hegner E, Jelínek E, Pécskay Z, Přichystal A, Upton BGJ, Zimák J, Foltýnová R (2013) Plio-Pleistocene basanitic and melilititic series of the Bohemian Massif: K-Ar ages, major/trace element and Sr–Nd isotopic data. Chem Erde 73:429–450. https://doi.org/10.1016/j.chemer.2013.02.001

WHO (2007) Health risks of heavy metals from long-range transboundary air pollution. World Health Organization, Germany, p 130

Zintwana MP, Cawthorn RG, Ashwal LD, Roelofse F, Cronwright H (2012) Mercury in the Bushveld complex, South Africa, and the Skaergaard intrusion, Greenland. Chem Geol 320–321:147–155. https://doi.org/10.1016/j.chemgeo.2012.06.001

Příloha II

Spectrochimica Acta Part B 118 (2016) 1–5

Contents lists available at ScienceDirect

Spectrochimica Acta Part B

journal homepage: www.elsevier.com/locate/sab

Analytical Note

The direct determination of HgS by thermal desorption coupled with atomic absorption spectrometry

Pavel Coufalík [a,b], Ondřej Zvěřina [a,c], Josef Komárek [a,*]

[a] Faculty of Science, Masaryk University, Kotlářská 2, 611 37 Brno, Czech Republic
[b] Institute of Analytical Chemistry, The Czech Academy of Sciences, v.v.i., Veveří 97, 602 00 Brno, Czech Republic
[c] Faculty of Medicine, Masaryk University, Kamenice 5, 62500 Brno, Czech Republic

ARTICLE INFO

Article history:
Received 21 July 2015
26 January 2016
Accepted 28 January 2016
Available online 3 February 2016

Keywords:
Mercury
HgS
Thermal desorption

ABSTRACT

This research was aimed at the direct determination of HgS in environmental samples by means of thermal desorption coupled with atomic absorption spectrometry. Operating parameters of the apparatus used for thermal desorption (including a prototype desorption unit) are described in this work, as well as the procedure for measuring mercury release curves together with an evaluation of the analytical signal including two methods of peak integration. The results of thermal desorption were compared with HgS contents obtained by sequential extraction. The limits of quantification of the proposed method for the selective determination of the black and red forms of HgS were 4 μg kg^{-1} and 5 μg kg^{-1}, respectively. The limit of quantification of red HgS in soils was 35 μg kg^{-1}. The developed analytical procedure was applied to soil and sediment samples from historical mining areas.

© 2016 Elsevier B.V. All rights reserved.

1. Introduction

Mercury production from red HgS represents a major anthropogenic impact on the natural Hg cycle in the environment. Elemental Hg released during ore processing and Hg forms contained in tailings constitute a considerable environmental burden. Areas of Hg mineral deposits [1] are also significant sources of environmental contamination. Mercury speciation in tailings depends on the initial speciation of Hg in the ore, the method of ore processing, and the physico-chemical parameters of the material. The main Hg forms in these localities are red HgS, black HgS, and metallic Hg [2]. The release of colloidal HgS and ongoing speciation changes allow the subsequent transport of the mercury.

Red HgS is the most important Hg mineral, which is often found in the form of veins or scatters in rocks in areas with hot springs. Mercury can be transported in hydrothermal fluids as the elemental form in aqueous solution or as gaseous Hg [3]. The geochemical mechanism of Hg mineral precipitation is the hydrothermal reworking of marine black shales, which leads to three types of Hg deposits [4]. The hot-spring type of Hg deposit is the most common and often geologically young [1]. Hydrothermal HgS crystallizes between 195 °C and 160 °C, a typical temperature range for the formation of Hg ore is from 200 °C to 100 °C [5]. Red HgS inverts to black HgS at 345 ± 2 °C (in a pure HgS system), but impurities (e.g., Fe and Zn) and also non-stoichiometry decrease the inversion temperature [4]. In addition, small particles of secondary Hg minerals are formed during ore processing. Black HgS is a relevant secondary mineral, which is formed in the course of the calcination process from the ore of silica-carbonate type of Hg deposit [1].

Accurate determination of HgS and nonsulfidic Hg forms in tailings enables the environmental risks of contaminated materials to be evaluated. Sequential extraction [6] is the most frequently used method for the determination of various Hg forms. An alternative method for the study of Hg speciation in solid samples is thermal desorption [7]. This method is based on the thermal release of individual Hg forms according to their thermal stability. The thermal behavior of Hg forms depends also on the intensity of their binding to the matrix. Instrumentation for this method, the preparation of calibration materials, the characteristic intervals for desorption temperatures, and the evaluation of mercury release curves have been described in the literature [8]. The method is particularly suitable for the identification of metallic Hg, matrix-bound Hg, and HgS [7]. Matrix-bound Hg is composed of bivalent and elemental Hg, mobile and semi-mobile Hg forms [7,8,9]. Matrix-bound Hg is formed by Hg readsorption during cooling of tailings. Metallic Hg can penetrate into the rocks at elevated temperature and adsorb within inner-sphere sorption sites [8].

The direct determination of HgS in solid samples stands in focus in this work. The thermal behavior of HgS was described in many papers [7,9,10]. Generally, the thermal desorption coupled with atomic absorption spectrometry (TD-AAS) is often realized by in-house fabricated devices coupled with common atomic absorption spectrometers [7] or by commercial pyrolyzer coupled with single-purpose mercury analyzer [11]. This paper describes in details a prototype of the desorption unit

* Corresponding author. Tel.: +420 549495027; fax: +420 549492494.
E-mail address: komarek@chemi.muni.cz (J. Komárek).

http://dx.doi.org/10.1016/j.sab.2016.01.004
0584-8547/© 2016 Elsevier B.V. All rights reserved.

used in previous works [9,12]. The previous publications are primarily concerned with the thermal stability of mercury compounds without any detailed description of the equipment.

The aim of this research was to develop an analytical procedure for the direct determination of red HgS in tailings, soils, and sediments. Specifically, the focus was on (i) developing a procedure to determine HgS by means of thermal desorption, (ii) the processing of mercury release curves, and (iii) the application of the suggested procedure on environmental samples.

2. Materials and methods

2.1. Locations and samples

Two deposits of red HgS in the Czech Republic were studied in this research. The first historical mine was Jedová hora (Poison Mountain) near Neřežín (N49°47′34″, E13°53′15″). The locality of Jedová hora forms part of the unmetamorphosed Ordovician sedimentary and volcanosedimentary sequences of the Barrandian Basin [5]. Mercury was mined here as a byproduct of iron ore mining from the 18th century until 1870 [2,13]. Hydrothermal vein mineralization was formed in this deposit. The presence of black HgS was not proven. The ore was processed directly in the mine grounds by melting in cylindrical retorts with the subsequent condensation of mercury into water [13].

The second locality was a negligible deposit near Bezdružice (N49°53′47″, E12°59′15″). The mineralization associated with metamorphosed shales of the Neoproterozoic, Cambrian–Ordovician and Silurian ages [5] also occurs as red HgS. The primary association of mercury with gold is uncertain due to its scattered occurrence in old heaps and in a nearby stream. The ore was mined in shallow pits and floated in situ in the 17th and 18th centuries [14].

Seven samples of soil (JH1–JH7) were collected in the vicinity of the former mining pit at Jedová hora. Each sample was collected as a soil profile (0–25 cm) after the removal of fresh organic material from the surface. Red HgS from Jedová hora obtained directly from the rock was also studied in this work. Two sediments from the stream (TS68 and TS83) and two soil samples (TP80 and TVP402) were taken in the vicinity of Bezdružice.

2.2. Reference materials and reagents

The following standard and certified reference materials were used: $Hg(NO_3)_2$ in 2 mol L^{-1} HNO_3 for AAS (1000 mg L^{-1} ± 4 mg L^{-1} Hg^{2+}, Fluka, Germany); CRM 020 Trace Metals—Sandy Loam 2 (RTC, USA) with a total mercury content of 1.12 ± 0.03 mg kg^{-1}; and CRM CC 580 Estuarine Sediment (No. 0160, IRMM, Belgium) with a total mercury content of 132 ± 3 mg kg^{-1}.

HCl (A.C.S. reagent, Hg < 0.0000005%, Sigma-Aldrich, Germany), KOH (p.a., ≥86%, Hg < 0.00001%, Fluka, Germany), HNO_3 (p.a., 65%, Hg < 0.0000005%, Sigma-Aldrich, Germany), $Na_2S{\cdot}nH_2O$ (32–38%, Sigma-Aldrich, Germany), and $K_2Cr_2O_7$ (A.C.S. reagent, Hg < 0.000001%, Merck, Germany) were used in the preparation of extraction or calibration solutions. The synthetic red form of HgS was obtained from Sigma-Aldrich (p.a., 99%). Black HgS was prepared by precipitation as follows: a solution of 0.1 mol L^{-1} $HgCl_2$ (A.C.S. reagent, 99.5%, Sigma-Aldrich, Germany) was added to an unsaturated Na_2S solution at laboratory temperature; precipitated HgS was repeatedly decanted and dried afterwards to a constant weight at laboratory temperature.

2.3. Preparation of samples and calibration materials

The samples from Jedová hora and Bezdružice were dried to a constant weight at laboratory temperature. Each sample was sieved and the proportion with particle sizes of below 2 mm was used for analysis. This proportion was pulverized in the mill (Pulverisette 7, Fritsch, Germany) to a particle size of below 63 μm. The processed samples were stored in polyethylene vials at 4 °C.

Sample dilution with sea sand (Penta, Czech Republic) was performed in an agate mortar for the samples with high mercury content (JH1 and JH5). The sand was previously heated at 1000 °C for 2 h. The dilution of CRM CC 580 by sand was performed at a ratio of 100 mg of certified material to 900 mg of sand. The sample of red HgS from Jedová hora was also ground in a mortar with sand. Calibration samples containing black or red HgS in sand were prepared with Hg concentrations ranging from 6 ng g^{-1} up to 1.2 μg g^{-1}.

Calibration solutions for the AMA-254 analyzer were prepared from CRM $Hg(NO_3)_2$ for AAS at concentrations of 1 μg L^{-1}, 10 μg L^{-1}, 100 μg L^{-1}, and 1000 μg L^{-1}. Solutions were stabilized using HNO_3 and $K_2Cr_2O_7$.

2.4. Instrumentation

The determination of total mercury content in all samples (including solid calibration materials and solutions) was performed using an AMA-254 analyzer (Altec, Czech Republic). This single-purpose, single-beam atomic absorption spectrometer enables the direct dosing of liquid and solid samples. The source of radiation is an Hg lamp with a wavelength of 253.65 nm. Two operating ranges of the analyzer are provided by means of two cuvettes with different lengths in the optical path.

Thermal desorption was performed using a Perkin Elmer 3030 atomic absorption spectrometer (USA) with deuterium background correction. An electrodeless discharge lamp (Perkin Elmer, USA) operating at a wavelength of 253.7 nm was used as the source (power 5 W). The spectral bandwidth was 0.7 nm. A quartz tube (of length 18.5 cm) in the optical path of the spectrometer was heated to 800 °C in an AEHT-01 heating block (RMI, Czech Republic). The output signal of the spectrometer was digitized using a converter to enable the processing of the analog signal. In-house fabricated TK15e unit is designed to allow controlled heating of a gas from laboratory temperature up to 480 °C. The instrument includes a control unit enabling the digital setting of parameters for gas heating and a heater. The scheme of the heater of TK15e unit and the quartz tube in the optical path is presented in Fig. 1. The heating of the gas is regulated by a temperature sensor fixed in the end part of the heater, into which a sample is inserted. The gas supplied to the heater is used both for sample heating (most of the flow) and as an analyte carrier. The separation of these two flows is enabled by a system of two concentric glass tubes—the inner tube contains a fritted capsule with the sample; gas flowing between the inner and outer tubes is used for heating. The flow of carrier gas is regulated by a commercial flowmeter placed on the output from quartz tube. The three main advantages of high flow of warming gas are (a) thermal stability of the system including regular heating of the sample particles, (b) minimum delay in the power control of the heating unit in relation to actual temperature of the sensor, and (c) prevention of the condensation of pyrolysis products (from materials with a high content of organic carbon).

2.5. Analytical procedure

The AMA-254 analyzer was calibrated in the range 0.05–200 ng Hg by means of calibration solutions. Calibration by liquid standards is more convenient than using solid standards [15]. The determination of total Hg content in solid samples was performed under the following conditions: 20 s drying time, 150 s decomposition, and 45 s delay. Six replicated analyses were performed for each sample.

Thermal desorption was carried out according to the following procedure. The inlet flow of argon was 10 L min^{-1}; the flux of the carrier gas was 500 mL min^{-1} or 100 mL min^{-1}, and the remainder of the flow was used as a warming gas in the heater. The heating rate was 30 °C min^{-1}; mercury release curves were observed in the temperature range 50–450 °C. Thus, the duration of each analysis was approximately

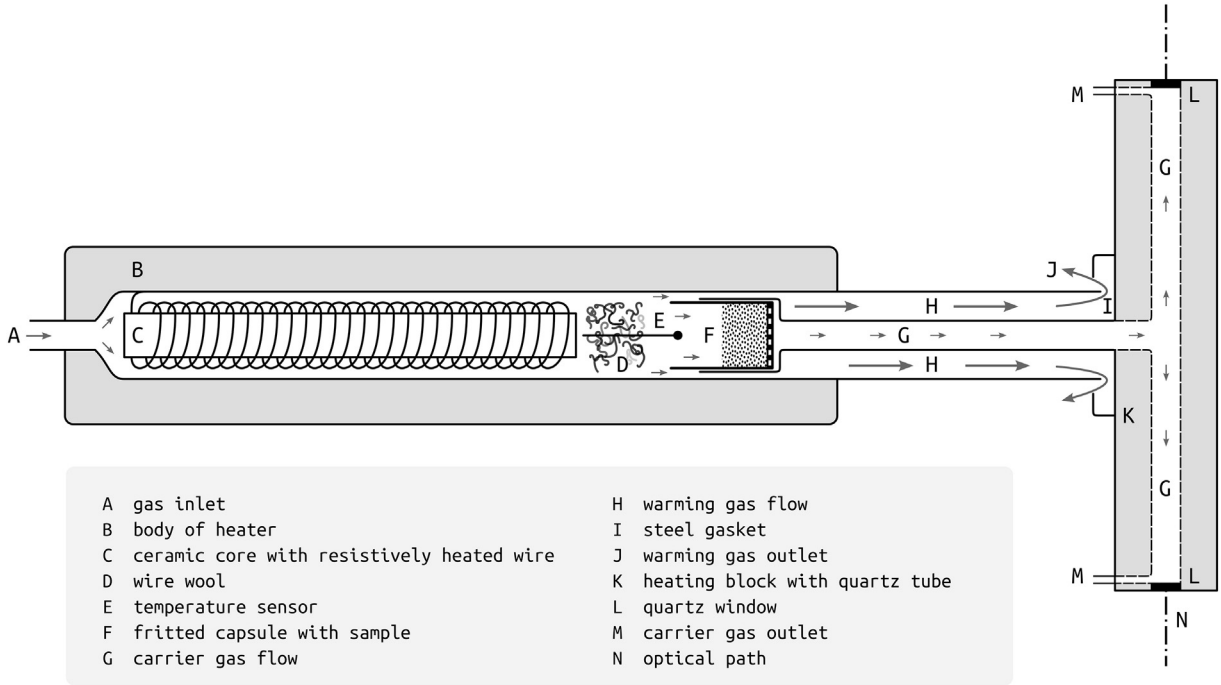

Fig. 1. The scheme of the heater with quartz tube in the heating block.

14 min (depending on the heating time required to reach a temperature of 50 °C). Cooling the system before the next analysis took approximately 10 min. Weights of samples from 10 mg up to 500 mg were used for the analyses. Sample was dosed into fritted glass capsule together with layers of quartz wool. This ensures the uniform heating of sample particles and minimal resistance to carrier gas flow. Calibration of the apparatus was performed in the range 3–26 ng Hg for a carrier gas flow of 100 mL min^{-1} and in the range 21–525 ng Hg for a flow of 500 mL min^{-1}. Red HgS was chosen for the calibration of the system. Three replicated analyses were carried out for both artificially prepared materials and environmental samples.

The analog output signal of the spectrometer in continuous mode (1 s interval) was digitized. The processing of curves and their integration were accomplished by means of Origin 6.1 (OriginLab, USA). Sulfidic and nonsulfidic Hg contents in environmental samples were quantified by the ratio of peak areas to the total area of the mercury release curve, which corresponded to the total Hg content. The integration of peaks was performed according to the peak-to-valley ratio (termed as whole-peak area integration in this work) and by the generally used method (termed as half-peak area integration), in which the first half of the first peak is doubled and deducted from the total area. Then, the content of HgS is calculated from the difference in areas [16, 17,18].

The determination of HgS by thermal desorption was compared with its determination using sequential extraction. Samples from Jedová hora and Bezdružice were subjected to sequential extraction using a published procedure [19]. The extraction was performed in four replicates for each sample. The mercury in fractions of the sequential extraction was determined by the AMA-254 analyzer. Total mercury contents in samples were fractionated into Hg releasable in water (F1), Hg releasable in acid conditions (F2), Hg bound to humic matter (F3), Hg(0) and amalgams (F4), HgS (F5), and residual Hg in the solid residue after extraction (Residual II). HgS content (F5) in a saturated solution of Na_2S cannot be accurately determined using an AMA-254 analyzer, and it is necessary to calculate it. Mercury contents in solid residues after step F4 (Residual I) were determined for two replicates of each sample; the other two replicates were subjected to the entire extraction process. The difference between Residual I and Residual II determines the content of HgS.

3. Results

The black and red forms of HgS were subjected to thermal desorption to determine the characteristic parameters of the mercury release curves. Desorption intervals were defined on the basis of the mercury release curves, which each exhibited a peak height at an absorbance of A = 0.012. Mercury release curves for black and red HgS at a gas flow of 500 mL min^{-1} are presented in Fig. 2a. Black HgS evinced a desorption interval between 210 and 330 °C, with a maximum at 273 °C; red HgS evinced an interval between 265 and 410 °C, with a maximum at 353 °C. The limit of quantification (LOQ) of HgS forms was determined experimentally on the basis of peak area at a peak height of A = 0.004. This LOQ corresponded to tenfold standard deviation of the blank measurement as well. The LOQ for black HgS was 33 μg kg^{-1}; the LOQ for red HgS was 42 μg kg^{-1}.

Certified reference materials with certified mercury species are not available with an exception of the methylmercury, which is not determined by this method because of insufficient LOQ for the most of environmental samples. Thus, internal reference materials were prepared using pure mercury species. The thermal behavior of red HgS was described in previous work [9]. The verification of the system calibration was performed by means of red and black HgS.

The thermal behavior of HgS forms was also observed for a carrier gas flow of 100 mL min^{-1} (Fig. 2b). The desorption interval for black HgS at the lower gas flow was shifted by approximately 20 °C, as was the temperature of maximum Hg release (252 °C). The LOQs of black and red HgS at the lower gas flow were 4 μg kg^{-1} and 5 μg kg^{-1}, respectively. These LOQs are relatively low, however, the limits relating to the determination of pure HgS in an inert matrix.

The carrier gas flow of 500 mL min^{-1} was used for the analysis of environmental samples. (LOQs are given below for this flow.) Mercury release curves for red HgS and soil from Jedová hora are shown in Fig. 2c. Desorption curves for environmental samples in Fig. 2c and Fig. 2d correspond to an absolute amount of 100 ng of Hg. The LOQ of

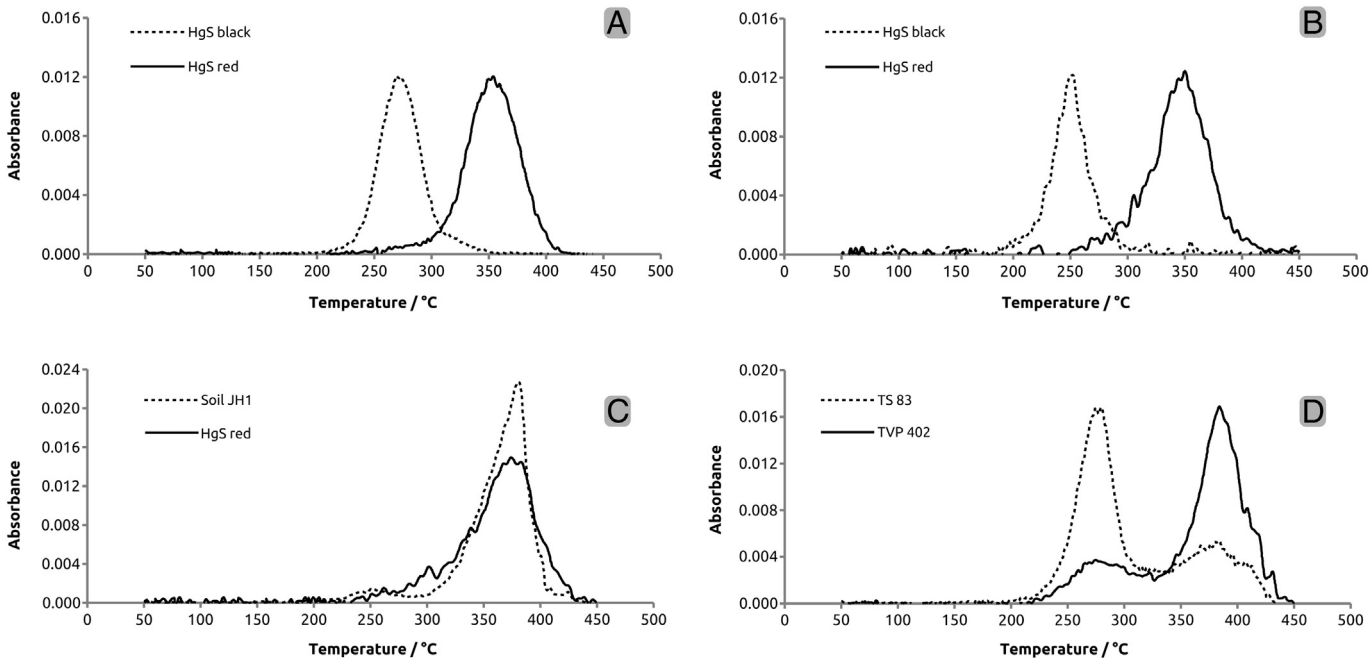

Fig. 2. Mercury release curves for synthetic HgS at a gas flow of 500 mL min^{-1} (a), synthetic HgS at a gas flow of 100 mL min^{-1} (b), samples from Jedová hora (c), samples from Bezdružice (d).

natural red HgS was 39 μg kg^{-1}, which was approximately equal to that of synthetic HgS. The LOQ of red HgS in soil was 35 μg kg^{-1}. Two peaks were evident on the desorption curves for soil samples from Jedová hora. The first peak (200–290 °C) can be defined as representing matrix-bound Hg. The second peak in the temperature interval of 290–430 °C (maximum at 375 °C) represents red HgS. Matrix-bound Hg (210–320 °C) and HgS (320–430 °C) were also observed in samples from Bezdružice (Fig. 2d).

Quantification of the contents of matrix-bound Hg and HgS in samples was carried out by the integration of peak areas. (The integration of each peak was performed using the measurement with the least absorbance of A = 0.004.) The contents of sulfidic and nonsulfidic Hg and the contents of total Hg in samples from both locations are presented in Table 1. Peak integration is given according to the peak-to-valley ratio (whole-peak area integration) and after calculation comprising area doubling of the first half of the first peak (half-peak area integration).

Total Hg contents in soil and sediment samples were also determined by an AMA-254 analyzer (Table 1). The LOQ of Hg determined by the AMA-254 analyzer in solid samples was 0.3 μg kg^{-1}. The determination of Hg in solid samples was verified using CRM 020 and CRM CC 580, with the achievement of contents 1.14 ± 0.03 and 131 ± 6 mg kg^{-1}, respectively. (CC 580 was diluted ten times.)

4. Discussion

A broad range of desorption intervals for Hg release from HgS has been published [8]. Differences in published values can be ascribed to differing measurement parameters and HgS origin. The broadening of peaks and other changes in their shape occur with increasing Hg concentration in the sample, which causes the resolution between Hg forms to deteriorate and complicates the specification of the desorption interval [9]. Therefore, it is advantageous to record characteristic mercury release curves at low absorbances (i.e., up to A = 0.1). A peak height of A = 0.012 can be recommended for the comparison of various Hg forms. Broadening of the peak occurs at high absorbance values, the overlap of peaks increases, and the correct resolution of individual species is worsened [9]. The LOQs of each Hg form are also influenced by peak

Table 1
The contents of total Hg, HgS and matrix-bound Hg (mg kg^{-1})[a].

Sample	AMA-254		TD-AAS				
	Hg_{total}	$HgS_{extraction}$	HgS[b]	HgS[c]	Hg_{matrix}[b]	Hg_{matrix}[c]	Hg_{total}
JH1	65 ± 3	60 ± 5	61 ± 4	65 ± 4	7.6 ± 0.3	4.0 ± 0.2	69 ± 4
JH2	2.6 ± 0.2	2.5 ± 0.3	2.1 ± 0.2	2.0 ± 0.2	0.2 ± 0.01	0.3 ± 0.02	2.3 ± 0.2
JH3	4.8 ± 0.3	3.8 ± 0.6	2.7 ± 0.3	3.0 ± 0.4	1.7 ± 0.1	1.4 ± 0.1	4.4 ± 0.4
JH4	4.5 ± 0.7	2.1 ± 0.5	2.8 ± 0.6	3.0 ± 0.6	2.2 ± 0.3	2.0 ± 0.3	5.0 ± 0.7
JH5	28 ± 3	25 ± 4	28 ± 4	29 ± 4	3.5 ± 0.2	1.9 ± 0.1	31 ± 4
JH6	4.4 ± 0.3	3.3 ± 0.4	3.2 ± 0.3	3.3 ± 0.3	0.8 ± 0.05	0.7 ± 0.04	4.0 ± 0.3
JH7	13 ± 1	13 ± 3	11 ± 1	11 ± 1	0.5 ± 0.03	0.3 ± 0.02	11 ± 1
TS68	2.8 ± 0.2[d]	1.3 ± 0.1[d]	0.9 ± 0.1	0.8 ± 0.1	1.6 ± 0.1	1.7 ± 0.1	2.5 ± 0.1
TS83	2.4 ± 0.1[d]	1.1 ± 0.1[d]	1.1 ± 0.2	0.9 ± 0.2	1.8 ± 0.1	2.0 ± 0.1	2.9 ± 0.3
TP80	1.2 ± 0.1[d]	0.26 ± 0.03[d]	0.1 ± 0.02	0.1 ± 0.02	1.4 ± 0.2	1.4 ± 0.2	1.5 ± 0.2
TVP402	8.4 ± 0.8[d]	6 ± 1[d]	6.2 ± 0.9	6.6 ± 0.9	1.8 ± 0.1	1.4 ± 0.1	8.0 ± 0.9

[a] $\bar{x}$ ± SD; $N = 6$ (AMA-254, Hg_{total}), $N = 2$ ($HgS_{extraction}$), $N = 3$ (TD-AAS).
[b] Whole-peak area integration.
[c] Half-peak area integration.
[d] Reference [20].

broadening. Thus, black HgS, with a narrower peak, may be determined at a lower concentration than red HgS.

Qualitative and quantitative parameters of the thermal desorption of both HgS forms were also observed for a carrier gas flow of 100 mL min^{-1}. The flow rate has minor effects on the desorption temperature of HgS [21]. Generally, lower gas flow through the quartz tube increased the concentration of atoms in the optical path. The peaks evinced the same shape but were less regular (Fig. 2b). The thermal stability of HgS is also dependent on the size of scattered particles in the sample [7]. In addition, slight differences in crystallinity and grain size can cause the formation of narrow peaks in the mercury release curve of red HgS [17]. The thermal shift of the peak for black HgS could be the result of the preparation of the calibration sample. Particles of black HgS were downsized during sample preparation by grinding with sand. This thermal shift did not appear for commercial red HgS because the particles had approximately the same size during preparation (red HgS was obtained in the form of a very fine powder). Natural red HgS from Jedová hora ground with sea sand evinced the same desorption interval as commercial HgS. It seems that a low gas flow could be suitable for the determination of trace HgS contents in environmental samples. However, peak broadening occurred in the course of soil and sediment analyses (for matrix-bound Hg), and, therefore, the resolution of nonsulfidic and sulfidic Hg was poor. This effect can be attributed to the complex matrix of environmental samples, which increases the thermal stability.

Two peaks were observed on the desorption curves for samples from both locations. The occurrence of black HgS was not confirmed in these locations. Thus, interference between black HgS and matrix-bound Hg can be excluded. The desorption interval of matrix-bound Hg (the first peak) can be shifted depending on the matrix composition. This mercury form is usually characterized by a regular peak. However, the peak symmetry may be misshapen, oftentimes due to the desorption of specific Hg forms contained in the sample, e.g., Hg bound to humic substances with a maximum release at 305 °C [9]. The resulting asymmetry can be expected especially for forest soils; for example, it is noticeable in the mercury release curve for sample TVP402 (Fig. 2d). The subsequent overestimation of sulfidic Hg is likely using the HgS calculation based on the first half of the first peak. The method of whole-peak area integration provided more accurate results with less variance in this case than the half-peak area integration with respect to the results of sequential extraction. Generally, sequential extraction based on the extraction power of reagents is burdened with overlaps between the fractions. The used procedure is based on the solubility of HgS in a saturated solution of Na_2S. Other Hg forms (nonsulfide fractions) are released in nitric acid in a previous step [6]. Moreover, previous extraction in water and sodium hydroxide reduces the risk of potential HgS dissolution in nitric acid [22]. Under these conditions, the results of HgS determination by sequential extraction should be burdened only by uncertainty resulting from sample homogeneity.

Thermal desorption enables the amount of matrix-bound Hg forms to be determined, and, thus, the potential amount of Hg releasable from the material into the environment to be estimated.

5. Conclusion

The described procedure enables the direct and rapid determination of red HgS and matrix-bound Hg in environmental samples. The amount of matrix-bound Hg determined can characterize the amounts of mobile and semi-mobile Hg forms in contaminated material. On the basis of comparison of the results of thermal desorption and sequential extraction, the evaluation of mercury release curves using integration according to the peak-to-valley ratio can be recommended. The method can be used to monitor the environmental burden in mining areas or in areas of ore processing.

Acknowledgments

The research was financially supported by the Grant Agency of the Czech Republic, Project P503/12/0682. The work was also supported by the Institute of Analytical Chemistry of the CAS under the Institutional Research Plan RVO: 68081715.

References

[1] J.J. Rytuba, Mercury from mineral deposits and potential environmental impact, Environ. Geol. 43 (2003) 326–338.
[2] M. Hojdová, T. Navrátil, J. Rohovec, V. Penížek, T. Grygar, Mercury distribution and speciation in soils affected by historic mercury mining, Water Air Soil Pollut. 200 (2009) 89–99.
[3] A.R. Lennie, J.M. Charnock, R.A.D. Pattrick, Structure of mercury(II)–sulfur complexes by EXAFS spectroscopic measurements, Chem. Geol. 199 (2003) 199–207.
[4] R.M. Hazen, J. Golden, R.T. Downs, G. Hystad, E.S. Grew, D. Azzolini, D.A. Sverjensky, Mercury (Hg) mineral evolution: a mineralogical record of supercontinent assembly changing ocean geochemistry, and the emerging terrestrial biosphere, Am. Mineral. 97 (2012) 1013–1042.
[5] D. Velebil, J. Zachariáš, Fluid inclusion study of the Horní Luby cinnabar deposit Saxothuringian Zone, Bohemian Massif: clues for the metamorphic remobilization of mercury, J. Geosci. 58 (2013) 283–298.
[6] N. Issaro, C. Abi-Ghanem, A. Bermond, Fractionation studies of mercury in soils and sediments: a review of the chemical reagents used for mercury extraction, Anal. Chim. Acta 631 (2009) 1–12.
[7] H. Biester, C. Scholz, Determination of mercury binding forms in contaminated soils: mercury pyrolysis versus sequential extractions, Environ. Sci. Technol. 31 (1997) 233–239.
[8] P. Coufalík, J. Komárek, The use of thermal desorption in the speciation analysis of mercury in soil, sediments and tailings, J. Anal. Chem. 69 (2014) 1123–1129.
[9] P. Coufalík, O. Zvěřina, J. Komárek, Determination of mercury species using thermal desorption analysis in AAS, Chem. Pap. 68 (2014) 427–434.
[10] H.E.L. Palmieri, H.A. Nalini, L.V. Leonel, C.C. Windmöller, R.C. Santos, W. de Brito, Quantification and speciation of mercury in soils from the Tripuí Ecological Station, Minas Gerais, Brazil, Sci. Total Environ. 368 (2006) 69–78.
[11] M. Rumayor, M. Diaz-Somoano, M.A. Lopez-Anton, M.R. Martinez-Tarazona, Mercury compounds characterization by thermal desorption, Talanta 114 (2013) 318–322.
[12] P. Coufalík, P. Krásenský, M. Dosbaba, J. Komárek, Sequential extraction and thermal desorption of mercury from contaminated soil and tailings from Mongolia, Cent. Eur. J. Chem. 10 (2012) 1565–1573.
[13] D. Velebil, Jedová hora Hill (Dědova hora Hill, Giftberg) near Neřežín, Czech Republic, Bull. mineral.-petrolog. Odd. Nár. Muz. (Praha) 11 (2003) 86–99. (in Czech)
[14] D. Velebil, Cinnabar (cinnabarite) mining near Bezdružice (Weseritz), SE of Teplá, Western Bohemia, Czech Republic, Bull. mineral.-petrolog. Odd. Nár. Muz. (Praha) 14–15 (2007) 47–54. (in Czech)
[15] C.T. Costley, K.F. Mossop, J.R. Dean, L.M. Garden, J. Marshall, J. Carroll, Determination of mercury in environmental and biological samples using pyrolysis atomic absorption spectrometry with gold amalgamation, Anal. Chim. Acta 405 (2000) 179–183.
[16] H. Biester, M. Gosar, S. Covelli, Mercury speciation in sediments affected by dumped mining residues in the drainage area of the Idrija mercury mine, Slovenia, Environ. Sci. Technol. 23 (2000) 3330–3336.
[17] R. Piany, S. Coveli, H. Biester, Mercury contamination in Marano Lagoon (Northern Adriatic sea, Italy): source identification by analyses of Hg phases, Appl. Geochem. 20 (2005) 1545–1559.
[18] T. Teršič, M. Gosar, H. Biester, Distribution and speciation of mercury in soil in the area of an ancient mercury ore roasting site, Frbejžene trate (Idrija area, Slovenia), J. Geochem. Explor. 110 (2011) 136–145.
[19] O. Zvěřina, P. Coufalík, J. Komárek, P. Gadas, J. Sysalová, Mercury associated with size-fractionated urban particulate matter: three years of sampling in Prague, Czech Republic, Chem. Pap. 68 (2014) 197–202.
[20] M. Abraham, M. Žáček, Final report of the project No. 11 1028, Distribuce rizikových prvků ve složkách životního prostředí ve vymezených oblastech ČR, the Ministry of the Environment of the Czech Republic, ČGS–Geofond, Praha, 2014 (in Czech).
[21] M. Sedlar, M. Pavlin, A. Popovič, M. Horvat, Temperature stability of mercury compounds in solid substrates, Open Chem. 13 (2015) 404–419.
[22] N. Mikac, D. Foucher, S. Niessen, S. Lojen, J.C. Fischer, Influence of chloride and sediment matrix on the extractability of HgS (cinnabar and metacinnabar) by nitric acid, Anal. Bioanal. Chem. 377 (2003) 1196–1201.

Příloha III

Environ Monit Assess (2018) 190:13
https://doi.org/10.1007/s10661-017-6397-1

The contents and distributions of cadmium, mercury, and lead in Usnea antarctica lichens from Solorina Valley, James Ross Island (Antarctica)

Ondřej Zvěřina · Pavel Coufalík · Miloš Barták · Michal Petrov · Josef Komárek

Received: 31 July 2017 / Accepted: 5 December 2017
© Springer International Publishing AG, part of Springer Nature 2017

Abstract Lichens are efficient and cost-effective biomonitors of the environment. Their geographic distribution together with their slow growth rate enable investigation of the deposition patterns of various elements and substances. In this research, levels of cadmium, lead, and mercury in *Usnea antarctica* lichens in the area of James Ross Island, Antarctica, were investigated. The lichens were microwave-digested, and the metals were determined by means of atomic absorption spectrometry with graphite furnace and a direct mercury analyzer. Median total contents of Cd, Hg, and Pb were 0.04, 0.47, and 1.6 mg/kg in whole lichens, respectively. The bottom-up distributions of these metals in the fruticose lichen thalli were investigated, and it was revealed that the accumulation patterns for mercury and lead were opposite to that for cadmium. The probable reason for this phenomenon may lie in the inner structure of thalli. The total contents of metals were comparable with those published for other unpolluted areas of maritime Antarctica. However, this finding was not expected for mercury, since the sampling locality was close to an area with some of the highest mercury contents published for Antarctic lichens. In short, lichens proved their usability as biological monitors, even in harsh conditions. However, the findings emphasize the need to take into account the distributions of elements both in the environment and in the lichen itself.

Keywords Lichen · Biomonitoring · Antarctica · Heavy metals

O. Zvěřina
Department of Public Health, Faculty of Medicine, Masaryk University, Kamenice 5, 625 00 Brno, Czech Republic

O. Zvěřina (✉) · P. Coufalík · J. Komárek
Department of Chemistry, Faculty of Science, Masaryk University, Kotlářská 2, 61137 Brno, Czech Republic
e-mail: zverina@med.muni.cz

P. Coufalík
Institute of Analytical Chemistry, The Czech Academy of Sciences, v.v.i., Veveří 97, 602 00 Brno, Czech Republic

M. Barták
Department of Plant Physiology and Anatomy, Institute of Experimental Biology, Masaryk University, Kamenice 5, 625 00 Brno, Czech Republic

M. Petrov
TESCAN Brno, s.r.o, Libušina třída 1, 623 00 Brno, Czech Republic

M. Petrov
Institute of Physical Engineering, Brno University of Technology, Technická 2, 616 69 Brno, Czech Republic

Introduction

As a very remote and inhospitable continent, Antarctica is often considered the last great wilderness. Circumpolar oceanic and atmospheric currents protect it from the entry of lower latitude air and water masses. These natural barriers taken together with the scarce human presence make the Antarctic the least polluted region in the world. However, it has not escaped the impact of man completely (Bargagli 2008).

Published online: 11 December 2017

Human presence in the Antarctic was first established in the eighteenth century with the arrival of the first explorers and hunters. During the twentieth century, many polar stations were built and scientific activities were further accelerated under the auspices of the International Geophysical Year 1957/58. Currently, more than 60 scientific stations are in operation below a latitude of 60° S (Culicov et al. 2017). In the last few decades, many historic sites in Antarctica have become destinations for mass tourism (Tin et al. 2009). Increased levels of Cd, Hg, and Pb have already been evaluated as the consequence of human activity on the South Shetland Islands (Lu et al. 2012). Besides these local sources of pollution, volatile contaminants such as POPs and mercury are transported to Antarctica via long-range transport from other continents, especially in the Southern Hemisphere (Bargagli 2008; Tin et al. 2009; Szopińska et al. 2016).

The direct monitoring of airborne contaminants in the Antarctic is limited due to the harsh conditions, and, thus, the analysis of naturally occurring cryptogams (such as lichens, mosses, or algae) offers a useful complementary approach to direct measurement (Bargagli 2016a). Lichens, in particular, are considered as reliable biomonitors of the deposition patterns of heavy metals. In polar regions, mosses are covered with snow for longer periods than lichens, which limits their direct exchange with the atmosphere. Another advantage of using lichens over mosses is that lichens usually entrap lower amounts of soil and dust particles (Bargagli 2016b).

A number of studies have investigated the content of heavy metals in Antarctic lichens including *Usnea antarctica*, but only a few have focused on the distribution of elements in the lichen thalli. Studies such as that conducted by Lim et al. (2009) showed that the distribution of individual elements varies significantly. Lichen morphology, thallus structure, and upper cortex surface characteristics play an important role in trapping both gaseous pollutants and particulate matter. Thanks to comparative studies, it is believed that lichens with foliose thallus morphology contain greater amounts of metals than fruticose lichens (Garty 2001). In lichens with fruticose thallus morphology, the concentration of heavy metals is reportedly 3–10 times lower and independent of substrate composition (Chiarenzelli et al. 1997, 2001). The accumulation of heavy metals in fruticose lichens depends mainly on the age of the particular thallus part and the structure of the top branched part. It might therefore be assumed that higher amounts of heavy metals are found in older thalli parts than in younger ones. On this basis, older basal thallus parts of fruticose lichens should have higher contents of heavy metals than younger upper thinly branched parts.

The samples investigated in this work were collected on James Ross Island, Antarctica (JRI, Fig. 1). Fruticose lichens of the *Usnea* genus are widespread and some of the most common lichens in maritime Antarctica (Bohuslavová et al. 2012). In the area of James Ross Island, *Usnea antarctica* species are among the most common lichens (Láska et al. 2011). Details on the occurrence of mercury and some other heavy metals were already investigated in local lichens (Zvěřina et al. 2014), in regolith and basaltic rocks (Coufalík et al. 2015; Zvěřina et al. 2012), and in the soils surrounding seal carcasses (Zvěřina et al. 2017). This work follows research into the ability of *Usnea antarctica* lichens to accumulate heavy metals. The main aim here was to investigate the contents and distributions of Cd, Hg, and Pb in lichens. Because the different parts of *Usnea antarctica* thalli vary significantly in both their outer structures (branching patterns) and inner structures (the relative proportions of the upper cortex, the photobiont layer, and the medulla), an uneven distribution of heavy metals was expected. Thus, a segmentation experiment was performed.

Materials and methods

Samples and sampling area

Samples were collected during the Czech expedition to the J.G. Mendel Czech Antarctic Station on James Ross Island, Antarctica (JRI). Occupying an area of approx. 2500 km^2, JRI is a relatively large island, with more than 80% of its surface permanently covered with ice. The northern part of the island is one of the largest ice-free areas along the tip of the Antarctic Peninsula (Láska et al. 2011). The proximity of both the Antarctic Peninsula and the Weddell Sea results in specific climatic conditions that can be characterized as a combination of oceanic and continental types of climate (Láska et al. 2011). During the period 2011–2013, the mean annual air temperature at sea level on JRI was − 8.0 °C (Hrbáček et al. 2016). Thawing seasons with prevailing positive near-surface ground temperatures usually take between ca. 100 and 150 days (Hrbáček et al. 2017).

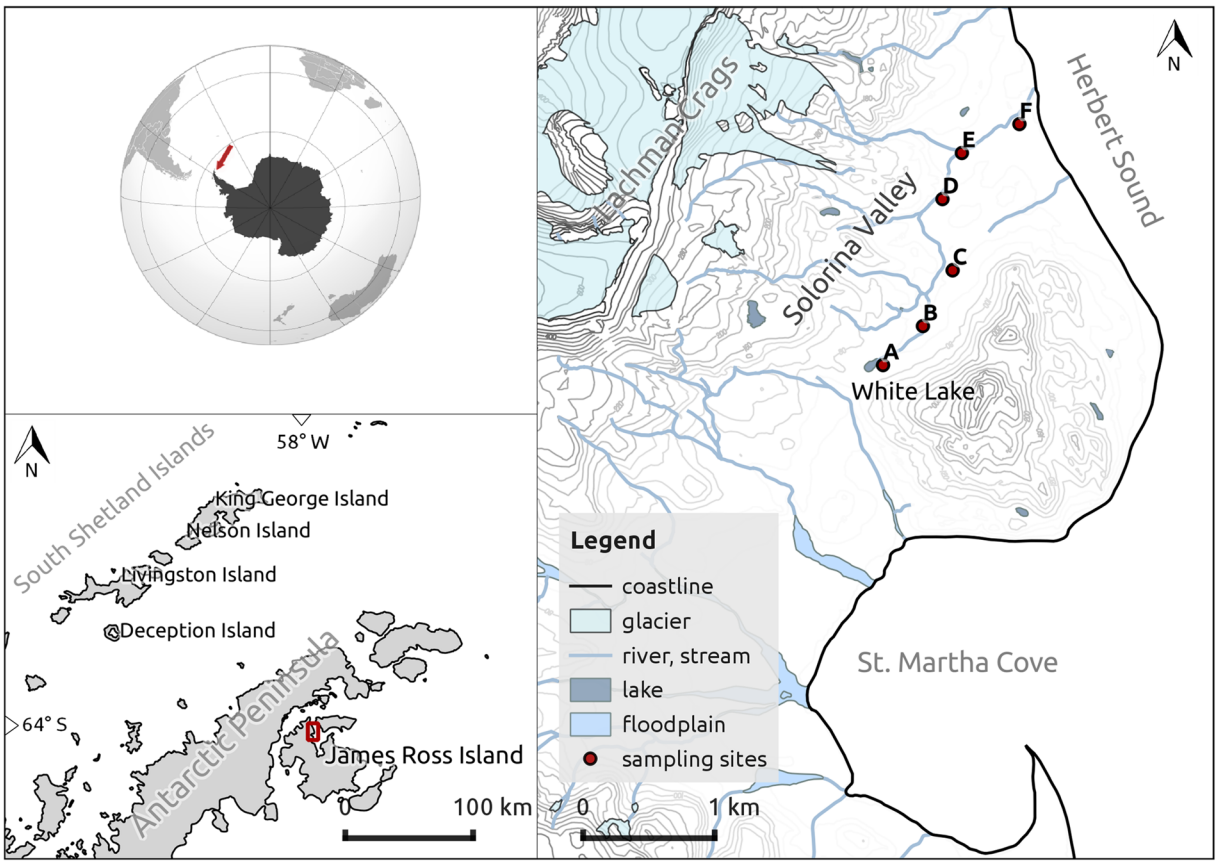

Fig. 1 Sampling locality. Modified map of James Ross Island—Northern part (Czech Geological Survey, 2009). Twenty meter of contours are shown

For the sampling of lichens, the locality of Solorina Valley was chosen. The valley is located on the northeast side of the island, approx. 10 km from Mendel Station. With a length of 3 km, Solorina is one of the longest valleys in the area of interest and is representative of the typical geomorphological landscape of this region. The valley is approx. 4 km from Brandy Bay (BB), an area for which some information on heavy metals in lichens was already reported (Zvěřina et al. 2014). The natural barrier of the Lachman Crags separates these two valleys. Solorina Valley differs substantially from the formerly investigated area: it is NE-oriented, which results in different conditions with respect to prevailing winds, the transport of sea spray, humidity, and temperature. Some of the lowest temperatures on JRI were measured here (e.g., − 39 °C during the austral winter of 2009 (Láska, unpublished data)). Although Solorina Valley is located far from any sources of local pollution, scientific field work is occasionally conducted in the valley.

The regolith from Solorina Valley was analyzed by Coufalík et al. (2015), who revealed that mercury levels in it were substantially lower than those observed in BB. However, the level of Hg in regolith is not a reliable indicator of the atmospheric deposition of this element, since Hg originates mainly from weathered bedrock. Thus, different trends in deposition patterns for Hg were expected in the selected area. Lichens, which dominate the local vegetation cover, were utilized to examine this assumption.

The lichens were collected along a 3 km-long stream flowing through the valley from White Lake down to the sea at Herbert Sound (Fig. 1). Along the stream, six sampling sites were selected, spaced 450 to 600 m apart. These sites had to be undisturbed with adequate vegetation cover and remote from birds' nesting areas. At each sampling site, 10 to 20 clusters of *Usnea antarctica* lichens were taken from basaltic rocks spread over an area of 10 × 10 m. Sample A was taken at the highest point of the sampling gradient, near the shore of White

Lake; samples B–E were collected along the stream, approx. 50 m from the riverbed; and sample F was collected from rocks at the seashore.

Analytical procedures

Collected lichen samples were thoroughly washed with deionized water to remove any dust or soil particles and clean thalli were then left to dry at 30 °C for 48 h. Subsequently, they were sealed in double polyethylene bags and stored frozen until analysis. The handling of samples was carried out in a clean laboratory equipped with HEPA filters.

The inner structures of different parts of thalli were examined by means of scanning electron microscopy. Small segments of selected well-developed linear thallus parts were carefully cut off and visualized using a Mira3 microscope (Tescan, Czech Republic). The images were acquired at an accelerating voltage of 10 keV and a working distance of 7.8 mm. The samples were processed at a chamber pressure of 20 Pa to prevent sample charging. Sample signals were detected by a low-energy BSE detector.

In order to investigate the vertical distribution of metals, ten lichen thalli were chosen for the segmentation experiment. According to the observed structure, these thalli were cut into three parts (basal, middle, and upper segments) and each one was processed individually (Fig. 2). To determine the total contents of elements, a few whole thalli from each sampling site were homogenized in a ball mill.

Both homogenized and partitioned thalli were brought into solution in Teflon vessels by means of microwave-assisted extraction (Milestone 1200 MLS, Italy). Two hundred fifty milligrams of each sample was digested with a mixture of 4 ml HNO_3 and 1 ml H_2O_2 according to the following program (power in W/time in min): 250/1, 0/2, 250/5, 400/5, and 600/5. The obtained solution was diluted to 25 ml, filtered, and stored in presealed polyethylene bottles until analysis.

The Cd and Pb contents were determined by the GF-AAS technique (graphite furnace atomic absorption spectrometry) using a Unicam Solaar 939 spectrometer

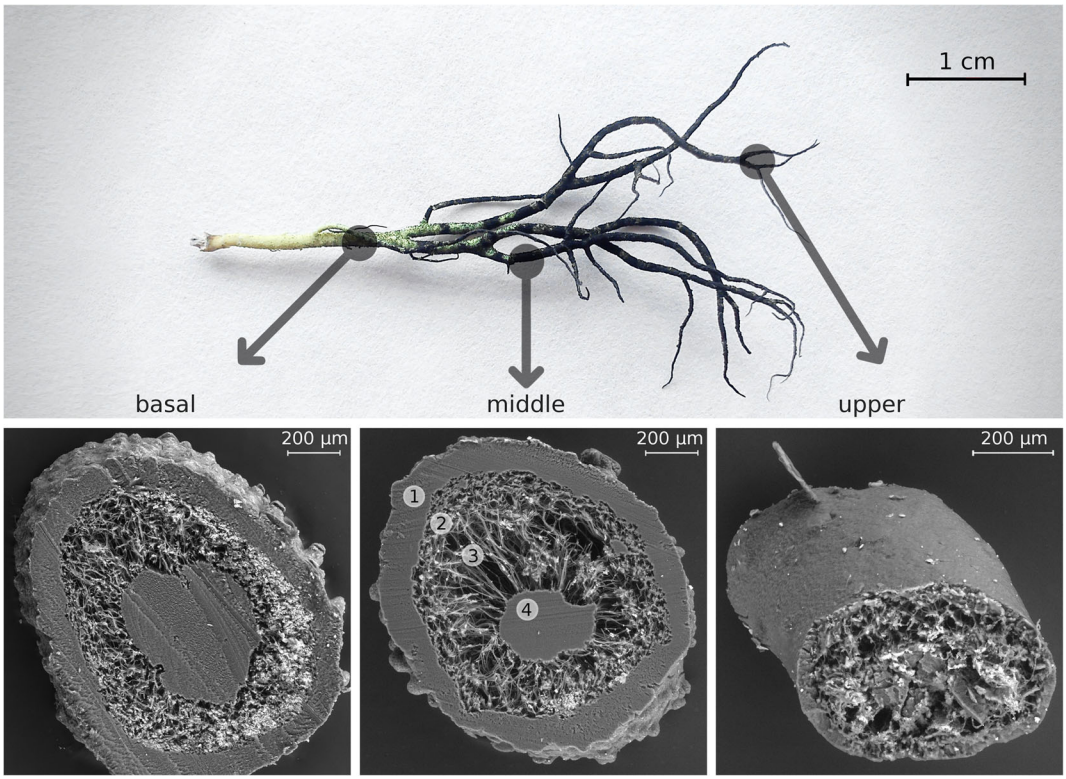

Fig. 2 Thalli of Usnea antarctica with indicated parts of the segmentation and corresponding cross-sectional visualizations showing (1) upper cortex, (2) photobiont layer, (3) medulla, and (4) central strand

(Cambridge, UK), equipped with deuterium background correction and an automatic sampler. A volume of 10 μl of sample solution was injected into a graphite cuvette of ELC type (extended lifetime cuvette) and mixed with 5 μl of a modifier containing 7.5 μg Pd and 5 μg $Mg(NO_3)_2$. The primary resonance lines of Cd (228.8 nm) and Pb (217.0 nm) were used for the determination. The solutions were dried at 120 °C. The pyrolysis and atomization temperatures were 800 and 1500 °C for Cd and 950 and 1850 °C for Pb, respectively. Quantification of the metals in samples was carried out by means of external calibration against aqueous standards.

The Hg content was determined by means of an AMA 254 single-purpose analyzer (Altec, Czech Republic). Such determination is based on the dry ashing of a sample in an oxygen flow, followed by the preconcentration of Hg vapor on a gold amalgamator. Then, the Hg is released by heat pulse and detected using AAS. The Hg content in whole homogenized thalli was determined directly in solid state. For segmented thalli, 200 μl of mineralization solution was injected.

Assurance of analytical quality

To ensure the analytical quality of the determinations, procedural blanks, certified reference material (CRM), and sample spikes were analyzed alongside the samples (Table 1). Accuracy was checked by the analysis of CRM BCR-482 Lichen (IRMM, Belgium), with recoveries of the three investigated elements ranging from 91 and 96%. The recoveries of the real sample spiked with a known amount of analytes varied between 95 and 102%.

Results and discussion

Thalli structure

The different inner structures of the different lichen parts are evident from the visualizations of cross-sections of the bottom, middle, and upper parts (Fig. 2). The proportions of the main components (i.e., upper cortex, photobiont layer, medulla, and central strand—if present) vary significantly along the thalli.

In general, the intrathalline distribution of heavy metals depends mainly on the length of exposure (the age of the individual parts of the thallus), the rate of growth processes, and the morphological properties of the anatomical structures. However, the ratio between the biomass and the photobiont/mycobiont in particular thalli parts may also play a role. These characteristics are derived from the analysis of cross-sections of the thalli of *Usnea* species across different parts of the thallus from base to apex (see e.g., Barták 2014). Typically, the basal, middle, and top parts of the *Usnea* thallus exhibit different proportions between the areas of the upper cortex layer, the photobiont layer, the medulla, and the central strand (Giełwanowska and Olech 2012).

Seymour et al. (2007) reported interspecific differences in the layers forming anatomical structures in the cross-sections of different lichen species of the genus *Usnea* from maritime Antarctica. Similarly, species-specific differences in the areas of particular layers in cross-sections are documented for Scandinavian species of the *Usnea* genus (Ericsson 2016). These anatomical characteristics may, because of the different densities of particular layers, play a role in the allocation of heavy metals. Guerra et al. (2011) showed the distribution of Pb to be well-distinguished in *U. aurantiacoatra* cross-sections. In this case, Pb was bioaccumulated mainly in

Table 1 Laboratory performance parameters (all values as mg/kg)

Analyte	Limit of detection*	CRM BCR-482		Spiked sample	
		Certified value	Found**	Added	Found**
Cd	0.005	0.56 ± 0.02	0.51 ± 0.04	0.05	0.048 ± 0.004
Hg	0.0003	0.48 ± 0.02	0.45 ± 0.03	0.5	0.51 ± 0.02
Pb	0.05	40.9 ± 1.4	39.1 ± 1.1	1	0.97 ± 0.03

*Limits of detection are calculated as three times the standard deviation of the procedural blanks ($n = 6$)

**Mean of three determinations ± standard deviation

the medulla region indicating that the central part of the thallus did not accumulate heavy metals.

In *U. antarctica*, surface structures of the upper cortex may also play a role in the allocation of elements, since the bottom, intermediate, and top thalli parts differ in the number of papillae and soralia (Seymour et al. 2007). Since papillae are numerous small, short cortex outgrowths they may enhance the uptake of deposited elements (see Fig. 2, basal and middle thallus parts). Moreover, it is well established that their growth and development are largely influenced by environmental parameters (Clerk 1998). Therefore, they differ in number in particular thalli parts, as well as between site-related morphotypes of *U. antarctica*.

Distribution of heavy metals in lichen

The segmentation of thalli into three parts was chosen on the basis of examining the inner structures of the different thallus parts by means of scanning electron microscopy. In the individual segments, a trend of increasing Hg and Pb contents from bottom to top was found (ANOVA, $p < 0.01$). In contrast, Cd exhibited a trend of slightly decreasing content from bottom to top (Fig. 3). Such results are in accordance with the data presented by Lim et al. (2009) for different species of the Antarctic lichen *U. aurantiacoatra.* They found relatively high concentrations of Cr, Al, and V in basal segments of the lichen thallus (i.e., in comparison to the top segments). The majority of heavy metals, however, had much higher concentrations in the top parts. This was particularly valid for Pb, whose contents were almost six-fold higher in upper thalli parts than in basal ones.

The higher contents of Hg and Pb in top thalli parts could be a consequence of the greater surface area of the tiny thalli parts in top parts compared to basal parts. Therefore, both wet and dry deposition could be enhanced in the upper parts. Such an explanation could be supported by the ecological and ecophysiological adaptations of lichens with fruticose thallus morphology in relation to water uptake. The upper branched parts of *U. antarctica* are efficient in capturing water from precipitation (both water drops and snow), and thus they preferentially absorb any dissolved ions which are present.

Another mechanism responsible for the higher accumulation of heavy metals in top thalli parts may be the thawing of yearly snow accumulated during the austral winter. During this process, a snow layer of between 20 and 50-cm in thickness melts in the close neighborhood of the tiny upper thalli parts. The black color of these parts may play a role in this phenomenon, since they become slightly warmer than the surrounding microenvironment. Thus, the upper thallus parts are capable of preferentially absorbing meltwater (and the heavy metal ions contained therein) from snow depositions covering the thalli. In this way, heavy metals could become more concentrated at the periphery of the branching structure (the top of the thallus) than at the bottom. Such a mechanism, however, would need to be investigated in follow-up field and laboratory-based studies.

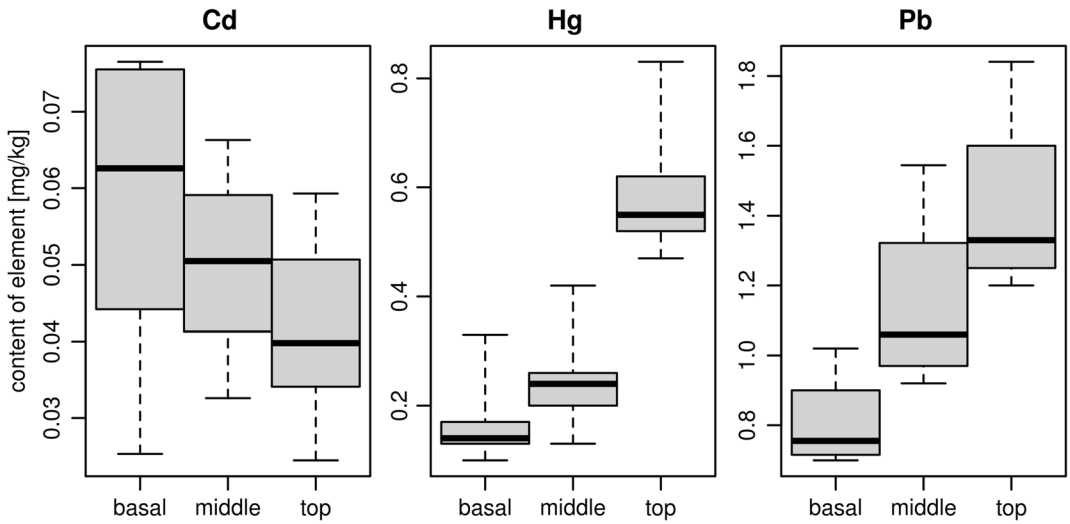

Fig. 3 Contents of Cd, Hg, and Pb in various segments of lichen thalli

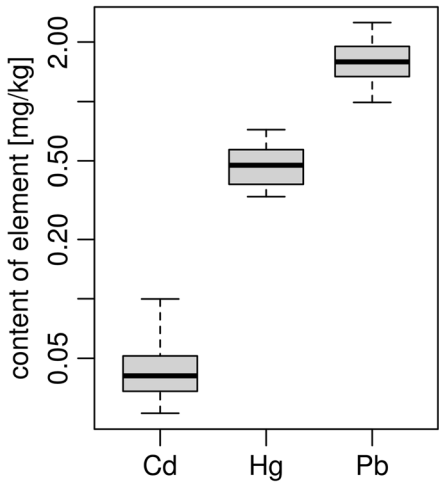

Fig. 4 Contents of Cd, Hg, and Pb determined in Usnea antarctica lichens. Note the logarithmic scale

Total contents of Cd, Hg, and Pb

The median contents of Cd, Hg, and Pb in the lichen samples were 0.04, 0.47, and 1.6 mg/kg, respectively, as shown in Fig. 4. For comparison, Table 2 summarizes already published contents of the investigated elements in *Usnea antarctica* from maritime Antarctica. In general, the contents of the investigated elements were similar to those reported for Antarctic lichens from other locations.

Hg contents were significantly lower than those reported for the lichens collected in Brandy Bay—an area only about 4 km from Solorina Valley (Zvěřina et al. 2014). The mean contents of Hg in lichens from these two locations differed by more than three times (*t* test, $p < 0.001$), whereas the contents of Cd and Pb did not differ significantly ($p > 0.2$). The morphology of both valleys as well as their orientation differ substantially and thus different prevailing winds and conditions can be expected.

Although Hg contents in lichens are generally two orders of magnitude higher than those in substrate, the relatively low Hg levels in lichens from Solorina Valley compared to those from Brandy Bay also correspond with the respective Hg levels in regolith (Coufalík et al. 2015).

An important factor influencing the deposition of atmospheric Hg in polar regions is the AMDE phenomenon (Atmospheric Mercury Depletion Event), i.e., the rapid oxidation and deposition of Hg promoted by halogens and ozone that takes place during and after the polar sunrise (Schroeder et al. 1998; Ebinghaus et al. 2002; Bargagli 2016b). Its consequences were clearly demonstrated in a study from Terra Nova Bay (Bargagli et al. 2005), where lichens in areas facing coastal polynya were affected by enhanced Hg deposition due to the AMDE. Similarly, in Brandy Bay, aerosols from the open waters of Prince Gustav Channel may promote AMDE and enhance the local deposition of Hg (Bargagli 2016b). Solorina Valley, in contrast, faces Herbert Sound and is sheltered from prevailing NW winds by the Lachman Crags messa, which, eventually, may reduce the extent of AMDE. It is noteworthy how different morphologies of microrelief and how the slightly different climatic conditions in both areas lead to considerably different accumulations of Hg.

Table 2 Reported Cd, Hg, and Pb contents in *Usnea antarctica*

Location, author	Cd (mg/kg)	Hg (mg/kg)	Pb (mg/kg)
King George Island (Olech 1991)	–	–	2
Northern Victoria Land, Graham Land, Deception Island, King George Island (Bargagli et al. 1993)	–	0.112–0.927 0.050–0.080 0.190–0.253 0.026–0.061	–
King George Island (Poblet et al. 1997)	0–0.3	–	0–2.85
King George Island (Osyczka et al. 2007)	< 1.8	–	< 0.9
James Ross Island, Brandy Bay (Zvěřina et al. 2014)	0.03–0.05	0.72–2.73	0.9–3
King George Island (Cipro et al. 2017)	–	0.152 ± 0.032	–
James Ross Island, Solorina Valley (this study, whole lichens)	0.03–0.10	0.33–0.72	0.99–2.51

Conclusion

Measurements of different parts of *U. antarctica* thalli revealed different accumulation patterns for the investigated elements. While most Pb and Hg was present in the top part, the trend of increasing Cd concentration along an individual thallus was in the opposite direction.

The total contents of Cd, Hg, and Pb in lichens from Solorina Valley, JRI, were consistent with other data published for unpolluted locations in maritime Antarctica. Surprisingly, Hg contents were more than three times lower than the contents published for nearby Brandy Bay. This finding points to a significant variation in Hg deposition patterns, which makes interpretation of the Hg contamination of geographically close areas rather difficult.

Although lichens are well-established biomonitors of airborne metals, their efficiency is highly dependent on climatic and microclimatic conditions. They can undoubtedly serve as a tool for mapping distribution patterns; however, when interpreting results, their sensitivity to local conditions must be kept in mind.

Acknowledgements We thank the CzechPolar-2 project for the possibility to use the facilities of the J. G. Mendel Station. We also thank all the personnel of the station and Diana Sychová for their assistance and support. The involvement of Pavel Coufalík was supported by the Institute of Analytical Chemistry of the CAS under the Institutional Research Plan RVO: 68081715. Miloš Barták was supported by Ecopolaris project CZ.02.1.01/0.0/0.0/16_013/0001708.

References

Bargagli, R. (2008). Environmental contamination in Antarctic ecosystems. *Science of the Total Environment, 400*(1-3), 212–226. https://doi.org/10.1016/j.scitotenv.2008.06.062.

Bargagli, R. (2016a). Atmospheric chemistry of mercury in Antarctica and the role of cryptogams to assess deposition patterns in coastal ice-free areas. *Chemosphere, 163*, 202–208. https://doi.org/10.1016/j.chemosphere.2016.08.007.

Bargagli, R. (2016b). Moss and lichen biomonitoring of atmospheric mercury: a review. *Science of the Total Environment, 572*, 216–231. https://doi.org/10.1016/j.scitotenv.2016.07.202.

Bargagli, R., Battisti, E., Focardi, S., & Formichi, P. (1993). Preliminary data on environmental distribution of mercury in northern Victoria Land, Antarctica. *Antarctic Science, 5*(01). https://doi.org/10.1017/S0954102093000021.

Bargagli, R., Agnorelli, C., Borghini, F., & Monaci, F. (2005). Enhanced deposition and bioaccumulation of mercury in Antarctic terrestrial ecosystems facing a coastal polynya. *Environmental Science and Technology, 39*(21), 8150–8155. https://doi.org/10.1021/es0507315.

Barták, M. (2014). Lichen photosynthesis. Scaling from the cellular to the organism level. In M. F. Hohmann-Marriott (Ed.), *The structural basis of biological energy generation* (pp. 379–400). Dordrecht: Springer Netherlands. https://doi.org/10.1007/978-94-017-8742-0_20.

Bohuslavová, O., Šmilauer, P., & Elster, J. (2012). Usnea lichen community biomass estimation on volcanic mesas, James Ross Island, Antarctica. *Polar Biology, 35*(10), 1563–1572. https://doi.org/10.1007/s00300-012-1197-0.

Chiarenzelli, J. R., Aspler, L. B., Ozarko, D. L., Hall, G. E. M., Powis, K. B., & Donaldson, J. A. (1997). Heavy metals in lichens, southern district of Keewatin, Northwest Territories, Canada. *Chemosphere, 35*(6), 1329–1341. https://doi.org/10.1016/S0045-6535(97)00168-9.

Chiarenzelli, J., Aspler, L., Dunn, C., Cousens, B., Ozarko, D., & Powis, K. (2001). Multi-element and rare earth element composition of lichens, mosses, and vascular plants from the Central Barrenlands, Nunavut, Canada. *Applied Geochemistry, 16*(2), 245–270. https://doi.org/10.1016/S0883-2927(00)00027-5.

Cipro, C. V., Montone, R. C., & Bustamante, P. (2017). Mercury in the ecosystem of Admiralty Bay, King George Island, Antarctica: Occurrence and trophic distribution. *Marine Pollution Bulletin, 114*(1), 564–570. https://doi.org/10.1016/j.marpolbul.2016.09.024.

Clerk, P. (1998). Species concept in the genus *Usnea* (lichenized Ascomycetes). *The Lichenologist, 30*(4-5), 321–340. https://doi.org/10.1006/lich.1998.0150.

Coufalík, P., Zvěřina, O., Krmíček, L., Pokorný, R., & Komárek, J. (2015). Ultra-trace analysis of Hg in alkaline lavas and regolith from James Ross Island. A*ntarctic Science, 27*(3), 281–290. https://doi.org/10.1017/S0954102014000819.

Culicov, O. A., Yurukova, L., Duliu, O. G., & Zinicovscaia, I. (2017). Elemental content of mosses and lichens from Livingston Island (Antarctica) as determined by instrumental neutron activation analysis (INAA). *Environmental Science and Pollution Research, 24*(6), 5717–5732. https://doi.org/10.1007/s11356-016-8279-4.

Ebinghaus, R., Kock, H. H., Temme, C., Einax, J. W., Löwe, A. G., Richter, A., Burrows, J. P., & Schroeder, W. H. (2002). Antarctic springtime depletion of atmospheric mercury. *Environmental Science and Technology, 36*(6), 1238–1244. https://doi.org/10.1021/es015710z.

Ericsson, A. (2016). *Water storage in the lichen genus Usnea in Sweden and Norway*. Master thesis. University of Umea, Sweden.

Garty, J. (2001). Biomonitoring atmospheric heavy metals with lichens: theory and application. *Critical Reviews in Plant Sciences, 20*(4), 309–371. https://doi.org/10.1080/20013591099254.

Giełwanowska, I., & Olech, M. (2012). New ultrastructural and physiological features of the thallus in Antarctic lichens. *Acta Biologica Cracoviensia Series Botanica, 54*(1). https://doi.org/10.2478/v10182-012-0004-0.

Guerra, M. B., Amarasiriwardena, D., Schaefer, C. E., Pereira, C. D., Spielmann, A. A., Nóbrega, J. A., & Pereira-Filho, E. R. (2011). Biomonitoring of lead in Antarctic lichens using laser ablation inductively coupled plasma mass spectrometry.

Journal of Analytical Atomic Spectrometry, 26(11), 2238. https://doi.org/10.1039/C1JA10198F.

Hrbáček, F., Láska, K., & Engel, Z. (2016). Effect of snow cover on the active-layer thermal regime – a case study from James Ross Island, Antarctic eninsula. *Permafrost and Periglacial Processes, 27*(3), 307–315. https://doi.org/10.1002/ppp.1871.

Hrbáček, F., Nývlt, D., & Láska, K. (2017). Active layer thermal dynamics at two lithologically different sites on James Ross Island, Eastern Antarctic Peninsula. *Catena, 149*, 592–602. https://doi.org/10.1016/j.catena.2016.06.020.

Láska, K., Barták, M., Hájek, J., Prošek, P., & Bohuslavová, O. (2011). Climatic and ecological characteristics of deglaciated area of James Ross Island, Antarctica, with a special respect to vegetation cover. *Czech Polar Reports, 1*(1), 49–62. https://doi.org/10.5817/CPR2011-1-5.

Lim, H. S., Han, M. J., Seo, D. C., Kim, J. H., Lee, J. I., Park, H., Hur, J. S., Cheong, Y. H., Heo, J. S., Yoon, H. I., & Cho, J. S. (2009). Heavy metal concentrations in the fruticose lichen Usnea aurantiacoatra from King George Island, South Shetland Islands, West Antarctica. *Journal of the Korean Society for Applied Biological Chemistry, 52*(5), 503–508. https://doi.org/10.3839/jksabc.2009.086.

Lu, Z., Cai, M., Wang, J., Yang, H., & He, J. (2012). Baseline values for metals in soils on Fildes Peninsula, King George Island, Antarctica: the extent of anthropogenic pollution. *Environmental Monitoring and Assessment, 184*(11), 7013–7021. https://doi.org/10.1007/s10661-011-2476-x.

Olech, M. (1991). Preliminary observations on the content of heavy metals in thalli of Usnea antarctica Du Rietz (Lichenes) in the vicinity of the "H. Arctowski" Polish Antarctic Station. *Polish Polar Research, 12*(1), 129–131.

Osyczka, P., Dutkiewicz, E. M., & Olech, M. (2007). Trace elements concentrations in selected moss and lichen species collected within Antarctic research stations. *Polish Journal of Ecology, 55*(1), 39–48.

Poblet, A., Andrade, S., Scagliola, M., Vodopivez, C., Curtosi, A., Pucci, A., & Marcovecchio, J. (1997). The use of epilithic Antarctic lichens (*Usnea aurantiacoatra* and *U. antartica*) to determine deposition patterns of heavy metals in the Shetland Islands, Antarctica. *Science of the Total Environment, 207*(2-3), 187–194. https://doi.org/10.1016/S0048-9697(97)00265-9.

Schroeder, W. H., Anlauf, K. G., Barrie, L. A., Lu, J. Y., Steffen, A., Schneeberger, D. R., & Berg, T. (1998). Arctic springtime depletion of mercury. *Nature, 394*(6691), 331–332. https://doi.org/10.1038/28530.

Seymour, F. A., Crittenden, P. D., Wirtz, N., Øvstedal, D. O., Dyer, P. S., & Lumbsch, H. T. (2007). Phylogenetic and morphological analysis of Antarctic lichen-forming Usnea species in the group Neuropogon. *Antarctic Science, 19*(01). https://doi.org/10.1017/S0954102007000107.

Szopińska, M., Namieśnik, J., & Polkowska, Ż. (2016). How important is research on pollution levels in Antarctica? Historical approach, difficulties and current trends. In P. Voogt (Ed.), *Reviews of Environmental Contamination and Toxicology Volume 239* (pp. 79–156). Springer International Publishing. https://doi.org/10.1007/398_2015_5008.

Tin, T., Fleming, Z. L., Hughes, K. A., Ainley, D. G., Convey, P., Moreno, C. A., Pfeiffer, S., Scott, J., & Snape, I. (2009). Impacts of local human activities on the Antarctic environment. *Antarctic Science, 21*(01), 3. https://doi.org/10.1017/S0954102009001722.

Zvěřina, O., Coufalík, P., Vaculovič, T., Kuta, J., Zeman, J., & Komárek, J. (2012). Macro and microelements in soil profile of the moss-covered area in James Ross Island, Antarctica. *Czech Polar Reports, 2*(1), 1–7. https://doi.org/10.5817/CPR2012-1-1.

Zvěřina, O., Láska, K., Červenka, R., Kuta, J., Coufalík, P., & Komárek, J. (2014). Analysis of mercury and other heavy metals accumulated in lichen Usnea antarctica from James Ross Island, Antarctica. *Environmental Monitoring and Assessment, 186*(12), 9089–9100. https://doi.org/10.1007/s10661-014-4068-z.

Zvěřina, O., Coufalík, P., Brat, K., Červenka, R., Kuta, J., Mikeš, O., & Komárek, J. (2017). Leaching of mercury from seal carcasses into Antarctic soils. *Environmental Science and Pollution Research, 24*(2), 1424–1431. https://doi.org/10.1007/s11356-016-7879-3

Příloha IV

JOURNAL OF ENVIRONMENTAL SCIENCE AND HEALTH, PART A
2016, VOL. 51, NO. 4, 364–370
http://dx.doi.org/10.1080/10934529.2015.1109413

Taylor & Francis
Taylor & Francis Group

Effects of the soil microbial community on mobile proportions and speciation of mercury (Hg) in contaminated soil

Jiřina Száková[a], Jitka Havlíčková[a], Adéla Šípková[a], Jiří Gabriel[b], Karel Švec[b], Petr Baldrian[b], Jiřina Sysalová[c], Pavel Coufalík[d,e], Rostislav Červenka[d], Ondřej Zvěřina[d,f], Josef Komárek[d], and Pavel Tlustoš[a]

[a]Department of Agroenvironmental Chemistry and Plant Nutrition, Czech University of Life Sciences Prague, Prague, Czech Republic; [b]Institute of Microbiology, Vídeňská, Prague, Czech Republic; [c]Atomic Absorption Spectrometry Laboratory, Institute of Chemical Technology, Prague, Czech Republic; [d]Department of Chemistry, Faculty of Science, Masaryk University, Brno, Czech Republic; [e]Institute of Analytical Chemistry, Academy of Sciences of the Czech Republic, Brno, Czech Republic; [f]Department of Public Health, Faculty of Medicine, Masaryk University, Brno, Czech Republic

Downloaded by [eská zemdlská univerzita v Praze], [Jirina Szakova] at 23:57 02 February 2016

ABSTRACT

The precise characterization of the behavior of individual microorganisms in the presence of increased mercury contents in soil is necessary for better elucidation of the fate of mercury in the soil environment. In our investigation, resistant bacterial strains isolated from two mercury contaminated soils, represented by *Paenibacillus alginolyticus, Burkholderia glathei, Burkholderia sp*., and *Pseudomonas sp*., were used. Two differently contaminated soils (0.5 and 7 mg kg^{-1} total mercury) were chosen. Preliminary soil analysis showed the presence of methylmercury and phenylmercury with the higher soil mercury level. Modified rhizobox experiments were performed to assess the ability of mercury accumulating strains to deplete the mobile and mobilizable mercury portions in the soil by modification; microbial agar cultures were used rather than the plant root zone. A sequential extraction procedure was performed to release the following mercury fractions: water soluble, extracted in acidic conditions, bound to humic substances, elemental, and bound to complexes, HgS and residual. Inductively coupled plasma mass spectrometry (ICP-MS) and a single-purpose atomic absorption spectrometer (AMA-254) were applied for mercury determination in the samples and extracts. Gas chromatography coupled to atomic fluorescence spectrometry (GC-AFS) was used for the determination of organomercury compounds. The analysis of the microbial community at the end of the experiment showed a 42% abundance of *Paenibacillus* sp. followed by *Acetivibrio sp., Brevibacillus sp., Cohnella sp., Lysinibacillus sp*., and *Clostridium sp*. not exceeding 2% abundance. The results suggest importance of *Paenibacillus* sp. in Hg transformation processes. This genus should be tested for potential bioremediation use in further research.

ARTICLE HISTORY
Received 30 July 2015

KEYWORDS
Mercury; microbial community; mobility; rhizobox; speciation

Introduction

Biological methods of soil remediation represent cost-effective and environmentally friendly methods to decrease the level of risk elements in soils. In the case of Hg, phytoremediation studies are still being conducted within the laboratory setting. Until now, no typical mercury hyperaccumulating plant has been described.[1] Plant species characterized by and increased ability to accumulate mercury, such as *Rumex scutatus ssp. Induratus, Marrubium vulgare*, and several crops such as *Hordeum spp., Lens culinaris, Cicer arietinum, Lupinus polyphyllus*, and *Triticum aestivum* have been mentioned.[2–4] However, the phytoextraction efficacy of these species is relatively low, requiring a long period of time to achieve a substantial decrease in the mercury content of the soil.

Investigations describing the role of soil microbial communities in mercury accumulation and/or transformation are relatively rare, and the precise characterization of the behavior of individual microorganisms in the presence of increased mercury contents in soil is still unclear in many aspects. Increasing levels of Hg generally depress microbial activity. However, the effects of Hg on soil microbial activity depend on the soil type and composition, particularly the organic matter content. Some bacteria are able to resist heavy metal contamination through chemical transformation by reduction, oxidation, methylation, and demethylation.[5] The genetic system that evolved as the "mer operon" is in fact the only well-known bacterial metal resistance system, allowing for the transformation of its toxic target into volatile nontoxic forms. Both organic (CH_3HgX) and inorganic (HgX) forms of mercurial compounds pass via MerC and MerT inner membrane proteins into cytosol where the action of the enzyme MerA results in volatilization and cellular release of only Hg^0 or both Hg^0 and CH_4, respectively.[6] These mechanisms enable the microorganisms to survive even in an extremely Hg contaminated environment[7] and have been observed in plasmids, chromosomes, transposons, and integrons of both Gram-negative and Gram-positive bacteria.[8]

The bioavailability of nutrients as well as potential risk elements and other pollutants is predominantly driven by soil

CONTACT Jiřina Száková szakova@af.czu.cz Department of Agroenvironmental Chemistry and Plant Nutrition, Czech University of Life Sciences Prague, Prague 165 21, Czech Republic.

Color versions of one or more of the figures in the article can be found online at www.tandfonline.com/lesa

© 2016 Taylor & Francis Group, LLC

Downloaded by [eská zemdlská univerzita v Praze], [Jirina Szakova] at 23:57 02 February 2016

conditions in the rhizosphere. Root exudates play an important role in this process, as they consist of a mixture of organic acids, chelates, vitamins, amino acids, purines, nucleosides, and inorganic ions.[9] For a detailed investigation into the processes in the rhizosphere, soil rhizobox experiments[10] can be done to assess changes in soil properties up to several millimeters from plant root surfaces. Instead of the depletion of nutrients and/or changing the mobility of risk elements and other pollutants in rhizosphere soil, these experiments are applied for the investigation of changing microbial activity in the rhizosphere soil as affected by the risk element level,[11–13] the interrelationship between soil nutrients and/or organic matter transformations, and the soil microflora.[14–16] Frequently, rhizobox experiments are provided as experiments describing the potential effects of various phytoremediation measures.[17–19] The efficacy of the biodegradation of organic pollutants *via* both plants and soil microflora in rhizosphere soil can be investigated using the rhizobox approach.[20–22]

In our study, the potential effect of resistant bacteria in mercury contaminated soil on the mobility, volatilization, and speciation of mercury was evaluated in a rhizobox experiment. The resistant bacterial strains isolated from mercury contaminated soils and identified preliminarily as the most resistant bacteria in contaminated soil (more details metioned below) were used for bioaugmentation of the soil in our experiment. The main objectives of the study were i) to assess rhizobox application for microbiological experiments using agar instead of plant roots for the culture of soil bacterial strains and ii) to evaluate the ability of Hg-resistant microorganisms to accumulate and transform Hg with regard to their potential bioremediation use.

Material and methods

Experimental design

The mining and smelting district of Příbram, Czech Republic is known for its Pb-Ag-Zn polymetallic mineral deposits which were mined and processed from the Middle Ages until the 1970s. Emissions from primary and secondary lead smelters are responsible for high concentrations of metallic contaminants (Pb, Cd, and Zn) in soils.[23] Increased Hg contents, especially in forest soils, have been observed in this area as well. Organic phenyl-mercury chloride, called Agronal, has also been used for protecting seeds from fungal diseases. The employment of this process was prohibited in the 1990s, and a newly developed seed dipping process has replaced it. However, the warehouse where dipping was performed is in the vicinity of Příbram, and represents an additional source of soil Hg contamination in this area.

Preliminary analysis of these soils has shown low contents of mobile Hg forms (water-soluble and plant-available fractions), but the location can be considered as hazardous to the environment due to the high content of total Hg (varying between 0.85 and 9.8 mg//kg) and potential occurrence of organometallic compounds.[24] The maximum permissible limits of elements in the soils of the Czech Republic is publically availablev;[25] according to this notice, the total Hg concentration is set as 0.8 mg kg^{-1}, confirming the high contamination level in our sampling area. Therefore, this area was chosen for sampling of representative soil samples for the model rhizobox experiment. At the time of this study soil pH was 7.0, the oxidizable carbon content (C_{ox}) was 3.24% and the cation exchange capacity (CEC) was 175 mMl/kg. Concerning the contents of available nutrients, the contents of elements extractable with the Mehlich III extraction procedure[26] were: 0.04 ± 0.00% of P, 0.62 ± 0.07% of K, 0.31 ± 0.00% of Mg, 0.26 ± 0.03% of Ca, and 0.07 ± 0.01% of S.

The microbial community isolated from these soil samples was cultivated in liquid agar culture amended with a solution of $HgCl_2$ to reach the final Hg concentration in the medium 0.1 mol L^{-1}. The bacteria being able to survive and grow in this medium were identified as the genera *Rhodanobacter, Frateuria, Luteibacter, Mycobacterium, Bacillus, Bradyrhizobium, Beijerinckia, Staphylococcus, Sphingomonas, Paenibacillus, Burkholderia*, and *Pseudomonas*. The methods applied for the analysis of the soil microbial community are described next.

Two sets of modified rhizobox experiments with two soils colected at the area of interest with different levels of soil Hg (0.5 and 7 mg kg^{-1} total mercury as determined before start of the experiment and labeled as Experiment 1 – lower level, and Experiment 2 – higher level of Hg, respectively), each with five rhizobox units, were provided to assess the ability of mercury accumulating strains to deplete the mobile and mobilizable mercury portions from soil. The soils were collected at the area of interest according to previous experiments,[24] air-dried, sieved through 2 mm diameter mesh and thoroughly homogenized.

Before start of the experiment, soil moisture was set up at 60% of the maximum water holding capacity (MWHC) using deionized water and kept at this level for whole experiment. No sterilization of the soil was provided to keep the natural microbial community in the soil and to estimate the potential ability of the organisms to penetrate the nylon membrane and the agar layer. Special designed rhizoboxes [10] allowing sampling of the soil rhizosphere vertical profile in a thickness of 1 mm per layer, were modified to apply microbial instead of plant root zone cultures as follows: the root zone of the rhizobox was filled up with the agar inoculated by the four organisms, *Paenibacillus alginolyticus, Burkholderia glathei, Burkholderia sp.*, and *Pseudomonas sp.* in the comparable amount of the organisms.

These organisms were chosen from the organisms isolated from the contaminated soil (see above) because of their best growth characteristics among the genera able to grow for a long-time in the medium containing 0.1 mol L^{-1} Hg. The agar layer was in contact with the "rhizosphere soil compartment"[10] *via* the nylon membrane. The "rhizosphere soil compartment" of the rhizobox with the agar layer was kept in the dark to avoid potential photochemical reactions. The "soil-plant compartment" was filled with the contaminated soil, as well to simulate the real conditions. The duration of the experiment was 90 days. The experiment was carried out in the greenhouse under controlled conditions at 20°C. At the end of the experiment, the soil was cut without freezing into root-parallel sections according to the distance from plant roots using a specially designed slicing device,[27] freeze-dried and homogenized. The agar layer with the microbial colonies was separated from the membrane and freeze-dried as well.

Downloaded by [eská zemdlská univerzita v Praze], [Jirina Szakova] at 23:57 02 February 2016

Analytical methods

For the determination of the bioavailable element portions in soils, 0.5 g of each sample was added to 10 mL of 0.11 mol L^{-1} solution of CH_3COOH and shaken overnight.[28] Each extraction was carried out in three replicates. For the centrifugation of extracts, a Hettich Universal 30 RF (Germany) instrument was used. The reaction mixture was centrifuged at 3000 rpm for 10 min at the end of each extraction procedure, and the supernatants were kept at 6°C prior to measurements.

The sequential extraction procedure releasing the particular fractions of Hg bound to individual soil components was performed as follows: 0.1 g of each sample was leached into 10 mL of extractant and the residue obtained after the extractions was used in the next step. The soil/liquid ratio was the same for all extraction reagents. The extraction procedure was performed on the bulk samples according to the following scheme: F1 with redistilled water–Hg leachable in water, F2 with 0.5 mol L^{-1} HCl–Hg leachable under acidic conditions, F3 with 0.2 mol L^{-1} KOH–Hg bound to humic substances, F4 with 50% HNO_3–elemental Hg and complexes, F5 with a saturated solution of Na_2S–mercury sulfide, and F6–solid residue. Experiments were carried out at laboratory temperature on shakers GFL 3006 (Burgwedel, Germany) at 300 rpm and the extraction time was 18 h in all fractionation steps. Subsequently, extracts were separated from the solid phase by centrifugation for 10 min at 4000 rpm.[29]

Inductively coupled plasma mass spectrometry (ICP-MS, Agilent 7700x, Agilent Technologies Inc., Wilmington, DE, USA) with an ASX-500 auto-sampler, a three-channel peristaltic pump, and MicroMist nebulizer and an AMA-254 single-purpose atomic absorption spectrometer (LECO model, Altec, Czech Republic) were applied for mercury determination in the individual samples and extracts. Agar from the microbial culture was dissolved in 6 M HCl and Hg was determined using the AMA-254.

For speciation analysis of organomercury compounds, 0.5 g of the sample was placed in a glass vial and extracted with 10 mL of 6 mol/L HCl using a GFL 3006 reciprocating shaker for 12 h. Then, 5 mL of liquid extract, after centrifugation on an EBA 20 Hettich centrifuge at 3500 rpm, was placed in a 40 mL glass vial and 17 mL of 4 mol/L sodium acetate was added to reach pH 5. The vial was closed immediately after the addition of 1 mL of hexane and 1 mL of 2% sodium tetraethylborate ($NaBEt_4$) and shaken on IKA Vortex Genius 3 shaker for 5 min. After phase separation, 2 μL of the extract were injected into the column of the chromatograph. Gas chromatography coupled to atomic fluorescence spectrometry (GC-AFS; Agilent Technologies 6890 N Network GC System with a PSA 10.750 fluorescence detector) was used for the determination of organomercury compounds, i.e., methylmercury (MeHg) and phenylmercury (PhHg). The GC separations were performed on a 30 m × 0.32 mm I.D. HP-5 capillary column. Optimized GC parameters were: splitless injection mode; injection port temperature, 220°C; argon flow, 2 mL/min; oven temperature programme, from 50°C to 130°C at ramp rate 15°C/min; from 130°C to 230°C at ramp rate 30°C/min; oven final temperature, 230°C; final time, 1 min.

Gaseous elemental mercury Hg^0 was measured at 253.7 nm by a portable single-purpose Lumex RA-915+ mercury analyzer (Lumex Ltd., St. Petersburg, Russia). The analyzer is based on Zeeman atomic absorption spectrometry with high-frequency modulation of light polarization. The radiation EDL source (mercury electrodeless discharge lamp at $\lambda = 253.7$ nm) absorbs only gaseous Hg^0. The measurements were repeated twice during the incubation, one and two months after the beginning of the experiment.

For microbial community analysis, DNA was extracted using the modified method of Miller[30] and purified as described previously.[31] The V4 region of bacterial 16S rRNA was amplified as a service by the Argonne National Laboratory with the barcoded primers 515F and 806R.[32] Amplicons were sequenced on an Illumina MiSeq. The amplicon sequencing data were processed with SEED 1.2.1.[33] Briefly, pair end reads were merged, chimeric sequences were deleted, and the remaining sequences were clustered using UPARSE[34] positioned at a 97% similarity level. Consensus sequences were constructed, and the closest hits at the genus or species level were identified using BLASTn search against the GenBank database. Full taxonomy was assigned to the identified hits using the SEED 1.2.1 permanent magnetic field.

Results and discussion

The high total Hg contents found in our anthropogenically contaminated soils did not differ from their contents in other industrial areas. For instance, Bloom et al.[35] determined soil Hg contents in various industrial locations reaching up to 73 mg kg^{-1}. Similarly, Millán et al.[36] determined the soil Hg contents up to 1710 mg kg^{-1} in the vicinity of a cinnabarite mine. Total contents of Hg in the individual rhizobox sections (Fig. 1) did not show any unambiguous changes with distance from the agar layer for both soil contamination levels. For acetic acid extractable Hg, the first experiment with lower total Hg content led to a similar conclusion, most probably due to the low extractable Hg contents falling close to the detection limits of the analytical method. However, at the higher Hg level in experiment 2, the results suggested a slight decrease in mobile Hg in the soil segments closest to the agar layer.

Similarly, Li et al.[37] investigated dynamic changes in the rhizosphere properties and antioxidant enzyme responses of wheat plants (*Triticum aestivum* L.) grown in three levels of Hg-contaminated soils and found that the soluble Hg in the rhizosphere soil solutions of the wheat plants decreased over time, especially in the highly Hg polluted soil compared to the slightly Hg polluted soil. They explained these changes by the decreasing pH in rhizosphere soil due to plant root activity. In our case, the effect of the exudates of the microbial community can be speculated on in this context.

The results of detailed Hg fractionation in the individual soil segments are summarized in Tables 1 and 2. As for total Hg, the results suggest ambiguous behavior of the Hg fractions as affected by the distance from the microbial culture, most probably due to the low mobile mercury pool in the soil regardless of the anthropogenic source of contamination. Water soluble Hg, mimicking the bioavailable Hg pool in soil, was low in accordance with other investigations where the most mobile Hg portions in industrially contaminated soils represented up

Downloaded by [eská zemdlská univerzita v Praze], [Jirina Szakova] at 23:57 02 February 2016

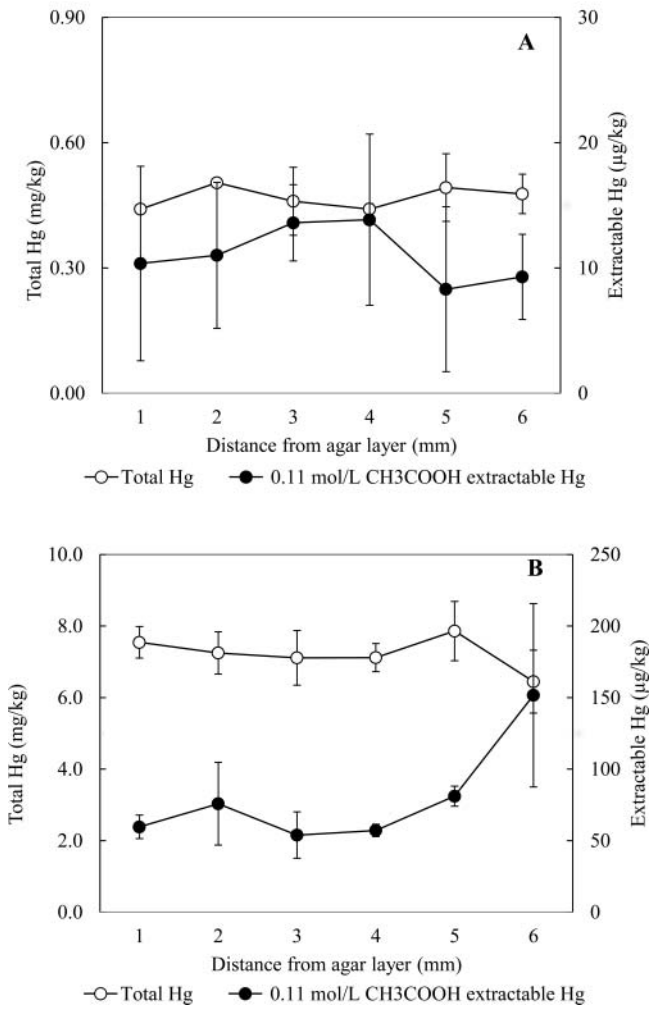

Figure 1. The total and mobile contents of Hg in soil according to distance from agar layer; A - experiment 1, B - experiment 2; data are presented as mean ± standard deviation, n = 5.

to 5% of the total Hg.[38] The distribution of Hg in the soil segments differed with the different soil contamination levels. With a lower Hg content in experiment 1, Table 1) the predominant Hg fraction was F3, i.e., the fraction representing the low mobile Hg pool bound to humic substances. In the more contaminated soil, the Hg was distributed predominantly among three fractions in the order F4 > F3 > F5. Thus, the most abundant Hg fraction was the semi-mobile elemental pool, as usually observed in highly contaminated industrial soils.[39] The high Hg pool was bound to sulfides, according to Liu et al.,[5] presenting a sulfidic Hg pool of around 10%.

The speciation of mercury in soils affected by industrial activity connected with a chlor-alkali plant in the Thur River basin (Alsace, France) was investigated by Remy et al.[40] Concentrations of MeHg reached up to 0.027 mg kg^{-1} and total Hg up to 29 mg kg^{-1}, confirming the low proportion of organomercury compounds in soils. In our case, detectable concentrations of organomercury compounds were observed only in experiment 2 with a higher soil Hg content (Fig. 2). The results show low levels of MeHg with no apparent trend according to the distance from the agar layer, whereas the PhHg levels tended to decrease with the distance from the agar layer. It has already been shown that the organic forms of mercury are more mobile than inorganic forms, and thus more toxic and more readily bio-accumulated.[41] Thus, we can speculate on the role of microbial exudates resulting in the mobilization of organic Hg species. The presence of PhHg is not surprising in the vicinity of a seed-dipping warehouse where phenylmercury chloride was applied, as documented by Hintelmann et al.[42]

The volatile pool of Hg was also detected in experiment 2 with the higher Hg level. The concentrations of volatile Hg^0 determined above the upper part of the rhizoboxes varied between 13 and 20 ng m^{-3} in the first measurement and from 16 to 19 ng m^{-3} in the second one, whereas the Hg° concentrations in the ambient air varied from 5 to 12 ng m^{-3}. Although abiotic reduction in soils occurs with the help of reductants (electron donors) such as Fe^{2+} and humic and fulvic com-

Table 1. Mercury contents in individual fractions after sequential extraction – experiment 1; F1 – Hg leachable in water, F2 – Hg leachable under acidic conditions, F3 – Hg bound to humic substances, F4 – elemental Hg and complexes, F5 - mercury sulfide, and F6 –residual H.

Distance from surface (mm)	F1 mg/kg	F2 mg/kg	F3 mg/kg	F4 mg/kg	F5 mg/kg	F6 mg/kg	Recovery %
1	<0.003	0.035 ± 0.007	0.29 ± 0.02	0.105 ± 0.021	0.070 ± 0.042	0.015 ± 0.007	95.5 ± 3.5
2	<0.003	0.040 ± 0.014	0.30 ± 0.03	0.100 ± 0.014	0.065 ± 0.021	0.015 ± 0.007	96.5 ± 2.1
3	<0.003	0.040 ± 0.014	0.31 ± 0.06	0.085 ± 0.021	0.080 ± 0.028	0.015 ± 0.007	91.5 ± 2.1
4	<0.003	0.040 ± 0.014	0.30 ± 0.06	0.090 ± 0.014	0.060 ± 0.028	0.015 ± 0.007	96.5 ± 3.5
5	<0.003	0.045 ± 0.007	0.28 ± 0.06	0.105 ± 0.007	0.050 ± 0.014	0.010 ± 0.000	92.0 ± 7.1
6	<0.003	0.050 ± 0.014	0.27 ± 0.03	0.135 ± 0.049	0.120 ± 0.085	0.010 ± 0.000	92.0 ± 1.4

Table 2. Mercury contents in individual fractions after sequential extraction – experiment 2; F1 – Hg leachable in water, F2 – Hg leachable under acidic conditions, F3 – Hg bound to humic substances, F4 – elemental Hg and complexes, F5 - mercury sulfide, and F6 –residual Hg.

Distance from surface (mm)	F1 mg/kg	F2 mg/kg	F3 mg/kg	F4 mg/kg	F5 mg/kg	F6 mg/kg	Recovery %
1	0.036 ± 0.006	0.062 ± 0.043	2.95 ± 0.68	3.28 ± 1.01	1.00 ± 0.52	0.034 ± 0.004	93.8 ± 4.1
2	0.038 ± 0.006	0.047 ± 0.036	2.30 ± 0.50	3.38 ± 0.97	1.16 ± 0.70	0.035 ± 0.006	90.7 ± 2.6
3	0.042 ± 0.008	0.032 ± 0.022	2.30 ± 0.49	3.35 ± 0.85	1.12 ± 0.65	0.049 ± 0.009	92.6 ± 7.0
4	0.040 ± 0.014	0.042 ± 0.034	2.15 ± 0.42	3.29 ± 0.94	1.05 ± 0.77	0.050 ± 0.015	90.3 ± 6.8
5	0.041 ± 0.009	0.034 ± 0.025	2.15 ± 0.35	3.48 ± 0.86	1.03 ± 0.78	0.056 ± 0.018	90.4 ± 1.4
6	0.039 ± 0.011	0.033 ± 0.028	2.15 ± 0.51	3.48 ± 0.85	0.97 ± 0.72	0.055 ± 0.010	95.5 ± 10.4

Downloaded by [eská zemdlská univerzita v Praze], [Jirina Szakova] at 23:57 02 February 2016

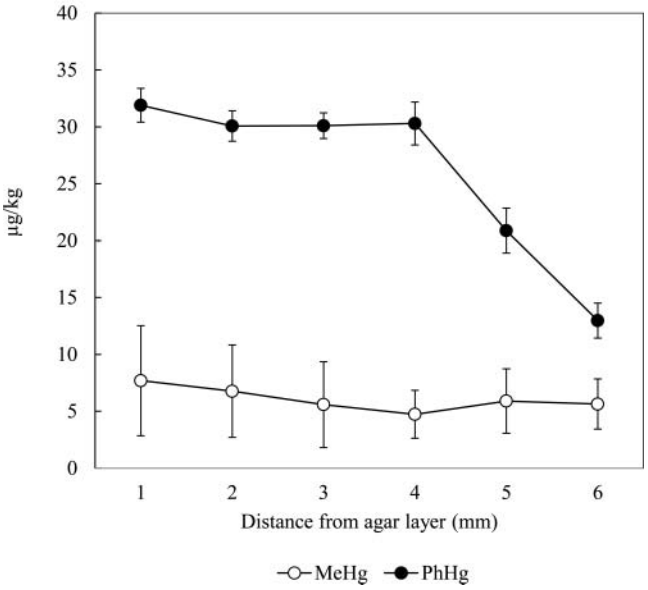

Figure 2. The contents of organomercury compounds (MeHg and PhHg) in soil according to distance from agar layer – experiment 2; data are presented as mean ± standard deviation, n = 5.

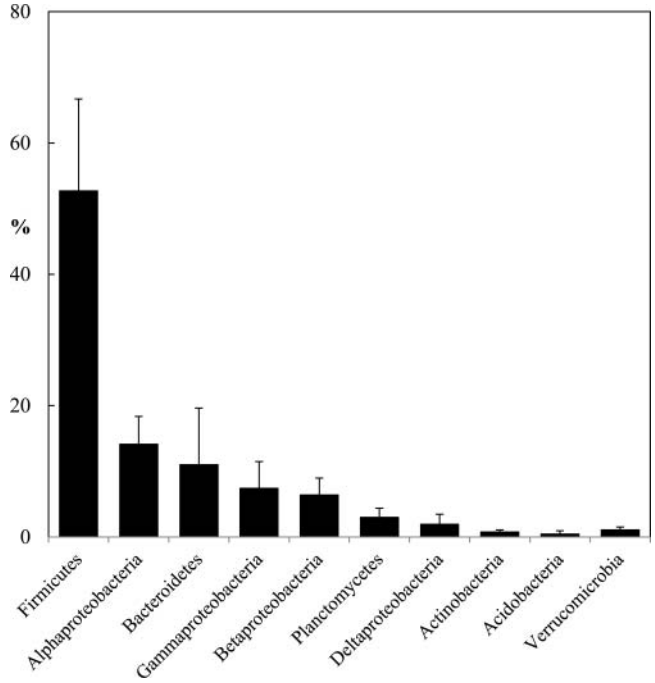

Figure 3. Relative abundance of individual phyla (for phyla representing > 1% abundance within the community) of microorganisms in the agar layer identified in the end of rhizobox experiment; data are presented as mean ± standard deviation, n = 5.

pounds,[43] the potential role of various soil microbial strains has been widely investigated. Under model laboratory conditions, organisms such as *Pseudomonas putida, Acidithiobacillus ferrooxidans*, or *Lysinibacillus fusiformis* are able to volatilize from 50% to almost 100% of Hg.[44–46]

For the estimation of Hg accumulation in the microbial biomass, the exposed agar layer was analyzed at the end of the experiment. The total Hg contents varied in the range from 0.11 to 0.36 mg kg^{-1} at the end of the first experiment and from 2.09 to 15.7 mg kg^{-1} after the second experiment (the pure agar contained 0.0034 mg kg^{-1} of Hg). In the second experiment, detectable values of organomercurials were found, ranging from 2.2 to 12.1 μg/kg of MeHg, and from the levels below the detection limit to 8.4 μg kg^{-1} of PhHg. Therefore, the microorganisms showed a high ability to accumulate Hg, especially in highly contaminated soil. Karunasagar et al.[47] investigated the Hg and MeHg biosorption ability of *Aspergillus niger* where the accumulated Hg contents reached up to 3.2 mg g^{-1} of the sorbent without any toxicity symptoms for the microorganisms. Similarly, the high Hg accumulation capacity of *Pseudomonas sp.* and *Bacillus sp.* was observed by Grassi and Netti[48] in extremely Hg contaminated coastal water.

To describe more precisely the soil microbial community at the agar layer in the end of the second experiment, the diversity of the individual strains was analyzed. The organisms representing 27 phyla were identified; those with more than 1% abundance are summarized in Fig. 3. Sorkhoh et al.[49] identified *Gammaproteobacteria, Actinobacteria*, and *Firmicutes* as the dominant mercury-resistant phyla. In our case, *Firmicutes* was the predominant phylum at the end of the experiment, and the detailed analysis of these organisms showed 42% abundance of *Paenibacillus* sp. followed by *Acetivibrio sp., Brevibacillus sp., Cohnella sp., Lysinibacillus sp.*, and *Clostridium sp.* where their abundances varied between 0.5 and 1.8%. Other genera of *Firmicutes* did not exceed 0.6% of the total amount of the organisms.

Within the *Paenibacillus* genus, *Paenibacillus agaridevorans* was the most abundant species, with abundance ranging from 7 to 32% of sequences.[50] The characteristics of the microbial community before start of the experiment and after 90 days of cultivation are substantially different. Among the four microorganisms inoculated to the agar layer *Paenibacillus* sp. abundance exceeded the remaining organisms where the abundance of *Pseudomonas* sp. (*Gammaproteobacteria*) reached 3.5%, and *Burkholderia* sp. (*Betaproteobacteria*) only 0.1%. Comparing the agar-dwelling microbial community with the community identified in the soil before start of the experiment, from the organisms able to grow in the 0.1 mol L^{-1} solution of Hg, only *Luteibacter* (*Gammaproteobacteria*), *Mycobacterium* (*Actinobacteria*), *Bacillus* (*Firmicutes*), *Staphylococcus* (*Firmicutes*), *Bradyrhizobium* (*Alphaproteobacteria*), and *Sphingomonas* (*Alphaproteobacteria*) in abundance between 0.01 and 0.6% were identified. Therefore, only *Paenibacillus sp.* proved to be the predominant organism growing for a long time in the specific conditions of the rhizobox experiments. The evaluation of the microbial strains behavior without presence of dominating *Paenibacillus sp.* should be provided in further research to assess which organisms are able to replace it.

Conclusions

Paenibacillus sp. are Gram-positive, aerobic or facultatively anaerobic, spore-forming bacteria and are known as promising organisms for the bioremediation of soil contaminated by polyaromatic hydrocarbons (particularly naphtalene) in soil.[51] However, their potential ability to accumulate and transform Hg in soil has never been tested. Microorganisms suitable for

Downloaded by [eská zemdlská univerzita v Praze], [Jirina Szakova] at 23:57 02 February 2016

bioremediation should be characterized by developed resistance mechanisms against the target pollutant, thereby avoiding potential cell damage.[52] Simultaneously, the bacteria should be able to absorb the pollutant and transform it into volatile compounds. For mercury, this represents the reduction of Hg^{2+} to Hg° followed by passive volatilization without a loss of energy.[53]

In such cases, the microbial biomass works as a catalyst without mercury accumulation in the biomass. In this context, *Deinococcus geothermalis, Cupriavidus metallidurans, Enterobacter cloacae, Alkaligenes faecalis*, and *Pseudomonas putida* has been suggested as promising organisms after model laboratory experiments.[54,55] Our results suggest that *Paenibacillus* sp. should be tested for potential bioremediation use as well. However, their ability to accumulate, transform and potentially volatilize mercury needs to be investigated in further research.

Acknowledgments

Special appreciation is extended to Dr. S. Grohová from the National Institute of Public Health, Prague, Czech Republic for her helpful assistance in gaseous elemental mercury measurements.

Funding

The authors appreciate financial support for the GAČR project P503/12/0682 and Czech University of Life Science project No. 21140/1313/3130; The work was supported by the research concept of the Institute of Microbiology of the ASCR (RVO61388971).

References

[1] Henry, J.R. *An Overview of the Phytoremediation of Lead and Mercury*, U.S. Environmental Protection Agency, Washington, DC, 2000. Available at http://clu-in.org (accessed March 2011).

[2] Moreno-Jimenez, E.; Gamarra, R.; Carpena-Ruiz, R.O.; Millan, R.; Penalosa, J.M.; Esteban, E. Mercury bioaccumulation and phytotoxicity in two wild plant species of Almaden area. Chemosphere **2006**, *63*, 1969–1973.

[3] Rodríguez, L.; López-Bellido, F.; Carnicer, A.; Alcalde-Morano, V. Phytoremediation of mercury-polluted soils using crop plants. Fresen. Environ. Bull. **2003**, *12*, 967–971.

[4] Rodríguez, L.; Rincon, J.; Asencio, I.; Rodriguez-Castellanos, L. Capability of selected crop plants for shoot mercury accumulation from polluted soils: Phytoremediation perspectives., Int. J. Phytoremed. **2007**, *9*, 1–13.

[5] Liu, Y.R.; Zheng, Y.M.; Shen, J.P.; Zhang, L.M.; He, J.Z. Effects of mercury on the activity and community composition of soil ammonia oxidizers. Environ. Sci. Pollut. Res. **2010**, *17*, 1237–1244.

[6] Mathema, V.B.; Thakuri, B.C.; Sillanpää, M. Bacterial *mer* operon-mediated detoxification of mercurial compounds: a short review. Arch. Microbiol. **2011**, *193*, 837–844.

[7] Rasmussen, L.D.; Zawadsky, C.; Binnerup, S.J.; Oregaard, G.; Sorensen, S.J.; Kroer, N. Cultivation of hard to culture subsurface mercury resistant bacteria and discovery of new merA gene sequences. Appl. Environ. Microbiol. **2008**, *74*, 3795–3803.

[8] Summers, A.O.; Silver, S. Microbial transformations of metals. Annu. Rev. Microbiol. **1978**, *32*, 367—672.

[9] Jones, D.L. Organic acids in the rhizosphere—a critical review. Plant Soil **1998**, *205*, 25–44.

[10] Wenzel, W.W.; Wieshammer, G.; Fitz, W.J.; Puschenreiter, M. Novel rhizobox design to assess rhizosphere characteristics at high spatial resolution. Plant Soil **2001**, *237*, 37–45.

[11] Dessureault-Rompré, J.; Luster, J.; Schulin, R.; Tercier-Waeber, M.L.; Nowack, B. Decrease of labile Zn and Cd in the rhizosphere of hyperaccumulating *Thlaspi caerulescens* with time. Environ. Pollut. **2010**, *158*, 1955–1962.

[12] Kim, K.R.; Owens, G.; Kwon, S. Influence of Indian mustard (*Brassica juncea*) on rhizosphere soil solution chemistry in long-term contaminated soils: A rhizobox study. J. Environ. Sci. **2010**, *22*, 98–105.

[13] Yang, W.; Zhang, T.; Li, S.; Ni, W. Metal removal from and microbial property improvement of a multiple heavy metals contaminated soil by phytoextraction with a cadmium hyperaccumulator *Sedum alfredii* H. J. Soils Sedim. **2014**, *14*, 1385–1396.

[14] Liu, D.; Fang, S.; Tian, Y.; Chang, S.X. Nitrogen transformations in the rhizosphere of different tree types in a seasonally flooded soil. Plant Soil Environ. **2014**, *60*, 249–254.

[15] Puglisi, E.; Pascazio, S.; Suciu, N.; Cattani, I.; Fait, G.; Spaccini, R.; Crecchio, C.; Piccolo, A.; Trevisan, M. Rhizosphere microbial diversity as influenced by humic substance amendments and chemical composition of rhizodeposits. J. Geochem. Explor. **2013**, *129*, 82–94.

[16] Schenck zu Schweinsberg-Mickan, M.; Jörgensen, R.G.; Müller, T. Rhizodeposition: Its contribution to microbial growth and carbon and nitrogen turnover within the rhizosphere. J. Plant Nutr. Soil Sci. **2012**, *175*, 750–760.

[17] Becerra-Castro, C.; Kidd, P.; Kuffner, M.; Prieto-Fernández, Á.; Hann, S.; Monterroso, C.; Sessitsch, A.; Wenzel, W.; Puschenreiter, M. Bacterially induced weathering of ultramafic rock and its implications for phytoextraction. Appl. Environ. Microbiol. **2013**, *79*, 5094–5103.

[18] Brennan, A.; Moreno Jiménez, E.; Puschenreiter, M.; Alburquerque, J.A.; Switzer, C. Effects of biochar amendment on root traits and contaminant availability of maize plants in a copper and arsenic impacted soil. Plant Soil **2014**, *379*, 351–360.

[19] Motaghian, H.R.; Hosseinpur, A.R. Effect of wheat (*Triticum aestivum* L.) rhizosphere and sewage sludge application on zinc desorption with dilute citric acid. Arch. Agron. Soil Sci. **2014**, *60*, 907–923.

[20] Gartler, J.; Wimmer, B.; Soja, G.; Reichenauer, T.G. Effects of rapeseed oil on the rhizodegradation of polyaromatic hydrocarbons in contaminated soil. Int. J. Phytoremed. **2014**, *16*, 671–683.

[21] Xie, X.; Liao, M.; Fang, S.; Peng, Y.; Yang, J.; Chai, J. Spacial characteristics of pyrene degradation and soil microbial activity with the distance from the ryegrass (*Lolium perenne* L.) root surface in a multi-interlayer rhizobox. J. Hazard. Mat. **2012**, *213–214*, 156–160.

[22] Zhong, Y.; Wang, J.; Song, Y.Z.; Liang, Y.T.; Li, G.H. Microbial community and functional genes in the rhizosphere of alfalfa in crude oil-contaminated soil. Front Environ. Sci. Eng. **2012**, *6*, 797–805.

[23] Ettler, V.; Rohovec, J.; Navrátil, T.; Mihaljevič, M. Mercury distribution in soil profiles polluted by lead smelting. Bull. Environ. Contam. Toxicol. **2007**, *78*, 13–17.

[24] Coufalík, P.; Zvěřina, O.; Komárek, J. Determination of mercury species using thermal desorption analysis in AAS. Chem. Pap. **2014**, *68*, 427–434.

[25] Anonymous. *Public notice No. 13/1994*, regulating some details concerning the preservation of agricultural lands available. Czech Ministry of the Environment: Prague, 1994.

[26] Mehlich, A. Mehlich 3 Soil test extractant: A modification of Mehlich 2 extractant, Commun. Soil Sci. Plant Anal. **1984**, *15*, 1409–1416.

[27] Fitz, W.J.; Wenzel, W.W.; Wieshammer, G.; Istenič, B. Microtome sectioning causes artifacts in rhizobox experiments. Plant Soil **2003**, *256*, 455–462.

[28] Quevauviller, P.; Ure, A., Muntau, H.; Griepink, B. Improvement of analytical measurements within the BCR – program – Single and sequential extraction procedures applied to soil and sediment analysis. Int. J. Environ. Anal. Chem. **1993**, *51*, 129–134.

[29] Coufalík, P.; Krásenský, P.; Dosbaba, M.; Komárek, J. Sequential extraction and thermal desorption of mercury from contaminated soil and tailings from Mongolia. Cent. Eur. J. Chem. **2012**, *10*, 1565–1573.

[30] Ságová-Marečková, M.; Čermák, L.; Novotná, J.; Plháčková, K.; Forstová, J.; Kopecký, J. Innovative methods for soil DNA purification

tested in soils with widely differing characteristics. Appl. Environ. Microbiol. **2008**, *74*, 2902–2907.

[31] Baldrian, P.; Kolařík, M.; Štursová, M.; Kopecký, J.; Valášková, V.; Větrovský, T.; Zifcakova, L.; Šnajdr, J.; Ridl, J.; Vlček, Č.; Voříšková, J. Active and total microbial communities in forest soil are largely different and highly stratified during decomposition. ISME J. **2012**, *6*, 248–258.

[32] Caporaso, J.G.; Lauber, C.L.; Walters, W.A.; Berg-Lyons, D.; Huntley, J.; Fierer, N.; Owens, S.M.; Betley, J.; Fraser, L.; Bauer, M.; Gormley, N.; Gilbert, J.A.; Smith, G.; Knight, R. Ultra-high-throughput microbial community analysis on the Illumina HiSeq and MiSeq platforms. ISME J. **2012**, *6*, 1621–1624.

[33] Větrovský, T.; Baldrian, P. Analysis of soil fungal communities by amplicon pyrosequencing: current approaches to data analysis and the introduction of the pipeline SEED. Biol. Fertil. Soils **2013**, *49*, 1027–1037.

[34] Edgar, R.C. UPARSE: highly accurate OTU sequences from microbial amplicon reads. Nat. Methods **2013**, *10*, 996–998.

[35] Bloom, N.S.; Preus, E.; Katon, J.; Hiltner, M. Selective extractions to assess the biogeochemically relevant fraction of inorganic mercury in sediments and soils. Anal. Chim. Acta **2003**, *479*, 233–248.

[36] Millán, R.; Sanchez, D.M.; Quejido, A.J.; Fernandez, M. Mercury and trace element fractionation in Almaden soils by application of different sequential extraction procedures. Anal. Bioanal. Chem. **2005**, *381*, 1507–1513.

[37] Li, Y.; Sun, H., Li, H.; Yang, L.; Ye, B.; Wang, W. Dynamic changes of rhizosphere properties and antioxidant enzyme responses of wheat plants (*Triticum aestivum* L.) grown in mercury-contaminated soils. Chemosphere **2013**, *93*, 972–977.

[38] Reis, A.T.; Rodrigues, S.M.; Davidson, C.M.; Pereira, E.; Duarte, A.C. Extractability and mobility of mercury from agricultural soils surrounding industrial and mining contaminated areas. Chemosphere **2010**, *81*, 1369–1377.

[39] Covelli, S.; Acquavita, A.; Piani, R., Predonzani, S.; De Vittor, C. Recent contamination of mercury in an estuarine environment (Marano lagoon, Northern Adriatic, Italy). Estuar. Coast. Shelf. Sci. **2009**, *82*, 273–284.

[40] Remy, S.; Prudent, P.; Probst, J.L. Mercury speciation in soils of the industrialised Thur River catchment (Alsace, France). Appl. Geochem. **2006**, *21*, 1855–1867.

[41] Bloom, S.; Porcella, D.B. Less mercury. Nature **1994**, *367*, 694.

[42] Hintelmann, H.; Hempel, M.; Wilken, R.D. Observation of unusual organic mercury species in soils and sediments of industrially contaminated sites. Environ. Sci. Technol. **1995**, *29*, 1845–1850.

[43] Gabriel, M.C.; Williamson, D.G. Principal biogeochemical factors affecting the speciation and transport of mercury through the terrestrial environment. Environ. Geochem. Health **2004**, *26*, 421–434.

[44] Cabral, L.; Giovanello, P.; Gianello, C.; Bento Menezes, F.; Andreazza, R.; Camargo, F.A.O. Isolation and characterization of bacteria from mercury contaminated sites in Rio Grande do Sul, Brazil, and assesment of methylmercury removal capability of a *Pseudomonas putina* V1 strain. Biodegradation **2013**, *24*, 319–331.

[45] Gupta, S.; Goyal, R.; Nirwan, J.; Cameotra, S.S.; Tejoprakash, N. Biosequestration, transformation, and volatilization of mercury by *Lysinibacillus fusiformis* isolated from industrial effluent. J. Microbiol. Biotechnol. **2012**, *22*, 684–689.

[46] Takeuchi, F.; Iwahori, K.; Kamimura, K.; Hegishi, A.; Maeda, T.; Sugio, T. Volatilization of mercury under acidic conditions from mercury-polluted soil by a mercury resistant *Acithiobacillus ferrooxidans* SUG 2–2. Biosci. Biotechnol. Biochem. **2001**, *65*, 1981–1986.

[47] Karunasagar, D.; Arunachalam, J.; Rashmi, K.; Naveena Lavanya Latha, J.; Maruthi Mohan, P. Biosorption of inorganic and methyl mercury by a biosorbent from *Aspergillus niger*. J. Microbiol. Biotechnol. **2003**, *19*, 291–295.

[48] Grassi, S.; Netti, R. Sea water intrusion and mercury pollution of some coastal aquifers in the province of Grosseto (Southern Tuscany-Italy). J. Hydrol. **2000**, *238*, 198–211.

[49] Sorkhoh, N.A.; Ali, N.; Dashti, N.; Al-Mailem, D.M.; Al-Awadhi, H.; Eliyas, M.; Radwan, S.S. Soil bacteria with the combined potential for oil utilization, nitrogen fixation, and mercury resistance. Int. Biodeter. Biodegrad. **2010**, *64*, 226–231.

[50] Winch, S.; Mills, H.J.; Kostka, J.E.; Fortin, D.; Lean, D.R.S. Identification of sulfate-reducing bacteria in methylmercury contaminated mine tailings by analysis of SSU rRNA genes. FEMS Microbiol. Ecol. **2009**, *68*, 94–107.

[51] Daane, L.L.; Harjono, I.; Barns, S.M.; Launen, L.A.; Palleroni, N.J.; Haggblom M.M. PAH-degradation by *Paenibacillus* spp. and description of *Paenibacillus naphthalenovorans* sp nov., a naphthalene-degrading bacterium from the rhizosphere of salt marsh plants. Int. J. Syst. Evol. Microbiol. **2002**, *52*, 131–139.

[52] Cursino, L., Mattos, S.V.M.; Azevedo, V.; Galarza, F.; Bucker, D.H., Chartone-Souza, E., Nascimento, A.M.A. Capacity of mercury volatilization by mer (from *Escherichiacoli*) and glutathione S-transferase (from *Schistosoma mansoni*) genes cloned in *Escherichia coli*. Sci. Total Environ. **2000**, *261*, 109–113.

[53] Dash, H.R.; Das, S. Bioremediation of mercury and the importance of bacterial *mer* genes. Int. Biodeter. Biodegr. **2012**, *75*, 207–213.

[54] Glick, B.R. Phytoremediation: synergistic use of plants and bacteria to clean up the environment. Biotechnol. Adv. **2003**, *174*, 383–393.

[55] Zhang, W.; Chen, L.; Liu, D. Characterization of a marine - isolated mercury - resistant *Pseudomonas putida* strain SP1 and its potential application in marine mercury reduction. Appl. Microbiol. Biotechnol. **2012**, *93*, 1305–1314.

Downloaded by [eská zemdlská univerzita v Praze], [Jirina Szakova] at 23:57 02 February 2016

Příloha V

Mercury distribution and mobility in contaminated soils from vicinity of waste incineration plant

A. Šípková[1], J. Száková[1], P. Coufalík[2], O. Zvěřina[2], L. Kacálková[3], P. Tlustoš[1]

[1]*Department of Agroenvironmental Chemistry and Plant Nutrition, Faculty of Agrobiology, Food and Natural Resources, Czech University of Life Sciences Prague, Prague, Czech Republic*
[2]*Department of Chemistry, Faculty of Science, Masaryk University, Brno, Czech Republic*
[3]*Department of Biology, Faculty of Science, University of Hradec Králové, Hradec Králové, Czech Republic*

ABSTRACT

The potential bioavailability of Hg from soil might be estimated by a variety of chemical extraction procedures, differing in the extraction agent, its concentration, the sample weight, and the time of extraction. In this study, a comparative analysis of several extraction methods, commonly used for obtaining the mobile and potentially mobilizable phase of the mercury was carried out. Concentrated HNO_3, 0.01 mol/L $Na_2S_2O_3$, 0.05 mol/L EDTA and 0.11 mol/L CH_3COOH were used as the single extraction agents. Moreover, the sequential extraction was performed. This procedure involved the following fractions: water soluble Hg, Hg extracted in acidic conditions, Hg bound to humic substances, elemental Hg and mercury bound to complexes, and residual Hg. The results showed that even strong acid HNO_3 is unable to release the mercury tightly bound to the soil matrix. This particular method with microwave digestion is commonly used for the estimation of anthropogenic pollution. Conversely, the lowest mercury yield was obtained using the acetic acid as the single extraction agent. In this case, the concentrations were below 0.15% of the total Hg content, which is a proportion generally defined as bioavailable to plants.

Keywords: bioavailability; extraction methods; inductively coupled plasma mass spectroscopy; advanced mercury analyzer AMA-254

Mercury can be released from soil by different extraction procedures. These procedures enable the determination of particular species present, the varying amounts of Hg bound to soil, and also the bioavailability and toxicity. The least tightly bound water-soluble fraction is obtained by the simple extraction using deionised water (Rodrigues et al. 2010). It estimates Hg portion present in soil pore water. This fraction of mercury is usually not in the form of the water-soluble ionic species but as species bound to dissolved organic matter; nevertheless, not directly on carbon (Biester and Scholz 1996). The application of diluted CH_3COOH as an extraction agent belongs to the methods simulating approximately composition of the soil solution similarly as other mild extraction procedures such as $CaCl_2$ solution (Novozamsky et al. 1993). The extraction solutions based on the chelating agents such as EDTA or DTPA represent another more efficient possibility. These agents are able to displace metals from insoluble organic or organometallic complexes in addition to those adsorbed on inorganic soil components (Rao et al. 2008). The other species are mercury fractions bound on iron sulphides, manganese hydroxides and carbonates, and Hg bound to the minerals. This strongly bound mercury species can be obtained by acids, e.g. HCl (Lechler et al. 1997).

Supported by the Czech Science Foundation, Grant No. P503/12/0682 and by the Czech University of Life Science Prague, Project No. 21140/1313/3130.

In soil, mercury can be bound very tightly to sulphur forming the insoluble HgS (Boszke et al. 2008). This phase of mercury can be obtained either by aqua regia extraction in a microwave oven (Fernándes-Martínez and Rucandio 2003), or using the saturated Na_2S solution from the residue remaining after the extraction procedures (Revis et al. 1989). The effect of the concentration of $Na_2S_2O_3$ on the extraction efficiency was in detail studied by Issaro et al. (2010).

The proportion of Hg, which is not firmly bound to the silicate matrix of soil, is often obtained by using HNO_3 as an extraction agent (Reis et al. 2010). The mercury concentration in these extracts enables an estimation of the amount of Hg from anthropogenic sources. In some cases, concentrated nitric acid combined with HCl (Teršič et al. 2011) or H_2SO_4 (Mailman and Bodaly 2005) is employed for total mercury content determination. It might also be used in sequential extraction procedures to obtain elemental Hg (Bloom et al. 2003). Sequential extractions are suitable methods for the mercury speciation analysis of solid samples. However, there is no universal sequential extraction concerning the individual Hg fraction determination. Several approaches were demonstrated by many authors (Renneberg and Dudas 2001, Sánchez et al. 2005, Han et al. 2006, Liu et al. 2006).

In this work, four various extraction agents as well as sequential extraction were applied for the assessment of Hg mobility and fractionation in one anthropogenically contaminated soil.

MATERIAL AND METHODS

Samples. Ten soil samples were collected from the former waste incineration plant in the suburb of Hradec Králové, Czech Republic. The selection of sampling sites was based on the experiment of Kacálková et al. (2009). Samples were collected in the vicinity of points 3 and 5. The plot 3 represented the average values of contamination (our samples 1–5), while extreme Hg content was measured in the plot 5 closer to the plant (our samples 6–10). Samples were taken from the top layer (0–30 cm), air-dried, sieved < 2 mm and kept at 4°C for several weeks. Following characteristics of soil were measured: pH_{CaCl_2} (Novozamsky et al. 1993), organic matter content (Sims and Haby 1971) and cation exchange capacity (ISO 1994). Total content of S was determined by X-ray fluorescence spectrometry (Spectro IQ, Kleve, Germany), mercury analyser AMA-254 (LECO model, Altec, Czech Republic, Plzeň) was used for total Hg determination. All experiments were carried out in three repetitions.

Extractable fractions of mercury. Four extraction agents HNO_3, $Na_2S_2O_3$, EDTA, and CH_3COOH were used to determine the mobile and mobilizable phases of Hg. For determination of potentially mobilizable mercury portions, 0.25 g of each sample was decomposed in 5 mL of concentrated HNO_3. The reaction mixture was digested at 280°C during 75 min by using microwave heating in MLS ultraCLAVE IV system (Milestone, Leutkirch im Allgäu, Germany) and then milli-q water was added to a final volume of 50 mL. The mild extraction procedures were performed as follows: (i) $Na_2S_2O_3$ extraction proceeded overnight in 10 mL of 0.01 mol/L solution, which was added to 1 g of the sample; (ii) 0.05 mol/L EDTA was adjusted with NaOH to pH 7. Subsequently, 1 g of soil was added to 10 mL of extraction solution and shaken for 1 h; (iii) 0.5 g of sample was added to 10 mL of 0.11 mol/L solution of CH_3COOH and shaken overnight. Subsequently, all the samples were centrifuged for 10 min at 3000 rpm.

Hg content in all extracts was measured by inductively coupled plasma mass spectrometry (Agilent 7700x, Agilent Technologies Inc., Santa Clara, USA). The isotope Hg(202) was measured and Pt(195) was used as an internal standard in concentration 10 μg/L. As reference material, San Joaquin Soil (SRM 2709) was utilized (theoretical Hg content is 1.4 ± 0.08 mg/kg; obtained recovery was 98%).

Sequential extraction. The sequential extraction procedure was designed by modifying the existing extraction schemes (Bloom et al. 2003, Boszke et al. 2008). 0.1 g of each sample was leached into 10 mL of chloroform, shaken for 3 h and centrifuged. This step was considered as F0 and residue obtained after the extractions was used in the next procedure. The soil/liquid ratio was the same for all extraction reagents. The extraction procedure was performed on the bulk samples according to the following scheme: F1 with redistilled water – Hg leachable in water, F2 with 0.5 mol/L HCl – Hg leachable under acidic conditions, F3 with 0.2 mol/L KOH – Hg bound to humic substances, F4 with 50% HNO_3 – elemental Hg and complexes, and F5 is solid residue. Experiments were carried out at laboratory temperature on shakers GFL 3006 (Burgwedel, Germany) at 300 rpm and the extraction

time was 18 h in all fractionation steps. Subsequently, extracts were separated from a solid phase by centrifugation for 10 min at 4000 rpm. The extraction agents from each single step were used as blank samples and the mercury content in all extracts was determined by using the AMA-254 analyser.

RESULTS AND DISCUSSION

Soil characteristic. The pH_{CaCl_2} of our samples equalled 7.18 ± 0.28 and the cation exchange capacity was 131.7 ± 3.8 $mmol_+$/kg. An oxidizable carbon and sulphur content ranged between 1.2–3.4% and 0.28–0.56%, respectively. The organic matter composition and/or content as well as mercury affinity to the individual fractions were described in the other works (Kacálková et al. 2009, Šípková et al. 2014). The measurements of the total Hg content indicated that in the vicinity of the former waste incineration plant there are places with relatively low Hg concentration; however, the sample with the amount of mercury reached even almost 29 mg/kg (Table 1). Kacálková et al. (2009) reported the same variability of the mercury content present in the same area showing the concentrations ranging from 0.15 to 12 mg/kg. Moreover, the highest organic matter content was observed in the samples representing the highest Hg values.

Single extractions. The extraction yields by individual extraction agents are shown in Table 1 and summarized in Figure 1 as relative Hg portions extractable from the total content. HNO_3 released around 50% of total Hg content in 8 of 10 samples. In the case of the most contaminated sample the concentration was approximately 70% and even 96%. Using $Na_2S_2O_3$ as an extraction agent the mercury yield was also highest in the last two samples. The average yield of these particular samples attains approximately 20% of the total. In other samples, the content of mercury ranged from 1.2% to 3.4%. Thus, it might be inferred that in places with higher anthropogenic contamination, the presence of mercury species bound to sulphur is higher than in less contaminated samples. In the case of the most contaminated site the rate of extractable Hg using $Na_2S_2O_3$ corresponds with the results reported by Issaro et al. (2010). They showed that the extraction yield of $Na_2S_2O_3$ usually reaches 50 ± 5% of Hg obtained by HNO_3 extraction from soils with high Hg levels from agricultural processes near Paris, France. Moreover, they showed that the rate of extractable Hg by $Na_2S_2O_3$ is decreasing with decreasing total Hg content. On the other hand, Subirés-Munoz et al. (2011) obtained by this type of extraction approximately 20% of the total Hg content. Their soils originated from the mining district of Almadén, Spain with high background Hg levels and influence of anthropogenic activities.

Further, using chelating agent EDTA, the values of extractable Hg ranged between 0.5% and 2% of the total Hg content, in all the experimental samples. These results correspond to those reported by Subirés-Munoz et al. (2011) who obtained less than 2% of the total Hg. This small variability suggests that the amount of mercury, which might serve as a source for plant uptake, is similar both in more and less contaminated places. Coinciding results were also obtained by extraction with a solution of CH_3COOH, which simulates natural conditions of soil solution. The yields of CH_3COOH were below 0.15% and confirmed no significant differences. The low availability therefore seems to indicate

Table 1. Total and extractable contents of mercury after single extractions (μg/kg)

Sample	Total	HNO_3	$Na_2S_2O_3$	EDTA	CH_3COOH
1	1070	578	14.3	6.92	0.49
2	236	132	7.04	1.99	0.34
3	415	201	7.82	5.21	0.37
4	419	234	8.03	8.80	0.48
5	550	273	10.4	6.27	0.45
6	2050	1132	52.1	9.37	0.73
7	396	223	13.5	2.95	0.44
8	580	300	6.95	2.94	0.78
9	28 800	20 108	5877	481	11.3
10	10 500	10 040	2094	64.7	8.64

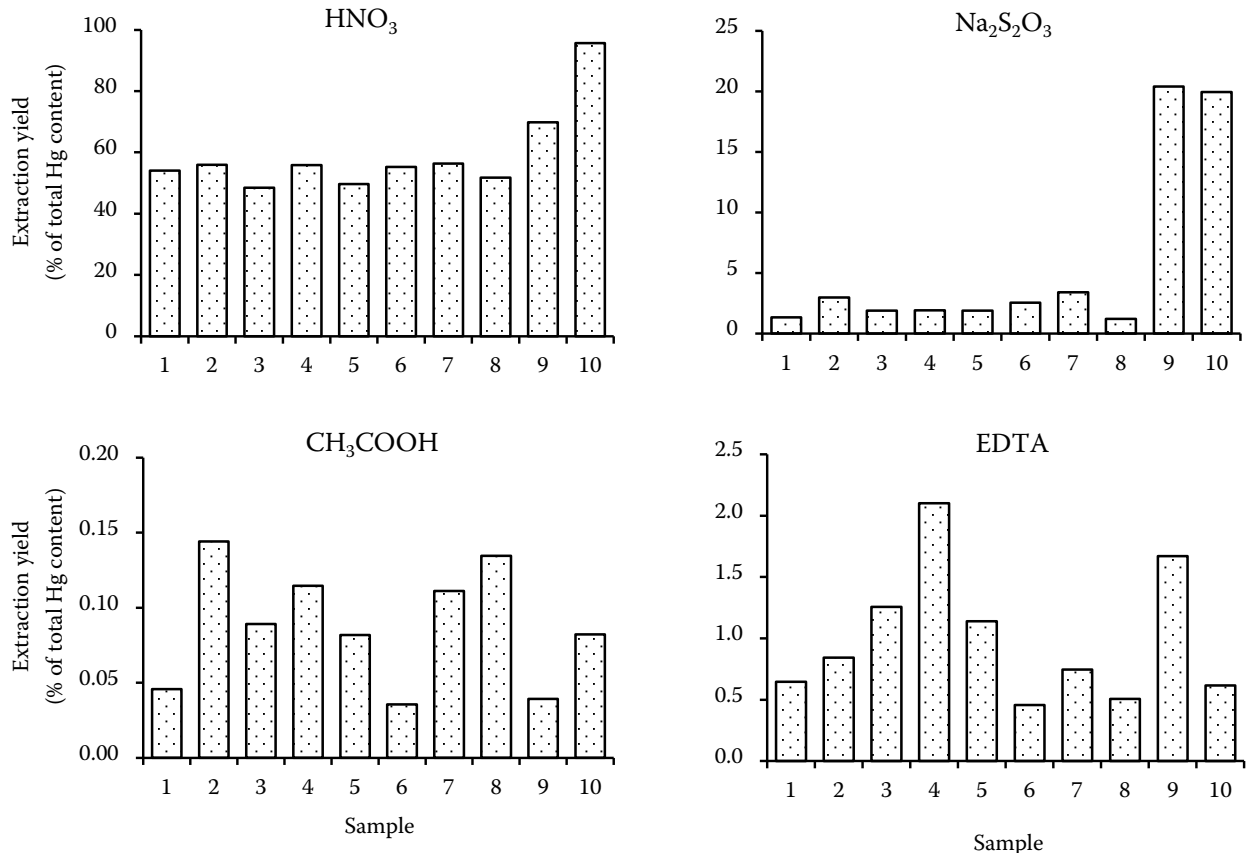

Figure 1. Extraction yield after single extraction using individual chemical agents

that mercury is strongly bound to sulphide phases and/or to insoluble clay minerals and organic matter in the samples (Rodrigues et al. 2010).

Sequential extraction. Mercury contents extracted in each step (F1–F5) are reported in Table 2. The sum of the amount removed by each extraction was in good agreement with the total amounts obtained by AMA-254. Values of recoveries ranged from 93% to 107%.

First fraction representing the total content of organomercury compounds (F0) was below the quantification limit (2 μg/kg) in all samples. Mobile fractions F1 and F2 were also very low for the majority of samples. Hg leachable in water was detectable only in the samples No. 9 and 10, containing the highest level of the total mercury content. Rodrigues et al. (2010) found similar value in samples from vicinity of chlor-alkali plant. The mercury leachable under acid conditions was measured in the aforementioned most contaminated samples and its content was less than 8%. Such high mercury content discovered in soil from the cinnabar refinery and mine by Miller et al. (1995). Low amount of this Hg species was found also in sample 6, which is the third site with high mercury concentration.

In the case of F3, Hg species values obtained were substantially higher. The semi-mobile mercury contents ranged from 18% to 30%. These Hg species bound to organic matter were regarded as stronger complexes and thus have limited mobility (Liu et al. 2006). Almost identical scale of the mercury fractions observed in the study of mercury mobility and bioavailability Boszke et al. (2008). The organic carbon content was also similar in this particular soil. Teršič et al. (2011) described mercury distribution in very contaminated soil from mining district of Idrija, Slovenia and in their study, Hg bound to organic or mineral soil matter reached from 35% to 40% of the total mercury content. These higher values can be connected with acidic pH because mercury is particularly bound to organic matter under the low pH (Schwesig et al. 1999). On the contrary, in our samples 9 and 10 the percentage ratios of this species were approximately 9% and differences among the amounts of mobile and semi-mobile fractions were relatively low.

Table 2. Mercury contents in individual fractions after sequential extraction (μg/kg)

Sample	F1	F2	F3	F4	F5
1	*	*	270	610	150
2	*	*	70	130	20
3	*	*	120	250	50
4	*	*	120	240	50
5	*	*	160	320	30
6	*	30	360	1400	220
7	*	*	80	280	30
8	*	*	130	350	70
9	400	2300	2500	16 200	5300
10	160	620	960	4900	3200

*data below the quantification limit (2 μg/kg). F1 – redistilled water; F2 – 0.5 mol/L HCl; F3 – 0.2 mol/L KOH; F4 – 50% HNO_3; F5 – residue

The highest Hg content was found in the case of non-mobile fraction, i.e. elemental mercury and Hg bound to complexes (F4). Although the sequential extraction by Lechler et al. (1997) was carried out with distinct extraction agent, results of Hg speciation showed the highest proportion of elemental mercury in the soil samples from former amalgamation milling of Ag-Au ores in Nevada, USA. Reis et al. (2010) divided the mercury species in a different way and their semi-mobile fraction included also elemental mercury. Thus, their values obtained from samples from the industrial complex and sulphide mine in Portugal, were similar to the results obtained in this study and the proportion ranged between 63% and 97%.

The content of mercury in solid residues after the extraction was in the majority of samples below 12%. However, in more contaminated samples these values were higher. Obviously, the substantial proportions of residues content are species bound to silica or Hg sulphides. Liu et al. (2006) found around 10% of Hg species bound to sulphur, which corresponds to our hypothesis.

In order to describe the mobility and bioavailability of mercury, several extraction agents and the sequential extraction described above were applied on soil collected near Hradec Králové, Czech Republic. In the area, several samples with high Hg concentration were found and the highest amount reached almost 29 mg/kg. Nevertheless, the total Hg content mostly achieved less than 2 mg/kg.

Based on the results of analyses, only a low amount of a mobile fraction, having the highest toxicity, was determined. In the majority of samples, which originated from the surroundings of the former waste incineration plant, less that 2% of the total Hg content was found. The lowest mercury yield was obtained using the acetic acid as a single extraction agent, which is a proportion generally defined as biologically available to plants (Quevauviller et al. 1993). In all experiments, the concentrations were below 0.15%.

Conversely, elemental Hg and mercury complexes were present in the highest amount and the proportion of this fraction ranged between approximately 50% and 70%. In the case of Hg bound to humic acids representing the semi-mobile species was determined as the second highest. Contrarily, higher Hg amounts were measured in the residuals of the two most contaminated samples. The results of this study concern on specific site and therefore the outcomes should not be taken as general characteristics of all anthropogenically contaminated soils.

REFERENCES

Biester H., Scholz C. (1996): Determination of mercury binding forms in contaminated soils. Mercury pyrolysis versus sequential extractions. Environmental Science and Technology, *31*: 233–239.

Bloom N.S., Preus E., Katon J., Hiltner M. (2003): Selective extractions to assess the biogeochemically relevant fractionation of inorganic mercury in sediments and soils. Analytica Chimica Acta, *479*: 233–248.

Boszke L., Kowalski A., Astel A., Barański A., Gworek B., Siepak J. (2008): Mercury mobility and bioavailability in soil from contaminated area. Environmental Geology, *55*: 1075–1087.

Fernández-Martínez R., Rucandio M.I. (2003): Study of extraction conditions for the quantitative determination of Hg bound to

sulfide in soils from Almaden (Spain). Analytical and Bioanalytical Chemistry, *375*: 1089–1096.

Han F.X., Su Y., Monts D.L., Waggoner C.A., Plodinec M.J. (2006): Binding, distribution, and plant uptake of mercury in a soil from Oak Ridge, Tennessee, USA. Science of the Total Environment, *368*: 753–768.

ISO 11260 (1994): Standard of Soil Quality – Determination of Effective cation Exchange Capacity and Base Saturation Level Using Barium Chloride Solution. International Organization for Standardization, Geneva.

Issaro N., Besancon S., Bermond A. (2010): Thermodynamic and kinetic study of the single extraction of mercury from soil using sodium-thiosulfate. Talanta, *82*: 1659–1667.

Kacálková L., Tlustoš P., Száková J. (2009): Phytoextraction of cadmium, copper, zinc and mercury by selected plants. Plant, Soil and Environment, *55*: 295–304.

Lechler P.J., Miller J.R., Hsu L.C., Desilets M.O. (1997): Mercury mobility at the Carson River superfund site, west-central Nevada, USA: Interpretation of mercury speciation data in mill tailings, soils, and sediments. Journal of Geochemical Exploration, *58*: 259–267.

Liu G., Cabrera J., Allen M., Cai Y. (2006): Mercury characterization in a soil sample collected nearby the DOE Oak Ridge Reservation utilizing sequential extraction and thermal desorption method. Science of the Total Environment, *369*: 384–392.

Mailman M., Bodaly R.A. (2005): Total mercury, methyl mercury, and carbon in fresh and burned plants and soil in Northwestern Ontario. Environmental Pollution, *138*: 161–166.

Miller E.L., Dobb D.E., Heithmar E.M. (1995): Speciation of mercury in soils by sequential extraction. In: Proceedings of USEPA Metal Speciation and Contamination of Surface Water Workshop, Jekyll Island.

Novozamsky I., Lexmond Th.M., Houba V.J.G. (1993): A single extraction procedure of soil for evaluation of uptake of some heavy metals in plants. International Journal of Environmental Analytical Chemistry, *51*: 47–58.

Quevauviller Ph., Ure A., Muntau H., Griepink B. (1993): Improvement of analytical measurements within the BCR-programme – Single and sequential extraction procedures applied to soil and sediment analysis. International Journal of Environmental Analytical Chemistry, *51*: 129–134.

Rao C.R.M., Sahuquillo A., Lopez Sanchez J.F. (2008): A review of the different methods applied in environmental geochemistry for single and sequential extraction of trace elements in soils and related materials. Water, Air, and Soil Pollution, *189*: 291–333.

Reis A.T., Rodrigues S.M., Davidson C.M., Pereira E., Duarte A.C. (2010): Extractability and mobility of mercury from agricultural soils surrounding industrial and mining contaminated areas. Chemosphere, *81*: 1369–1377.

Renneberg A.J., Dudas M.J. (2001): Transformations of elemental mercury to inorganic and organic forms in mercury and hydrocarbon co-contaminated soils. Chemosphere, *45*: 1103–1109.

Revis N.W., Osborne T.R., Sedgley D., King A. (1989): Quantitative method for determining the concentration of mercury(II) sulphide in soils and sediments. Analyst, *114*: 823–825.

Rodrigues S.M., Henriques B., Coimbra J., Ferreira da Silva E., Pereira M.E., Duarte A.C. (2010): Water-soluble fraction of mercury, arsenic and other potentially toxic elements in highly contaminated sediments and soils. Chemosphere, *78*: 1301–1312.

Sánchez D.M., Quejido A.J., Fernández M., Hernández C., Schmid T., Millán R., González M., Aldea M., Martín R., Morante R. (2005): Mercury and trace element fractionation in Almaden soils by application of different sequential extraction procedures. Analytical and Bioanalytical Chemistry, *381*: 1507–1513.

Schwesig D., Ilgen G., Matzner E. (1999): Mercury and methylmercury in upland and wetland acid forest soils of a watershed in Ne-Bavaria, Germany. Water, Air, and Soil Pollution, *113*: 141–154.

Sims J.R., Haby V.A. (1971): Simplified colorimetric determination of soil organic matter. Soil Science, *112*: 137–141.

Šípková A., Száková J., Tlustoš P. (2014): Affinity of selected elements to individual fractions of soil organic matter. Water, Air, and Soil Pollution, *225*: 1802.

Subirés-Munoz J.D., García-Rubio A., Vereda-Alonso C., Gómez-Lahoz C., Rodríguez-Maroto J.M., García-Herruzo F., Paz-García J.M. (2011): Feasibility study of the use of different extractant agents in the remediation of a mercury contaminated soil from Almaden. Separation and Purification Technology, *79*: 151–156.

Teršič T., Gosar M., Biester H. (2011): Distribution and speciation of mercury in soil in the area of an ancient mercury ore roasting site, Frbejžene trate (Idrija area, Slovenia). Journal of Geochemical Exploration, *110*: 136–145.

Received on August 29, 2013
Accepted on January 23, 2014

Corresponding author:

Ing. Adéla Šípková, Česká zemědělská univerzita v Praze, Fakulta agrobiologie, potravinových a přírodních zdrojů, Katedra agroenvironmentální chemie a výživy rostlin, Kamýcká 129, 16521 Praha 6-Suchdol, Česká republika
e-mail: sipkovaa@af.czu.cz

Příloha VI

Antarctic Science 27(3), 281–290 (2015) © Antarctic Science Ltd 2014 doi:10.1017/S0954102014000819

Ultra-trace analysis of Hg in alkaline lavas and regolith from James Ross Island

PAVEL COUFALÍK[1,2], ONDŘEJ ZVĚŘINA[1,3], LUKÁŠ KRMÍČEK[4,5], RICHARD POKORNÝ[6] and JOSEF KOMÁREK[1]

[1]*Faculty of Science, Masaryk University, Kotlářská 2, 61137 Brno, Czech Republic*
[2]*Institute of Analytical Chemistry, Academy of Sciences of the Czech Republic, v.v.i., Veveří 97, 60200 Brno, Czech Republic*
[3]*Faculty of Medicine, Masaryk University, Kamenice 5, 62500 Brno, Czech Republic*
[4]*Faculty of Civil Engineering, Brno University of Technology, Veveří 95, 60200 Brno, Czech Republic*
[5]*Institute of Geology, Academy of Sciences of the Czech Republic, v.v.i., Rozvojová 269, 16500 Prague 6, Czech Republic*
[6]*Faculty of Environmental Studies, University J. E. Purkyně, Králova výšina 3132/7, 40096 Ústí nad Labem, Czech Republic*
coufalik@iach.cz

Abstract: Polar regions represent a unique environment for the study of mercury cycling in the global ecosystem. Our research was focused on the assessment of the origin and mobility of mercury in the geochemical cycle in Maritime Antarctic (James Ross Island) by means of atomic absorption spectrometry. Mercury content in a set of extrusive (subaerial, subaqueous) and intrusive (dyke) alkaline basalts ranged between 1.6 μg kg^{-1} (for samples without xenoliths) and 8 μg kg^{-1} (for samples containing crustal xenoliths). The mercury content in alkaline basalts indicates a very low concentration of mercury in peridotitic mantle sources. Samples of regolith from James Ross Island were subjected to a comprehensive analytical procedure proposed for ultra-trace mercury concentrations involving fractionation and thermal analysis. Total mercury contents in regolith (2.7–11.3 μg kg^{-1}) did not deviate from the natural background in this part of Antarctica. Additionally, the obtained results are about two orders of magnitude smaller than values formerly assumed for primary mercury contents in basaltic lavas. Our results from Antarctica were compared with mercury contents in basaltic rocks from Greenland and the findings were confirmed. It seems that the input of mercury of geological origin into the polar ecosystem is apparently lower than expected.

Received 19 May 2014, accepted 22 September 2014, first published online 10 December 2014

Key words: basaltic volcanite, fractionation, mercury, polar region, weathered material

Introduction

Contamination of the Antarctic ecosystem by pollutants from lower latitudes is one of the main research topics concerning Antarctica (Bargagli 2008). Although Antarctica is isolated by the circulation of air masses and ocean currents, the concentration of metals and persistent compounds in environmental samples indicate long-range transport of pollutants from continents of the Southern Hemisphere (Bargagli 2008). These pollutants include mercury, which concentrates in polar regions after deposition and re-emission cycles (Bargagli *et al.* 2007, Brooks *et al.* 2008a). Antarctica is contaminated less than the Arctic by mercury from anthropogenic activities (Pfaffhuber *et al.* 2012). The main sources of mercury in Antarctica are marine aerosols, volcanic activity and atmospheric deposition (Bargagli *et al.* 1998). Contaminants are also introduced into the terrestrial ecosystem by seabirds nesting on the shore (Nie *et al.* 2012).

Polar coastal ecosystems seem to be cold traps for global atmospheric mercury burden (Bargagli 2005). Atmospheric mercury consists mainly of the elemental form (Bargagli *et al.* 2005). The Northern Hemisphere has a higher mercury content (*c.* 30%) in the atmosphere than the Southern Hemisphere (Bargagli 2005). Gaseous elemental mercury can have a residence time in the atmosphere of *c.* 1 year (Martínez-Cortizas *et al.* 1999). However, in polar regions, the lifetime of $Hg^{(0)}$ in the atmosphere is shorter than at lower latitudes (Bargagli *et al.* 2005). Mercury cycling in the Antarctic environment is well described in many works (e.g. Bargagli 2005, Brooks *et al.* 2008a, Pfaffhuber *et al.* 2012). Reactive halogens in aerosols promote the oxidation and deposition of mercury in coastal areas (Bargagli *et al.* 2007). The oxidation of $Hg^{(0)}$ by bromine after the polar sunrise increases the amount of reactive gaseous mercury (Bargagli *et al.* 2005). These speciation changes increase the amount of mercury deposited in snowfall (Brooks *et al.* 2008b). A significant proportion of the deposited mercury is returned to the atmosphere by photochemical reduction (Bargagli *et al.* 2007). A portion of divalent mercury deposited on snow enters into the terrestrial ecosystem in meltwater (largely in bioavailable form), which leads to increased concentrations of total

CAMBRIDGE JOURNALS
http://journals.cambridge.org Downloaded: 28 Apr 2015 IP address: 147.231.204.183

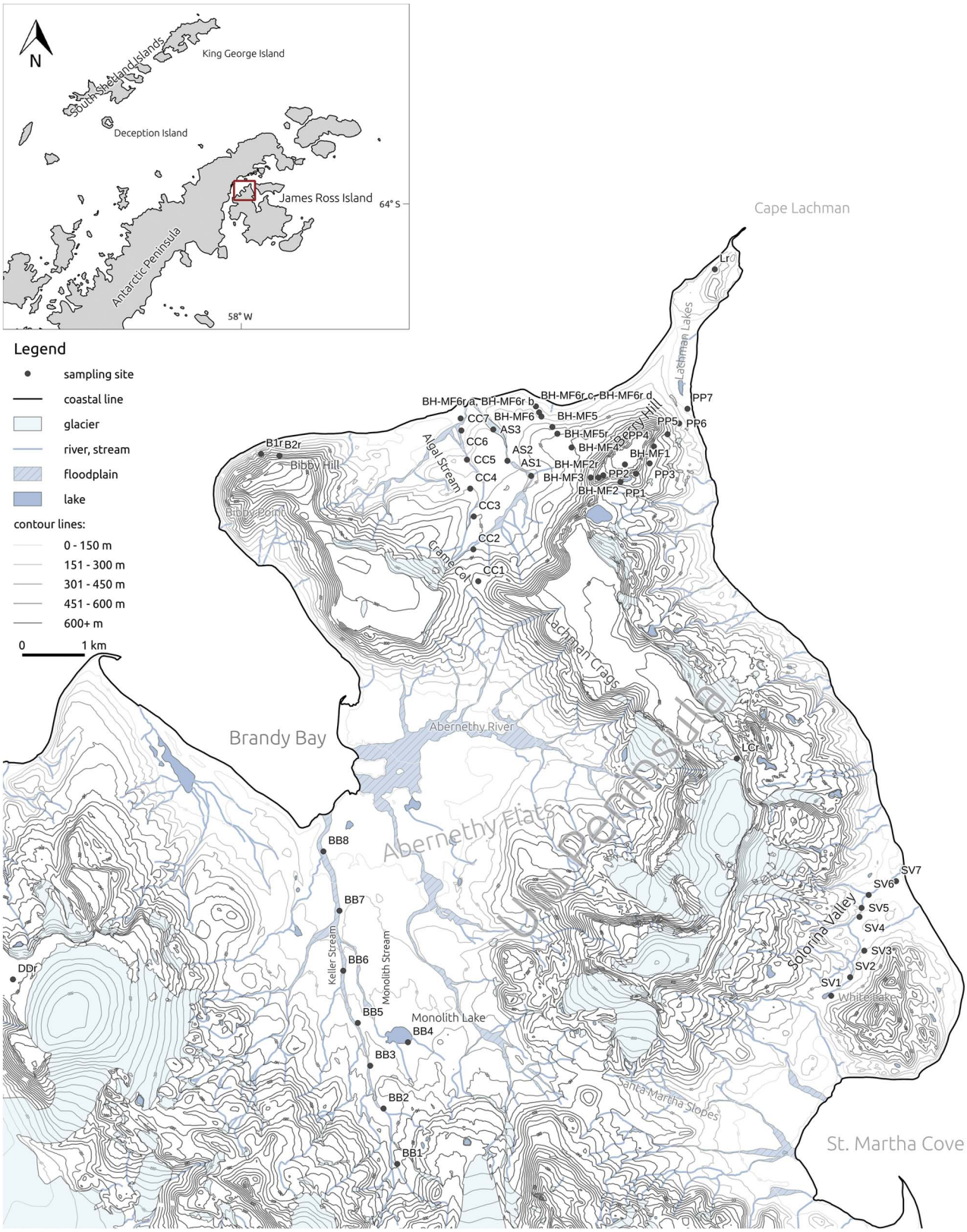

Fig. 1. Sampling sites of volcanites and weathered materials (after CGS 2009). AS = Algal Stream, B = Bibby Hill, BB = Brandy Bay, BH-MF = Berry Hill–Mendel Formation, CC = Crame Col saddle, DD = Davies Dome, L = Cape Lachman, LC = Lachman Crags, PP = Panorama Pass saddle, SV = Solorina Valley.

CAMBRIDGE JOURNALS
http://journals.cambridge.org Downloaded: 28 Apr 2015 IP address: 147.231.204.183

mercury in runoff (Bargagli *et al.* 2005). Nevertheless, unlike the Arctic, an increase in mercury bioaccumulation was not confirmed in Antarctica according to the analysis of sediment cores (Bargagli *et al.* 2007). The mercury content in organisms in areas close to the Antarctic Peninsula is relatively low (De Moreno *et al.* 1997). However, terrestrial environment is more susceptible to the contamination. Bioaccumulation in lichens and mosses has been observed (Bargagli *et al.* 1993, Bargagli *et al.* 1998, Bargagli *et al.* 2005).

Very few studies have been dedicated to the description of total mercury content in igneous rocks. Based on the review by Fleischer (1970), mercury content in most igneous rocks are usually below 100 μg kg^{-1}, except for alkaline basalts and kimberlites which contain several hundred μg kg^{-1} on average. Mercury is emitted into the air during volcanic eruption (e.g. Martin *et al.* 2012). Due to the effective ionic radii of Hg^{2+}, mercury might be expected to accompany Ba, Sr and Ca in rock-forming minerals, which probably accounts for the high concentrations reported for alkaline basalt rocks (Fleischer 1970). Moreover, elevated mercury content was observed in tholeiitic igneous rocks. Dissanayake & Vincent (1975) published total mercury content in whole-rocks and minerals from the layered Skaergaard Intrusion in East Greenland, which is a part of the North Atlantic large igneous province together with coeval flood basalts. The average value was 257 μg kg^{-1} determined by radiochemical neutron-activation analysis. Furthermore, the authors confirmed the hypothesis that mercury is enriched in plagioclase-rich igneous rocks.

To assess the origin, mobility and fate of mercury in the Antarctic ecosystem, information obtained by fractionation analysis can be used. The concentrations of mercury in weathered material in deglaciated parts of Antarctica may represent a background dependent on local geological conditions or may be affected by another source, such as the atmospheric deposition of mercury from distant areas. The aim of this research was to evaluate the geological influence of alkaline basaltic bedrock on the mercury content in weathered material and to consider the extent of mercury contamination in the maritime ecosystem of the Antarctic Peninsula region. Devising an appropriate analytical procedure for the determination of low concentrations of mercury forms in samples was an important task of this research.

Materials and methods

Location of the study

James Ross Island (64°10'S, 57°45'W) is located on the north-eastern, leeward side of the Antarctic Peninsula (Fig. 1). Its northern part, the Ulu Peninsula (CGS 2009), is one of the largest deglaciated areas in the Antarctic Peninsula region. The retreat of glaciers in this area occurred in the late Glacial at 12.9 ± 1.2 ka (Nývlt *et al.* 2014). The Ulu Peninsula is predominantly formed by Cretaceous marine sediments of the James Ross Basin (e.g. Vodrážka & Crame 2011) that were overlain by back-arc alkaline volcanites of the James Ross Island Volcanic Group (Košler *et al.* 2009) together with a late Miocene sedimentary sequence of terrestrial glacigenic, glaciomarine and marine sediments of the Mendel Formation (Nývlt *et al.* 2011). The $^{40}Ar/^{39}Ar$ age of volcanites in the Ulu Peninsula, which are created from hyaloclastic breccias, pillow-lavas and subaerial lava flows accompanied by basaltic dykes and subvolcanic plugs, is estimated to be in the range of 6–4 Ma (Smellie *et al.* 2008 and references therein).

Regarding the type of weathering processes in Antarctica, where simple mechanical disintegration predominates, the differences between parent rock and weathered material are minor (Campbell & Claridge 1987). However, compared to Continental Antarctica, the surface of James Ross Island is influenced to a significantly greater extent by liquid water, which promotes weathering and enables the mobility of dissolved minerals and nutrients. In addition, the surface at wet sites is often covered with a layer of microorganisms or moss. In these places, organic matter occurs in the upper layer of the regolith.

Collection of samples

The collection of volcanic rocks and weathered materials was performed during the Czech polar expedition at the Johann Gregor Mendel station in the summers of 2011–12 and 2012–13. In total, 11 rock samples and 33 regolith samples were collected. Considering the objectives of the research, two types of regolith were distinguished. Weathered material from dry surfaces (plateaus, hillsides and stony hillocks) was termed as type 1, whereas samples from streams (deposits in watercourses) were termed as type 2. It can be assumed that both types differ in the degree of particle leaching which may evince the mercury content. The regolith was collected using a stainless scoop; samples of type 1 were removed from a depth of 2–10 cm and type 2 from the edge of streams. The top layer of type 1 was not taken due to the potential presence of microbiota or guano. The samples were subsequently dried in the laboratory at the station for 48 hours (at *c*. 15°C) and sieved to a size fraction below 2 mm. Only this fraction was used in further investigations. The samples were stored at 4°C in polyethylene containers. The collected material was transported to the laboratory in the Czech Republic in a cooling box.

The following transects through the selected localities (Fig. 1) were suggested: Crame Col saddle, Berry Hill–Mendel Formation, Panorama Pass saddle, Brandy Bay

CAMBRIDGE JOURNALS
http://journals.cambridge.org Downloaded: 28 Apr 2015 IP address: 147.231.204.183

Table I. Samples from the comparative locality in Greenland.

Sample	GPS co-ordinates	Petrographical type
DIK01	69°15'13.536"N, 53°29'22.956"W	Olivine-phyric basalt dyke
DIK05B	69°15'56.808"N, 53°32'51.792"W	Amygdaloidal feldspar-phyric dolerite
DIK05C	69°15'56.808"N, 53°32'51.792"W	Olivine-phyric basalt lava
DIK06	69°15'15.480"N, 53°30'48.636"W	Amygdaloidal olivine basalt clast from hyaloclastite breccia
DIK07	69°15'10.836"N, 53°29'45.276"W	Feldspar-phyric basalt lava
DIK08	69°15'39.060"N, 53°27'35.604"W	Olivine-phyric basalt lava
DIK09	69°15'44.532"N, 53°31'58.044"W	Olivine and feldspar-phyric lava

and Solorina Valley. Additionally, samples from Algal Stream were also taken. The Berry Hill–Mendel Formation transect included the sampling of erratic granite and microgranite pebbles from the Mendel Formation, as well as hyaloclastite breccias and massive basalts above the Mendel Formation. Due to the assessment of mercury content in alkaline volcanites of the Ulu Peninsula, various petrographical samples out of the transects were also collected. Subvolcanic plugs and dykes formed by Na-rich basalt–hawaiite were sampled along the northern slope of Bibby Hill. Basalt pillow lava was collected on Cape Lachman, while subaerial dolerite lava was sampled on exposed upper parts of the Lachman Crags and Davies Dome.

With respect to the low levels of mercury detected in basaltic lavas from the James Ross Island Volcanic Group, an additional polar field campaign focused on the sampling of Palaeocene flood basalts was performed. Exposed basalts in the vicinity of the Arctic Station (University of Copenhagen) in Qeqertarsuaq, Disko Island, West Greenland (e.g. Larsen & Pedersen 2009) were chosen as a comparative locality. Sampling sites and the petrographical features of the collected material are defined in Table I.

Analytical procedures

Thin sections of representative rock were prepared for detailed petrographical investigation (structural/textural characteristics, identification of the constituent mineral phases). Photographs were acquired using an Olympus BX 51 polarizing microscope equipped with a Canon EOS 1100D digital camera.

Prior to analysis, the rock samples were ground to a size fraction below 2 mm. Afterwards, all samples of rock and regolith were milled to a size fraction below 63 μm using short durations of milling to prevent sample heating. The total mercury content in all samples was determined using an AMA-254 Analyzer (Altec, Czech Republic). This atomic absorption spectrometer incorporating thermo-oxidative decomposition of the sample allows the measurement of liquid and solid samples and the pre-concentration of mercury atoms on a gold amalgamator. Three parallel analyses were performed for each sample. The determination of total mercury in solid samples was verified by means of the certified reference material CRM 020 Trace Metals – Sandy Loam 2 (RTC, USA). The limit of quantification for all measurements was 0.3 μg kg^{-1}.

The samples from the transect in Brandy Bay were subjected to fractionation analysis. The following procedure of sequential extraction was designed for the determination of low concentrations of mercury forms. Total mercury was fractionated into mobile mercury (extracted in 0.5 mol l^{-1} HCl), mercury bound to organic matter (extracted in 0.2 mol l^{-1} KOH), elemental mercury (extracted in 50% HNO_3) and residual mercury (the content in solid residue after extraction in HNO_3). The extraction was carried out using a return shaker at laboratory temperature, with a solid/liquid ratio of 100 mg of sample to 10 ml of extractant; the time of extraction was 18 hours for each step. Extracts were separated by centrifugation; solid residues were dried at 30°C. The determination of individual mercury forms from the solid residues was performed after each extraction step (for the entire weight of each sample). The concentrations of the mercury forms were calculated from the differences in mercury contents between the steps. Therefore, a new portion of the sample was required for each step of the extraction. Three parallel extractions were performed; thus, one sample was extracted in nine repetitions. The measurement of solid samples allows the determination of lower mercury concentrations than the measurement of liquid extracts.

The content of $Hg^{(0)}$ in samples from Brandy Bay was also determined using thermal desorption. The $Hg^{(0)}$ was calculated from the difference in mercury contents before and after heating at 105°C for 48 hours (Coufalík *et al.* 2014). In addition, the thermal stability of mercury in samples from Brandy Bay was also studied. Samples were heated in an oven from 50–250°C, with the temperature increasing in steps of 50°C over 2 hours. The determination of mercury content in the samples was performed at each temperature step.

In addition, the organic carbon content in samples from Brandy Bay was determined after the previous removal of carbonates by HCl. Measurements were performed on a Vario TOC Cube Analyzer (Germany).

CAMBRIDGE JOURNALS
http://journals.cambridge.org Downloaded: 28 Apr 2015 IP address: 147.231.204.183

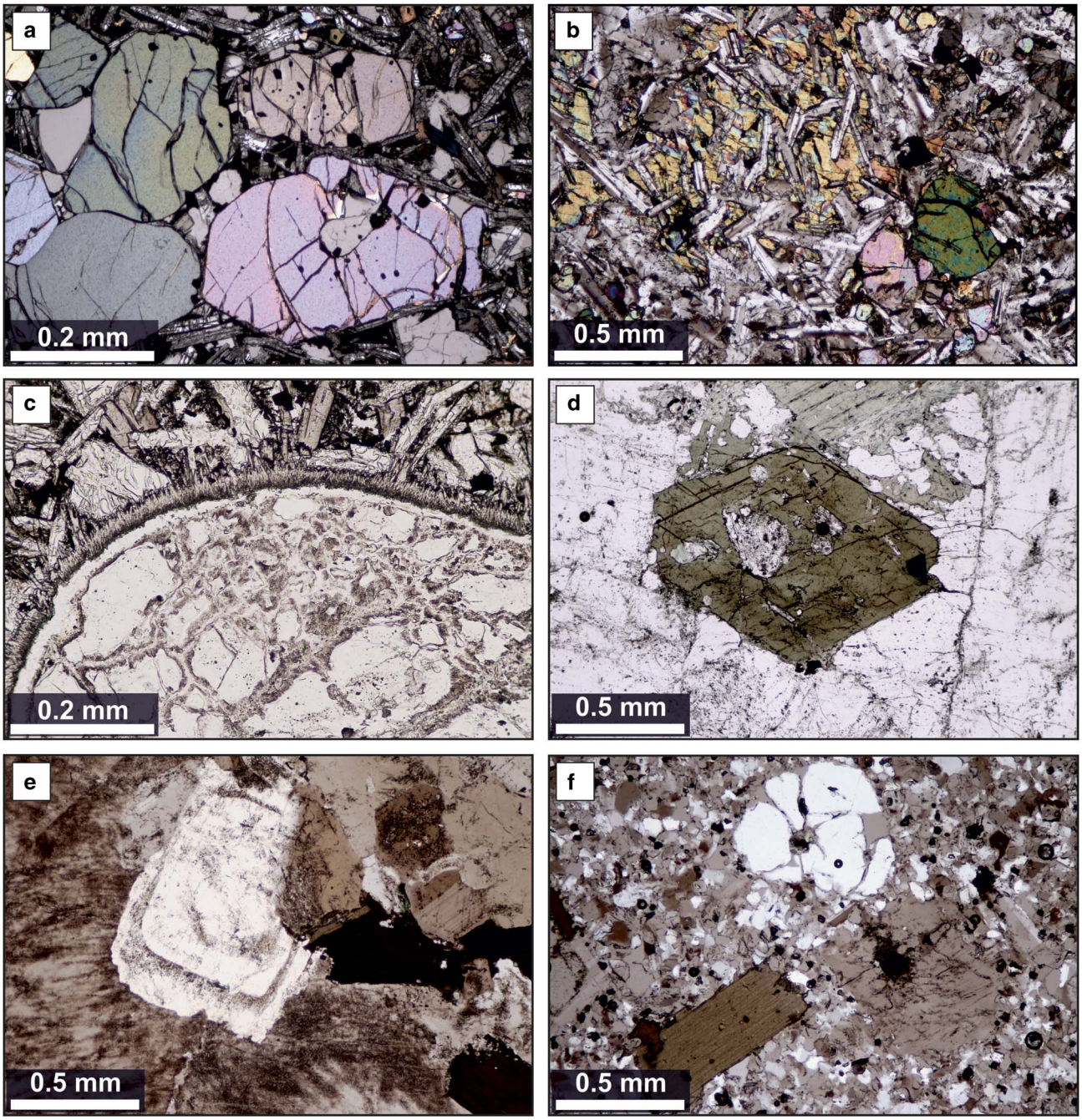

Fig. 2. Photomicrographs of the analysed rocks. **a**. Glomeroporphyritic olivine containing euhedral Cr-spinel (B2r, hawaiite, Bibby Hill; crossed polars). **b**. Plagioclase laths enclosed in anhedral clinopyroxene (BH-MF5r, platy basalt flow above the Mendel Formation; crossed polars). **c.** Reaction rim around quartz xenolith (B2r; parallel polars). **d.** Amphibole from mafic enclave in granite (BH-MF6r_b, pebble from the Mendel Formation; parallel polars). **e.** Plagioclase with compositionally different zones highlighted by selective sericitization (BH-MF6r_d, granite pebble from the Mendel Formation; crossed polars). **f.** Quartz, feldspar and biotite in a felsic fine-grained matrix (BH-MF6r_c, pebble of porphyric microgranite newly identified from the Mendel Formation; crossed polars).

Results

Petrography of the parent rocks

The bedrock of most of the transects is represented by alkaline olivine basalts and dolerites of the James Ross Island Volcanic Group. The sampled sites covered products with textural features of both subaerial and subaqueous volcanic activity. Among the primary minerals, volcanites contain phenocrysts of euhedral olivine, occurring as individual crystals and as glomeroporphyritic aggregates (Fig. 2a). Olivine crystals contain inclusions of spinel group minerals. Olivine is

CAMBRIDGE JOURNALS
http://journals.cambridge.org Downloaded: 28 Apr 2015 IP address: 147.231.204.183

Table II. Total mercury content in rock samples in μg kg^{-1}.

James Ross Island Sample		Greenland Sample	
BH-MF2r	1.9	DIK01	3.2
BH-MF5r	8.0	DIK05B	1.3
BH-MF6r a	4.0	DIK05C	1.7
BH-MF6r b	1.8	DIK06	3.8
BH-MF6r c	2.9	DIK07	1.5
BH-MF6r d	0.7	DIK08	1.1
B1r	1.6	DIK09	2.0
B2r	2.6		
Lr	8.0		
LCr	3.4		
DDr	2.8		

Table III. Total mercury content in regolith in μg kg^{-1}.

Sample	Type 1	Type 2	Sample	Type 1	Type 2
CC1	4.5		BB1	7.6	7.2
CC2	9.8		BB2	8.3	5.3
CC3	8.2		BB3	9.4	9.1
CC4	4.7		BB4	7.9	6.3
CC5	5.0		BB5	7.3	7.2
CC6	4.9		BB6	8.3	5.5
CC7	5.4		BB7	10.3	4.3
AS1		7.8	BB8	11.0	5.2
AS2		7.6	SV1	3.8	6.3
AS3		5.5	SV2	3.0	4.6
BH-MF1	5.5		SV3	5.6	5.2
BH-MF2	11.3		SV4	4.1	
BH-MF3	5.6		SV5		4.2
BH-MF4	5.6		SV6	3.6	4.5
BH-MF5	6.7		SV7	2.7	3.8
BH-MF6	5.6				
PP1	8.0				
PP2	5.1				
PP3	7.2				
PP4	5.4				
PP5	8.4				
PP6	3.1				
PP7	4.3				

also present in the matrix, where it is accompanied by laths of plagioclase with ophitic to trachytic arrangements. Plagioclase crystals can be enclosed in subhedral to anhedral clinopyroxene (Fig. 2b). Additionally, a variable amount of glass can also be found in quickly chilled samples. The majority of accessory minerals are formed by magnetite and ilmenite. Secondary minerals include alteration products of olivine, zeolite group minerals in amygdules, and the palagonitic alteration of glass in hyaloclastic breccias. A characteristic textural feature of the studied basalts is the presence of xenoliths from underlying Cretaceous sediments of the James Ross Basin (Fig. 2c).

The broad petrographical variability of the bedrock of James Ross Island is represented by the erratic fraction of Mendel Formation sediments (Berry Hill–Mendel Formation transect). Among the prevalent basaltic lavas and tephra of local origin, there are also present gravel-to-boulder clasts of magmatic (granitoids, diorites and gabbros) and metamorphic (cherts, phyllites, biotite gneisses, orthogneisses and amphibolites) rocks with a presumed origin from the Antarctic Peninsula Batholith and the surrounding crystalline basement. Various types of medium-grain granites (both porphyric and epigranular) are the most abundant. Granites exhibit textures of interaction with basic melt demonstrated by the presence of abundant mafic microgranular enclaves of dioritic composition rich in green amphibole and biotite (Fig. 2d). Even granites without visible mafic microgranular enclaves show evidence of magma mixing, as they contain feldspar crystals with

Table IV. Content of mercury forms in samples from Brandy Bay in μg kg^{-1}.

Sample	Organic carbon	Sequential extraction				Thermal desorption
	(%)	Mobile Hg	Organic bound Hg	Hg^0	Residual Hg	Hg^0
$BB1_{type1}$	0.45	1.7	2.8	2.7	0.4	2.7
$BB1_{type2}$	0.41	1.9	1.7	3.3	0.3	1.8
$BB2_{type1}$	0.31	2.4	3.3	2.2	0.4	2.4
$BB2_{type2}$	0.28	1.8	1.3	1.9	0.3	0.9
$BB3_{type1}$	0.31	5.1	1.8	2.0	0.5	1.7
$BB3_{type2}$	0.21	4.4	0.7	2.8	1.2	2.5
$BB4_{type1}$	0.45	2.2	3.1	2.1	0.5	1.8
$BB4_{type2}$	1.24	1.4	3.0	1.5	0.4	1.2
$BB5_{type1}$	0.24	3.6	1.5	1.6	0.6	1.1
$BB5_{type2}$	0.49	2.2	3.0	1.6	0.4	1.5
$BB6_{type1}$	0.32	4.9	0.7	2.2	0.5	1.4
$BB6_{type2}$	0.30	3.1	0.4	1.6	0.4	1.2
$BB7_{type1}$	0.38	6.3	0.6	3.0	0.4	1.9
$BB7_{type2}$	0.23	2.1	–	1.9	0.3	1.6
$BB8_{type1}$	0.60	4.4	4.3	1.6	0.7	1.7
$BB8_{type2}$	0.22	1.4	2.1	1.2	0.5	1.1

– = below the limit of quantification.

CAMBRIDGE JOURNALS
http://journals.cambridge.org Downloaded: 28 Apr 2015 IP address: 147.231.204.183

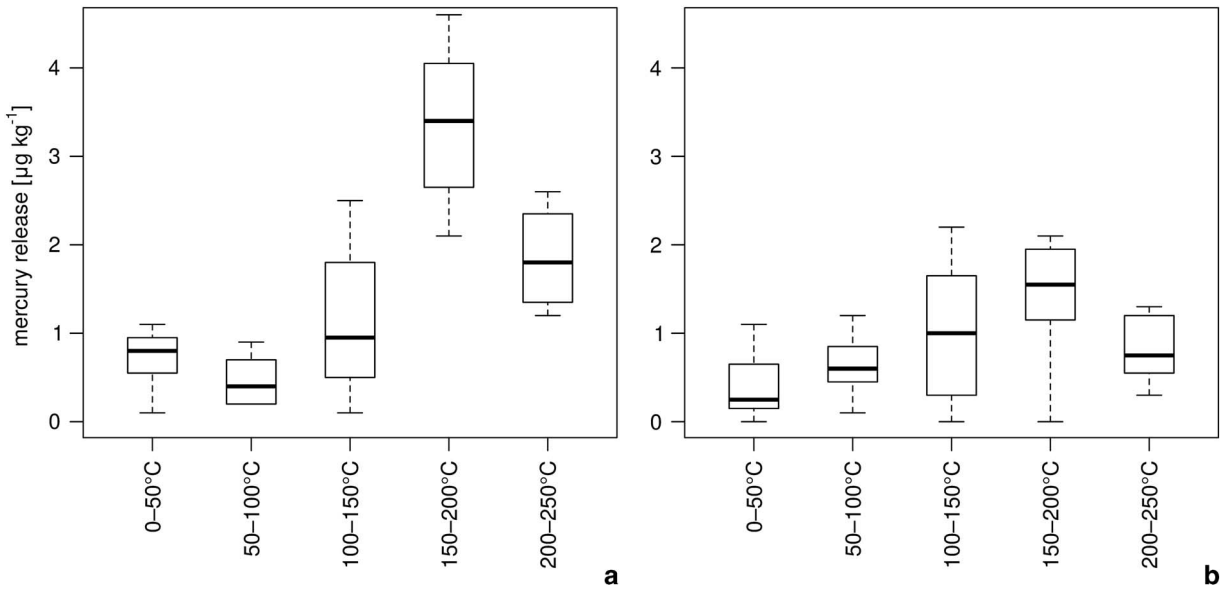

Fig. 3. Release of mercury from samples from Brandy Bay. **a.** Type 1. **b.** Type 2.

rounded zones resembling those grown under magma-mixing conditions. Growing zones are highlighted by selective alteration (Fig. 2e). Dyke equivalents of granites–porphyric microgranites, which are characterized by phenocryst of quartz, alkaline feldspars and biotite (Fig. 2f), were newly recognized within the Mendel Formation.

Total mercury contents

The studied samples of regolith and bedrock from James Ross Island cover various petrographical types. Therefore, the relatively low range of total mercury content (0.7–11.3 µg kg^{-1}) was unexpected (Table II and Table III). The relative standard deviation (RSD) of the determination was within 3% for all samples.

The determined concentrations of total mercury in rock samples from James Ross Island and Greenland are presented in Table II. While the results obtained for granites and microgranites of the Mendel Formation (0.7–4.0 µg kg^{-1}) were in the expected range, the very low mercury content found in the alkaline volcanites (1.6–8.0 µg kg^{-1}) were quite unexpected. The results obtained for mineralogically and texturally similar basaltic lavas from Greenland were also in the low range (1.1–3.8 µg kg^{-1}). Since volcanites in polar regions are not strongly affected by chemical weathering, these results can be considered as reliable and significant.

Fractionation analysis and thermal desorption

Fractionation analysis was performed on samples with the highest mercury content, i.e. those from the transect in Brandy Bay. Results of the determination of individual mercury forms together with organic carbon content are presented in Table IV. Elemental mercury was determined using both sequential extraction and thermal desorption. The RSD of the determination was up to 8% for all mercury forms. The decrease in mercury content in samples from Brandy Bay with increasing temperature (in steps) for both regolith types is presented in Fig. 3.

Discussion

Total mercury content

The results of older studies (cf. Fleischer 1970, Dissanayake & Vincent 1975) were not confirmed. Similarly, Zintwana *et al.* (2012) found significantly lower mercury concentrations for the Skaergaard Intrusion than in previous measurements, and the authors found no evidence of mercury enrichment in plagioclase-rich igneous rocks, as was reported previously. Zintwana *et al.* (2012) attributed this difference to the inaccurate analytical methodology of early measurements.

Rudnick & Gao (2003) published the following mercury contents in the Earth's crust: 50 µg kg^{-1} for the upper continental crust, 8 µg kg^{-1} for the middle continental crust and 6 µg kg^{-1} for the lower continental crust. The mercury content in the primitive mantle is estimated to be 6 µg kg^{-1} (Palme & O'Neill 2003). Nevertheless, it seems that these estimates are being reduced with increasing data. The relatively high range of mercury content determined for basalts from James Ross Island in comparison with Greenland samples is probably the result of contamination of basaltic melt by crustal material. Numerous findings of xenoliths from the underlying Cretaceous sedimentary rocks represent evidence of this contamination. The influence of

CAMBRIDGE JOURNALS
http://journals.cambridge.org Downloaded: 28 Apr 2015 IP address: 147.231.204.183

sediments on the composition of lavas on James Ross Island is also recorded in the Li isotope system (Košler *et al.* 2009). The homogeneous distribution of mercury in the primitive mantle cannot be expected. Thus, mercury content in the primitive mantle could even be lower.

Concentrations of total mercury in regolith samples from all transects are presented in Table III. The transects were designed to run through the geological layers along with the change in altitude. A trend of mercury accumulation with a drop in altitude or a significantly higher concentration in some localities was not observed. The determined concentrations were relatively low in relation to published data. The lowest mercury content (0.5 μg kg^{-1}) was determined in sediments from Deception Island, outside fumaroles (De Ferro *et al.* 2014). Higher mercury concentrations were found in other parts of Antarctica, mostly up to 100 μg kg^{-1} (Bargagli *et al.* 1993, 1998, 2005, Nie *et al.* 2012), compared to those found for James Ross Island (this study).

The total mercury content in samples may be considerably affected by speciation. Mobile mercury forms are subjected to the influence of external conditions, i.e. leaching from particles of weathered material; thus, the mercury content in geological layers increases at lower elevations. The secondary enrichment of material by mobile forms is noticeable in the case of samples from Solorina Valley (type 2). However, this form of enrichment caused by mercury transport via surface water cannot be compared to the effect of bio-vectors such as penguins or seals (Nie *et al.* 2012).

The calculated baseline concentration of mercury (without an anthropogenic contribution) on King George Island (South Shetland Islands) is 13 μg kg^{-1} (Lu *et al.* 2012). Mercury content in rock and regolith samples did not differ significantly. The determined concentrations in James Ross Island could be considered as a background in this part of Antarctica. Nevertheless, the possible contamination of the area by long-range transport is not excluded. Mercury deposition from the atmosphere may not be evident in these inorganic samples.

Fractionation analysis and thermal desorption

Determination of the mobility (i.e. bioavailability) and thermal stability (i.e. inclination towards re-emission) of mercury in material is essential for the assessment of mercury fate in the Antarctic environment. A proportion of mercury releasable in water exhibits a considerable variability depending on the location. It may be caused by the adsorption of ions onto particles after the evaporation of meltwater (Bargagli *et al.* 2007). In this case, the first extraction step also consisted of mercury bound to alkaline components of the material. The content of mobile mercury varied between 23–61% of the total content in samples. Mercury in surface soil is mostly bound to organic matter or clay (Bargagli *et al.* 2005). In general, the content of organic material in Antarctic soils and sediments is very low (Campbell & Claridge 1987), as can be seen here (Table IV). A soil poor in carbon may have an excess of metal with respect to the number of bonding groups in organic material, which increases the soluble fraction (Bargagli *et al.* 2007). Mercury bound to organic matter formed up to 53% of total mercury content. This is probably the result of strong interactions between mercury and organic matter, even if the mercury content did not correlate with the content of organic carbon (Bargagli *et al.* 1998). A direct correlation of mercury levels with carbon was confirmed for samples with higher carbon content (Bargagli *et al.* 1993) or in the case of ornithogenic sediments (Nie *et al.* 2012). Elemental mercury constituted 15–47% of the mercury in samples. Residual mercury formed 4–14%; this fraction consists of insoluble and immobile mercury forms, such as mercury sulfide.

The results of $Hg^{(0)}$ determination obtained by thermal desorption and sequential extraction evinced a sufficient degree of conformity in relation to low concentrations. The values determined thermally were equal to or lower than the concentrations determined by the extraction. A difference of at least 1 μg kg^{-1} was observed for the BB1 and BB2 samples (type 2) and for the BB7 sample (type 1). Thus, the extraction of amalgams or complex compounds together with elemental mercury could be expected for these samples in this extraction step.

Mercury, which condenses in areas with a cold climate, tends to have low thermal stability (Martínez-Cortizas *et al.* 1999). Mercury re-emission from the surface depends on the intensity of metal interaction with the matrix, the surface of the particles and the thermal stability of the mercury species contained. Thermal stability may also be enhanced by adsorption to internal surfaces of the particles (Coufalík *et al.* 2014).

Significant mercury release was not observed up to 50°C, which may be the result of the relatively high temperature of the deglaciated surface of James Ross Island during sunny days in the summer period. The proportion of mercury with low thermal stability (up to 100°C) was lower than that of thermally determined $Hg^{(0)}$. Thus, a portion of elemental mercury is not free and is adsorbed in pores of the particles. The highest mercury release was observed between 150 and 200°C; the mercury released here was the divalent form, which is not bound to organic matter. The remaining content after the heating of samples to 250°C can be defined as thermally stable mercury. This proportion was always higher for type 2 than for type 1 and formed up to 43% of the total content. The content of residual mercury (Table IV) was very low. For this reason, thermally stable mercury was not comprised only of mercury sulfide but also contained

CAMBRIDGE JOURNALS
http://journals.cambridge.org Downloaded: 28 Apr 2015 IP address: 147.231.204.183

other divalent mercury forms, such as the mercury bound to organic matter (Coufalík *et al.* 2014).

Based on the results obtained, the following mercury cycle in the Antarctic Peninsula region could be expected. Low mercury concentrations which are released from the bedrock by weathering processes represent the background. The input of additional mercury from the atmosphere is probable, which may increase the amount of mobile divalent mercury in the ecosystem. A proportion of deposited mercury is subjected to re-emission. Transport and adsorption occur at temperatures above 0°C. Generally, the content of organic matter and mineral particles in regolith is very low. Thus, insignificant capture by particles of material poor in carbon occurs and a substantial portion of the mercury migrates. For this reason, there is no obvious contamination in inorganic components of the environment. Mercury can accumulate by adsorption to the finest particles (e.g. in lakes) or flow out into the sea. The degree of contamination of the environment in this area cannot be determined on the basis of the analysis of inorganic samples. The solution may consist of the analysis of living organisms. To assess Hg^0 input from the atmosphere, the analysis of lichens can be suggested; the analysis of cyanobacterial coatings could be proposed to evaluate the extent of mercury accumulation in the aquatic environment.

Conclusion

Mercury content in basaltic lavas is significantly lower than previously considered, which indicates a very low mercury concentration in the peridotitic mantle source. Background concentrations of mercury in regolith in Antarctica are dependent mainly on the concentrations in parent rocks, especially because of the low retention capacity of weathered material with a low content of organic matter and particles with a large surface. It seems that mercury deposition from the atmosphere occurs in the region of the Antarctic Peninsula. However, its extent cannot be evaluated on the basis of the analysis of inorganic samples.

Acknowledgements

We greatly appreciate editorial handling of John Smellie as well as the thoughtful reviews of two anonymous reviewers. The main financial support was provided by the Grant Agency of the Czech Republic, Project P503/12/0682. The authors are grateful to the Czech Antarctic Station "J.G. Mendel", James Ross Island, Antarctica and the Arctic Station in Qeqertarsuaq, Disko Island, West Greenland for allowing them access to their facilities. The work was also supported by the Institute of Analytical Chemistry of the ASCR under the Institutional Research Plan RVO: 68081715, and by the project RVO 67985831 of the Institute of Geology of the ASCR. The involvement of Lukáš Krmíček in polar research was covered by the "EXCELLENT TEAMS" project at Brno University of Technology; registration number CZ.1.07/2.3.00/30.0005. Richard Pokorný also acknowledges the projects CZ.1.07/2.3.00/35.0046 and FZP IG 1/2014. Special thanks go to Diana Sychová for technical assistance.

References

Bargagli, R. 2005. *Antarctic ecosystems. Environmental contamination, climatic change, and human impact*. Berlin: Springer, 395 pp.

Bargagli, R. 2008. Environmental contamination in Antarctic ecosystems. *Science of the Total Environment*, **400**, 212–226.

Bargagli, R., Monaci, F. & Bucci, C. 2007. Environmental biogeochemistry of mercury in Antarctic ecosystems. *Soil Biology & Biochemistry*, **39**, 352–360.

Bargagli, R., Agnorelli, C., Borghini, F. & Monaci, F. 2005. Enhanced deposition and bioaccumulation of mercury in Antarctic terrestrial ecosystems facing a coastal polynya. *Environmental Science & Technology*, **39**, 8150–8155.

Bargagli, R., Battisti, E., Focardi, S. & Formichi, P. 1993. Preliminary data on environmental distribution of mercury in northern Victoria Land, Antarctica. *Antarctic Science*, **5**, 3–8.

Bargagli, R., Sanchez-Hernandez, J.C., Martella, L. & Monaci, F. 1998. Mercury, cadmium and lead accumulation in Antarctic mosses growing along nutrient and moisture gradients. *Polar Biology*, **19**, 316–322.

Brooks, S., Arimoto, R., Lindberg, S. & Southworth, G. 2008a. Antarctic polar plateau snow surface conversion of deposited oxidized mercury to gaseous elemental mercury with fractional long-term burial. *Atmospheric Environment*, **42**, 2877–2884.

Brooks, S., Lindberg, S., Southworth, G. & Arimoto, R. 2008b. Springtime atmospheric mercury speciation in the McMurdo, Antarctica coastal region. *Atmospheric Environment*, **42**, 2885–2893.

Campbell, I.B. & Claridge, G.G.C. 1987. *Antarctica: soils, weathering processes and environment*. Amsterdam: Elsevier, 368 pp.

CGS. 2009. *James Ross Island – northern part*. Topographical map, 1:25000. Prague: Czech Geological Survey.

Coufalík, P., Zvěřina, O. & Komárek, J. 2014. Determination of mercury species using thermal desorption analysis in AAS. *Chemical Papers*, **68**, 427–434.

De Ferro, A.M., Mota, A.M. & Canário, J. 2014. Pathways and speciation of mercury in the environmental compartments of Deception Island, Antarctica. *Chemosphere*, **95**, 227–233.

De Moreno, J.E.A., Gerpe, M.S., Moreno, V.J. & Vodopivez, C. 1997. Heavy metals in Antarctic organisms. *Polar Biology*, **17**, 131–140.

Dissanayake, C.B. & Vincent, E.A. 1975. Mercury in rocks and minerals of the Skaergaard intrusion, East Greenland. *Mineralogical Magazine*, **40**, 33–42.

Fleischer, M. 1970. Summary of the literature on the inorganic geochemistry of mercury. *In Mercury in the environment*. Geological Survey Professional Paper 713. Washington, DC: United States Geological Survey, 67 pp.

Košler, J., Magna, T., Mlčoch, B., Mixa, P., Nývlt, D. & Holub, F.V. 2009. Combined Sr, Nd, Pb and Li isotope geochemistry of alkaline lavas from northern James Ross Island (Antarctic Peninsula) and implications for back-arc magma formation. *Chemical Geology*, **258**, 207–218.

Larsen, L.M. & Pedersen, A.K. 2009. Petrology of the paleocene picrites and flood basalts on Disko and Nuussuaq, West Greenland. *Journal of Petrology*, **50**, 1667–1711.

Lu, Z.B., Cai, M.H., Wang, J., Yang, H.Z. & He, J.F. 2012. Baseline values for metals in soils on Fildes Peninsula, King George Island, Antarctica: the extent of anthropogenic pollution. *Environmental Monitoring and Assessment*, **184**, 7013–7021.

CAMBRIDGE JOURNALS
http://journals.cambridge.org Downloaded: 28 Apr 2015 IP address: 147.231.204.183

Martin, R.S., Witt, M.L.I., Sawyer, G.M., Thomas, H.E., Watt, S.F.L., Bagnato, E., Calabrese, S., Aiuppa, A., Delmelle, P., Pyle, D.M. & Mather, T.A. 2012. Bioindication of volcanic mercury (Hg) deposition around Mt. Etna (Sicily). *Chemical Geology*, **310**, 12–22.

Martínez-Cortizas, A., Pontevedra-Pombal, X., García-Rodeja, E., Nóvoa-Muñoz, J.C. & Shotyk, W. 1999. Mercury in a Spanish peat bog: archive of climate change and atmospheric metal deposition. *Science*, **284**, 939–942.

Nývlt, D., Košler, J., Mlčoch, B., Mixa, P., Lisá, L., Bubík, M. & Hendriks, B.W.H. 2011. The Mendel Formation: evidence for late Miocene climatic cyclicity at the northern tip of the Antarctic Peninsula. *Palaeogeography, Palaeoclimatology, Palaeoecology*, **299**, 363–384.

Nývlt, D., Braucher, R., Engel, Z., Mlčoch, B. & ASTER team. 2014. Timing of the northern Prince Gustav Ice Stream retreat and the deglaciation of northern James Ross Island, Antarctic Peninsula during the last glacial-interglacial transition. *Quaternary Research*, **82**, 441–449.

Nie, Y., Liu, X.D., Sun, L.G. & Emslie, S.D. 2012. Effect of penguin and seal excrement on mercury distribution in sediments from the Ross Sea region, East Antarctica. *Science of the Total Environment*, **433**, 132–140.

Palme, H. & O'Neill, H.S.C. 2003. Cosmochemical estimates of mantle composition. *In* Holland H.D. & Turekian K.K., *eds. Treatise on geochemistry*, vol. 2. New York, NY: Elsevier, 1–38.

Pfaffhuber, K.A., Berg, T., Hirdman, D. & Stohl, A. 2012. Atmospheric mercury observations from Antarctica: seasonal variation and source and sink region calculations. *Atmospheric Chemistry and Physics*, **12**, 3241–3251.

Rudnick, R.L. & Gao, S. 2003. Composition of the continental crust. *In* Holland H.D. & Turekian K.K., *eds. Treatise on geochemistry*, vol. 3. New York, NY: Elsevier, 1–64.

Smellie, J.L., Johnson, J.S., McIntosh, W.C., Esser, R., Gudmundsson, M.T., Hambrey, M.J. & de Vries, B.V. 2008. Six million years of glacial history recorded in volcanic lithofacies of the James Ross Island Volcanic Group, Antarctic Peninsula. *Palaeogeography, Palaeoclimatology, Palaeoecology*, **260**, 122–148.

Vodrážka, R. & Crame, J.A. 2011. First fossil sponge from Antarctica and its paleobiogeographical significance. *Journal of Paleontology*, **85**, 48–57.

Zintwana, M.P., Cawthorn, R.G., Ashwal, L.D., Roelofse, F. & Cronwright, H. 2012. Mercury in the Bushveld Complex, South Africa, and the Skaergaard Intrusion, Greenland. *Chemical Geology*, **320**, 147–155.

CAMBRIDGE JOURNALS
http://journals.cambridge.org Downloaded: 28 Apr 2015 IP address: 147.231.204.183

Příloha VII

Bull Environ Contam Toxicol (2014) 93:503–508
DOI 10.1007/s00128-014-1289-3

Seasonal Variability of Mercury Contents in Street Dust in Brno, Czech Republic

Pavel Coufalík · Ondřej Zvěřina · Pavel Mikuška · Josef Komárek

Received: 6 February 2014 / Accepted: 29 April 2014 / Published online: 10 May 2014
© Springer Science+Business Media New York 2014

Abstract Environmental contamination by mercury carries serious risks to the biosphere. Urban agglomerations burdened with traffic are characterized by substantial dust levels, including high concentrations of pollutants bound to particulate matter. In this research, the content of particulate mercury in street dust was investigated in relation to the season and traffic intensity. In total, 80 street dust samples were collected in the centre of Brno (Czech Republic) in which total and bioaccessible mercury contents were determined. Total mercury content in the samples ranged from 0.03 to 2.67 mg/kg. The content of bioaccessible mercury was below the limit of quantification in all samples. Thus, street dust did not increase the daily mercury intake by the population in studied area. A clear trend of mercury accumulation in street dust depending on traffic intensity in the investigated streets was not observed over the whole year.

Keywords Particulate mercury · Accumulation · Street dust · Re-suspension

Air pollution with heavy metals represents a serious health hazard (WHO 2007). Mercury is a highly dangerous contaminant which is transported over long distances from its source. Anthropogenic sources include industrial production as well as fuels burning in vehicles (Stamenkovic et al. 2007), which contribute to the contamination of the urban environment especially in larger agglomerations. In urban areas, mercury concentrations exhibit a higher variability than in rural areas. This trend is partly influenced by meteorological conditions. The condensation of mercury forms on particles in the atmosphere occurs more in winter months, which increases the content of particulate mercury (HgP) in the dust (Liu et al. 2007).

The harmful effects of dust particles are proportional to their aerodynamic diameter; particles below 10 μm in size (PM_{10}) and especially below 2.5 μm ($PM_{2.5}$) pose serious health risks (Amato et al. 2010; Charlesworth et al. 2011). In the urban environment, re-suspended street dust is often a source of these particles (Charlesworth et al. 2011; Žibret et al. 2013). Contamination by dust particles can be studied after the sampling of aerosols (Liu et al. 2007) or after the direct sampling of street dust (Amato et al. 2011; Hu et al. 2011). Street profile is significant for the accumulation of pollutants in street dust due to the character of the air flow in the built-up area, which can be described by a mathematical model (Kauhaniemi et al. 2011). Street canyons formed by close buildings with a specific air flow (Pospíšil and Jícha 2010) affect the re-suspension of deposited particulate material. The immediate meteorological conditions, particularly wind speed, humidity and precipitation, are also important in the re-suspension process. The re-suspension of particles larger then 2.5 μm is the most important source of urban air contamination during dry periods (Pospíšil and Jícha 2010). Dust particle re-emission also varies according to the region (Amato et al. 2011).

This research was aimed at an assessment of the seasonal contamination of street dust by mercury in an urban environment burden with heavy traffic.

P. Coufalík (✉) · O. Zvěřina · J. Komárek
Faculty of Science, Masaryk University, Kotlářská 2, 611 37 Brno, Czech Republic
e-mail: coufalik@iach.cz

P. Coufalík · P. Mikuška
Institute of Analytical Chemistry, Academy of Sciences of the Czech Republic, v.v.i., Veveří 97, 602 00 Brno, Czech Republic

Materials and Methods

The city of Brno (49°12′N, 16°36′E) was selected for the study of the seasonal variability of street dust contamination by mercury. Brno is the second largest city in the Czech Republic with approximately 400,000 inhabitants. Pollutant limits for human health are exceeded in this location over long periods; traffic was identified as the main source of pollutants in Brno (CHMI 2012; Skeřil and Elfenbein 2010). The long-term measurement of PM_{10} and $PM_{2.5}$ concentrations is performed by the Czech Hydrometeorological Institute (CHMI) through a network of measuring stations.

The highest average annual concentrations of PM_{10} were recorded at the following stations: Brno – Svatoplukova (39 μg/m^3 in 2011, 34.6 μg/m^3 in 2012) with daily peaks up to 70 μg/m^3, Brno – Centre on Kotlářská Street (37.5 μg/m^3 in 2012), and Brno – Úvoz (30.7 μg/m^3 in 2011, 30.3 μg/m^3 in 2012). The $PM_{2.5}$ annual limit (defined as the average annual concentration of $PM_{2.5}$ of 25 μg/m^3) was exceeded at the following stations: Brno – Svatoplukova and Brno – Zvonařka (in 2011). The number of days in 2011 with concentrations of PM_{10} above the daily limit (i.e. 50 μg/m^3) was highest at the following stations: Brno – Svatoplukova (85 day), Brno – Centre (77 day) and Brno – Úvoz (45 day) (CHMI 2012; CHMI 2013). Concentrations of particulate matter (CHMI 2012; CHMI 2013) in three sampling sites before the dates of sampling are presented in Table 1.

Streets forming a transit route through the city are significantly burdened with heavy traffic. Zvonařka Street and Opuštěná Street are known as sites with the heaviest traffic in the city centre, with approximately 37,800 vehicles per day, of which 12 % are heavy goods vehicles (RMD 2010). These are followed by Kotlářská Street with 32,500 vehicles per day, of which 3 % are heavy goods vehicles (Adamec et al. 2010), and Poříčí Street with 29,500 vehicles per day, of which 12 % are heavy goods vehicles (RMD 2010).

Table 1 Average concentrations of PM before dates of sampling (μg/m^3)

	PM in time interval before dates of sampling			
	4th–10th May	20th–25th Aug	27th Oct–10th Nov	23rd Jan–2nd Feb
Zvonařka PM10	22.7	–	53.5	56.9
Zvonařka PM2.5	16.4	–	52.3	54.9
Úvoz PM10	23.6	26.2	60.6	56.4
Centre PM10	27.8	36.1	80.5	76.8

– Data not available

Ten sampling sites were selected for the collection of street dust samples. Two samples were collected from each site (road), 100–200 m apart (Fig. 1). The aim was to cover the streets with the heaviest traffic (i.e. Zvonařka, Opuštěná, Poříčí, Úvoz, Kotlářská, Provazníkova, Lidická, Štefánikova), reference sites with low traffic intensity (i.e. Tučkova, Hrnčířská, Heinrichova, Muchova, Lužova), and the historical centre (i.e. Veselá). Sample collection was carried out directly from the road surface by sweeping an area of 1 m^2 using polyethylene (PE) implements. Sample collection was conducted during dry weather without any rainfall (the time interval is specified in Table 1) and without prior road cleaning. Collections were carried out on the 10th May, 25th August, and 10th November, 2011, and on the 2nd February, 2012. First, the samples were dried at room temperature in a clean laboratory and then sieved through a nylon sieve (Linker Industrie-Technik, Germany). The size fraction below 63 μm was used for further analysis. Samples were stored in PE containers in a refrigerator at a constant temperature of 4°C.

Samples of street dust were analyzed immediately after treatment. Total mercury contents in dust samples were determined using an AMA-254 atomic absorption spectrometer (Altec, Czech Republic). This single-purpose spectrometer is designed for the direct measurement of liquid and solid samples and is equipped with an amalgamator for the preconcentration of mercury atoms. Calibration was performed using the certified reference material CRM for AAS – $Hg(NO_3)_2$ in 2 mol/L HNO_3 (1,000 mg/L ± 4 mg/L Hg^{2+}, Fluka, Germany). Six parallel analyses were carried out for each sample (the weight of 100 mg per one analysis). The determination of total mercury content in solid material was verified by the CRM 020 Trace Metals – Sandy Loam 2 (RTC, USA) with a total mercury content of 1.12 ± 0.03 mg/kg.

In addition, the content of inaccessible mercury forms in dust samples was also measured. Two extraction procedures were used: SBET (Hu et al. 2011; Oomen et al. 2002), defined as the extraction simulating a release under gastric fluid conditions, and an extraction into deionized water (Coufalík et al. 2012). Mercury content in the extracts was also determined by the AMA-254 analyzer.

Results and Discussion

The total mercury content was determined in all collected samples of street dust. The limit of quantification for total mercury content in solid samples was 0.3 μg/kg. The results are presented in Fig. 2, including standard deviations of the measurements. The character of street dust contamination, including the influence of local conditions, can be evaluated from the obtained set of data covering

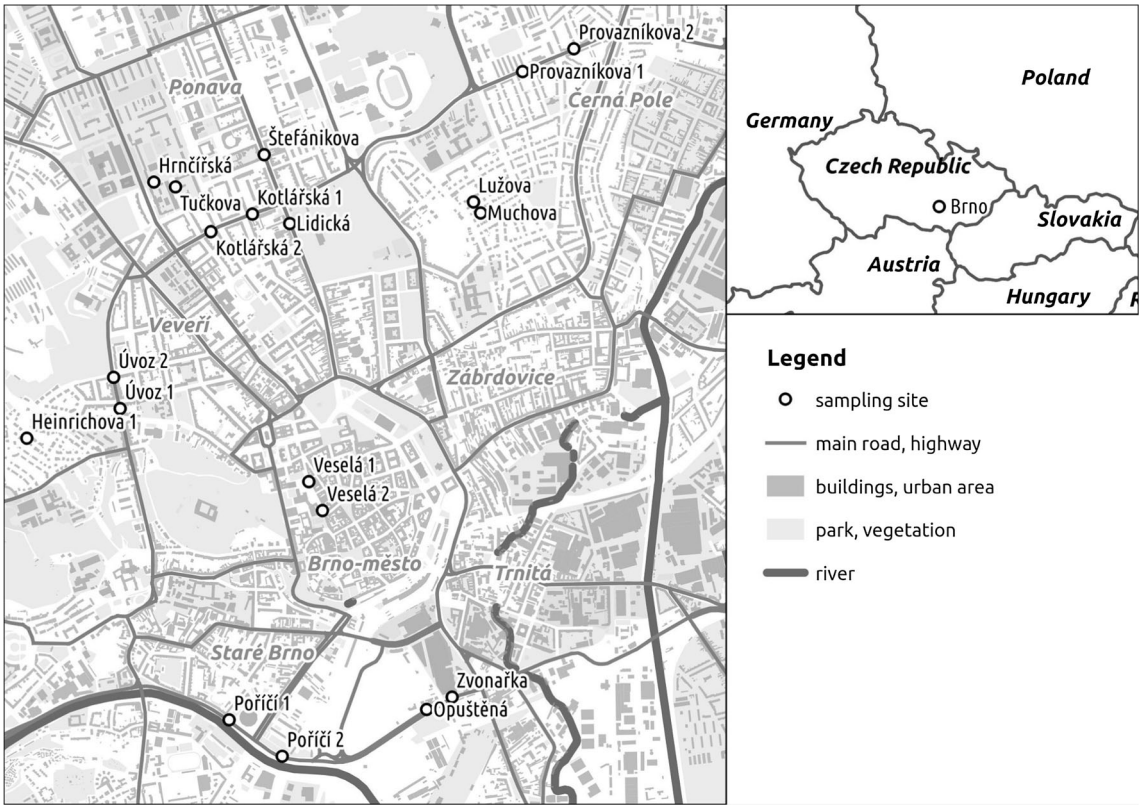

Fig. 1 Sampling sites in the city of Brno

twenty sampling sites over four seasons. Parallel collection at the investigated sampling sites is indicated by the presentation of results in the same chart (Fig. 2a–j). However, the conformity of mercury concentrations in the monitored sections of road cannot be expected due to the relatively large distances between sampling sites.

It is obvious that the degree of environmental contamination relating to mercury at the investigated sites corresponds to polluted urban areas (Hu et al. 2011). Nevertheless, total mercury concentrations fluctuated by up to 0.4 mg/kg, even in streets with heavy traffic. The only exception was Veselá Street in the historical centre (Fig. 2h). In general, the mercury content in exhaust gas from burning petroleum-based fuels is relatively low, nevertheless, exact data on the concentration and fate of the mercury in common fuels is lacking (Wilhelm and Bloom 2000). The impact of traffic was also observable in this case. The lowest total mercury concentrations were determined in residential neighbourhoods with low traffic intensity (Fig. 2i and j). The total mercury contents in Úvoz and Kotlářská Street (Fig. 2c and d) were several times higher. However, this trend is not entirely transparent. 37,800 vehicles per day passed through sampling sites represented in Fig. 2a, 29,500 through the Poříčí 2 site (Fig. 2b), and 19,300 vehicles through the Poříčí 1 site (RMD 2010). Thus, the ratio of total mercury concentrations between samples corresponded approximately to the traffic intensity.

The re-suspension, i.e. re-emission, of formerly deposited particles in relation to street profile can be an important factor in explaining differences in mercury concentration at individual sampling sites. Most of Poříčí Street is not lined by buildings, which allows the free runoff of particles by airflow induced by the movement of vehicles (Jícha et al. 2000). Kotlářská Street is considered to be a street canyon (Pospíšil and Jícha 2010); nonetheless, samples from this street exhibited increased concentrations only in spring 2011 (Fig. 2d). Úvoz Street, with a similar character of buildings, had also increased mercury contents (Fig. 2c). It is a question whether the extremely high autumn concentration in Veselá Street in the historical centre was associated with a deposition of particulate material or was only random contamination of the roadway of an anthropogenic character, e.g. from a broken thermometer (Fig. 2h). Enhanced total mercury concentrations in dust samples were observed in May 2011 in streets that are part of the transit route around the city centre (Fig. 2a, c, d and e). This phenomenon could be the result of increased re-emissions due to road cleaning in the spring period (Salonen et al. 2004).

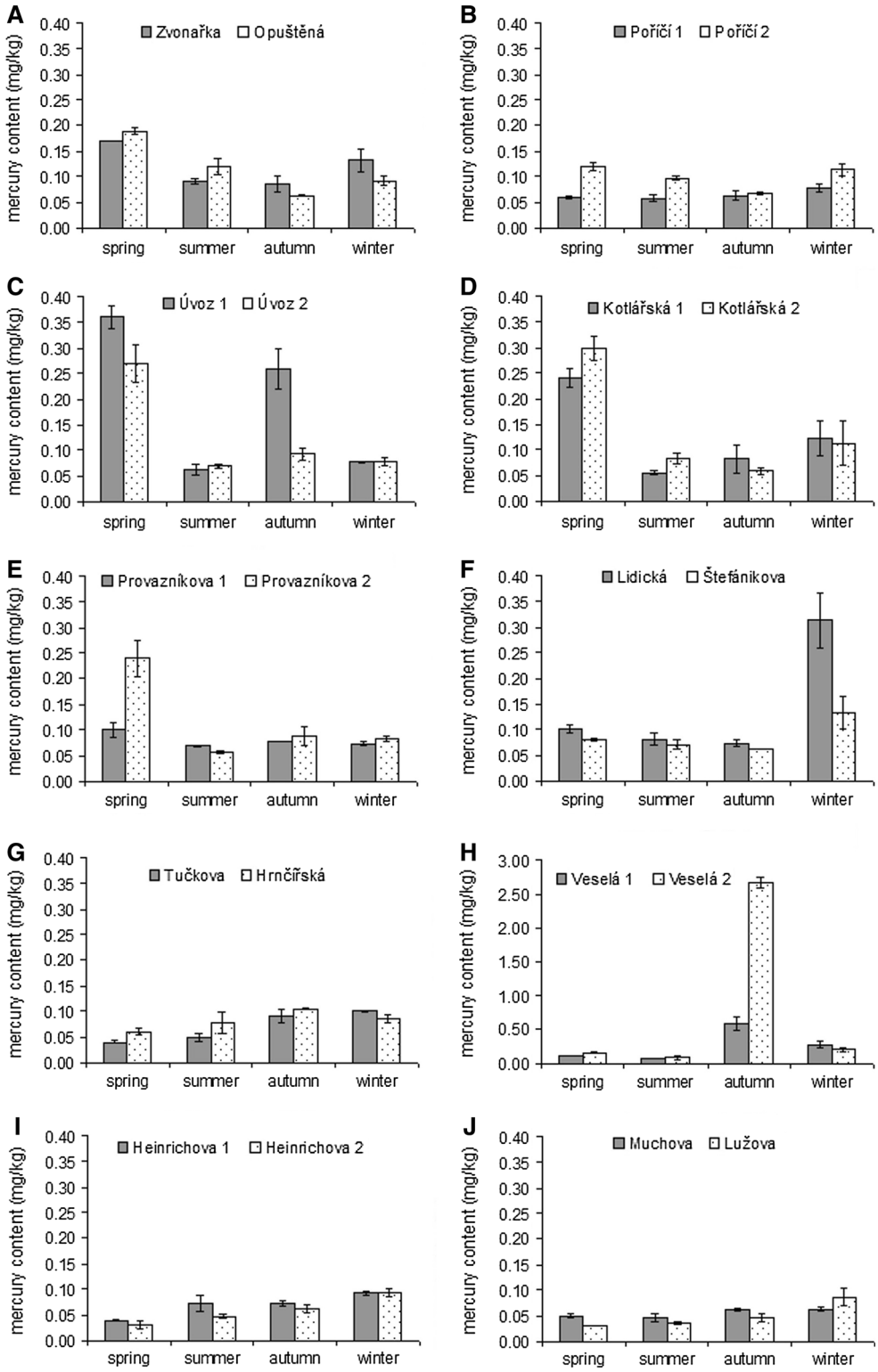

Fig. 2 Mercury contents in street dust

The degree of contamination at the studied sites differed between seasons partially due to the number of days with high levels of dustiness before the date of sampling (Table 1). High concentrations of dust particles in air were registered mainly in November 2011 and in January and February 2012 (CHMI 2012; CHMI 2013). November 2011 was also characterized by very low rainfall. Data related to the dustiness in Brno are available only for few sampling sites with heavy traffic. The highest dustiness was observed in autumn and winter, which probably originated

from enhanced emissions due to biomass and coal combustion. Increased amount of particulate matter could increase mercury concentrations in deposition areas – i.e. areas with low air flow or low traffic intensity. It can be assumed, that the time interval without any precipitation also affects the amount of particulate matter. An adsorption of gaseous mercury on present aerosol was confirmed for PM >2.5 μm (Keeler et al. 1995). According to the data from Zvonařka Street (Table 1), the particulate matter consists mainly of size fraction PM 2.5 during the sampling period in autumn and winter. It may be the reason, that the dustiness did not directly impact the mercury concentrations in street dust in Zvonařka Street and Úvoz Street. Another important accumulation factor for mercury is air temperature. The periods prior to the sampling in autumn 2011 and especially in winter 2012 were characterized by a high number of days with minimum temperatures below 0°C (CHMI 2014). These circumstances are also evident in the results, especially in the case of streets with low traffic intensity (Fig. 2g, i and j), which can better demonstrate the influence of accumulation conditions. Concentrations of gaseous mercury in the atmosphere are influenced by the temperature, but also the concentrations of particulate mercury tend to be higher in winter. Besides, this mercury form deposits near the source of pollution (Schroeder and Munthe 1998). Thus, it is apparent that the contamination of street dust by mercury varied during the year depending on casual re-suspension, weather conditions and, in general, was not directly linked to the traffic intensity in a particular street.

Bioaccessible mercury can constitute a significant part of the total content in highly polluted urban areas (Hu et al. 2011). The concentration of bioaccessible mercury in the dust samples was also studied in this research because of the possible health risk to the population. However, the content of bioaccessible mercury in all collected samples in Brno was below the limit of quantification for both extractions −1.5 μg/kg for SBET extraction and 2 μg/kg for extraction in water. It appears that street dust did not directly increase the daily intake of mercury by the population at the studied localities.

Conclusion

Mercury contamination of street dust in Brno, Central Europe, reached concentrations comparable with large Chinese agglomerations, although it was not extreme. On the basis of the analysis of samples from selected urban sites, traffic as well as dustiness, rainfall and temperature were proven to have simultaneous influence on the accumulation of mercury in the dust. The resulting total mercury concentrations were probably related to the re-suspension of deposited material. Bioaccessible mercury was below the limit of quantification over the whole year at all studied sites. Thus, particulate mercury in Brno did not represent a direct health risk.

Acknowledgments This research was financially supported by the Grant Agency of the Czech Republic, project P503/12/0682. The work was also supported by the Institute of Analytical Chemistry of the ASCR under the Institutional research plan RVO: 68081715.

References

Adamec V, Huzlík J, Ličbinský R, Effenberger K, Mikuška P, Večeřa Z, Dočekal B, Vojtěšek M (2010) Morphology, chemical and toxicological characterisation of road dust and particulate matter including sources apportionment. Final report – project SP/1a3/55/08, 2008–2010, Ministry of the Environment of the Czech Republic (in Czech)

Amato F, Querol X, Johanson C, Nagl C, Alastuey A (2010) A review on the effectiveness of street sweeping, washing and dust suppressants as urban PM control methods. Sci Total Environ 408:3070–3084

Amato F, Pandolfi M, Moreno T, Furger M, Pey J, Alastuey A, Bukowiecki N, Prevot ASH, Baltensperger U, Querol X (2011) Sources and variability of inhalable road dust particles in three European cities. Atmos Environ 45:6777–6787

Charlesworth S, De Miguel E, Ordóñez A (2011) A review of the distribution of particulate trace elements in urban terrestrial environments and its application to considerations of risk. Environ Geochem Health 33:103–123

CHMI (2012) Air pollution in the Czech Republic in 2011. Czech Hydrometeorological Institute, Praha

CHMI (2013) Air pollution in the Czech Republic in 2012. Czech Hydrometeorological Institute, Praha

CHMI (2014) Historical data from meteorological station Brno-Tuřany 2011 and 2012. http://portal.chmi.cz/portal/dt?action=content&provider=JSPTabContainer&menu=JSPTabContainer/P3_0_Informace_pro_Vas/P3_9_Historicka_data/P3_9_1_Pocasi/P3_9_1_9_Mesicni_data&nc=1&portal_lang=en#PP_Mesicni_data. Accessed 29th January, 2014

Coufalík P, Krásenský P, Dosbaba M, Komárek J (2012) Sequential extraction and thermal desorption of mercury from contaminated soil and tailings from Mongolia. Center Eur J Chem 10:1565–1573

Hu X, Zhang Y, Luo J, Wang T, Lian H, Ding Z (2011) Bioaccessibility and health risk of arsenic, mercury and other metals in urban street dusts from a mega-city, Nanjing, China. Environ Pollut 159:1215–1221

Jícha M, Pospíšil J, Katolický J (2000) Dispersion of pollutants in street canyon under traffic induced flow and turbulence. Environ Monit Assess 65:343–351

Kauhaniemi M, Kukkonen J, Härkönen J, Nikmo J, Kangas L, Omstedt G, Ketzel M, Kousa A, Haakana M, Karppinen A (2011) Evaluation of a road dust suspension model for predicting the concentrations of PM_{10} in a street canyon. Atmos Environ 45:3646–3654

Keeler G, Glinsorn G, Pirrone N (1995) Particulate mercury in the atmosphere: its significance, transport, transformation and sources. Water Air Soil Pollut 80:159–168

Liu B, Keeler GJ, Dvonch JT, Barres JA, Lynam MM, Marsik FJ, Morgan JT (2007) Temporal variability of mercury speciation in urban air. Atmos Environ 41:1911–1923

Oomen AG, Hack A, Minekus M, Zeijdner E, Cornelis C, Schoeters G, Verstraete W, Van De Wiele T, Wragg J, Rompelberg CJM, Sips AJAM, Van Wijnen JH (2002) Comparison of five in vitro digestion models to study the bioaccessibility of soil contaminants. Environ Sci Technol 36:3326–3334

Pospíšil J, Jícha M (2010) Particle re-suspension in city areas with intensive traffic. In: Adamec V, Jandová V (eds) Transport Health and Environment. Transport Research Centre, Brno, pp 39–46

RMD (2010) Traffic intensity 2010. Road and motorway directorate of the Czech Republic http://scitani2010.rsd.cz. Accessed 29th January, 2014 (in Czech)

Salonen RO, Hälinen AI, Pennanen AS, Hirvonen MR, Sillanpää M, Hillamo R, Shi T, Borm P, Sandell E, Koskentalo T, Aarnio P (2004) Chemical and in vitro toxicologic characterization of wintertime and springtime urban-airparticles with an aerodynamic diameter below 10 μm in Helsinky. Scand J Work Environ Health 30:80–90

Schroeder WH, Munthe J (1998) Atmospheric mercury: an overview. Atmos Environ 32:809–822

Skeřil R, Elfenbein Z (2010) The traffic influence on the air-quality in Brno. In: Adamec V, Jandová V (eds) Transport Health and Environment. Transport Research Centre, Brno, pp 63–67

Stamenkovic J, Lyman S, Gustin MS (2007) Seasonal and diel variation of atmospheric mercury concentrations in the Reno (Nevada, USA) airshed. Atmos Environ 41:6662–6672

WHO (2007) Health risks of heavy metals from long-range transboundary air pollution. World Health Organization, Germany

Wilhelm SM, Bloom N (2000) Mercury in petroleum. Fuel Process Technol 63:1–27

Žibret G, Van Tonder D, Žibret L (2013) Metal content in street dust as a reflection of atmospheric dust emissions from coal power plants, metal smelters, and traffic. Environ Sci Pollut Res 20:4455–4468

Příloha VIII

Environ Sci Pollut Res (2017) 24:1424–1431
DOI 10.1007/s11356-016-7879-3

RESEARCH ARTICLE

Leaching of mercury from seal carcasses into Antarctic soils

Ondřej Zvěřina[1,2] · Pavel Coufalík[2,3] · Kristián Brat[4,5] · Rostislav Červenka[6] · Jan Kuta[6] · Ondřej Mikeš[6] · Josef Komárek[2]

Received: 21 April 2016 / Accepted: 10 October 2016 / Published online: 25 October 2016
© Springer-Verlag Berlin Heidelberg 2016

Abstract More than 400 seal mummies and skeletons are now mapped in the northern part of James Ross Island, Antarctica. Decomposing carcasses represent a rare source of both organic matter and associated elements for the soil. Owing to their high trophic position, seals are known to carry a significant mercury body burden. This work focuses on the extent of the mercury input from seal carcasses and shows that such carcasses represent locally significant sources of mercury and methylmercury for the environment. Mercury contents in soil samples from the surrounding areas were determined using a single-purpose AAS mercury analyzer. For the determination of methylmercury, an ultra-sensitive isotopic dilution HPLC-ICP-MS technique was used. In the soils lying directly under seal carcasses, mercury contents were higher, with levels reaching almost 40 μg/kg dry weight of which methylmercury formed up to 2.8 % of the total. The spatial distribution implies rather slow vertical transport to the lower soil layers instead of a horizontal spread. For comparison, the background level of mercury in soils of the investigated area was found to be 8 μg/kg dry weight, with methylmercury accounting for less than 0.1 %. Apart from the direct mercury input, an enhanced level of nutrients in the vicinity of carcasses enables the growth of lichens and mosses with accumulative ability with respect to metals. The enhanced capacity of soil to retain mercury is also anticipated due to the high content of total organic carbon (from 1.6 to 7.5 %). According to the results, seal remains represent a clear source of mercury in the observed area.

Keywords Mercury · Methylmercury · Seal · Soil · Antarctica

Responsible editor: Philippe Garrigues

✉ Ondřej Zvěřina
zverina@med.muni.cz

[1] Department of Public Health, Faculty of Medicine, Masaryk University, Kamenice 5, 625 00 Brno, Czech Republic

[2] Department of Chemistry, Faculty of Science, Masaryk University, Kotlářská 2, 611 37 Brno, Czech Republic

[3] Institute of Analytical Chemistry, The Czech Academy of Sciences, v.v.i., Veveří 97, 602 00 Brno, Czech Republic

[4] Department of Respiratory Diseases and TB, Faculty of Medicine, Masaryk University, Kamenice 5, 625 00 Brno, Czech Republic

[5] Department of Respiratory Diseases and TB, University Hospital Brno, Jihlavská 20, 625 00 Brno, Czech Republic

[6] Research Centre for Toxic Compounds in the Environment (RECETOX), Faculty of Science, Masaryk University, Kamenice 5, 625 00 Brno, Czech Republic

Introduction

Antarctica is a continent partially isolated from the input of lower latitude contaminants by natural barriers, such as circumpolar atmospheric and oceanic currents (Barker and Thomas 2004). Thanks to this, the anthropogenic impact is limited mainly to the vicinity of scientific stations (Santos et al. 2005; Bargagli 2008). Specific conditions of polar regions provide a unique opportunity to study mercury (Hg) cycling in the ecosystem (Bargagli 2005, 2008). This work follows recent studies on Hg occurrence and cycling in the ecosystems and geosystems of James Ross Island (JRI; Fig. 1), Antarctica. Previously conducted research revealed some particularities of Hg distribution and speciation in soils, sediments, and lichens in the JRI area (Zvěřina et al. 2014; Coufalík et al. 2015). In this study, the focus was placed on decaying carcasses of seals, scattered numerously across the ice-free areas of JRI, as potential sources of Hg for Antarctic soils.

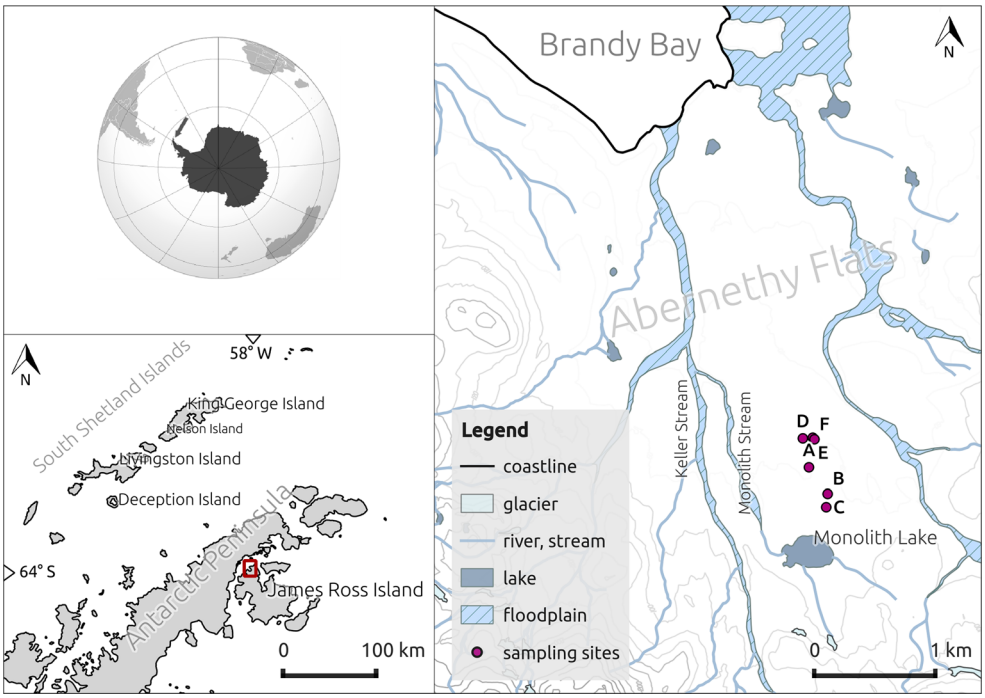

Fig. 1 Map showing the locations of sample collection. Twenty-meter contours are shown. Modified map of James Ross Island—northern part (Czech Geological Survey 2009)

Unlike other metals, Hg is biomagnified in the marine food chain (Gray 2002). It is well documented that high-trophic level organisms have considerably higher Hg contents in comparison with those at the bottom of the food chain (Bargagli et al. 1998; Nie et al. 2012). Compared to the rather low levels of Hg found in primary producers in Antarctica, levels found in predators seem to be similar to those reported for animals of the northern hemisphere (Bargagli et al. 1998). Top predators such as birds or seals are the main accumulators and carriers of trace metals in the ice-free areas of Antarctica (Yin et al. 2007; Nie et al. 2012). The biological transport of pollutants by biovectors such as gregarious animals is often ignored. In many cases, however, it can become a predominant pathway for contaminants (Blais et al. 2007). Due to the excessively high number of dead seals scattered across the northern part of JRI, the environmental consequences are worth exploring. The advantage of the studied area lies in the fact that Hg levels in soils are low and relatively homogeneous (Coufalík et al. 2015). Due to a very low natural background level of Hg, the area offers unique opportunity for research into the spread of Hg from point sources and its fate in the environment.

Mummified seals have been studied in many Antarctic and sub-Antarctic regions (Péwé et al. 1959; Gordon and Harkness 1992; Nelson et al. 2008). Today, more than 400 seal mummies and skeletons are mapped in the northern part of JRI (Nelson et al. 2008; Nývlt et al. 2016). Decomposing carcasses represent a rare source of both organic matter and associated elements for the soil. Since pinnipeds remain at the top of the Antarctic food web, it is known that they contain a significant concentration of Hg. Levels of Hg have already been determined in seal fur, blood, kidney, liver, and other tissues (Yamamoto et al. 1987; Szefer et al. 1993; de Moreno et al. 1997; Bargagli et al. 1998; Wagemann et al. 2000), ranging from tenths to more than hundredths of milligrams per kilogram. It was reported that seal hair contains the greatest Hg concentration, followed by liver, kidney, and muscle (Szefer et al. 1993; Brookens et al. 2008).

Being generally the most abundant seal species, the crabeater seal (*Lobodon carcinophagus*) is also the predominant species within the seal remains found in the investigated area. A typical adult weighs approximately 200 kg (Laws et al. 2003). In most biomagnification studies, whole organisms at the bottom of the food chain are analyzed in contrast to specific tissues of larger animals at the top of the food chain (Gray 2002). Thus, estimation of the total amount of mercury accumulated in the seal body is problematic. A total body burden of about 7 mg Hg was estimated in Pacific harbor seal pups younger than 2 months (Brookens et al. 2008). However, the Hg concentration in the seal body increases with age (Ikemoto et al. 2004; Brookens et al. 2007).

Since Hg is highly toxic, pinnipeds have developed various protective mechanisms (Bargagli et al. 1998). The Hg is cumulated in the liver due to the fact that this organ is responsible for its detoxification (Wagemann et al. 2000). Apart from the formation of insoluble mercury selenide (HgSe) in the liver, the main processes of seal detoxication are based on metallothionein metabolism and the production of new pelage via Hg excretion in hair (Bargagli et al. 1998; Wagemann et al. 2000; Yin et al. 2007; Habran et al. 2011; Jakimska et al. 2011; Cossaboon et al. 2015). Molted pelage was recently identified

as a significant source of Hg for the coastal environment and as a source of top-down contamination of the marine food chain (Cossaboon et al. 2015).

When a seal dies, decomposition begins and the carcass gradually releases both nutrients and contaminants into the environment. In low temperature regions such as Antarctica, the decay process advances very slowly. The decay (taphonomic) state, geographic distribution, and several other parameters describing seal carcasses in the northern part of JRI were already documented (Nelson et al. 2008; Nývlt et al. 2016). According to the preservation state, seal carcasses are classified into five categories from T1, characterized as a well-preserved complete seal corpse, to T5, characterized as a group of disarticulated bones (Nývlt et al. 2016).

In this study, samples of soil surrounding seal carcasses were collected and analyzed for their contents of Hg, methylmercury (MeHg), and total organic carbon (TOC). The main aim was to assess the extent of Hg input from these seal carcass sources. As the levels of Hg in surface soils of Antarctica are generally low (Matsumoto et al. 1983; Bargagli et al. 2007; Coufalík et al. 2015), it is assumed that the input of Hg can be significant on a local scale.

Sampling area

Samples for this study were collected during the Czech Antarctic expedition to the Johann Gregor Mendel (JGM) research station in the austral summer of 2015. The station is located in the northern part of James Ross Island (Fig. 1). JRI is the largest single outcrop of the James Ross Island Volcanic Group (JRIVG)—a c. 6000 km^2 large basaltic volcanic field situated in the northern Antarctic Peninsula (Košler et al. 2009; Smellie 2013). The island itself has an area of ca. 2500 km^2, of which about 20 % is permanently deglaciated (Rabassa et al. 1982). The coastal areas became ice-free by approx. 12.9 ka (Nývlt et al. 2014). The landscape of the northern part of JRI is characterized by Cretaceous marine sediments of the James Ross Basin that were overlain by alkaline volcanic rocks of JRIVG (Crame et al. 1991; Nývlt et al. 2011; Davies et al. 2013; Nehyba and Nývlt 2015). Erratic boulders are scattered over sedimentary and volcanic bedrock, and only small glaciers remain in the present landscape (Engel et al. 2012; Davies et al. 2013). The samples were collected in the flat and low-lying Abernethy Flats, which are readily accessible for seals from the shallow sea bay (Nývlt et al. 2016). The landscape of the valley is relatively flat, characterized by a gradual increase in altitude from the broad Brandy Bay towards the south. The samples for this work were collected in the vicinity of Monolith Lake, which lies at 67 m a.s.l.

In total, more than 400 individual seal carcasses are documented in the northern part of JRI (Nývlt et al. 2016). Most of them are located in the ice-free part of Abernethy Flats, with the crabeater seal (*L. carcinophagus*) being by far the most abundant species (Nelson et al. 2008; Nývlt et al. 2016). Most carcasses are located at elevations below 100 m a.s.l. over a 10-km^2 area of Abernethy Flats (Nývlt et al. 2016). For this work, six carcasses of crabeater seal were selected in the vicinity of Monolith Lake at the southern part of Abernethy Flats (Fig. 1). Crabeater seals were identified by their characteristic jagged teeth (Nelson et al. 2008).

According to their taphonomic state, the seal carcasses were classified into the five categories mentioned above (Nývlt et al. 2016). Carcasses in states T1 and T5 were not selected. As T1 is defined as a well-preserved seal corpse, no leaching of body fluids or tissues into the environment can be expected. At the other extremes, as T5, the most advanced decay state, is characterized by individual bones, little information can be gleaned about the former position or age of such mummies (up to one century old; (Nývlt et al. 2016)). According to the purposes of the present study, seals in decay states T2 (samples A, B), T3 (samples C, D), and T4 (samples E, F) were selected (Fig. 2).

Soil samples were systematically collected directly under the seal carcass and at distances 0.5 and 1 m in four directions from the carcass (Fig. 2). In addition, samples of uncontaminated soil from the nearby surroundings of each seal were taken. Samples of both the upper (0–5 cm) and lower soil layers (5–10 cm) were carefully collected using a stainless steel shovel. In total, 120 soil samples were collected in the vicinities of six seal carcasses. At the laboratory of the JGM Antarctic station, the samples were dried at approximately 15 °C for 48 h to constant weight. The dry material was sieved through nylon sieve and the fraction under 2 mm was used. The samples were then stored in double polyethylene bags and kept at −18 °C until analysis.

Analytical procedures

Total mercury contents (Hg_T) in soil samples were determined using a single-purpose analyzer AMA-254 (Altec,

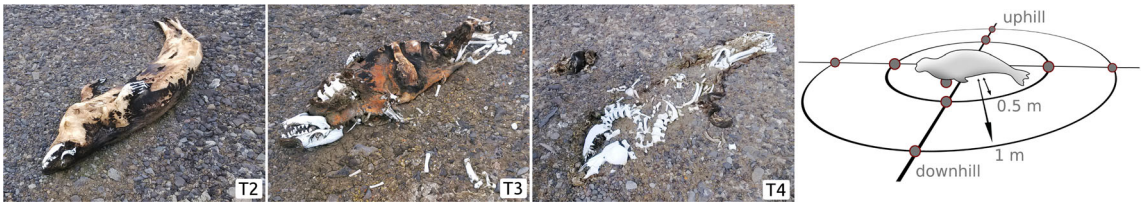

Fig. 2 Seal carcasses A, D, and F in decay states T2, T3, and T4, respectively

Czech Republic). An amount of 150 mg of each sample was introduced into the analyzer directly in the solid state. Determination was based on dry decomposition followed by amalgamation preconcentration and AAS detection. The accuracy of the method was verified by means of the reference material CRM 020 Trace Metals - Sandy Loam 2 (RTC, USA) with a total mercury content of 1.12 ± 0.03 mg/kg. The excellent analytical recovery of 99.4 ± 1 % was obtained. The limit of quantification was 0.3 μg Hg/kg.

MeHg contents in samples were determined after acid digestion and liquid-liquid extraction and back-extraction to the aqueous phase. First, 500 mg of soil sample was extracted with 7 mL of 6 mol/L HCl (Sigma-Aldrich, Germany) on an end-over-end shaker. After centrifugation, an aliquot of 2 mL was spiked with a solution of ^{198}Hg-enriched methylmercury (EMMS-1, National Research Council, Canada) and extracted twice with 3 mL of toluene (Sigma-Aldrich, Germany). The combined organic extract was subjected to back-extraction with 0.5 mL of an aqueous solution of 1 % L-cysteine (Sigma-Aldrich, Germany). Final analysis was performed by means of HPLC-ICP-MS. A reversed-phase chromatographic column (Synergi Hydro–RP, 150 mm × 4.6 mm, 4 μm) combined with an Agilent 7700× quadrupole ICP-MS spectrometer was used for analysis. The accuracy of the procedure was checked using certified reference material ERM-CC580 estuarine sediment (IRMM, Belgium) with a certified MeHg content of 75 ± 4 μg/kg. Measured concentrations of MeHg were within the certified range. Method precision (relative standard deviation, RSD) estimated from three replicate analyses of soil samples ranged from 4.2 to 9.4 %. Mean recovery of MeHg from ^{198}MeHg-spiked real samples was 89 ± 4 %.

The contents of organic carbon were determined using a Vario TOC cube analyzer (Elementar, Germany). An amount of 50 mg of sample was weighed into a Ag foil. The sample was then treated by the addition of sufficient amount of 1 M HCl and dried at 75 °C. Determination of the organic carbon content has been performed by catalytic high-temperature oxidation of the samples with non-dispersive infrared detection.

All the procedures were conducted in a clean laboratory equipped with HEPA filters. The glassware used was thoroughly decontaminated with HNO_3 (1:3) and also by heating to 250 °C for 2 h.

Results and discussion

Total mercury contents

Generally, the total mercury content (Hg_T) in uncontaminated Antarctic soils usually ranges from tenths to almost hundredths of micrograms per kilogram (Bargagli et al. 1993, 1998, 2005; Lu et al. 2012; Nie et al. 2012; Coufalík et al. 2015). Background mercury levels in the northern part of JRI were already described in the previous studies (Zvěřina et al. 2014; Coufalík et al. 2015). In the samples collected in Abernethy Flats, Hg_T ranged from 7.3 to 11.0 μg/kg (Coufalík et al. 2015). Comparable background level of Hg_T (9 ± 1 μg/kg) was reported by Yin et al. (2007) for weathering soils of Nelson Island in South Shetlands (Fig. 1). For the Fildes Peninsula of King George Island, Lu et al. (2012) calculated the baseline of Hg in soil as 13 μg/kg. Highly variable contents of Hg_T from 0.5 μg/kg (in stream sediments) and 10 mg/kg (in the center of fumarole) were reported for Deception Island by de Ferro et al. (2014). Nevertheless, the Hg_T levels in the surface regolith across the northern part of JRI are considered to be rather uniform and homogeneous (Coufalík et al. 2015). Similarly to the abovementioned studies, an Hg content of 8.0 ± 1.2 μg/kg dry weight (dry wt.) was determined as the background level in the area of interest of this work.

Samples collected at distances of 0.5 and 1 m from the carcasses in different radial directions did not contain elevated mercury levels, with Hg_T ranging from 6.3 to 8.6 μg/kg dry wt. No relative elevation was observed even in samples collected in a downhill direction from the carcasses. However, elevated Hg levels were found in samples collected under the seal carcasses. As noted in Fig. 3, Hg levels in soils lying directly under the carcasses were up to five times higher than the background level. Relatively higher Hg_T contents were observed in the upper soil layers under the carcasses in decay states T2 and T3. Higher contents in lower layers were observed under carcasses in decay state T4. Overall, the highest Hg content, 39.6 μg Hg/kg dry wt., was found in a lower soil layer under seal F (decay state T4). This observation indicates the vertical transport of Hg to lower soil layers over time. As the samples did not contain visible organic material from seals or seal hair, the Hg presumably originates from released body fluids gradually transported by melting water. During the summer season, temperatures above the freezing point enable the transport of Hg. The ground temperature at a depth of 5 cm was measured by Hrbáček et al. (2015) who concluded that in the investigated area, the freezing season lasts for most of the year. During January to March, the active layer reaches a maximum of more than 50 cm (Hrbáček et al. 2015). Generally, Antarctic soils are poor in carbon and mineral particles, which results in a low retention capacity for Hg (Coufalík et al. 2015). However, our results indicate that the vertical transport of Hg proceeds slowly, as the progression between taphonomic states is a matter of several decades (Nývlt et al. 2016).

It should be emphasized that elevated mercury levels were found only in samples from locations in close proximity to seal carcasses. This observation indicates that the horizontal transport of deposited Hg is strictly limited. Thus, seal carcasses present a source of mercury only for the immediate surroundings. Similar observation has been previously

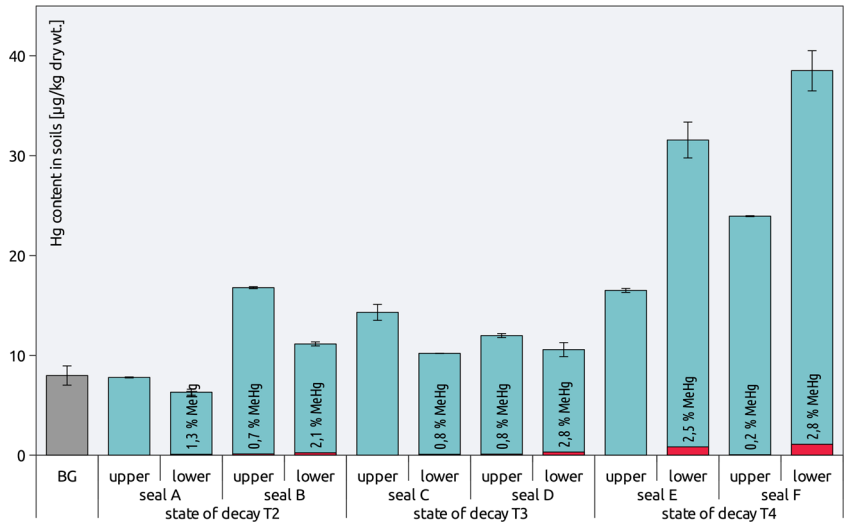

Fig. 3 Total mercury and methylmercury contents (in *red*) in soils lying under seal carcasses. *Error bars* (±1 SD) indicate that each sample was analyzed at least three times. The background mercury level "BG" was estimated as the mean level from a total of 12 soil samples collected in the vicinity of seals

published in the study describing nutrient release from the decaying bison carcasses in the primeval forest in Poland (Melis et al. 2007).

Methylmercury content

Information on the occurrence of methylmercury in the Antarctic soils is very limited. As a consequence of ultra-trace Hg levels, speciation analysis presents a challenge for analytical chemistry (Caroli et al. 2001). De Ferro reported levels of MeHg of between 0.06 and 0.1 µg/kg in sediments from the vicinity of fumaroles at Deception Island (Mão de Ferro et al. 2014). Usually, MeHg forms a 0.1–1.5 % proportion of Hg_T in natural sediments (Leermakers et al. 2005; Lin et al. 2012).

MeHg contents in uncontaminated background soils were under the limit of detection (LOD = 8 ng/kg dry wt.). MeHg was not detected even in the surrounding soils sampled at distances of 0.5 and 1 m from the carcasses. This means that the proportion of MeHg is less than 0.1 % with respect to Hg_T in the background soils.

However, MeHg was detected in most of the samples collected directly under seal carcasses (Fig. 3). Higher proportions of MeHg were found in lower soil layers compared to topsoil. The highest content of MeHg (1.1 µg/kg dry wt.), representing 2.8 % of Hg_T, was found in the lower soil sample from seal F, which also exhibited the highest total content of Hg. Overall, MeHg contents correlated closely with total Hg contents ($R_s = 0.85$, $p < 0.05$).

During their lives, seals take up Hg mainly in the form of MeHg from muscle tissue of fish. However, it is known that they retain only a small proportion of Hg in methylated form (Boening 2000; Wagemann et al. 2000). This is because of a natural protective mechanism in seals involving the demethylation of MeHg with selenium. The Hg is then stored in the less toxic form of mercury-selenide complexes (Wagemann et al. 2000). It has been shown that about one half of the Hg deposited in the livers of seals is inactivated into the form of non-toxic biomineral HgSe; inorganic Hg constitutes a smaller fraction, and the most toxic form, MeHg, represents only about 2–15 % of the total Hg content (Wagemann et al. 2000; Yin et al. 2007; Brookens et al. 2008). In contrast to liver, the proportion of MeHg is significantly higher in seal muscle (Smith and Armstrong 1978; Wagemann et al. 2000).

Recently, seals were identified as a significant source of MeHg for the environment due to the seasonal molting of their pelage (Cossaboon et al. 2015). Hg is present in seal hair in concentrations of up to several hundred milligrams per kilogram, and it is believed that the main constituent is MeHg, similarly as in human hair (dos Santos et al. 2006; Magos and Clarkson 2008; Cossaboon et al. 2015). The bioavailability of MeHg bound in hair as well as its mobility is not known (Cossaboon et al. 2015). Since no seal hair was visible in the collected samples, the MeHg measured in samples probably originated from released body fluids. However, it cannot be excluded that the microscopic remains of seal hair can contribute to the content of Hg_T and MeHg. Therefore, seal mummies represent a source of methylmercury for Antarctic soils, at least on the local scale.

Organic carbon content

Due to the harsh polar conditions, Antarctic soils are usually poorly developed and tend to contain low levels of organic matter, even in the areas covered by vegetation (Claridge et al. 1995). In the samples of uncontaminated surrounding soils, the level of TOC was homogeneous with a median of 0.3 %. In soils under seal carcasses, the TOC content ranged from 1.6 to 7.5 %, with a median of 3.2 %. Such contents of TOC in Antarctic soils are rare and higher than those commonly reported, e.g., for vegetation-covered soils (Bargagli et al. 1993; Zvěřina et al. 2012) and ornithogenic soils from penguin

colonies (Nie et al. 2012; Ma et al. 2013; Poggere et al. 2016). As the close surroundings of seal carcasses are often colonized by lichens and mosses, it should be emphasized that collected samples did not contain any vegetation that would otherwise affect and distort the results.

Organic matter increases the ability of soil to retain Hg; thus, a positive relationship between Hg and TOC has been observed repeatedly in Antarctic soils (Matsumoto et al. 1983; Bargagli et al. 2005; Mão de Ferro et al. 2014). However, in this study, the correlation between Hg_T and TOC was not significant ($R = 0.35$, $p = 0.24$). Nevertheless, it is very likely that both Hg and organic carbon had the same source in this case. In the samples classified according to state of decay of respective seal carcass, the correlations are much stronger; however, the number of samples is small. Figure 4 illustrates the relationship between TOC and Hg contents in the categorized samples. As already mentioned, Hg is distributed irregularly in seal tissues and body fluids, which is the probable reason for the weak Hg_T-TOC correlation.

It is assumed that organic matter not only acts as a carrier of Hg but also has the ability to absorb Hg(II) from the environment (Bargagli et al. 1993; Nie et al. 2012). In general, Antarctic soils are not able to retain Hg deposited from the atmosphere. A large proportion of Hg is taken away by thawing water (Coufalík et al. 2015). Thus, a significantly increased level of TOC in close proximity of a seal carcass can enable the accumulation of Hg. It is also well documented how the input of nutrients enables the growth of lichen and mosses in the vicinity of carcasses and directly on the carcasses themselves (Nývlt et al. 2016). Those organisms are well known for their ability to capture and accumulate Hg from the atmosphere (Zvěřina et al. 2014). In relation to that, further elevation of Hg concentrations might be expected at such locations.

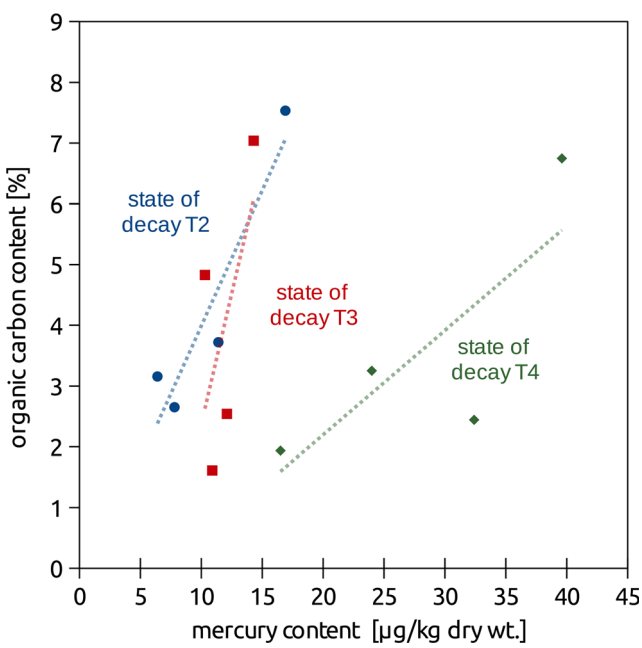

Fig. 4 Relationship between content of mercury and total organic carbon in soils directly underlying seals in different states of decay

Conclusion

Although most studies of Hg contamination in Antarctica concern the natural long-range transport of Hg to the Antarctic environment, biovectors including fallen animals seem to be an important pathway for Hg transport from marine to terrestrial Antarctic ecosystems.

This study has shown that Hg is gradually releasing from seal remains, scattered around the northern part of James Ross Island (and also in other parts of Antarctica). Although the Hg contamination is limited to the immediate subsoil of seal carcasses, it may present a significant source of Hg for the ecosystem due to the high number of individual seal carcasses. In soil samples collected under seal carcasses, Hg contents reached up to five times the background level. Methylmercury constituted up to 3 % of total Hg, while in background levels, it accounted for less than 0.1 %. It should be noted that no elevated Hg levels were observed at distances of 0.5 and 1 m from seal carcasses. However, the slow vertical transport of released Hg to lower soil layers is apparent. Moreover, we have observed an increase in concentrations of both Hg and MeHg with the state of decay of the carcasses.

Concerning Hg contamination, it should be taken into account that seal carcasses increase the Hg load also indirectly by means of the input of nutrients and organic matter into the environment. Organic matter in soil increases the capacity of soil to retain Hg, while the nutrients enable the growth of lichen and mosses, which are efficient bioaccumulators of Hg and other pollutants. The observed levels of TOC were among the highest reported for Antarctic soils. The correlation between TOC and Hg in samples was weak, which might be explained by the irregular distribution of the mercury within the seal body.

It seems that the nutrient-enriched oases which form around seal carcasses are also hot spots for the input of Hg and its further accumulation. Future research should explore this topic further in order to identify more associations and consequences with respect to both contaminants and nutrients releasing from seal carcasses.

Acknowledgments The authors are grateful to the Czech Polar project for use of its facilities (Johann Gregor Mendel Station) and for financial support from the Grant Agency of the Czech Republic, project P503/12/0682. The involvement of Pavel Coufalík was supported by the Institute of Analytical Chemistry of the CAS under the Institutional Research Plan RVO: 68081715. This work was also supported by the Czech Ministry of Education, Youth and Sports (LO1214 and LM2015051).

References

Bargagli R (2005) Antarctic ecosystems: environmental contamination, climate change, and human impact. Springer-Verlag, Berlin

Bargagli R (2008) Environmental contamination in Antarctic ecosystems. Sci Total Environ 400:212–226. doi:10.1016/j.scitotenv.2008.06.062

Bargagli R, Battisti E, Focardi S, Formichi P (1993) Preliminary data on environmental distribution of mercury in northern Victoria Land, Antarctica. Antarct Sci 5:3–8. doi:10.1017/S0954102093000021

Bargagli R, Monaci F, Sanchez-Hernandez JC, Cateni D (1998) Biomagnification of mercury in an Antarctic marine coastal food web. Mar Ecol Prog Ser 169:65–76. doi:10.3354/meps169065

Bargagli R, Agnorelli C, Borghini F, Monaci F (2005) Enhanced deposition and bioaccumulation of mercury in Antarctic terrestrial ecosystems facing a coastal polynya. Environ Sci Technol 39:8150–8155. doi:10.1021/es0507315

Bargagli R, Monaci F, Bucci C (2007) Environmental biogeochemistry of mercury in Antarctic ecosystems. Soil Biol Biochem 39:352–360. doi:10.1016/j.soilbio.2006.08.005

Barker PF, Thomas E (2004) Origin, signature and palaeoclimatic influence of the Antarctic Circumpolar Current. Earth-Science Rev 66: 143–162. doi:10.1016/j.earscirev.2003.10.003

Blais JM, Macdonald RW, Mackay D et al (2007) Biologically mediated transport of contaminants to aquatic systems. Environ Sci Technol 41:1075–1084. doi:10.1021/es061314a

Boening DW (2000) Ecological effects, transport, and fate of mercury: a general review. Chemosphere 40:1335–1351. doi:10.1016/S0045-6535(99)00283-0

Brookens TJ, Harvey JT, O'Hara TM (2007) Trace element concentrations in the Pacific harbor seal (*Phoca vitulina richardii*) in central and northern California. Sci Total Environ 372:676–692. doi:10.1016/j.scitotenv.2006.10.006

Brookens TJ, O'Hara TM, Taylor RJ et al (2008) Total mercury body burden in Pacific harbor seal, *Phoca vitulina richardii*, pups from central California. Mar Pollut Bull 56:27–41. doi:10.1016/j.marpolbul.2007.08.010

Caroli S, Cescon P, Walton DWH (2001) Environmental contamination in Antarctica: a challenge to analytical chemistry. Elsevier, Oxford

Claridge GGC, Campbell IB, Powell HKJ et al (1995) Heavy metal contamination in some soils of the McMurdo Sound region, Antarctica. Antarct Sci 7:9–14

Cossaboon JM, Ganguli PM, Flegal AR (2015) Mercury offloaded in northern elephant seal hair affects coastal seawater surrounding rookery. Proc Natl Acad Sci 112:12058–12062. doi:10.1073/pnas.1506520112

Coufalík P, Zvěřina O, Krmíček L et al (2015) Ultra-trace analysis of Hg in alkaline lavas and regolith from James Ross Island. Antarct Sci 27:281–290. doi:10.1017/S0954102014000819

Crame JA, Pirrie D, Riding JB, Thomson MRA (1991) Campanian Maastrichtian (Cretaceous) stratigraphy of the James-Ross-Island area, Antarctica. J Geol Soc Lond 148:1125–1140. doi:10.1144/gsjgs.148.6.1125

Czech Geological Survey (2009) James Ross Island—northern part. Topographic map 1: 25,000. CGS, Prague

Davies BJ, Glasser NF, Carrivick JL et al (2013) Landscape evolution and ice-sheet behaviour in a semi-arid polar environment: James Ross Island, NE Antarctic Peninsula. Antarct Palaeoenvironments Earth-Surface Process 381:1–43. doi:10.1144/SP381.1

de Moreno JEA, Gerpe MS, Moreno VJ, Vodopivez C (1997) Heavy metals in Antarctic organisms. Polar Biol 17:131–140. doi:10.1007/s003000050115

dos Santos IR, Silva-Filho EV, Schaefer C et al (2006) Baseline mercury and zinc concentrations in terrestrial and coastal organisms of Admiralty Bay, Antarctica. Environ Pollut 140:304–311. doi:10.1016/j.envpol.2005.07.007

Engel Z, Nývlt D, Láska K (2012) Ice thickness, areal and volumetric changes of Davies dome and whisky glacier (James Ross Island, Antarctic peninsula) in 1979–2006. J Glaciol 58:904–914. doi:10.3189/2012JoG11J156

Gordon JE, Harkness DD (1992) Magnitude and geographic variation of the radiocarbon content in Antarctic marine life: implications for reservoir corrections in radiocarbon dating. Quat Sci Rev 11:697–708. doi:10.1016/0277-3791(92)90078-M

Gray JS (2002) Biomagnification in marine systems: the perspective of an ecologist. Mar Pollut Bull 45:46–52. doi:10.1016/S0025-326X(01)00323-X

Habran S, Debier C, Crocker DE et al (2011) Blood dynamics of mercury and selenium in northern elephant seals during the lactation period. Environ Pollut 159:2523–2529. doi:10.1016/j.envpol.2011.06.019

Hrbáček F, Láska K, Engel Z (2015) Effect of snow cover on the active-layer thermal regime—a case study from James Ross Island. Antarctic Peninsula Permafr Periglac Process. doi:10.1002/ppp.1871

Ikemoto T, Kunito T, Watanabe I et al (2004) Comparison of trace element accumulation in Baikal seals (*Pusa sibirica*), Caspian seals (*Pusa caspica*) and northern fur seals (*Callorhinus ursinus*). Environ Pollut 127:83–97. doi:10.1016/S0269-7491(03)00251-3

Jakimska A, Konieczka P, Skóra K, Namieśnik J (2011) Bioaccumulation of metals in tissues of marine animals, part I: the role and impact of heavy metals on organisms. Pol J Environ Stud 20:1117–1125

Košler J, Magna T, Mlčoch B et al (2009) Combined Sr, Nd, Pb and Li isotope geochemistry of alkaline lavas from northern James Ross Island (Antarctic Peninsula) and implications for back-arc magma formation. Chem Geol 258:207–218. doi:10.1016/j.chemgeo.2008.10.006

Laws RM, Baird A, Bryden MM (2003) Size and growth of the crabeater seal *Lobodon carcinophagus* (Mammalia: Carnivora). J Zool 259: 103–108. doi:10.1017/S0952836902003072

Leermakers M, Baeyens W, Quevauviller P, Horvat M (2005) Mercury in environmental samples: speciation, artifacts and validation. Trends Anal Chem 24:383–393. doi:10.1016/j.trac.2004.01.001

Lin Y, Vogt R, Larssen T (2012) Environmental mercury in China: a review. Environ Toxicol Chem 31:2431–2444. doi:10.1002/etc.1980

Lu Z, Cai M, Wang J et al (2012) Baseline values for metals in soils on Fildes Peninsula, King George Island, Antarctica: the extent of anthropogenic pollution. Environ Monit Assess 184:7013–7021. doi:10.1007/s10661-011-2476-x

Ma D, Zhu R, Ding W et al (2013) Ex-situ enzyme activity and bacterial community diversity through soil depth profiles in penguin and seal colonies on Vestfold Hills, East Antarctica. Polar Biol 36:1347–1361. doi:10.1007/s00300-013-1355-z

Magos L, Clarkson T (2008) The assessment of the contribution of hair to methyl mercury excretion. Toxicol Lett 182:48–49. doi:10.1016/j.toxlet.2008.08.010

Mão de Ferro A, Mota AM, Canário J (2014) Pathways and speciation of mercury in the environmental compartments of Deception Island, Antarctica. Chemosphere 95:227–233. doi:10.1016/j.chemosphere.2013.08.081

Matsumoto G, Chikazawai K, Hanyai T (1983) Distribution and correlation of total organic carbon and mercury in Antarctic dry valley soils, sediments and organisms. Geochem J 17:247–255. doi:10.2343/geochemj.17.241

Melis C, Selva N, Teurlings I, Skarpe C, Linnell JD, Andersen R (2007) Soil and vegetation nutrient response to bison carcasses in Białowieża Primeval Forest, Poland. Ecol Res 22:807–813. doi:10.1007/s11284-006-0321-4

Nehyba S, Nývlt D (2015) "Bottomsets" of the lava–fed delta of James Ross Island Volcanic Group, Ulu Peninsula, James Ross Island, Antarctica. Polish Polar Res 36:1–24. doi:10.1515/popore-2015-0002

Nelson AE, Smellie JL, Williams M, Moreton S (2008) Age, geographical distribution and taphonomy of an unusual occurrence of mummified crabeater seals on James Ross Island, Antarctic Peninsula. Antarct Sci 20:485–493. doi:10.1017/S095410200800134X

Nie Y, Liu X, Sun L, Emslie SD (2012) Effect of penguin and seal excrement on mercury distribution in sediments from the Ross Sea region, East Antarctica. Sci Total Environ 433:132–140. doi:10.1016/j.scitotenv.2012.06.022

Nývlt D, Košler J, Mlčoch B et al (2011) The Mendel Formation: evidence for Late Miocene climatic cyclicity at the northern tip of the Antarctic Peninsula. Palaeogeogr Palaeoclimatol Palaeoecol 299: 363–384. doi:10.1016/j.palaeo.2010.11.017

Nývlt D, Braucher R, Engel Z, Mlčoch B (2014) Timing of the Northern Prince Gustav Ice Stream retreat and the deglaciation of northern James Ross Island, Antarctic Peninsula during the last glacial–interglacial transition. Quat Res 82:441–449. doi:10.1016/j.yqres.2014.05.003

Nývlt D, Fišáková MN, Barták M et al (2016) Death age, seasonality, taphonomy and colonization of seal carcasses from Ulu Peninsula, James Ross Island, Antarctic Peninsula. Antarct Sci 28:3–16. doi:10.1017/S095410201500036X

Péwé TL, Rivard NR, Llano GA (1959) Mummified seal carcasses in the McMurdo Sound Region, Antarctica. Science 130:716. doi:10.1126/science.130.3377.716

Poggere GC, Melo VF, Francelino MR et al (2016) Characterization of products of the early stages of pedogenesis in ornithogenic soil from Maritime Antarctica. Eur J Soil Sci 67:70–78. doi:10.1111/ejss.12307

Rabassa J, Skvarca P, Bertani L, Mazzoni E (1982) Glacier inventory of James Ross and Vega Islands, Antarctic Peninsula. Ann Glaciol 3: 260–264

Santos IR, Silva-Filho EV, Schaefer CEGR et al (2005) Heavy metal contamination in coastal sediments and soils near the Brazilian Antarctic Station, King George Island. Mar Pollut Bull 50:185–194. doi:10.1016/j.marpolbul.2004.10.009

Smellie JL (2013) Geological map of James Ross Island 1. James Ross Island Volcanic Group. BAS GEOMAP 2 Ser Sheet 5, Br Ant – Arct Surv Cambridge 110. doi:10.1029/2006GC001450.20

Smith TG, Armstrong FAJ (1978) Mercury and selenium in ringed and bearded seal tissues from Arctic Canada. Arctic 31:75–84. doi:10.2307/40508886

Szefer P, Czarnowski W, Pempkowiak J, Holm E (1993) Mercury and major essential elements in seals, penguins, and other representative fauna of the Antarctic. Arch Environ Contam Toxicol 25:422–427

Wagemann R, Trebacz E, Boila G, Lockhart WL (2000) Mercury species in the liver of ringed seals. Sci Total Environ 261:21–32. doi:10.1016/S0048-9697(00)00592-1

Yamamoto Y, Honda K, Hidaka H, Tatsukawa R (1987) Tissue distribution of heavy metals in Weddell seals (*Leptonychotes weddellii*). Mar Pollut Bull 18:164–169. doi:10.1016/0025-326X(87)90240-2

Yin X, Sun L, Zhu R, Liu X, Ruan D, Wang Y (2007) Mercury-selenium association in antarctic seal hairs and animal excrements over the past 1,500 years. Environ Toxicol Chem 26:381–386. doi:10.1897/06-128.1

Zvěřina O, Coufalík P, Vaculovič T et al (2012) Macro-and microelements in soil profile of the moss-covered area in James Ross Island, Antarctica. Czech Polar Reports 2:1–7. doi:10.5817/CPR2012-1-1

Zvěřina O, Láska K, Červenka R et al (2014) Analysis of mercury and other heavy metals accumulated in lichen Usnea Antarctica from James Ross Island, Antarctica. Environ Monit Assess 186:9089–9100. doi:10.1007/s10661-014-4068-z

Příloha IX

Environ Monit Assess (2014) 186:9089–9100
DOI 10.1007/s10661-014-4068-z

Analysis of mercury and other heavy metals accumulated in lichen *Usnea antarctica* from James Ross Island, Antarctica

Ondřej Zvěřina · Kamil Láska · Rostislav Červenka · Jan Kuta · Pavel Coufalík · Josef Komárek

Received: 12 February 2014 / Accepted: 16 September 2014 / Published online: 28 September 2014
© Springer International Publishing Switzerland 2014

Abstract The study was designed to investigate the content and distribution of selected heavy metals (As, Cd, Co, Cr, Cu, Hg, Mn, Ni, Fe, Pb and Zn) in samples of fruticose macrolichen *Usnea antarctica* from James Ross Island. A special emphasis was devoted to mercury and its species (elemental mercury and methylmercury). It was found that mercury contents were relatively high (up to 2.73 mg kg^{-1} dry weight) compared to other parts of the Antarctic Peninsula region, while the concentrations of most other elements were within reported ranges. Mercury contents in lichens originating from the interior were higher than those from the coast, which is probably the result of local microclimate conditions. Similar trends were observed for Hg^0 and $MeHg^+$, whose contents were up to 0.14 and 0.098 mg kg^{-1} dry weight, respectively. While mercury did not show a significant correlation with any other element, the mutual correlation of some litophile elements probably refers to the influence on thalli of resuspended weathered material. The influence of habitat and environmental conditions could play an essential role in the bioaccumulation of contaminants rather than just the simple presence of sources. Thus, the study of the thalli of this species can bring a new perspective on the interpretation of contaminant accumulation in lichens of the polar region.

Keywords Antarctica · Heavy metal · Mercury · Lichen

O. Zvěřina · P. Coufalík · J. Komárek (✉)
Department of Chemistry, Faculty of Science, Masaryk University, Kotlářská 2, 61137 Brno, Czech Republic
e-mail: komarek@chemi.muni.cz

O. Zvěřina
Department of Public Health, Faculty of Medicine, Masaryk University, Kamenice 5, 625 00 Brno, Czech Republic

K. Láska
Department of Geography, Faculty of Science, Masaryk University, Kotlářská 2, 61137 Brno, Czech Republic

R. Červenka · J. Kuta
Research Centre for Toxic Compounds in the Environment (RECETOX), Faculty of Science, Masaryk University, Kamenice 753/5, 62500 Brno, Czech Republic

P. Coufalík
Institute of Analytical Chemistry, Academy of Sciences of the Czech Republic, v.v.i., Veveří 97, 602 00 Brno, Czech Republic

Introduction

Due to its remote location, Antarctica presents a unique opportunity to study the long distance transport and allocation of chemicals generated naturally or produced by humans on other continents. Although it is protected from the entry of lower latitude air masses by natural atmospheric circulation, Antarctica represents a potential sink for the deposition of long-range transported pollutants including mercury (Bargagli 2008). The atmospheric transport of pollutants is considered to be a significant pathway of Antarctic environment contamination (Montone et al. 2003; Bargagli 2008; Cipro et al. 2011). Therefore, studies on the amounts of particular chemicals

in different compartments of Antarctic ecosystems are of great importance.

Mercury is an atmospheric pollutant of global concern. Its biogeochemical cycle includes various physical, chemical and photochemical interactions, both wet and dry deposition, and reemission from environmental surfaces (Schroeder and Munthe 1998; Wängberg et al. 2001). In the atmosphere, mercury occurs mainly as Hg^0 (elemental mercury vapour), along with reactive gaseous mercury ((RGM)—Hg^{2+} divalent mercury compounds) and mercury associated with particulate matter. The presence of methylated mercury species has also been reported (Slemr et al. 1981, 1985; Fitzgerald et al. 1991; Lin and Pehkonen 1999). Hg^0 is stable and its residence time of 6–24 months allows its transport over large distances on a global scale (Schroeder and Munthe 1998; William et al. 1998; Wängberg et al. 2001). The rate of deposition is largely affected by Hg^0 to Hg^{2+} conversion, since RGM includes highly surface-reactive species and is rapidly deposited through both wet and dry deposition (Lindberg and Stratton 1998). It is known that, in polar regions, intensive Hg deposition occurs during and after the polar sunrise during mercury depletion events (MDEs). Elemental mercury undergoes photochemical oxidation to RGM by reactive halogens, and thereafter is rapidly deposited on the Earth's surface. MDE is considered to be a critical factor for mercury input in coastal polar ecosystems.

Concerns have been raised about the possible environmental effects of changes in the regional climate on the role of Antarctica as a "cold trap". The warming of both land and ocean causes increased outgassing and also changes in sea-ice cover and in precipitation patterns (Lindberg et al. 2002; Bargagli 2005; Bargagli et al. 2005). The west side of the Antarctic Peninsula has experienced the largest increase in annual surface air warming over the last few decades. An annual temperature growth of +0.56 °C per decade was reported at the Faraday/Vernadsky station between 1951 and 2001 (Turner et al. 2005), while warming in the northwest Antarctic Peninsula was considerably greater than the mean Antarctic trend (Vaughan et al. 2001). The mean annual air temperatures also rose substantially along the eastern coast of the Antarctic Peninsula, accelerating glacier retreat and an increase in permafrost temperature (Strelin et al. 2006; Cook and Vaughan 2010). The recent breakup of the Prince Gustav shelf in 1995 (Rott et al. 1996) is one of the consequences of this temperature increase. It can also be assumed that open water connected with sea aerosol input may additionally increase the deposition of Hg and other metals into the surveyed area.

As the retreating ice is uncovering bedrock in coastal areas, new terrestrial ecosystems are being established. Lichens are among the first colonisers of exposed rock and snow-free ground (Bargagli et al. 1999). Along with mosses, they are able to tolerate extreme temperatures together with long periods of desiccation and are the main components of Antarctic terrestrial flora (Bargagli et al. 1998; Wojtuń et al. 2013).

Lichens are known for their ability to capture and accumulate gaseous atmospheric pollutants and are commonly used as biomonitors of airborne metals including Hg (Bargagli and Barghigiani 1991; Loppi and Bonini 2000; Conti and Cecchetti 2001; Pisani et al. 2011; Mlakar et al. 2011; Lodenius 2013; Mão de Ferro et al. 2014). Five processes by which both nutrients and contaminants are deposited onto lichens are described. These are wet deposition (including snowfall), occult precipitation (fog, dew and mist), sedimentation (particles >1–4 mm), impaction (particles <1–4 mm carried by wind) and direct uptake (particularly when wetted) (Knops et al. 1991). Unlike higher plants, lichens have neither roots nor stomata, and a weak or absent cuticle enables easy exchange between the environment and their cell walls. Owing to their high cation exchange capacity, lichens have the ability to accumulate available ions of all gaseous, dissolved and particulate elements in air, snow and melting water (Bargagli et al. 1998). In addition, due to the lichens having a complicated surface structure, contaminants are absorbed over the whole thallus surface (Lupsina et al. 1992; Lodenius 2013). Different lichen morphotypes vary in their active surface for ion uptake. From this perspective, the fruticose type of thallus represents an ideal material with a large surface area. The fruticose macrolichen *Usnea antarctica* has already been utilised for monitoring the levels of heavy metals (Bargagli et al. 1993; Poblet et al. 1997; Osyczka et al. 2007; Cansaran-Duman 2011; Wojtuń et al. 2013).

There is a continuous need to monitor pollutants in the polar environment. In contrast to numerous studies on the Arctic, information on the levels of heavy metals in Antarctic lichens is still scarce. Moreover, most of the studies concerning this topic are focused on the South Shetland Islands and no similar report has been published on mercury levels in the Antarctic Peninsula and on James Ross Island in particular. The small amount of

available data from the Antarctic hinders the assessment of mercury (and other heavy metal) concentrations and the complex comparison of such concentrations and their trends between different geographical locations. James Ross Island represents an ideal area for the investigation of heavy metal concentrations and their geographical distribution, as it is one of the largest deglaciated areas along the eastern coast of the Antarctic Peninsula with only small glaciers remaining in the present landscape (Engel et al. 2012).

The objectives of this research were to determine the contents of Hg (including $MeHg^+$ and Hg^0 species) and some other heavy metals (As, Cd, Co, Cr, Cu, Mn, Ni, Fe, Pb and Zn) and to investigate their distribution in lichen samples originating from the northern part of James Ross Island. The geographical distribution of sampling points affected by local factors and climatic conditions (distance from the seashore, snow accumulation and fog occurrence) was expected to be the most influential factor.

Materials and methods

Sample origin and treatment

James Ross Island (JRI, 64° 10′ S, 57° 45′ W) is situated on the east side of the Antarctic Peninsula tip (Fig. 1). About 20 % of its total area of 2500 km^2 is recently deglaciated (Rabassa et al. 1982). The Ulu Peninsula, the northern part of JRI, represents the largest deglaciated area, with several lava-fed deltas, abundant outcrops of glacial sedimentary rock and exposures of Cretaceous marine sediments (Crame et al. 1991; Kristjánsson et al. 2005; Nývlt et al. 2014). The area of the Abernethy Flats was selected for sampling considering the articulation of the recently deglaciated terrain, which is characterised by a gradual increase in altitude from 0 to 134 m at San Jose Pass. The morphology of the valley is relatively flat and formed mostly by less resistant Cretaceous marine deposits. Local and small elevations in the central part of the valley are mostly formed by exhumed volcanic dykes. Monolith Stream, one of the largest watercourses in the area, is dewatering the vicinity of Monolith Lake towards the broad and shallow Brandy Bay. The river is located in the western and southern part of the asymmetric depression Abernethy Flats.

Climatic conditions of the Ulu Peninsula are characterised by a short summer (December–February) with positive air temperatures up to 10 °C and an annual mean air temperature of around −7 °C (Láska et al. 2011a). Total precipitation is estimated at between 300 and 500 mm water equivalent per year, with snowfall occurring even in the summer period (Bromwich et al. 2004; Dethloff et al. 2010). The snow-free period can vary from 1 to 3 months with large year-to-year variations. The daily mean incoming solar radiation is around 250 W m^{-2} in summer, which significantly reduces snow cover (Láska et al. 2011b). In order to describe local wind conditions, 30-min surface wind observations from the nearby meteorological station at Johnson Mesa were used. The flat surface of Johnson Mesa at an elevation of 320 m a.s.l. was found as a representative site for evaluation of the prevailing wind direction. In the study, the relative frequency of wind direction measured at 6 m above ground was estimated for the period 2008–2010.

Samples were collected from the gravel plain Abernethy Flats and also in the area of the continuous and stable slope of Keller Stream and Monolith Lake during the 2012 Czech Antarctic expedition. Fruticose macrolichens *U. antarctica* were sampled along a 6-km transect beginning inland and running down across the Abernethy Flats to the seashore (Fig. 1). In the laboratory, the lichens were washed in deionised water in order to remove dust and any unwanted particles and dried for 48 h at 30 °C. Then, the thalli were homogenised in a ball mill and stored at −20 °C until analysis.

Analytical procedures

Total mercury concentrations in the samples were determined by means of an AMA-254 analyser (Altec, Czech Republic). Determination is based on dry decomposition followed by preconcetration by amalgamation and AAS detection (Száková et al. 2004).

Elemental mercury was determined by means of thermal desorption. Aliquots of samples were heated at 105 °C for 48 h and the mercury concentrations subsequently measured. The contents of elemental mercury were calculated as the differences between total concentrations and those measured in treated aliquots. The pyrolytical determination of Hg^0 was first suggested by Biester and Scholz (1997) and applied as a single-step analysis by Nóvoa-Muñoz et al. (2008). This method was also conducted for Hg^0 determination

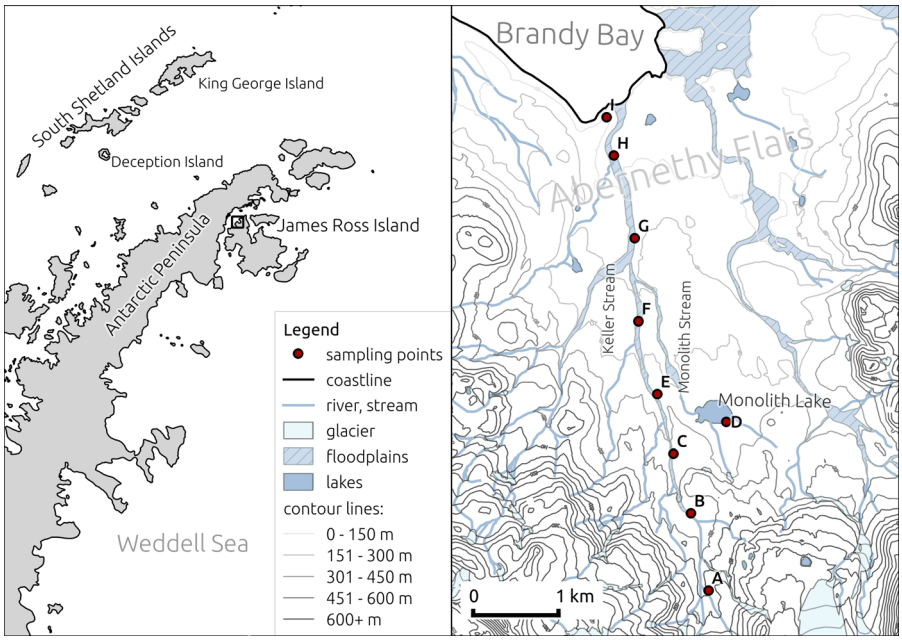

Fig. 1 Maps of the Antarctic Peninsula region (*left*) and the Abernethy Flats sampling locality on James Ross Island (*right*). Modified map of James Ross Island-Northern part (Czech Geological Survey 2009)

in samples with a high content of organic carbon (Coufalík et al. 2013a).

For methylmercury determination, 300-mg samples were extracted with 10 mL of 6 mol L^{-1} HCl (Sigma-Aldrich, Germany). The extraction was conducted for 2 h in an ultrasound bath and then for another 18 h on an end-over-end shaker (150 RPM). The obtained extracts were filtered through glass microfibre filters (Whatman) and the pH of the solution was adjusted to 5 with acetate buffer. The contained polar methylmercury was then converted to nonpolar volatile ethylated methylmercury using $NaBEt_4$ (Sigma-Aldrich, Germany), and the resulting solution was extracted with hexane (Sigma-Aldrich, Germany). Finally, an aliquot of 2 μl was injected into an Agilent 6890N gas chromatograph with a PSA 10.750 atomic fluorescence detector (Cai et al. 2000; Leermakers et al. 2005; Kuballa et al. 2008; Nevado et al. 2011; Červenka et al. 2011).

For the determination of selected metal contents (As, Cd, Co, Cr, Cu, Mn, Ni, Fe, Pb and Zn), the homogenised lichen thalli were digested in an HNO_3/H_2O_2 (both Sigma-Aldrich, Germany) mixture in a microwave digester (Berghof MSW3+ speedwave) according to EPA 3052 method. The contents of elements in digestions were subsequently measured using an Agilent 7500 CE quadrupole ICP-MS spectrometer (Agilent, Japan) according to the EPA 6020A method. The spectrometer was equipped with an octopole reaction cell to avoid isobaric interferences, a Babington nebuliser and a double-pass Scott chamber. The conditions were optimised to obtain maximum sensitivity and minimum CeO^+/Ce^+ and Ce^{++}/Ce^+ ratios.

All analyses were performed in an ultra-clean laboratory equipped with HEPA filters. The used chemicals were ACS reagent grade, especially pure for mercury. Prior to use, all glassware was cleaned by two-stage decontamination in an HNO_3 bath and heated to 250 °C for 2 h.

The accuracy of the methods was verified by means of the following reference materials: IRMM BCR-482 Lichen (for elements As, Cd, Cr, Cu, Hg, Ni, Pb, Zn) and IAEA-336 Lichen (for elements As, Co, Cu, Hg, Fe, Mn, Zn). Recoveries of all elements were consistently within the ranges of certified values. Typical relative standard deviations for triplicate analysis of reference materials and lichen samples were within the order of units of percents. Contents of particular elements in samples were at least one order of magnitude higher than the method detection limits.

Statistical analysis

To summarise the collected data, general descriptive statistics including Spearman rank order correlation

and Bartels' rank test (investigation of trend occurrence) (Bartels 1982) were performed using R version 3.0.2 (R Development Core Team 2013). Nonparametric tests were used due to the non-normality of the data.

Results and discussion

Surface wind conditions

Figure 2 shows the relative frequency of the wind direction at the Johnson Mesa in the period 2008–2010. The prevailing wind directions were observed in the south-western sector. Southerly and westerly winds were the most common, with a frequency of occurrence of 18.8 and 14.4 % of all cases, respectively. On average, the summertime and wintertime wind directions were slightly different, but were observed within the same sector. Northerly, northwesterly and southeasterly winds had the lowest frequency of occurrence. From the observed wind pattern, it is evident that the orography of the Antarctic Peninsula affects the airflow along the eastern side of the Peninsula and the northern coast of James Ross Island.

Total mercury contents

Figure 3 shows the total Hg contents in lichen samples. Hg concentrations ranged from 0.72 to 2.73 mg kg^{-1} dry weight (d.w.) with a median value of 1.59 mg kg^{-1} d.w. Bartels' test for randomness was used to examine the probability of trend occurrence (Bartels 1982). A p value of 0.82 indicates a gradual mercury content increase in the direction from the coast to the interior.

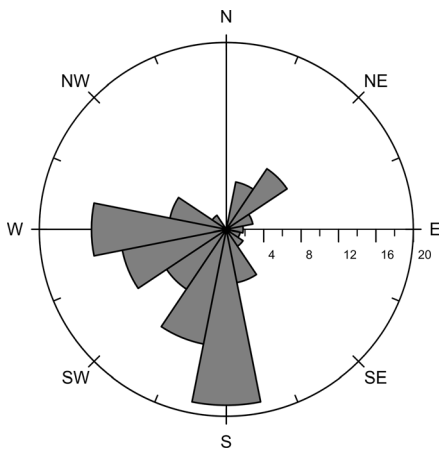

Fig. 2 Relative wind frequency at the Johnson Mesa in the period 2008–2010

Marine aerosol has been suggested as the main contributor of mercury contamination in lichens together with volcanic emissions (Mão de Ferro et al. 2014). The lowest mercury content determined in coastal sample I, together with the above mentioned trend, indicates that sea spray does not represent a significant Hg source in this case. This fact can be partly attributed to the prevailing winds blowing towards the sea (Fig. 2). Moreover, lichens growing in localities further inland may be more affected by moisture at higher elevations. An increase in relative air humidity of 5 % from seashore to higher-elevated plateaus was observed in a previous study (Láska et al. 2011a). Increased mercury input into lichens caused by the effect of fog was already observed (Evans and Hutchinson 1996).

Abernethy Flats is a valley with suitable conditions for snow accumulation and subsequent melting. At the beginning of the sampling transect (in the vicinity of sampling points A and partially in the vicinity of B), there is the probability of increased accumulation of wind-blown snow from the glaciers south of the sampling area (e.g. Whisky Glacier). Dissolved Hg^{2+} compounds are known to be readily absorbed by lichens when snow melts (Skov et al. 2004; Bargagli et al. 2005).

In fact, the concentrations of mercury in lichens are two to three orders of magnitude higher than those determined in soils from the same sampling localities (0.0073–0.011 mg kg^{-1}) (Coufalík et al. 2013b). The enrichment factor between lichens and the underlying soil would reach a value of several hundred. This ratio excludes crustal aerosols as a strongly influential factor (Carignan et al. 2009). Therefore, atmospheric deposition could be considered the main source of mercury in lichens.

In comparison with mercury contents reported in lichens from the Antarctic Peninsula region, the values obtained in this work are substantially higher. Table 1 summarises published Hg levels for lichen samples originating from the South Shetland Islands, the closest area for which similar information has been published. The likely explanation is the fact that the environments of JRI and the South Shetlands are influenced by the circulation of different air masses. The climate of the South Shetlands is mainly affected by relatively warm (oceanic) air masses associated with synoptic-scale systems moving across the Bellingshausen Sea (Martin and

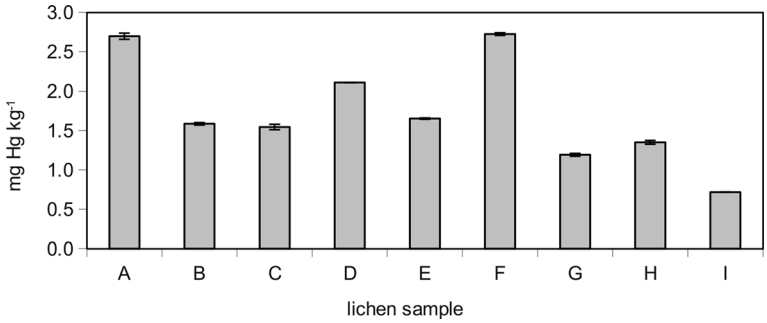

Fig. 3 Total mercury concentrations in samples of *Usnea antarctica* (n=5, ±SD) from inland site (*A*) towards the seashore (*I*)

Peel 1978). JRI, however, is moderated by cold air masses of continental origin coming from the south and southwest, along the eastern coast of the Antarctic Peninsula. The advection of oceanic air masses towards James Ross Island is reduced by the pronounced orographic effect of the Peninsula (King 2003). Therefore, the frequency of the occurrence of continental and oceanic air masses determines the climate of the study site. These factors are assumed to play a crucial role in the distribution of long-range transported pollutants such as mercury.

Elemental mercury

An amount of up to 0.14 mg Hg kg^{-1} d.w. was released by thermal desorption experiments, which presents less than 5 % of the total mercury in the samples (Fig. 4). The amounts of the desorbed portions correlate closely with total mercury contents (Spearman's correlation coefficient r_s=0.93, p<0.001). Similarly to the total Hg concentration, the desorbed fraction also increased along the sampling transect from the coast to the interior (p value of Bartels' test is 0.78).

Recently, laboratory experiments have shown the ability of some plants to take up Hg^0 directly from the atmosphere and bond it strongly with almost no losses from evaporation or leaching (Lodenius et al. 2003). It has been demonstrated that, on the lichen surface, elemental mercury is converted into a strongly held form or diffuses into the lichen cells and is released less readily; possibly, it is converted into an inorganic form—Hg^{2+} (Krishna et al. 2003, 2004). The high concentration of mercury in some plants could be created by an irreversible accumulation process determined by oxidation of the adsorbed Hg^0 followed by complexation of Hg^{2+} by -SH groups of amino acids (Bacci et al. 1994). Some authors suggest that Hg is captured by lichens mainly after its atmospheric oxidation to the more soluble Hg^{2+} (Krishna et al. 2003). The above-described processes are probably the reason for the small proportion of total mercury that was desorbed at 105 °C, although Hg^0, the main mercury form in the atmosphere, is readily released under these conditions.

Table 1 Reported mercury levels in lichens of *Usnea* species originating from the South Shetland Islands

Study, location	Lichen specie	Hg [mg kg^{-1}]	MeHg [mg kg^{-1}]
(Mão de Ferro et al. 2014)			
Deception Island	*Usnea sphacelata*	0.14–0.24	0.021–0.026
(Bargagli et al. 1993)			
King George Island	*Usnea antarctica*	0.026–0.061	–
Deception Island	*Usnea antarctica*	0.190–0.253	–
(Wojtuń et al. 2013)			
King George Island	Several lichen species including *Usnea antarctica*	0.18	–
(dos Santos et al. 2006)			
King George Island	*Usnea spp.*	0.0363	–

"–" means that methylmercury was not determined in this study

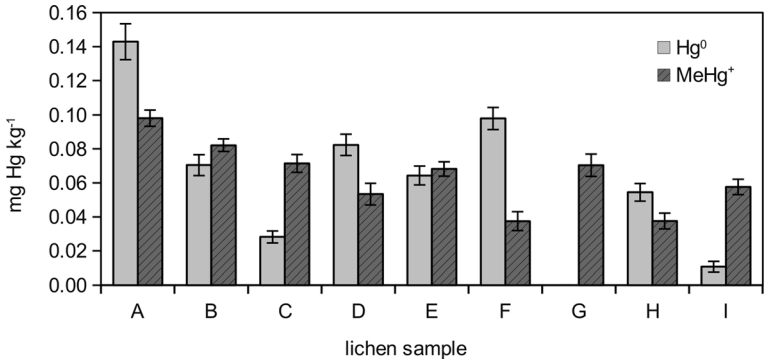

Fig. 4 Elemental mercury and methylmercury contents in samples of *Usnea antarctica* ($n=3$, ±SD) from inland site (*A*) towards the seashore (*I*)

Locally, Hg vapours can be evaporated from the top soil layer. According to literature, the Hg evaporation rate from bare uncontaminated soils increases linearly from 10 °C (the lowest measured temperature) to 15–20 °C and then exponentially to 35 °C, while the volatile species (such as Hg^0 and $(CH_3)_2Hg$) are supposed to dominate Hg evaporation from soil (Schlüter 2000). However, previously reported results suggest that Hg content in Abernethy Flats soils is stable at temperatures up to 50 °C (Coufalík et al. 2013b). Moreover, a recent study showed that the mean monthly surface temperature on the Ulu Peninsula ranges from −11 to 6 °C (Láska et al. 2011a), which implies a low rate of Hg evaporation. Furthermore, a surface temperature higher than 10 °C is exceeded only for several days in the summer (December–February).

Methylmercury

The methylmercury concentration in samples ranged from 0.037 to 0.098 mg kg^{-1} d.w. with a median of 0.068 mg kg^{-1} d.w., which represents a portion of 1.4 to 8.1 % of total Hg. A trend of increasing $MeHg^+$ content from the cost to the interior was observed (Bartels' test *p* value is 0.82).

So far, little data has been published on the occurrence of methylmercury in lichens. It was reported for lichen (*Usnea sphacelata* from Deception Island) to have a higher capacity for Hg and MeHg bioaccumulation than that observed for moss (*Polytrichum strictum Brid.* and *Sanionia georgico-uncinata*), while published $MeHg^+$ levels (Tab. 1) were slightly lower than those observed in this work (Mão de Ferro et al. 2014). Similar concentrations of $MeHg^+$ were also determined in *Hypogymnia physodes* lichens from Slovenia: 5–106 μg kg^{-1} (0.06–3.70 % of total Hg). In addition, a good statistical correlation with total Hg was found (Lupsina et al. 1992). In contrast, our data shows no correlation between total Hg and $MeHg^+$ ($r_s=-0.05$, $p=0.9$). Moreover, $MeHg^+$ contents were in anti-correlation with contents of most of the measured elements (Fig. 5).

Several processes of $MeHg^+$ production in the polar environment have been suggested, but the pathways and methylation/demethylation processes which occur are still not fully understood (Steffen et al. 2008). Snowmelt water has been identified as a significant source of $MeHg^+$ in the High Arctic, and elevated levels of bioavailable Hg were found in snow after the MDE (Loseto et al. 2004; Steffen et al. 2008).

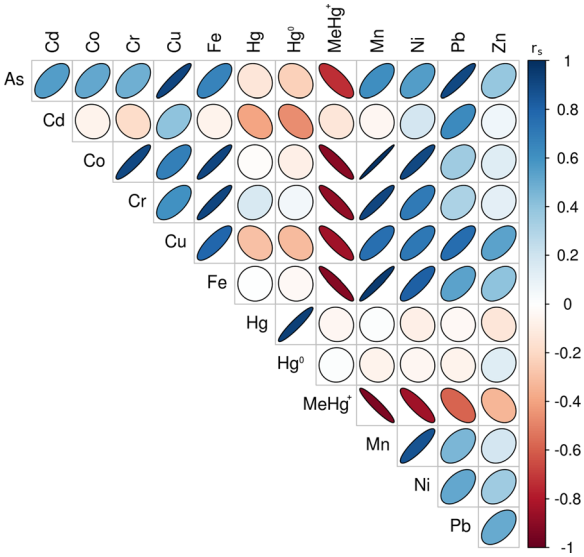

Fig. 5 Matrix of Spearman rank correlations between measured elements. The r_s coefficients are denoted both by *different shapes of ellipse and different colours* (Murdoch and Chow 1996). *Thin and deeply coloured ellipses* refer to the strongest correlations, *the inclination of an ellipse* indicates the sign of the correlation. (*Thin blue ellipses* refer to the strongest positive correlations, *thin red* to the negative.)

Table 2 Contents of heavy metals in samples and reported contents for *Usnea antarctica* [mg kg^{-1} d.w.]

Element	As	Cd	Co	Cr	Cu	Mn	Ni	Fe	Pb	Zn
Range	0.9–2.3	0.03–0.05	0.3–1.6	1.9–4.6	1.8–6.7	10–47	1–5.1	1800–6400	0.9–3	12–27
Median	1.5	0.04	0.8	2.7	3.9	26	2.5	3900	2.0	20
Bartels' negative rank[a]	0.97	0.47	0.77	0.85	0.98	0.80	0.39	0.82	0.59	0.55
(Olech 1991)[b]	–	–	–	5.6	2.9	–	2	170	2	7
(Poblet et al. 1997)	–	0–0.03	–	–	–	16–56	2.2–9.5	283–1115	0–2.9	–
(Osyczka et al. 2007)[b]	–	<1.8	–	<1.7	6±1	25±5	–	–	<0.9	26±5

[a] *p* value of Bartels' negative rank test indicates the probability of a decreasing trend of element content from seashore to the interior

[b] reference samples of *Usnea antarctica* originating from areas remote to polar stations on the South Shetland Islands

"–" means that the element was not determined in this work

Ocean evasion of volatile Hg compounds (including dimethylmercury) was postulated as a source of these compounds in glacial meltwater streams (Vandal et al. 1998). The MeHg levels reported for Antarctic waters were some of the highest observed in the open ocean (Cossa et al. 2011). Unique conditions enable the oxidation of atmospheric Hg by halogens followed by its deposition into the sea. Subsequently, it is scavenged by organic particles and together with organic matter it presents a substrate for methylating bacteria in the hypoxic zone. The upwelling water is low in oxygen and rich in MeHg (Cossa et al. 2011). The sampling area is adjacent to Brandy Bay; therefore, the sea may represent a potential source of MeHg for lichens. However, no elevated MeHg levels were found in samples originating from the Brandy Bay seashore (Fig. 4).

In situ methylation in sediment, followed by diffusion into overlaying water, is another suggested cause of the presence of MeHg in the polar environment (Vandal et al. 1998). In the investigated area, conditions for methylation are expected in Monolith Lake and its close vicinity. The bottom of the lake is covered by a thick cyanobacterial mat accumulated on sediment, which allows particularly suitable conditions for microbial methylation. However, no elevated $MeHg^+$ level was observed in sample D. The highest level of $MeHg^+$ (0.098 mg kg^{-1} d.w.) was detected in sample A, originating from the headwater area of Keller Stream with thicker snow accumulation. Lichens in this locality are frequently wetted by meltwater from both the glacial Keller Stream and also snow, which is brought by wind from the south-western sector, where the higher-located glaciers occur.

The methylation abilities of lichens themselves are not well explored. The methylation of arsenic compounds was confirmed for *Hypogymnia* lichen as a part of the detoxification process (Mrak et al. 2008). It was suggested that lichens do not act as simple passive biomonitors, but are actively involved in the uptake, accumulation and/or biotransformation of arsenic, and possibly other elements as well (Machado et al. 2006). Nevertheless, little is known about the transformation of mercury in lichens. Further research has to be undertaken to investigate the applicability of lichens as bioindicators of organometallic compounds.

Selected heavy metals

The concentrations of selected heavy metals (As, Cd, Co, Cr, Cu, Mn, Ni, Fe, Pb and Zn) are presented in Table 2. Generally, the contents of most metals were similar to those already reported for *U. antarctica* in other studies (Table 2). The only exception is Fe, which content is slightly higher than published values; however, it is still of the same order of magnitude. The significant correlation of lithophile elements (Co, Cr, Fe, Mn and Ni) indicate that lichen thalli may be affected by absorbed soil particles. Elevated Fe levels are likely caused by dust particles deposited onto lichen by impaction. A significant relationship has been reported to exist between the concentration of lithophile elements (including Fe and particularly Cu) in Antarctic soils and lichens (Bargagli et al. 1999). Therefore, bedrock composition is supposed to be an influencing factor, since most other metal levels are within the

ranges reported for *U. antarctica* from reference areas.

As follows from the Bartels' test p values (Table 2), the contents of As and Cu decrease with distance from the ocean. This indicates sea spray as a potential source of these metals. In contrast, no significant trend was observed for Cd, Ni, Pb or Zn.

There was no significant correlation found between the content of Hg and that of any other metal (Spearman's correlation coefficient $r_s<0.4$, $p>0.3$, Fig. 5). The same lack of correlation between Hg and some other heavy metals (Pb, Cd) has been reported (Carignan et al. 2009), suggesting decoupling between these elements during emission and/or transport.

Conclusion

Local climate and microclimate conditions are key determinants with respect to total mercury content and its variability in the Antarctic Peninsula region. While the levels of most monitored metals were within already published ranges, total Hg levels determined in the samples of *U. antarctica* originating from the area of Brandy Bay were some of the highest reported in Antarctica. According to the results of this research, elemental mercury and methylmercury accounted for up to 5.0 and 8.1 % of total mercury, respectively. It remains unclear whether these species were accumulated from the environment or whether they are products of lichen metabolism. The effects of atmospheric deposition and sea spray are most likely overlapped by the different abilities of individual thalli to effectively capture pollutants from their immediate surroundings. Nevertheless, lichen species selected for this purpose appeared to be suitable for the monitoring of heavy metals and their deposition patterns in the polar environment. Mercury speciation and the clarification of undergoing biotransformation in lichens should be important tasks for future studies.

Acknowledgments The authors are grateful to the CzechPolar project for the provision of infrastructure (Johann Gregor Mendel Station) and for financial support from the Grant Agency of the Czech Republic, project P503/12/0682. The work of K. Láska was supported by the Masaryk University project MUNI/A/0902/2012 "Global environmental changes and their impacts" (GlobE). The research has been co-funded from the European Social Fund and the state budget of the Czech Republic.

References

Bacci, E., Gaggi, C., Duccini, M., Bargagli, R., & Renzoni, A. (1994). Mapping mercury vapours in an abandoned cinnabar mining area by azalea (Azalea indica) leaf trapping. *Chemosphere*. doi:10.1016/0045-6535(94)90036-1.

Bargagli, R. (2005). *Antarctic ecosystems: environmental contamination, climate change, and human impact*. Berlin: Springer.

Bargagli, R. (2008). Environmental contamination in Antarctic ecosystems. *Science of the Total Environment*. doi:10.1016/j.scitotenv.2008.06.062.

Bargagli, R., & Barghigiani, C. (1991). Lichen biomonitoring of mercury emission and deposition in mining, geothermal and volcanic areas of Italy. *Environmental Monitoring and Assessment*. doi:10.1007/BF00397614.

Bargagli, R., Battisti, E., Focardi, S., & Formichi, P. (1993). Preliminary data on environmental distribution of mercury in northern Victoria Land, Antarctica. *Antarctic Science*. doi:10.1017/S0954102093000021.

Bargagli, R., Sanchez-Hernandez, J. C., Martella, L., & Monaci, F. (1998). Mercury, cadmium and lead accumulation in Antarctic mosses growing along nutrient and moisture gradients. *Polar Biology*. doi:10.1007/s003000050252.

Bargagli, R., Sanchez-Hernandez, J. C., & Monaci, F. (1999). Baseline concentrations of elements in the antarctic macrolichen Umbilicaria decussata. *Chemosphere*. doi:10.1016/S0045-6535(98)00211-2.

Bargagli, R., Agnorelli, C., Borghini, F., & Monaci, F. (2005). Enhanced deposition and bioaccumulation of mercury in Antarctic terrestrial ecosystems facing a coastal polynya. *Environmental Science and Technology*. doi:10.1021/es0507315.

Bartels, R. (1982). The rank version of von Neumann's ratio test for randomness. *Journal of the American Statistical Association*. doi:10.1080/01621459.1982.10477764.

Biester, H., & Scholz, C. (1997). Determination of mercury binding forms in contaminated soils: mercury pyrolysis versus sequential extractions. *Environmental Science and Technology*. doi:10.1021/es960369h.

Bromwich, D. H., Guo, Z., Bai, L., & Chen, Q. (2004). Modeled antarctic precipitation. Part I: spatial and temporal variability*. *Journal of Climate*. doi:10.1175/1520-0442(2004)017<0427:MAPPIS>2.0.CO;2.

Cai, Y., Monsalud, S., Jaffé, R., & Jones, R. D. (2000). Gas chromatographic determination of organomercury following aqueous derivatization with sodium tetraethylborate and sodium tetraphenylborate. Comparative study of gas chromatography coupled with atomic fluorescence spectrometry, atomic emission spectrome. *Journal of Chromatography A, 876*, 147–155.

Cansaran-Duman, D. (2011). Study on accumulation ability of two lichen species Hypogymnia physodes and Usnea hirta at iron-steel factory site, Turkey. *Journal of Environmental Biology, 32*, 839–844.

Carignan, J., Estrade, N., Sonke, J. E., & Donard, O. F. X. (2009). Odd isotope deficits in atmospheric Hg measured in lichens. *Environmental Science and Technology*. doi:10.1021/es900578v.

Červenka, R., Bednařík, A., Komárek, J., Ondračková, M., Jurajda, P., Vítek, T., et al. (2011). The relationship between

the mercury concentration in fish muscles and scales/fins and its significance. *Central European Journal of Chemistry*. doi:10.2478/s11532-011-0105-8.

Cipro, C. V. Z., Yogui, G. T., Bustamante, P., Taniguchi, S., Sericano, J. L., & Montone, R. C. (2011). Organic pollutants and their correlation with stable isotopes in vegetation from King George Island, Antarctica. *Chemosphere*. doi:10.1016/j.chemosphere.2011.07.047.

Conti, M. E., & Cecchetti, G. (2001). Biological monitoring: lichens as bioindicators of air pollution assessment-a review. *Environmental Pollution, 114*, 471–492.

Cook, A. J., & Vaughan, D. G. (2010). Overview of areal changes of the ice shelves on the Antarctic Peninsula over the past 50 years. *Cryosphere*. doi:10.5194/tc-4-77-2010.

Cossa, D., Heimbürger, L.-E., Lannuzel, D., Rintoul, S. R., Butler, E. C. V., Bowie, A. R., et al. (2011). Mercury in the Southern Ocean. *Geochimica et Cosmochimica Acta*. doi:10.1016/j.gca.2011.05.001.

Coufalík, P., Zvěřina, O., & Komárek, J. (2013a). Atmospheric mercury deposited in a peat bog, the Jeseníky Mountains, Czech Republic. *Journal of Geochemical Exploration*. doi:10.1016/j.gexplo.2013.06.005.

Coufalík, P., Zvěřina, O., Komárek, J. (2013b). Ultra-trace analysis of mercury deposition in soils and sediments from James Ross Island, Antarctica. In: *poster Present. 11th Int. Conf. Mercur. as a Glob. Pollut. Edinburgh, Scotland, 28.7.-2.8*. (p 611). http://www.mercury2013.com/view-abstract.php?id=447

Crame, J. A., Pirrie, D., Riding, J. B., & Thomson, M. R. A. (1991). Campanian Maastrichtian (Cretaceous) Stratigraphy of the James-Ross-Island Area, Antarctica. *Journal of the Geological Society (London)*. doi:10.1144/gsjgs.148.6.1125.

Czech Geological Survey. (2009). *James Ross Island—northern part. Topographic map 1:25,000*. Prague: CGS.

Dethloff, K., Glushak, K., Rinke, A., & Handorf, D. (2010). Antarctic 20th century accumulation changes based on regional climate model simulations. *Advances in Meteorology*. doi:10.1155/2010/327172.

Development Core Team, R. (2013). *R: a language and environment for statistical computing*. Vienna: R Foundation for Statistical Computing.

Dos Santos, I. R., Silva-Filho, E. V., Schaefer, C., Maria Sella, S., Silva, C. A., Gomes, V., et al. (2006). Baseline mercury and zinc concentrations in terrestrial and coastal organisms of Admiralty Bay, Antarctica. *Environmental Pollution*. doi:10.1016/j.envpol.2005.07.007.

Engel, Z., Nývlt, D., & Láska, K. (2012). Ice thickness, areal and volumetric changes of Davies Dome and Whisky Glacier (James Ross Island, Antarctic Peninsula) in 1979–2006. *Journal of Glaciology*. doi:10.3189/2012JoG11J156.

Evans, C. A., & Hutchinson, T. C. (1996). Mercury accumulation in transplanted moss and lichens at high elevation sites in Quebec. *Water, Air, and Soil Pollution*. doi:10.1007/BF00282663.

Fitzgerald, W. F., Mason, R. P., & Vandal, G. M. (1991). Atmospheric cycling and air-water exchange of mercury over mid-continental lacustrine regions. *Water, Air, and Soil Pollution*. doi:10.1007/BF00342314.

King, J. C. (2003). The spatial coherence of interannual temperature variations in the Antarctic Peninsula. *Geophysical Research Letters*. doi:10.1029/2002GL015580.

Knops, J. M. H., Nash Iii, T. H., Boucher, V. L., & Schlesinger, W. H. (1991). Mineral cycling and epiphytic lichens: implications at the ecosystem level. *Lichenologist*. doi:10.1017/S0024282991000452.

Krishna, B. M. V., Karunasagar, D., & Arunachalam, J. (2003). Study of mercury pollution near a thermometer factory using lichens and mosses. *Environmental Pollution*. doi:10.1016/S0269-7491(03)00041-1.

Krishna, B. M. V., Karunasagar, D., & Arunachalam, J. (2004). Sorption characteristics of inorganic, methyl and elemental mercury on lichens and mosses: implication in biogeochemical cycling of mercury. *Journal of Atmospheric Chemistry*. doi:10.1007/s10874-004-1242-7.

Kristjánsson, L., Gudmundsson, M. T., Smellie, J. L., Mcintosh, W. C., & Esser, R. (2005). Palaeomagnetic, 40 Ar/39 Ar, and stratigraphical correlation of Miocene–Pliocene basalts in the Brandy Bay area, James Ross Island, Antarctica. *Antarctic Science*. doi:10.1017/S0954102005002853.

Kuballa, T., Leonhardt, E., Schoeberl, K., & Lachenmeier, D. W. (2008). Determination of methylmercury in fish and seafood using optimized digestion and derivatization followed by gas chromatography with atomic emission detection. *European Food Research and Technology*. doi:10.1007/s00217-008-0949-0.

Láska, K., Barták, M., Hájek, J., Prošek, P., & Bohuslavová, O. (2011a). Climatic and ecological characteristics of deglaciated area of James Ross Island, Antarctica, with a special respect to vegetation cover. *Czech Polar Reports*. doi:10.5817/CPR2011-1-5.

Láska, K., Prošek, P., Budík, L., & Budíková, M. (2011b). Method of estimation of solar UV radiation in high latitude location based on satellite ozone retrieval with improved algorithm. *International Journal of Remote Sensing, 32*, 3165–3177.

Leermakers, M., Baeyens, W., Quevauviller, P., & Horvat, M. (2005). Mercury in environmental samples: speciation, artifacts and validation. *TrAC Trends in Analytical Chemistry*. doi:10.1016/j.trac.2004.01.001.

Lin, C.-J., & Pehkonen, S. O. (1999). The chemistry of atmospheric mercury: a review. *Atmospheric Environment*. doi:10.1016/S1352-2310(98)00387-2.

Lindberg, S. E., & Stratton, W. J. (1998). Atmospheric mercury speciation: concentrations and behavior of reactive gaseous mercury in ambient air. *Environmental Science and Technology*. doi:10.1021/es970546u.

Lindberg, S. E., Brooks, S., Lin, C. J., Scott, K. J., Landis, M. S., Stevens, R. K., et al. (2002). Dynamic oxidation of gaseous mercury in the Arctic troposphere at polar sunrise. *Environmental Science and Technology*. doi:10.1021/es0111941.

Lodenius, M. (2013). Use of plants for biomonitoring of airborne mercury in contaminated areas. *Environmental Research*. doi:10.1016/j.envres.2012.10.014.

Lodenius, M., Tulisalo, E., & Soltanpour-Gargari, A. (2003). Exchange of mercury between atmosphere and vegetation under contaminated conditions. *Science of the Total Environment*. doi:10.1016/S0048-9697(02)00566-1.

Loppi, S., & Bonini, I. (2000). Lichens and mosses as biomonitors of trace elements in areas with thermal springs and fumarole activity (Mt. Amiata, central Italy). *Chemosphere*. doi:10.1016/S0045-6535(00)00026-6.

Loseto, L. L., Lean, D. R. S., & Siciliano, S. D. (2004). Snowmelt sources of methylmercury to high arctic ecosystems. *Environmental Science and Technology*. doi:10.1021/es035146n.

Lupsina, V., Horvat, M., Jeran, Z., & Stegnar, P. (1992). Investigation of mercury speciation in lichens. *Analyst, 117*, 673–675.

Machado, A., Šlejkovec, Z., Elteren, J. T., Freitas, M. C., & Baptista, M. S. (2006). Arsenic speciation in transplanted lichens and tree bark in the framework of a biomonitoring scenario. *Journal of Atmospheric Chemistry*. doi:10.1007/s10874-006-9013-2.

Mão de Ferro, A., Mota, A. M., & Canário, J. (2014). Pathways and speciation of mercury in the environmental compartments of Deception Island, Antarctica. *Chemosphere*. doi:10.1016/j.chemosphere.2013.08.081.

Martin, P. J., & Peel, D. A. (1978). The spatial distribution of 10m temperatures in the Antarctic Peninsula. *Journal of Glaciology, 20*, 311–317.

Mlakar, T. L., Horvat, M., Kotnik, J., Jeran, Z., Vuk, T., Mrak, T., et al. (2011). Biomonitoring with epiphytic lichens as a complementary method for the study of mercury contamination near a cement plant. *Environmental Monitoring and Assessment*. doi:10.1007/s10661-010-1825-5.

Montone, R. C., Taniguchi, S., & Weber, R. R. (2003). PCBs in the atmosphere of King George Island, Antarctica. *Science of the Total Environment*. doi:10.1016/S0048-9697(02)00649-6.

Mrak, T., Slejkovec, Z., Jeran, Z., Jaćimović, R., & Kastelec, D. (2008). Uptake and biotransformation of arsenate in the lichen Hypogymnia physodes (L.) Nyl. *Environmental Pollution*. doi:10.1016/j.envpol.2007.06.011.

Murdoch, D. J., & Chow, E. D. (1996). A graphical display of large correlation matrices. *American Statistician*. doi:10.2307/2684435.

Nevado, J. J. B., Martín-Doimeadios, R. C. R., Krupp, E. M., Bernardo, F. J. G., Fariñas, N. R., Moreno, M. J., et al. (2011). Comparison of gas chromatographic hyphenated techniques for mercury speciation analysis. *Journal of Chromatography A*. doi:10.1016/j.chroma.2011.05.036.

Nóvoa-Muñoz, J. C., Pontevedra-Pombal, X., Martínez-Cortizas, A., & García-Rodeja Gayoso, E. (2008). Mercury accumulation in upland acid forest ecosystems nearby a coal-fired power-plant in southwest Europe (Galicia, NW Spain). *Science of the Total Environment*. doi:10.1016/j.scitotenv.2008.01.044.

Nývlt, D., Braucher, R., Engel, Z., & Mlčoch, B. (2014). Timing of the Northern Prince Gustav Ice Stream retreat and the deglaciation of northern James Ross Island, Antarctic Peninsula during the last glacial–interglacial transition. *Quaternary Research*. doi:10.1016/j.yqres.2014.05.003.

Olech, M. (1991). Preliminary observations on the content of heavy metals in thalli of Usnea antarctica Du Rietz (Lichenes) in the vicinity of the "H. Arctowski" Polish Antarctic Station. *Polish Polar Research, 12*, 129–131.

Osyczka, P., Dutkiewicz, E., & Olech, M. (2007). Trace elements concentrations in selected moss and lichen species collected within Antarctic research stations. *Polish Journal of Ecology, 55*, 39–48.

Pisani, T., Munzi, S., Paoli, L., Bačkor, M., Kováčik, J., Piovár, J., et al. (2011). Physiological effects of mercury in the lichens Cladonia arbuscula subsp. mitis (Sandst.) Ruoss and Peltigera rufescens (Weiss) Humb. *Chemosphere*. doi:10.1016/j.chemosphere.2010.10.062.

Poblet, A., Andrade, S., Scagliola, M., Vodopivez, C., Curtosi, A., Pucci, A., et al. (1997). The use of epilithic Antarctic lichens (Usnea aurantiacoatra and U. antartica) to determine deposition patterns of heavy metals in the Shetland Islands, Antarctica. *Science of the Total Environment*. doi:10.1016/S0048-9697(97)00265-9.

Rabassa, J., Skvarca, P., Bertani, L., Mazzoni, E. (1982). *Glacier inventory of james ross and vega islands, antarctic peninsula**. p. 260–264.

Rott, H., Skvarca, P., & Nagler, T. (1996). Rapid collapse of Northern Larsen Ice Shelf, Antarctica. *Science*. doi:10.1126/science.271.5250.788.

Schlüter, K. (2000). Review: evaporation of mercury from soils. An integration and synthesis of current knowledge. *Environmental Geology*. doi:10.1007/s002540050005.

Schroeder, W. H., & Munthe, J. (1998). Atmospheric mercury—an overview. *Atmospheric Environment*. doi:10.1016/S1352-2310(97)00293-8.

Skov, H., Christensen, J. H., Goodsite, M. E., Heidam, N. Z., Jensen, B., Wåhlin, P., et al. (2004). Fate of elemental mercury in the Arctic during atmospheric mercury depletion episodes and the load of atmospheric mercury to the Arctic. *Environmental Science and Technology*. doi:10.1021/es030080h.

Slemr, F., Seiler, W., & Schuster, G. (1981). Latitudinal distribution of Mercury over the Atlantic Ocean. *Journal of Geophysical Research*. doi:10.1029/JC086iC02p01159.

Slemr, F., Schuster, G., & Seiler, W. (1985). Distribution, speciation, and budget of atmospheric mercury. *Journal of Atmospheric Chemistry*. doi:10.1007/BF00053870.

Steffen, A., Douglas, T., Amyot, M., Ariya, P., Aspmo, K., Berg, T., et al. (2008). A synthesis of atmospheric mercury depletion event chemistry in the atmosphere and snow. *Atmospheric Chemistry and Physics*. doi:10.5194/acp-8-1445-2008.

Strelin, J., Sone, T., Mori, J., Torielli, C., Nakamura, T. (2006). New Data Related to Holocene Landform Development and Climatic Change from James Ross Island, Antarctic Peninsula. *Antarct SE, 58*. doi: 10.1007/3-540-32934-X_58.

Száková, J., Kolihová, D., Miholová, D., & Mader, P. (2004). Single-purpose atomic absorption spectrometer AMA-254 for mercury determination and its performance in analysis of agricultural and environmental materials. *Chemical Papers, 58*, 311–315.

Turner, J., Colwell, S. R., Marshall, G. J., Lachlan-Cope, T. A., Carleton, A. M., Jones, P. D., et al. (2005). Antarctic climate change during the last 50 years. *International Journal of Climatology*. doi:10.1002/joc.1130.

Vandal, G. M., Mason, R. P., McKnight, D., & Fitzgerald, W. (1998). Mercury speciation and distribution in a polar desert lake (Lake Hoare, Antarctica) and two glacial meltwater streams. *Science of the Total Environment*. doi:10.1016/S0048-9697(98)00095-3.

Vaughan, D. G., Marshall, G. J., Connolley, W. M., King, J. C., & Mulvaney, R. (2001). Climate change. Devil in the detail. *Science*. doi:10.1126/science.1065116.

Wängberg, I., Munthe, J., Pirrone, N., Iverfeldt, Å., Bahlman, E., Costa, P., et al. (2001). Atmospheric mercury distribution in Northern Europe and in the Mediterranean region.

Atmospheric Environment. doi:10.1016/S1352-2310(01)00105-4.

William, H. S., Munthe, J., & Schroeder, W. H. (1998). Atmospheric mercury—an overview. *Atmospheric Environment*. doi:10.1016/S1352-2310(97)00293-8.

Wojtuń, B., Kolon, K., Samecka-Cymerman, A., Jasion, M., & Kempers, A. J. (2013). A survey of metal concentrations in higher plants, mosses, and lichens collected on King George Island in 1988. *Polar Biology*. doi:10.1007/s00300-013-1306-8.

Příloha X

Microchemical Journal 140 (2018) 8–13

Contents lists available at ScienceDirect

Microchemical Journal

journal homepage: www.elsevier.com/locate/microc

Determination of methylmercury in cryptogams by means of GC-AFS using enzymatic hydrolysis

Pavel Coufalík [a,b,*], Natália Meszarosová [a], Kateřina Coufalíková [a], Ondřej Zvěřina [a,c], Josef Komárek [a]

[a] Department of Chemistry, Faculty of Science, Masaryk University, Kotlářská 2, 611 37 Brno, Czech Republic
[b] Institute of Analytical Chemistry of the Czech Academy of Sciences, v.v.i., Veveří 97, 602 00 Brno, Czech Republic
[c] Department of Public Health, Faculty of Medicine, Masaryk University, Kamenice 5, 625 00 Brno, Czech Republic

ARTICLE INFO

Article history:
Received 24 January 2018
Received in revised form 29 March 2018
Accepted 29 March 2018
Available online 30 March 2018

Keywords:
Methylmercury
Cyanobacterium
Alga
Lichen
GC-AFS

ABSTRACT

Since methylmercury is a highly toxic compound, there is undoubtedly a need for the monitoring of methylmercury in the ecosystem. However, its isolation from the organic matrix using an appropriate analytical procedure and sensitive detection technique are necessary due to trace levels of methylmercury in biomonitors. This study focuses on the determination of methylmercury in plant matrices by means of GC-AFS. The developed extraction procedure is based on the enzymatic hydrolysis of the matrix by cellulase, followed by the extraction of methylmercury in hydrochloric acid and the extraction of derivatized methylmercury into the organic phase. The limit of detection of methylmercury in environmental samples was 4 μg kg^{-1}. The method demonstrated sufficient precision, accuracy, and repeatability with respect to the determination of methylmercury in cryptogams. High contents of methylmercury (up to 60.9 ± 4.4 μg kg^{-1}) were determined in cyanobacterial mats from James Ross Island (Antarctic Peninsula). Thus, freshwater lakes and wetlands in Antarctica can be sources of methylmercury for the local ecosystem.

© 2018 Elsevier B.V. All rights reserved.

1. Introduction

Mercury is a global pollutant whose concentration in ecosystems is growing. The contamination of polar regions caused by long-range transport of Hg and its deposition in cold regions of the Earth poses a significant environmental risk due to the high bioaccumulation of Hg and its forms. The biogeochemical cycle of Hg is already very well explored [1–8] as well as the atmospheric chemistry in Antarctica regarding Atmospheric Mercury Depletion Events (AMDEs) [1,2]. Generally, Hg concentrations in biomonitors are commonly measured to assess Hg deposition from the atmosphere. Antarctic regolith has been found to be unusable as an indicator because of its low Hg retention [4]. The deposition of bioavailable Hg is increased in deglaciated Antarctic regions; therefore, Hg contents in Antarctic cryptogams are the same or higher than in the Northern Hemisphere [2,9]. Lakes and wetlands with colonies of microorganisms (cyanobacterial mat) represent an important part of the biomass occurring on land. In addition to lichens and mosses, cyanobacterial mats are major accumulators of Hg from melt water during the summer season [1,3]. Cyanobacterial mats have a complex internal structure and are often formed by a large number of species of cyanobacteria, algae, and diatoms [3], which results in a variable ability to accumulate metals.

The biotic and abiotic formation of methylmercury (MeHg) are key processes with respect to Hg speciation changes in the aquatic environment [8]. Methylmercury is formed primarily in anoxic aquatic environments, especially in sediments [5,7]. Biogeochemical changes in the ecosystem are particularly noticeable in lakes without any outflow because they accumulate dissolved compounds and solid particles [1]. The rate of methylation depends on the bioavailability of Hg^{2+} and the activity of methylating microorganisms [5]. The intake of metals by organisms in water involves two steps: the reaction of metal ions with reactive sites on the biological membrane and transport into the organism. However, there is competition with dissolved ligands (e.g. sulphides) in the water column and colloids [10].

A large number of analytical procedures for the determination of MeHg in sediments have been published; for these, see the review published by Jagtap and Maher [11]. Substantially fewer studies are concerned with the determination of MeHg in cyanobacterial mats [3] or in lichens [9]. The quantitative extraction of MeHg from the matrix is necessary for its determination in environmental samples. During the extraction step, Hg speciation must not be changed. Acid and alkaline extraction, and also distillation were used to extract MeHg from the sample matrix [6,12–14]. HCl [9], HBr [15], HNO_3 [16,17], and H_2SO_4 [18] were used for the acid extraction of MeHg in plant material.

* Corresponding author at: Institute of Analytical Chemistry of the Czech Academy of Sciences, v.v.i., Veveří 97, 602 00 Brno, Czech Republic.
E-mail address: coufalik@iach.cz. (P. Coufalík).

https://doi.org/10.1016/j.microc.2018.03.040
0026-265X/© 2018 Elsevier B.V. All rights reserved.

Methanolic solutions of KOH are most commonly used for alkaline extraction [12,19,20].

A number of analytical methods for the determination of MeHg have been used [14], of which gas chromatography (GC) [21] or high performance liquid chromatography (HPLC) [13] are the most commonly used separation techniques. Atomic fluorescence spectrometry (AFS) [3,9,21], cold vapor atomic fluorescence spectrometry (CV-AFS) [12,13,17,19,20,22,23], microwave-induced plasma atomic emission spectrometry (MIP-AES) [21], inductively coupled plasma mass spectrometry (ICP-MS) [16,24], atomic absorption spectrometry (AAS) [18], and electron capture detection (ECD) [15] are used as the detection techniques. The derivatization of Hg species is necessary for the most frequent determination of MeHg by a tandem technique involving GC. The ethylation or phenylation of MeHg with sodium tetraethylborate or sodium tetraphenylborate is carried out at a pH of 4.5–5 adjusted with acetate buffer, acids, or bases [3,16,19,21,25]. Derivatization is followed by extraction into the organic phase (e.g. hexane, toluene), thereby also concentrating the analyte prior to GC separation [14,15,21]. Besides analytical procedures using extract purification [20], pre-concentration by solid phase extraction [13] and a non-chromatographic separation technique (liquid/liquid extraction) [14,18] were developed for the determination of MeHg in environmental samples.

The main objective of this research was to develop a new analytical method for the determination of trace levels of MeHg in plant material using gas chromatography coupled to atomic fluorescence spectrometry (GC-AFS). The second aim was to study MeHg bioaccumulation in the Antarctic cyanobacterial mat.

2. Material and methods

2.1. Reagents and standards

All chemicals were obtained from Sigma-Aldrich. Cellulase from *Aspergillus niger* was used for the enzymatic hydrolysis of samples. The following chemicals were used for MeHg extraction, the treatment of extracts, and derivatization: HCl (≥37%, Hg ≤ 0.0000005%), NaOH (≥98%, Hg ≤ 0.000005%), CH_3COOH (≥99.8%), CH_3COONa (ACS reagent), $(CH_3CH_2)_4BNa$ (97%). Hexane (≥99%) was used for the pre-concentration of the analyte.

CH_3HgCl and Mercury Standard for AAS (1000 ± 4 mg L^{-1} Hg in 2 mol L^{-1} HNO_3) were used for the preparation of calibration solutions. The standard of MeHg (1 g L^{-1}) was prepared by the dissolution of CH_3HgCl in methanol (99.9%). Calibration solutions of MeHg were prepared by dilution of the standard in deionized water. An aqueous solution containing Hg^0 was prepared by saturating deionized water with metallic mercury.

Certified reference material (CRM) of BCR-482 Lichen (IRMM, Belgium) with a total Hg content of 0.48 ± 0.02 mg kg^{-1} was used during the development of the analytical method.

2.2. Samples of cyanobacterial mat

Samples of the Antarctic cyanobacterial mat from James Ross Island (Antarctic Peninsula) were studied in this work. The characteristics of the studied area are described in the literature [4,9,26]. Samples were collected in the deglaciated area of the Ulu Peninsula from Johnson Mesa Lake, Monolith Lake, the Interlagos ponds, and seepage near J.G. Mendel Czech Antarctic Station. Detailed description of the localities, and of the sampling and sample characteristics (including species of microorganisms) are reported in Coufalík et al. [26]. Lyophilized and homogenized samples were used for the analysis.

2.3. Extraction procedure

The following aspects of the extraction procedure were considered: the quantitative extraction of MeHg; the avoidance of losses, contamination, and speciation changes; and the pre-concentration of trace contents. Accordingly, a suitable extraction method should include the use of sufficient sample weights, the use of the maximum volume of sample extract, and an advantageous ratio between aqueous and organic phases.

The developed extraction procedure is presented in Fig. 1. One hundred milligram of homogenized sample or CRM was weighed into a centrifuge tube and suspended in an acetate buffer (pH = 5) prepared from acetic acid and sodium acetate. An ultrasonic bath was used to thoroughly wet the sample particles. One milligram of cellulase (freshly dissolved in deionized water) was added to the sample and the sample was incubated in a water bath placed in an oven at 40 °C for 24 h. Subsequently, acid extraction with hydrochloric acid was performed in an ultrasonic bath for 4 h. The temperature of the ultrasonic bath was maintained at about 40 °C. After sample centrifugation, 3 mL of the extract was used for analysis. Follow-up treatment of the aqueous extract was carried out in a Kimble Mini Reaction Vial with a Screw Cap Mininert Valve (10 mL, Chromatography Research Supplies, USA). (This vial is suitable for the work with volatile analytes.) The extract was diluted with deionized water and a portion of the hydrochloric acid in the extract was neutralized by the addition of sodium hydroxide solution. Solid sodium acetate was added to the solution and the vial was sealed. The solution had a pH = 5. The pH of the solutions was monitored using a S220 SevenCompact pH Meter (Mettler Toledo). Hexane and derivatizing agent were added via the septum. (An aqueous solution of sodium tetraethylborate was prepared under an argon atmosphere every day and stored in a CERTAN capillary bottle.) MeHg was extracted into the organic phase. The determination of MeHg in the prepared extracts was performed on the same day. The removal of 4 μL of extract for analysis was performed using a Hamilton syringe with the vial turned upside down. Thus, the hexane phase created a thicker layer for convenient offtake in the conical part of the vial. In addition, the risk of analyte losses through the headspace was minimized.

For maximum pre-concentration of the analyte in the organic phase, the following conditions were changed during optimization of the procedure: the amount of sample (10–100 mg), the pH of the buffer during enzymatic hydrolysis (pH = 4 or pH = 5), the amount of enzyme (1–4 mg), the amount of hexane (0.2–1 mL), and the amount of derivatizing agent (0.1–0.5 mL) and its concentration (1–2%, w/v). Filtration using Whatman quartz filters (Grade GF/B) was performed in the case of insufficient separation of the solid sample during centrifugation.

2.4. Determination of mercury

An Agilent Technologies 6890 N Network gas chromatograph (USA) with a PSA 10.750 atomic fluorescence spectrometer (UK) was used for the determination of MeHg in extracts. In this commercial system, the detector was coupled to gas chromatograph via a pyrolysis oven held at 800 °C. The source of radiation in the atomic fluorescence detector was a mercury lamp with a wavelength of 253.7 nm. The HP-5 capillary column had an inner diameter of 0.25 mm and a length of 30 m. For MeHg determination, 4 μL of sample was injected in Splitless mode at an injector temperature of 220 °C. The column was heated according to the following temperature program: from 50 °C to 130 °C at 13 °C min^{-1}, from 130 °C to 230 °C at 100 °C min^{-1}. Argon at a flow rate of 0.9 mL min^{-1} was used as the carrier gas. Data were evaluated in the Agilent ChemStation.

The total Hg content in samples was determined by an AMA-254 mercury analyzer (Altec, Czech Republic). This atomic absorption spectrometer allows the dosing of solid and liquid samples. The Hg content in solid samples was determined for weights of about 100 mg. The total Hg content in liquid solutions was determined from volumes of 100 μL.

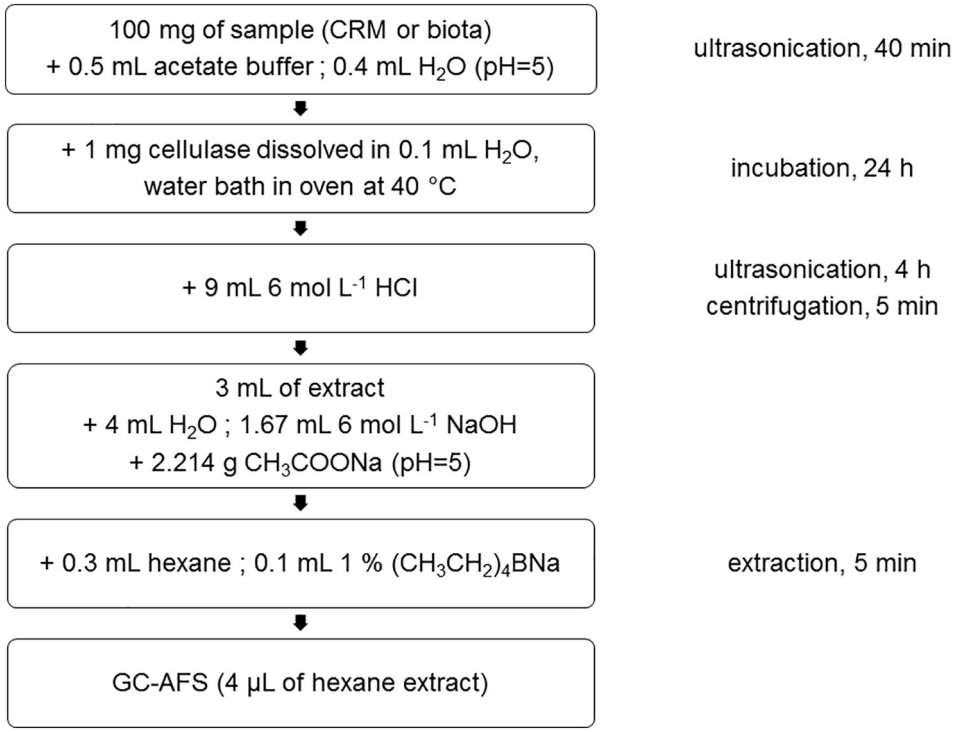

Fig. 1. The scheme of the extraction procedure.

2.5. QA/QC control

Emphasis was placed on the efficiency of MeHg extraction and the monitoring of potential contamination or losses during the individual extraction steps. The stabilities of the calibration solutions and derivatizing agent were also monitored.

Laboratory glass was cleaned in diluted HNO_3 for 24 h, rinsed with deionized water, and heated in the oven to 250 °C for 2 h. The work was carried out in a clean laboratory equipped with HEPA filters. Blank measurements were performed among the measurements of samples and calibration solutions; the preparation of blanks included all extraction steps as samples and standards. The limit of detection (LOD) and the limit of quantification (LOQ) of the method were determined as three times, and ten times the standard deviation (SD) of the experimental blanks, respectively. Potential Hg losses or contamination of the blank from the glassware were continuously monitored using rinses with a clean solution of HCl in which the total Hg content was determined. Control rinses were performed randomly.

The linearity of calibration curve was observed across the range of 0.1–10 ng MeHg (in absolute amounts); the first calibration point was measured near the LOD of the method. Fresh calibration solution (0.1 mg L^{-1}) was prepared daily by dilution of the standard. The retention times of Hg^0, MeHg, and Hg^{2+} were determined using deionized water with Hg^0 and standards of MeHg and Hg^{2+}. For the assessment of possible matrix interference, calibration using standard solutions was compared with that using a standard addition method. As no significant difference in the slopes of the two calibration methods was observed, the quantification of MeHg in real samples was performed against the calibration curve.

The method was developed using a CRM BCR-482. The extraction yield was assessed according to MeHg spikes to 100 mg of BCR-482 and the selected sample of cyanobacterial mat (Interlagos ponds). The contents of MeHg in samples of cyanobacterial mat were determined from three analyses.

3. Results and discussion

3.1. Determination of MeHg by GC-AFS

The determination of MeHg using the developed procedure demonstrated sufficient accuracy, trueness, repeatability, and linearity, as well as a sufficient LOQ with respect to the determination of trace concentrations of MeHg in the organic matrix of cryptogams. Fig. 2a presents the chromatograms of Hg species corresponding to Hg^0 (t_R = 2.00 min), MeHgEt (t_R = 3.45 min, i.e. ethylated MeHg), and $HgEt_2$ (t_R = 4.37 min, i.e. ethylated Hg^{2+}). The peaks of Hg^0 and Hg^{2+} in Fig. 2a correspond to the additions of Hg^0 in deionized water and the standard of Hg^{2+}. The peaks of MeHg correspond to the calibration points for 0.3, 3, 5, and 10 ng MeHg (in absolute amounts). Linear regression equation, LOD and LOQ of MeHg are given in Table 1. The range of the calibration curve (0.1–10 ng MeHg) corresponded to 3–333 ng g^{-1} MeHg in the solid sample. No MeHg was detected during blank measurements; thus, any contamination by MeHg or Hg methylation during the extraction procedure were avoided.

The extraction recovery of MeHg and the accuracy of determination in the presence of the organic matrix were determined by spikes (10 ng MeHg) to three parallel weights of 100 mg BCR-482 and 100 mg of cyanobacterial mat (Interlagos ponds); the recoveries were 99.5–103% and 99.0–101.8%, respectively. Thus, there were no losses or speciation changes of MeHg during the extraction. The repeatability was also determined by spikes to BCR-482; the relative standard deviation (RSD) of the determination was 3% for six parallel analyses.

The MeHg content in the CRM BCR-482 was determined according to the calibration curve in unspiked and spiked (10 ng MeHg) samples (Fig. 2b). The content of MeHg in unspiked CRM BCR-482 was 30.9 ± 0.9 μg kg^{-1}. The MeHg content in BCR-482 after spike subtraction was within the quoted uncertainty. The MeHg content in mat from the Interlagos ponds was 17.0 ± 1.4 μg kg^{-1} (Table 2). The MeHg content in the spiked sample also corresponded to the content determined after the subtraction of the spike.

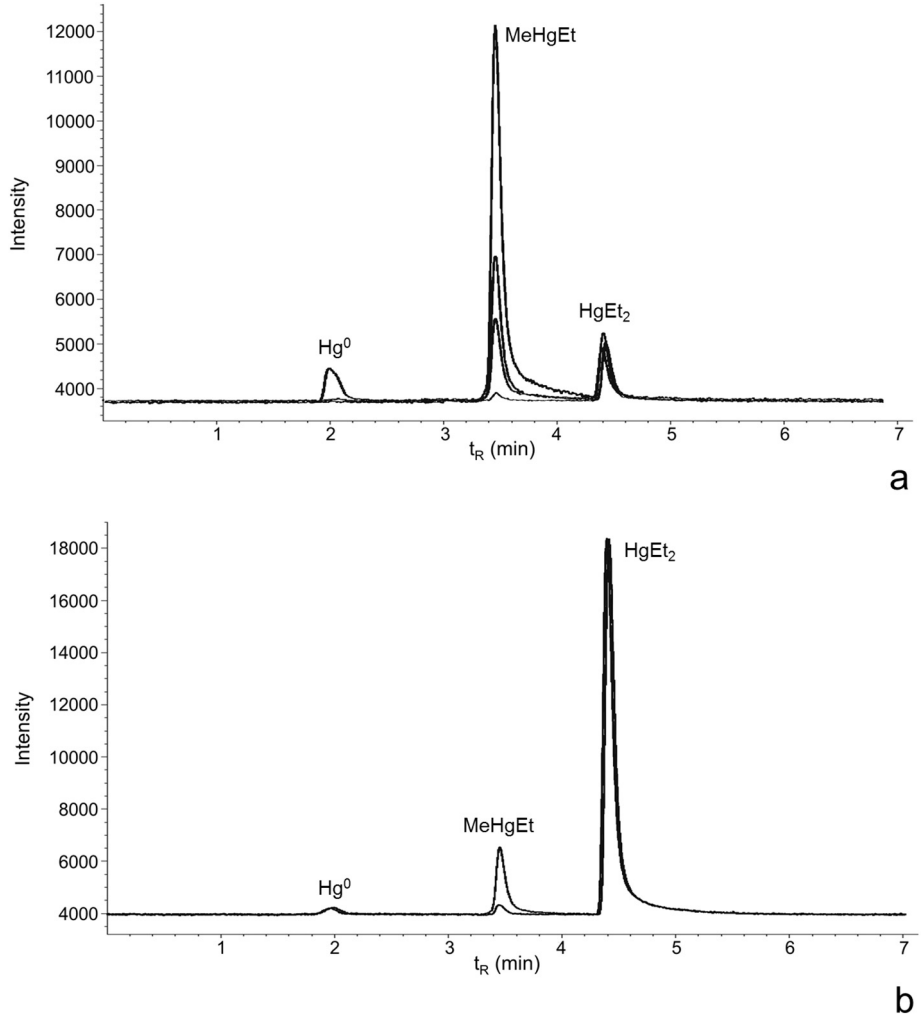

Fig. 2. GC chromatograms: a – calibration solutions of Hg^0 ($t_R = 2.00$), MeHg ($t_R = 3.45$), and Hg^{2+} ($t_R = 4.37$); b – spiked and unspiked CRM BCR-482.

The optimization of extraction parameters was performed regard to the extraction recovery of MeHg in spiked samples. One milligram of cellulase was sufficient for the enzymatic hydrolysis of 100 mg of sample. Enzymolysis at pH = 4 and pH = 5 did not differ; an acetate buffer with a pH of 5 was selected. Derivatization of spiked samples was performed quantitatively with 100 μL of 1% sodium tetraethylborate, higher amounts of derivatizing agent were unnecessary. Two hundred microliter of hexane can be used for the maximum concentration of the analyte; however, the use of 300 μL of the organic phase allows easier sampling. Larger volume of organic phase deteriorates LOD.

The acid extraction of samples in 6 mol L^{-1} HCl followed by ethylation and extraction in hexane was used to determine MeHg levels in microorganisms and in lichens [9,25]. However, this procedure only works well with higher dilutions of the sample in acetate buffer and a larger volume of the final organic phase. The MeHg content in the sample must be sufficient for such dilution. Otherwise, a higher volume of the extract should be used and the analyte should be concentrated into a small volume of the organic phase. However, this approach increases matrix effects. Because of the low Hg contents in Antarctic cyanobacterial mat, extraction with the highest pre-concentration factor was necessary. Thus, three milliliter of HCl extract was used for MeHg determination when using a small volume of the organic phase. (3 mL of extract had to be diluted with 4 mL of water because of the high content of inorganic salts in the treated sample for MeHg derivatisation.)

In the first experiments, a very low recovery (about 5%) was found for spiked BCR-482, but the recovery increased (22%) in the case of lower sample weights (10 mg). A dense foam formed during the extraction of MeHg from the aqueous phase into hexane and the hexane was turbid. A distinct precipitate formed in 1 mL of hexane in the case of a higher dilution of aqueous extract. Precipitate formation was also observed for samples of cyanobacterial mat. The emerging precipitate from the organic matrix made the analysis of environmental samples impossible.

90–95% of the thallus of lichens is comprised of hyphae. The photobionts in lichens are often composed of cyanobacteria (e.g., *Nostoc*, *Calothrix*) [27], whose presence was confirmed in mat samples [26]. Lichens have high contents of polysaccharides, chitin, lichenin, isolichenin, hemicellulose and other substances [27]. In general, carbohydrates protect the organisms from environmental stress and increase their tolerance to temperature changes [28]. Lichenin ("moss starch") undergoes enzymolysis with cellulase [29]. Therefore, a modified form of enzymatic hydrolysis [30] was employed prior to the extraction of MeHg to prevent the formation of precipitate in the hexane phase.

Table 1
Linear regression equations, LOD and LOQ of methylmercury and total mercury.

Mercury species	Linear regression equation	R^2	LOD (μg kg^{-1})	LOQ (μg kg^{-1})
MeHg	$y^a = 4106x$	0.998	4	12.6
Total Hg	$y^b = 0.0995x$	0.999	0.1	0.3

[a] y – peak area, x – Hg (ng); GC-AFS.
[b] y – peak height, x – Hg (ng); mercury analyzer.

Table 2
Contents[a] of total mercury and methylmercury in samples of cyanobacterial mat.

Sample	Total Hg (μg kg^{-1})	MeHg$^+$ (μg kg^{-1})	MeHg$^+$ (%)
Johnson Mesa L. – site A	88.5 ± 0.1	–	–
Johnson Mesa L. – site B	309 ± 5.6	13.7 ± 0.7	4.4 ± 0.2
Monolith L. inlet – site A	37.2 ± 1.0	15.0 ± 0.3	40.2 ± 0.7
Monolith L. inlet – site B	26.0 ± 1.0	11.6 ± 3.4	45 ± 13
Interlagos ponds	46.4 ± 1.0	17.0 ± 1.4	36.7 ± 3.1
Seepage – site A	80.9 ± 0.4	60.9 ± 4.4	75.3 ± 5.4
Seepage – site B	25.6 ± 1.1	–	–
Seepage – site C	27.2 ± 1.2	9.8 ± 1.8	36.1 ± 6.8

– the content under LOD.
[a] $\bar{x} \pm$ SD; $N = 3$.

Precipitation or turbidity in extracts did not occur thanks to the activity of cellulase from *Aspergillus niger*. The proposed procedure of the enzymatic hydrolysis of the organic matrix appears to be universally applicable to samples with similar chemical compositions to lichens (algae, cyanobacteria and bryophytes), these also having a high carbohydrate content [28].

3.2. Bioaccumulation of MeHg in cyanobacterial mat

After verification of the analytical method, total Hg and MeHg were determined in samples of Antarctic cyanobacterial mat. The results are summarized in Table 2. The determination of total Hg by the AMA-254 analyzer was verified using CRM; the content in BCR-482 was 0.484 ± 0.004 mg kg^{-1}, which corresponded to the certified value. (LOD and LOQ of total Hg are in Table 1.) Total Hg contents in mat samples ranged from 25.6 μg kg^{-1} to 308.7 μg kg^{-1}; the RSD of the determination reached a maximum value of 4.5%.

The MeHg contents in mats ranged from 9.8 to 60.9 μg kg^{-1}; two samples had contents below the LOD. The RSD of the determination reached a maximum of 8.2% at values above the LOQ (12.6 μg kg^{-1}). MeHg formed a significant proportion of total Hg in most samples.

The contents of total Hg in regolith and sediments on James Ross Island range between 2.7 and 11.3 μg kg^{-1}, which can be considered as a background value in this part of Antarctica [4]. Sea spray was confirmed to have a small influence in the case of cyanobacterial mats in the studied localities [26]. Sea spray is not a significant source of Hg in this area according to the analysis of *Usnea antarctica* lichens. A large proportion of Hg in the local ecosystem likely originates from atmospheric deposition [9].

Generally, total Hg contents in Antarctic cyanobacterial mat can be up to hundreds of μg kg^{-1}. *Usnea* lichens accumulate higher Hg concentrations than the mat in the same area [2]. Concentrations of total Hg in mat samples (Table 2) were comparable to other areas in Antarctica [2] and significantly lower than concentrations in *Usnea antarctica* lichens in the studied area [9]. Hg concentrations in cyanobacterial mat may not be associated with their biological activity but with the growth rate of microbial colonies [3]. The bioaccumulation of Hg in mat can be increased by organic sulfur and sulphides [1]. Nevertheless, the determined Hg contents in samples did not demonstrate any correlation with sulfur [26] in this case.

The determined MeHg concentrations in cyanobacterial mat were comparable to MeHg concentrations in *Usnea antarctica* lichens [9]. Thus, the ratio of MeHg to total Hg in mats was very high, even in comparison with cyanobacterial mats in other Antarctic regions [3]. Increased methylation of Hg often occurs at elevated temperatures and with the prolongation of thermally favourable conditions [5]. It is probable that the biological activity of microorganisms methylating inorganic Hg is high because of the temperatures of the surface water in the studied area during the summer season [26].

4. Conclusion

The developed analytical procedure enables the determination of trace levels of MeHg in plant material by means of GC-AFS. The activity of *cellulase* enzyme caused the hydrolysis of the organic matrix, which avoided precipitate formation in the organic phase during the extraction of MeHg. The procedure was developed on lichen, algae and cyanobacteria, and, thus, can be used for organic matrices with a similar chemical composition. The method offers sufficient precision, accuracy, and repeatability with respect to measurements of environmental samples. MeHg concentrations in Antarctic cyanobacterial mat were determined. Cyanobacterial mats on James Ross Island exhibited very high contents of MeHg, which indicated ongoing methylation processes.

Acknowledgement

The authors are grateful for use of the facilities of the J.G. Mendel Czech Antarctic Station. The research was supported by Masaryk University under the MUNI/A/0886/2016 project, and by the Institute of Analytical Chemistry of the CAS under the Institutional Research Plan RVO: 68081715.

References

[1] R. Bargagli, F. Monaci, C. Bucci, Environmental biogeochemistry of mercury in Antarctic ecosystems, Soil Biol. Biochem. 39 (2007) 352–360.
[2] R. Bargagli, Atmospheric chemistry of mercury in Antarctica and the role of cryptogams to assess deposition patterns in coastal ice-free areas, Chemosphere 163 (2016) 202–208.
[3] A. Camacho, C. Rochera, R. Hennebelle, C. Ferrari, A. Quesada, Total mercury and methyl-mercury contents and accumulation in polar microbial mats, Sci. Total Environ. 509–510 (2015) 145–153.
[4] P. Coufalík, O. Zvěřina, L. Krmíček, R. Pokorný, J. Komárek, Ultra-trace analysis of Hg in alkaline lavas and regolith from James Ross Island, Antarct. Sci. 27 (2015) 281–290.
[5] H. Hintelmann, Organomercurials. Their formation and pathways in the environment, in: A. Sigel, H. Sigel, R.K.O. Sigel (Eds.), Organometallics in Environment and Toxicology: Metal Ions in Life Sciences, RSC Publishing, Cambridge 2010, pp. 365–401.
[6] M. Leermakers, W. Baeyens, P. Quevauviller, M. Horvat, Mercury in environmental samples: speciation, artifacts and validation, Trends Anal. Chem. 24 (2005) 383–393.
[7] I. Lehnherr, Methylmercury biogeochemistry: a review with special reference to Arctic aquatic ecosystems, Environ. Rev. 22 (2014) 229–243.
[8] F.M.M. Morel, A.M.L. Kraepiel, M. Amyot, The chemical cycle and bioaccumulation of mercury, Annu. Rev. Ecol. Syst. 29 (1998) 543–566.
[9] O. Zvěřina, K. Láska, R. Červenka, J. Kuta, P. Coufalík, J. Komárek, Analysis of mercury and other heavy metals accumulated in lichen *Usnea antarctica* from James Ross Island, Antarctica, Environ. Monit. Assess. 186 (2014) 9089–9100.
[10] P.P. Gorski, D.E. Armstrong, J.P. Hurley, M.M. Shafer, Speciation of aqueous methylmercury influences uptake by a freshwater alga (*Selenastrum capricornutum*), Environ. Toxicol. Chem. 25 (2006) 534–540.
[11] R. Jagtap, W. Maher, Measurement of mercury species in sediments and soils by HPLC–ICPMS, Microchem. J. 121 (2015) 65–98.
[12] B.D. Hall, V.L.S.T. Louis, Methylmercury and total mercury in plant litter decomposing in upland forests and flooded landscapes, Environ. Sci. Technol. 38 (2004) 5010–5021.
[13] D. Schwesig, O. Krebs, The role of ground vegetation in the uptake of mercury and methylmercury in a forest ecosystem, Plant Soil 253 (2003) 445–455.

[14] J.E.S. Uría, A. Sanz-Medel, Inorganic and methylmercury speciation in environmental samples, Talanta 47 (1998) 509–524.
[15] J. Canário, M. Caetano, C. Vale, Validation and application of an analytical method for monomethylmercury quantification in aquatic plant tissues, Anal. Chim. Acta 580 (2006) 258–262.
[16] H. Hintelman, H.T. Nguyen, Extraction of methylmercury from tissue and plant samples by acid leaching, Anal. Bioanal. Chem. 381 (2005) 360–365.
[17] M.D. Tabatchnick, G. Nogaro, C.R. Hammerschmidt, Potential sources of methylmercury in tree foliage, Environ. Pollut. 160 (2012) 82–87.
[18] M. Válega, S. Abreu, P. Pato, L. Rocha, A.R. Gomes, M.E. Pereira, A.C. Duarte, Determination of organic mercury in biota, plants and contaminated sediments using a thermal atomic absorption spectrometry technique, Water Air Soil Pollut. 174 (2006) 223–234.
[19] M. Desrosiers, D. Planas, A. Mucci, Total mercury and methylmercury accumulation in periphyton of Boreal Shield Lakes: influence of watershed physiographic characteristics, Sci. Total Environ. 355 (2006) 247–258.
[20] L. Liang, M. Horvat, E. Cernichiari, B. Gelein, S. Balogh, Simple solvent extraction technique for elimination of matrix interferences in the determination of methylmercury in environmental and biological samples by ethylation – gas chromatography – cold vapor atomic fluorescence spectrometry, Talanta 43 (1996) 1883–1888.
[21] Y. Cai, S. Monsalud, R. Jaffé, R.D. Jones, Gas chromatographic determination of organomercury following aqueous derivatization with sodium tetraethylborate and sodium tetraphenylborate comparative study of gas chromatography coupled with atomic fluorescence spectrometry, atomic emission spectrometry and mass spectrometry, J. Chromatogr. A 876 (2000) 147–155.
[22] Y. Gao, W. Yang, C. Zheng, X. Hou, L. Wu, On-line preconcentration and in situ photochemical vapor generation in coiled reactor for speciation analysis of mercury and methylmercury by atomic fluorescence spectrometry, J. Anal. At. Spectrom. 26 (2011) 126–132.
[23] C. Zheng, Y. Li, Y. He, Q. MA, X. Hou, Photo-induced chemical vapor generation with formic acid for ultrasensitive atomic fluorescence spectrometric determination of mercury: potential application to mercury speciation in water, J. Anal. At. Spectrom. 20 (2005) 746–750.
[24] Y. Wu, Y. Lee, L. Wu, X. Hou, Simple mercury speciation analysis by CVG-ICP-MS following TMAH pre-treatment and microwave-assisted digestion, Microchem. J. 103 (2012) 105–109.
[25] J. Száková, J. Havlíčková, A. Šípková, J. Gabriel, K. Švec, P. Baldrian, J. Sysalová, P. Coufalík, R. Červenka, O. Zvěřina, J. Komárek, P. Tlustoš, Effects of the soil microbial community on mobile proportions and speciation of mercury (Hg) in contaminated soil, J. Environ. Sci. Health A 51 (2016) 364–370.
[26] P. Coufalík, P. Prochazková, O. Zvěřina, K. Trnková, K. Skácelová, D. Nývlt, J. Komárek, Freshwater mineral nitrogen and essential elements in autotrophs in James Ross Island, West Antarctica, Pol. Polar Res. 37 (2016) 477–491.
[27] A.P. Podterob, Chemical composition of lichens and their medicinal applications, Pharm. Chem. J. 42 (2008) 582–588.
[28] D.J. Roser, D.R. Melick, H.U. Ling, R.D. Seppelt, Polyol and sugar content of terrestrial plants from continental Antarctica, Antarct. Sci. 4 (1992) 413–420.
[29] A.S. Perlin, S. Suzuki, The structure of lichenin: selective enzymolysis studies, Can. J. Chem. 40 (1962) 50–56.
[30] L. Li, Y. Guo, L. Zhao, Y. Zu, H. Gu, L. Yang, Enzymatic hydrolysis and simultaneous extraction for preparation of genipin from bark of Eucommia ulmoides after ultrasound, microwave pretreatment, Molecules 20 (2015) 18717–18731.

Příloha XI

International Journal of Coal Geology 165 (2016) 157–172

Contents lists available at ScienceDirect

International Journal of Coal Geology

journal homepage: www.elsevier.com/locate/ijcoalgeo

Petrological and geochemical characteristics of Palaeogene low-rank coal on the Faroe Islands: Restricted effects of alteration by basaltic lava flows

Simona Kubouškova [a], Lukáš Krmíček [a,b,c,*], Pavel Coufalík [d,e], Richard Pokorný [f]

[a] Department of Geological Sciences, Faculty of Science, Masaryk University, Kotlářská 2, CZ-611 37 Brno, Czech Republic
[b] Institute of Geology, The Czech Academy of Sciences, v.v.i., Rozvojová 269, CZ-165 02 Prague 6, Czech Republic
[c] Brno University of Technology, Faculty of Civil Engineering, AdMaS Centre, Veveří 95, CZ-602 00 Brno, Czech Republic
[d] Department of Chemistry, Faculty of Science, Masaryk University, Kotlářská 2, CZ-611 37 Brno, Czech Republic
[e] Institute of Analytical Chemistry, The Czech Academy of Sciences, v.v.i., Veveří 97, CZ-602 00 Brno, Czech Republic
[f] Faculty of Environment, Jan Evangelista Purkyně University, Králova Výšina 3132/7, CZ-400 96 Ústí nad Labem, Czech Republic

ARTICLE INFO

Article history:
Received 9 February 2016
Received in revised form 8 August 2016
Accepted 9 August 2016
Available online 10 August 2016

Keywords:
Faroe Islands
Coal composition
Alteration
Depositional environment

ABSTRACT

The first combined petrographic and geochemical investigation of coal from the Faroe Islands was performed as a case study to understand thermal effects from basaltic lava flows on immature coal. The samples were divided into two distinct groups: "normal" coal (xylite and detroxylite) and "altered organic matter" (charcoal and organic particles dispersed in samples rich in altered clastic mineral components or enriched via hydrothermal fluids). The "normal" coal consists primarily of huminite-group material dominated by ulminite. The proportions of material from inertinite and liptinite groups vary from sample to sample. The studied macerals are anisotropic with no observed reaction rims or vacuoles. According to the mean ulminite reflectance in combination with ultimate and proximate analyses, the coal reached the lignite and subbituminous stages. The maceral compositions together with coal palynology indicate a predominance of gelified wood-derived tissues and demonstrate that the coal evolved in wet forest swamps under limno-telmatic to telmatic conditions.

Alteration effects on immature coals from overlying basalt flows were relatively limited. Due to relatively rapid heat loss from the basaltic lava, as verified by the presence of volcanic glass (tachylyte), its imposed thermal effects resulted only in development of a thin "anthracite-like" crust on samples with no elevated coal rank. Associated hydrothermal fluids induced coal hydrofracturing with subsequent mineral precipitation and decomposition of the ambient feldspar-rich volcaniclastic sediments. Altered organic matter is enriched in SiO_2, Al_2O_3 and FeO_{tot}, as well as in trace elements such as Ni and Cr. In contrast, these samples are depleted in Hg (<10 ppb).

© 2016 Elsevier B.V. All rights reserved.

1. Introduction

The Faroe Islands (1400 km^2; 4° S of the Arctic Circle) belong geologically to the North Atlantic Igneous Province (Saunders et al., 1997). Massive basalt lava flows of Palaeocene age (Storey et al., 2007) are interbedded with sedimentary layers containing thin coal lenses and seams. Continental interlava volcaniclastic sediments on the Faroe Islands provide only limited palaeontological evidence (plant remains, rare trace fossils) and their depositional environment has been highly debated (Pokorný et al., 2015 and references therein).

Coal has been a key fuel for the Faroe Islands, particularly in the past, due to their isolated geographical position and the limited import of fossil fuels. Because of its importance the coal was locally named "black gold" and has been mined in many adits since the 18th century to ensure energy self-sufficiency. Coal productivity in 1930 was approximately 5000 tons/year. Since the beginning of the 21st century, production has decreased to 100 tons/year (Øster-Mortensen, 2002). For this reason, only one coal mine has been in operation since 2008.

The coal deposits are mentioned peripherally in several publications within basic geological descriptions of the Faroe Islands (e.g., Ellis et al., 2002; Laier et al., 1997; Lund, 1989; Parra et al., 1987; Passey, 2014; Rasmussen and Noe-Nygaard, 1969, 1970; Stokes, 1874). Nevertheless, they have not yet been systematically studied in terms of quality.

The chemical composition of coal varies considerably on the global scale (Mukherjee et al., 2008). The differences involve major element compositions (e.g., the commonly observed sulphur content) and trace element contents. The increasing environmental burden associated with the burning of fossil fuels places demands on the regulation of pollutants emitted into the atmosphere. Coal combustion leads to the vaporization of metals, which subsequently condense as an aerosol of submicron-sized particles. The emission of metals into the atmosphere depends on the vapour pressure of each element (Finkelman et al.,

* Corresponding author at: Institute of Geology, The Czech Academy of Sciences, v.v.i., Rozvojová 269, CZ-165 02 Prague 6, Czech Republic.
E-mail address: l.krmicek@gmail.com (L. Krmíček).

http://dx.doi.org/10.1016/j.coal.2016.08.009
0166-5162/© 2016 Elsevier B.V. All rights reserved.

1990). Trace elements in coals are subdivided into five categories according to the degree of possible health risk (Zhang et al., 2004). The most hazardous metals are: As, Cd, Cr and especially Hg (Swaine and Goodarzi, 1995). The negative influence of non-metals such as fluorine emitted during indoor combustion of a F-rich coal containing a binder clay has also been observed (Dai et al., 2007).

Mercury begins to be released from coal at temperatures below 200 °C; above 600 °C it occurs in the form of Hg^0 (Mukherjee et al., 2008). For this reason, mercury released into the atmosphere during coal combustion (Yudovich and Ketris, 2005a, 2005b) is a significant pollutant, despite its generally low concentrations in coal (Ketris and Yudovich, 2009; Xu et al., 2013). However, extremely-high Hg concentrations (up to 12.1 ppm) were reported from some Chinese coals and coal ashes (Dai et al., 2006, 2012a, 2014). Long-range mercury transport, enabled by cycles of deposition and reemission, considerably increases mercury concentrations in subpolar and polar regions (Poissant et al., 2008). This effect is also apparent from the increased levels of mercury in Faroese peat. Maximum concentrations of 498 ppb total Hg were determined in peat from 1954, at the peak of coal production (Shotyk et al., 2005).

The composition of coal can be affected by volcanic activity. Several authors have studied various properties of thermally altered coal from all over the world (Bussio and Roberts, 2016; Dai and Ren, 2007; Golab and Carr, 2004; Merritt, 1985; Rahman and Rimmer, 2014; Singh et al., 2007, 2008; Wang et al., 2014; Ward et al., 1989; Yao and Liu, 2012). Ward et al. (1989) categorized the layers around an igneous body into four zones: i) zone of porous cinder close to the contact; ii) zone of visibly banded cinder with remnants of the original lithotype stratification; iii) zone of heat-affected coal without porosity and other microscopic and macroscopic signs of coking; iv) zone of unaffected coal. Kwiecińska and Petersen (2004) defined cinder from the contact zone as natural char and coke. Physical and chemical effects of intrusions on peat and coal depend on exposure to heat, time of igneous emplacement, temperature, thickness and form of the igneous body, pressure, hydrology, as well as the composition and initial coal rank of the affected formation, lithology of the surrounding rocks and other local factors (Bostick and Pawlewicz, 1984; Crelling and Dutcher, 1968; Suchý et al., 2002). In heat-affected coal, microconstituents formed by the alteration of vitrinite and liptinite macerals, having different textural and optical properties than the original macerals, are commonly recognized (Taylor et al., 1998). Typical optical changes in coal caused by intrusion/effusion involve microbrecciation, increases in vitrinite reflectance, development of devolatilization pores and fissures, coke textures and the presence of pyrolytic carbon. Pores of natural coke are empty or filled with mineral or carbonaceous matter formed from volatile material (Amijaya and Littke, 2006; Goodarzi and Cameron, 1990; Khorasani et al., 1990; Kisch and Taylor, 1966; Mastalerz et al., 2009; Suchý et al., 2002). The product formed from vitrinite and liptinite of the bituminous coal at temperatures above 500 °C is an anisotropic coke with a mosaic structure and higher reflectance than the original vitrinite (Kwiecińska and Petersen, 2004).

The goal of this pilot study is threefold: i) to describe the petrography and geochemistry as well as the coal rank of Palaeogene coal from the Faroe Islands; ii) to assess its depositional environment; iii) to characterize the effect of basaltic effusions overlying coal-bearing strata on the coal composition.

2. Geological setting

The Faroe Islands were formed during extensive volcanic activity within the North Atlantic Igneous Province in response to the opening of the Atlantic Ocean (Jolley and Bell, 2002). This part of the North Atlantic Igneous Province is named the Faroe Islands Basalt Group and extends to the east and southeast from the current Faroe Islands to the Faroe-Shetland Basin. Volcanic rocks of the Faroe Islands Basalt Group are petrographically classified as aphyric basalts with a fine-grained groundmass, plagioclase-phyric basalts and olivine-phyric basalts (Noe-Nygaard and Rasmussen, 1968).

Rasmussen and Noe-Nygaard (1969, 1970) described three tholeiitic basalt series (~6.6 km thick): lower, middle and upper basaltic lava formations that are thought to overlie older continental crust (Bohnhoff and Makris, 2004, Bott et al., 1974; Casten, 1973; Richardson et al., 1998).

The oldest basalt flow yielded an $^{40}Ar/^{39}Ar$ plateau age of 63.1 ± 1.8 Ma (Waagstein et al., 2002). After termination of the initial volcanic phase, sediment deposition began. Subsequent volcanic activity produced the middle basaltic lavas and when this ceased, a coal-bearing sedimentary sequence was formed during the period between 58 and 56 Ma (Jolley and Bell, 2002; Storey et al., 2007). Finally, the coal-bearing sedimentary sequence was covered by the upper basalt flows.

According to Passey and Jolley (2009), tholeiitic lavas of the Faroe Islands can be further subdivided into seven lithostratigraphic formations (Figs. 1, 2). The basal Lopra Formation (1.1 km thick) is known only from the onshore Lopra-1/1A borehole and consists of basalts, volcaniclastic sandstones and hyaloclastites. The subsequent 3.25-km-thick Beinisvørð Formation is made up of basaltic lavas, volcaniclastics and sandy claystone to mudstone sediments that may contain thin coal lenses. The Beinisvørð Formation is overlain by up to 15 m thick coal-bearing Prestfjall Formation, deposited between eruptions, which consists predominantly of tuffitic claystones and volcaniclastic conglomerates. The Prestfjall formation is overlain by the syn-eruption Hvannhagi Formation of pyroclastic sediments, up to 50 m thick. This formation is covered by basaltic lava flows with a total thickness of 1.4 km named the Malinstindur Formation and the 30-m-thick sedimentary Sneis Formation dominated by sandstones and conglomerates. The volcanic activity terminated with basaltic lava flows forming the 900-m-thick Enni Formation that is interbedded with volcaniclastic sequences. The landscape of the Faroe Islands was subsequently reshaped by Pleistocene glacial activity.

3. Samples and methods

To examine the petrological and geochemical composition of Faroese coal, a total of 22 bench samples with well-known positions within the coal-bearing sequence were taken from the Prestfjall Formation on Suðuroy Island and one from the Beinisvørð Formation on Mykines Island (Fig. 1, Table 1). Sampling was performed both in coal mines and coal-bearing sedimentary profiles (Fig. 3A–F), following ISO 5069-1:1983 standard procedure. The sampled localities were described in detail by Kubouškovа et al. (2015). Coal samples were air-dried and stored in polyethylene bags for transport.

Additionally, on Suðuroy Island it was possible to collect basalt samples (Malinstindur Formation; 5 samples) directly overlying the Prestfjall Formation that contains the studied coal occurrences (Fig. 3D, E) and two samples of tuffitic coal-bearing claystone changed to porcelanite along the contact of these formations. Thin sections made from these samples were investigated using an Olympus BX50 petrographic microscope.

3.1. Petrographic analyses

The coal samples were the subject of petrographic investigation, i.e., maceral analysis of huminite, liptinite, inertinite groups and mineral group divided into clay minerals, sulphides, carbonates and other particularly accessorial minerals and altered minerals, and measurement of the reflectance of ulminite and altered organic matter (ISO 7404-3: 2009, Taylor et al., 1998).

For petrographic analyses, polished sections were prepared and studied both in reflected and ultraviolet light using an Olympus BX51 microscope with Zeiss Photomultiplier MK3 system and fluorescence mode using immersion lens with 40× magnification. The Pelcon point counter was used for the maceral analysis. Coal rank was determined by reflectance measurements on ulminite B from particulate polished sections by SpectraVision software calibrated with yttrium aluminium garnet (R = 0.894%), sapphire (R = 0.596%), spinel (R = 0.422%) and

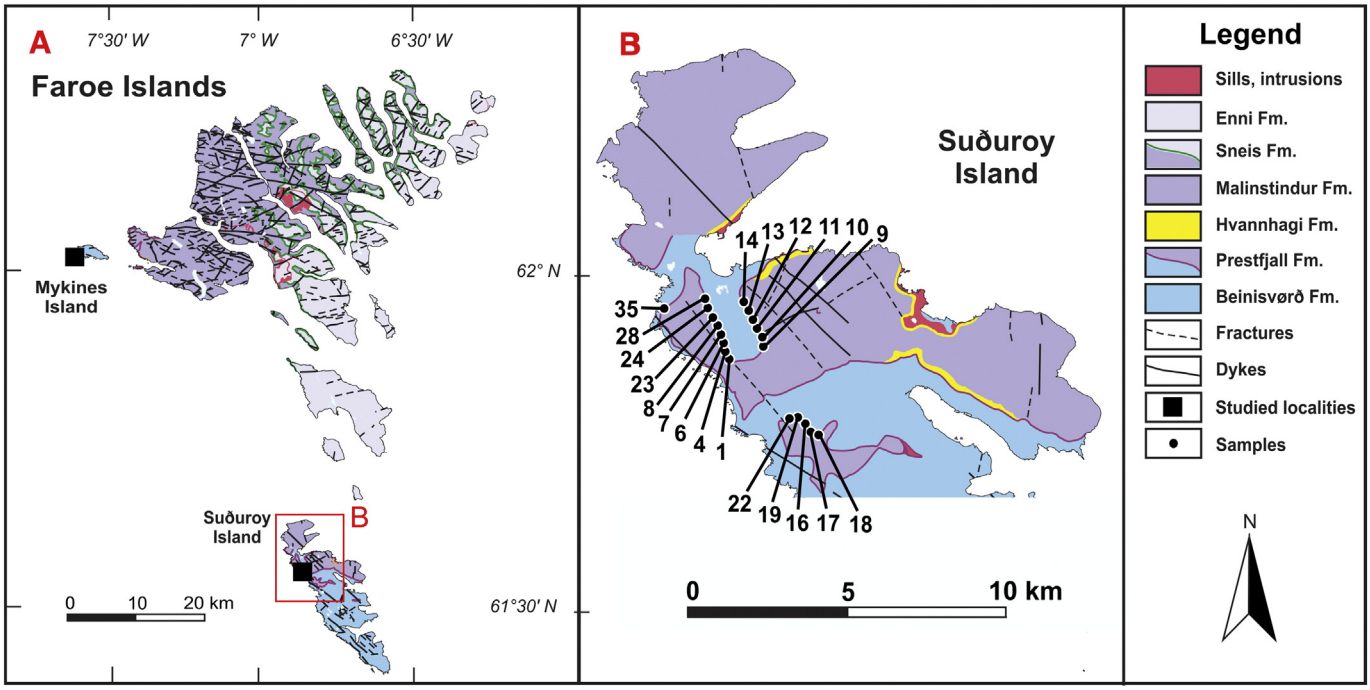

Fig. 1. A – Geological map of the Faroe Islands modified after Passey and Jolley (2009) with overview of studied areas; B – Main coalfield on Suðuroy Island associated with the Prestfjall Formation. Numbers of sampled localities correspond with samples ID in tables.

gadolinium-gallium-garnet (R = 1.717%) standards. Abbreviations of minerals on photomicrographs were used according to Whitney and Evans (2010).

3.2. Chemical analyses

Samples were examined for moisture, ash, elemental composition and calorific values following standard procedures (ČSN 44 1377; ČSN ISO 1171; ČSN ISO 29541). Calorific values were determined by adiabatic bomb calorimetry (Parr 6300 adiabatic bomb calorimeter; Parr Instrument Company, Moline, IL, USA). The ultimate analysis (C, H, N, S and O) was performed using a Thermo Finnigan FA 1112 Series CHNS/O analyzer.

The contents of major oxides and trace elements in the coal were measured by X-ray fluorescence (XRF) spectrometry (Delta Premium). The following certified reference standards were used for calibration of XRF spectrometer for organomineral matrix: GBW07603 (GSV-2) and NIST 2702. Trace amounts of mercury were determined by atomic absorption spectrometry (AAS) using an AMA-254 Advanced Mercury Analyzer (Altec, Czech Republic). The absolute detection limits of this facility are 10 pg Hg. The limit of quantification for Hg measurements was 0.3 ppb (this limit was defined as 10× standard deviation of the blank).

From the mercury data, the "Hg coal affinity index" (CAI_{Hg}), which shows how efficiently the coal acted as a crustal geochemical barrier for the mercury, was calculated according to Yudovich and Ketris (2005a) as the ratio of measured Hg contents in the coal and the average Hg content in the Upper Continental Crust (UCC) given by Rudnick and Gao (2014):

$$CAI_{Hg} = \frac{\text{Hg in the coal[ppb]}}{50\ \text{ppb(UCC)}} \quad (1)$$

4. Results

The samples investigated in this study represent two distinct groups (Table 1): i) "normal" coal (xylite and detroxylite) and ii) altered organic matter (charcoal and organic particles dispersed in mineral-rich samples).

Accordingly, geochemical and organic petrographic signatures were used to compare two different types of the samples. This approach has been applied by evaluating ultimate and proximate analyses, maceral descriptions and inorganic geochemical compositions.

4.1. Field and macroscopic characteristics

The thicknesses of the coal seams range from a few centimetres to 1.5 m, the thicker of which have been exploited in coal mines (Fig. 3A, B). The studied coal varies from xylitic, containing relict wooden fragments (SK14B), to a compact, "anthracite-like" character with a noticeable resinous lustre and conchoidal fracture (e.g., SK01, SK22). However, the "anthracite-like" character of the coal appears only at the surface of several samples (Fig. 3C). The coal is covered by limonite in places and cubic crystals of pyrite were occasionally observed.

4.2. Ultimate and proximate parameters

The ultimate and proximate analyses illustrate the variability of the sample groups (Table 2, Fig. 4A–C). Overall ranges (in wt.%) were 5.63 to 71.5 for total carbon (C^d), 1.43 to 5.13 for total hydrogen (H^d), 0.03 to 0.99 for total sulphur (S^d), 0.05 to 0.83 for total nitrogen (N^d) and 7.46 to 25.89 for total oxygen (O^d).

Samples classified as "altered organic matter" (except of charcoal) have elevated ash yields (A^d) between 74.05 and 86.2 wt.%, very low calorific value (Q_s^d) 0.75–3.2 MJ/kg along with very high content of volatile compounds (V^{daf}) 43.51–96.17 wt.%. In contrast, charcoal and samples classified as "normal" coal have medium to high V^{daf} (30.11–45.31 wt.%), and relatively high Q_s^d (23.80–29.06 MJ/kg) accompanied by low to medium A^d (2.26–18.71 wt.%).

The carbon content (C^d) was chosen as the primary parameter for coals due to its slight separation potential. Subsequently, correlation with hydrogen and oxygen content was carried out (Fig. 4A, B). All 18 samples classified as a "normal" coal are thermally immature and belong to low-rank, respectively lignite to subbituminous stage (ECE-UN, 1998).

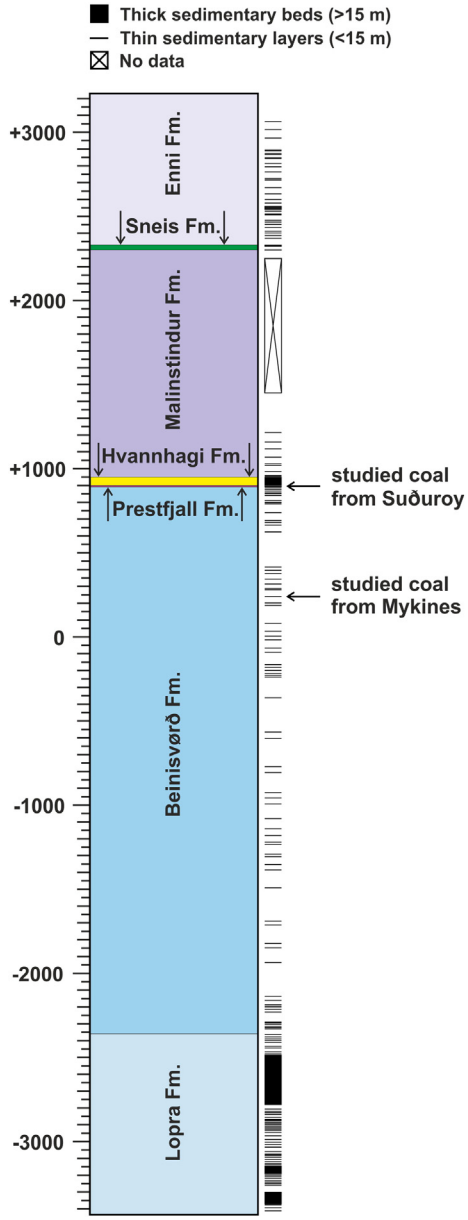

Fig. 2. Litostratigraphic subdivision of the Faroe Islands Basalt Group. Volcaniclastic sediment layers are highlighted on the right side of the scheme together with positions of studied coal-bearing sequences (Pokorný et al., 2015, modified). Position of sampled coal-bearing strata on Mykines Island was correlated with a study of Passey and Varming (2010). Negative stratigraphic profile is inferred from Lopra-1/1A borehole.

Table 1
List of coal samples and their geographic locations.

Sample ID	Sample type	Locality	Island	Longitude (N)	Latitude (W)
SK01A	xylite	New Prestfjall mine	Suðuroy	61°34′9.7″	6°56′4.6″
SK01B	detroxylite	New Prestfjall mine	Suðuroy	61°34′9.7″	6°56′4.6″
SK01C	detroxylite	New Prestfjall mine	Suðuroy	61°34′9.7″	6°56′4.6″
SK04	detroxylite	Kolaminur	Suðuroy	61°34′12″	6°56′10.3″
SK06	xylite	Kolaminur	Suðuroy	61°34′18.6″	6°56′15.3″
SK07	detroxylite	Kolaminur	Suðuroy	61°34′21.3″	6°56′14.5″
SK08	detroxylite	Kolaminur	Suðuroy	61°34′25.4″	6°56′13.5″
SK09	detroxylite	Rókhagi	Suðuroy	61°34′31.9″	6°55′0.9″
SK10	mineral-rich	Rókhagi	Suðuroy	61°34′39.2″	6°55′9.4″
SK12	detroxylite	Rókhagi	Suðuroy	61°34′41.7″	6°55′13.1″
SK13	detroxylite	Rókhagi	Suðuroy	61°34′44.4″	6°55′17.8″
SK14A	xylite	Rókhagi	Suðuroy	61°34′46.4″	6°55′19.8″
SK14B	charcoal	Rókhagi	Suðuroy	61°34′46.4″	6°55′19.8″
SK16	xylite	Rangibotnur	Suðuroy	61°33′11.4″	6°53′44.2″
SK17	xylite	Rangibotnur	Suðuroy	61°33′9.4″	6°53′43.1″
SK18	detroxylite	Rangibotnur	Suðuroy	61°33′2.7″	6°53′30.6″
SK19	xylite	Gudmund's mine	Suðuroy	61°33′16.7″	6°53′48.6″
SK22	xylite	Gudmund's mine	Suðuroy	61°33′17.1″	6°54′10.6″
SK23	mineral-rich	Kolavegurin	Suðuroy	61°34′31.4″	6°56′15.3″
SK24	mineral-rich	Kolavegurin	Suðuroy	61°34′33.9″	6°56′16.2″
SK28	detroxylite	Kolavegurin	Suðuroy	61°34′42″	6°56′22.9″
SK35	mineral-rich	Suður í Haga	Suðuroy	61°35′08″	6°58′14.2″
SK40	xylite	Mykineshólmur	Mykines	62°06′01.1″	7°39′41.4″

4.3. Coal petrography

Precise characterization of coal and coaly material has been successfully achieved by the investigating of individual macerals (e.g., Taylor et al., 1998). Maceral descriptions focused partly on specific alteration features, and gelification related to changes in maceral composition was evaluated (Fig. 5, Table 3). Maceral analysis allowed discrimination of various sample types. In particular, xylite, detroxylite, charcoal and organic particles dispersed in mineral matter could be distinguished.

4.3.1. Maceral composition

All "normal" coal samples are classified as a gelified xylite-rich coal. The fossil wood remnants in these coals contain mainly huminite macerals (55.7–97 vol.%) of predominantly ulminite B (38.9–93 vol.%) with poorly discernible tissue structures, and less densinite (1.7–11.7 vol.%). Light grey ulminite B dominates in all samples and forms a homogenous groundmass in most coals, whereas contents of darker grey ulminite A with reflectance values between 0.25 and 0.33% do not exceed 2 vol.% in samples SK01B, SK06, SK13, SK28 and SK40. Most corpohuminite (1.8–9.9 vol.%) occurs in-situ in wood and bark tissues as phlobaphinite (Fig. 6A, B, C), smaller amounts may also occur dispersed in densinite or in clay minerals. Corpohuminite is formed in well-preserved oval to elongated (compressed) cell structures that can be gas-charged or filled by mineralization products, as very well developed in sample SK40. Textinite is irregularly distributed and its content is relatively low (up to 6.4 vol.% in sample SK12). Gelinite was not found.

Liptinite contents vary between 1.5 vol.% and 25.5 vol.%. This maceral group is dominated by resinite (1.1–11.2 vol.%), and less cutinite (0.3–8 vol.%), liptodetrinite (0.8–4.4 vol.%), sporinite (0.7–5.3 vol.%) and suberinite (0.4–3.6 vol.%). Resinite mostly occurs in-situ in wood cell tissues and leaf fragments (Fig. 6B, C, D). Small isolated resinite bodies commonly forms greyish rounded or elongated grains which are often slightly altered and show weak yellow to brown fluorescence and often contain fine pores as result of degassing. Resinite is mostly dispersed in densinite and clay minerals. Cutinite is predominantly derived from coniferous leaves that are variable deformed and humified. Fragments of separate tenuicutinite were identified only in a few samples SK01C, SK06, SK08, SK13 and SK28 (Fig. 6D). Liptodetrinite occurs as long bands, individually as small nests or dispersed in densinite and clay minerals. Sporinite appears most frequently as dark brown oval structures within liptodetrinite. Suberinite was often found in bark tissues and less in rootlet cortex together with phlobaphinite (Fig. 6C).

Inertinite contents vary between 0.9 vol.% and 23 vol.% and is represented predominantly by fusinite, macrinite, semifusinite and inertodetrinite. Secretinite and funginite are rare. Whereas macrinite occurs mainly as irregularly shaped particles of >10 μm size (Fig. 6E), inertodetrinite appears as discrete <10 μm sized fragments. In mineral-rich samples (SK10, SK23, SK24) it can occur dispersed throughout the mineral mass.

Mineral matter contents range between 1.5 vol.% and 30.2 vol.% in xylite-rich coal. Compositions of mineral matter are very variable, particularly in samples SK01B and SK04. Mineral admixture consists

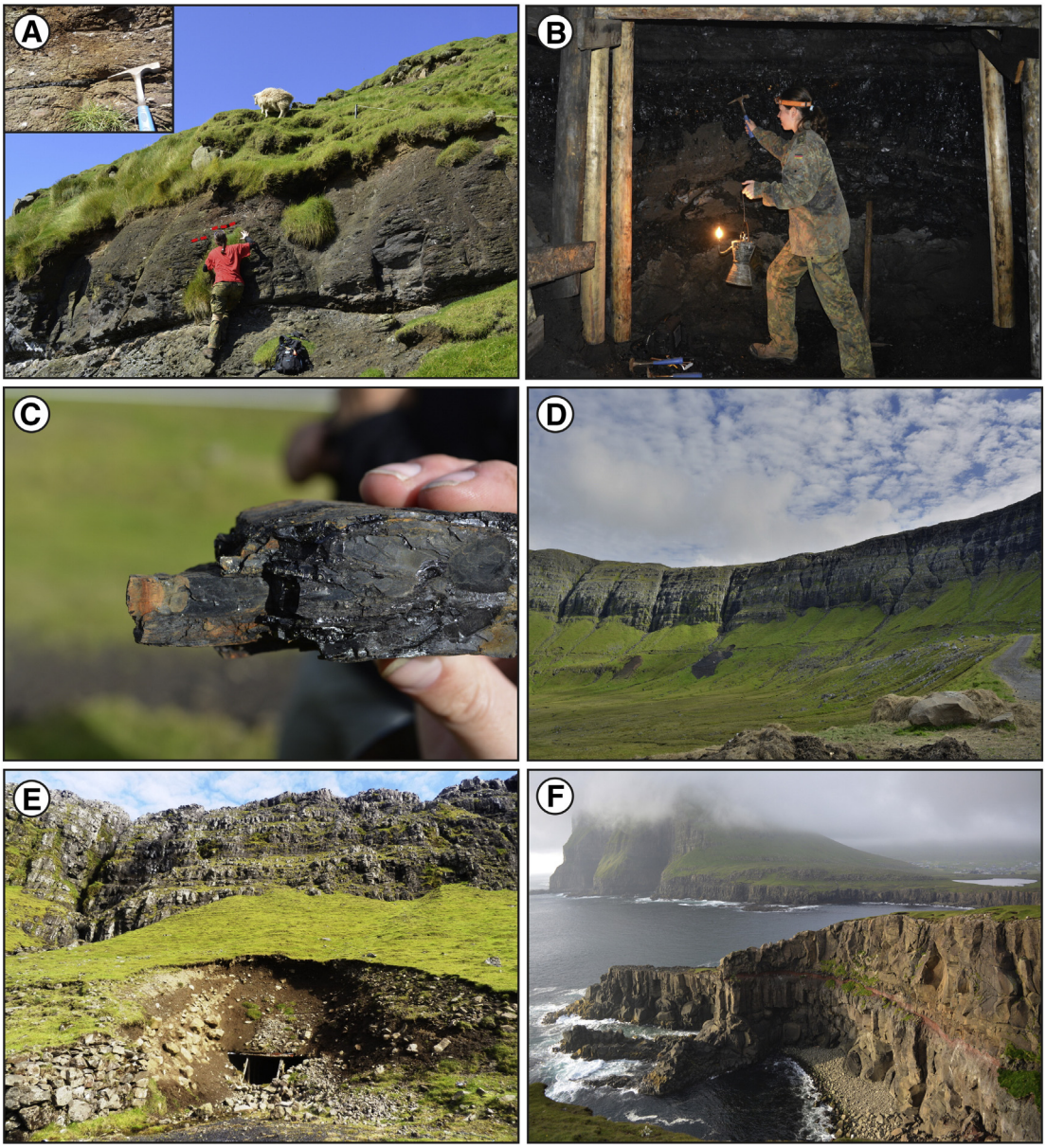

Fig. 3. Photographs from the field investigation of the coal occurrences. A – Sampling of SK40 sample from thin coal layers (red lines) within the sedimentary profile at Mykineshólmur coastline affected by crossed faults; inset in the upper left corner shows a detail view on a coal lens; B – 1-m-thick coal seam exposed at the production heading in New Prestfjall mine (Suðuroy); C – Coal sample (SK08) with "anthracite-like" thin crust partially covered by limonite (Suðuroy); D – Coalfield of Rókhagi mine overlain by basalts of Malinstindur Formation (Suðuroy); E – Partially buried adit portal of Rókhagi mine (Suðuroy). F – Reddish coal-bearing sedimentary sequence exposed at Hvalba cliffs, Suður í Haga (Suðuroy).

primarily of fine-grained clay minerals, especially smectites and kaolinites (Parra et al., 1987), which are dispersed in fine-grained densinite, or form isolated layers (Fig. 6E, F). Pyrite appears either as fracture fillings of epigenetic origin (Fig. 7A), or as syngenetic framboidal globules and aggregates (Fig. 7B) in amounts not exceeding 3 vol.%, particularly in samples SK12 and SK13. Quartz and carbonates occur irregularly and their contents do not exceed 3 vol.% in "normal" coal. Carbonates are predominantly siderite and calcite with well-shaped crystals showing noticeable cleavage. The coal can be slightly oxidized, which becomes evident at the margins of huminite grains as 10–20 μm thick oxidized rims of darker grey colour, or as a thin limonite crust. The mineral composition of xylite-rich coal is quite unusual. Various minerals which could not be identified using microscopic techniques were included into the group "other" (Table 3).

All samples of "altered organic matter" (SK10, SK14B, SK23, SK24 and SK35) are altered with respect of their mineral and organic content (Fig. 8A–D). Organic material consists mainly of altered particles of huminite and inertinite (average reflectance 0.56–1.35%) and char particles with the highest average reflectance of 1.93% (Fig. 8C, D). Rarely present are unaltered particles of ulminite with average reflectance of 0.39–0.42% (Fig. 8B) and inertinite. The most common minerals observed in samples grouped into "altered organic matter" are clay minerals, indicating a transition from pure coal to coaly claystone. The interesting charcoal sample SK14B (Fig. 8A) consists of altered textinite and ulminite with corpohuminite lacking resinite, respectively fusinite and semifusinite within a fine-grained clayey matrix. Altered wood material in this sample has reflectance values of up to 0.87% (Table 4).

4.3.2. Coal rank

The random reflectance values (R_r) of ulminite B in "normal" coal range from 0.34% to 0.53% with standard deviation in the range

Table 2
Ultimate and proximate analyses of Faroese samples.

Sample ID	W^a [wt.%]	A^d [wt.%]	Q_s^d [MJ/kg]	H^d [wt.%]	N^d [wt.%]	C^d [wt.%]	S^d [wt.%]	O^d [wt.%]	V^{daf} [wt.%]
SK01A	8.52	4.53	28.96	4.53	0.75	69.62	0.38	20.19	35.74
SK01B	8.44	18.71	23.80	4.36	0.48	56.15	0.42	19.88	45.31
SK01C	6.90	12.50	26.03	4.78	0.62	62.89	0.46	18.78	43.42
SK04	9.69	3.47	29.01	4.78	0.66	71.24	0.29	19.56	36.43
SK06	9.73	2.64	29.06	4.61	0.72	71.22	0.28	20.53	37.85
SK07	10.15	3.90	28.36	5.02	0.56	67.30	0.42	22.80	38.20
SK08	9.22	14.60	24.52	4.24	0.61	61.21	0.22	19.11	42.97
SK09	9.91	2.39	28.87	4.21	0.58	66.89	0.11	25.89	35.79
SK10	2.97	86.20	0.75	1.43	0.10	2.38	0.03	9.91	96.17
SK12	10.2	2.26	28.97	4.63	0.60	71.49	0.23	20.79	36.23
SK13	8.85	8.41	27.14	4.67	0.61	66.98	0.99	18.34	37.79
SK14A	10.12	5.35	27.84	5.10	0.52	66.56	0.57	21.90	36.37
SK14B	4.62	12.30	26.63	3.67	0.25	69.08	0.03	14.65	30.11
SK16	9.71	2.46	28.95	4.77	0.33	71.50	0.17	20.77	37.38
SK17	9.08	5.43	27.40	5.13	0.44	65.60	0.61	22.79	38.39
SK18	9.09	3.53	28.32	4.71	0.44	70.49	0.25	20.58	37.51
SK19	9.57	7.97	25.80	4.80	0.62	62.27	0.53	23.81	39.51
SK22	10.43	4.99	27.82	4.53	0.83	68.47	0.43	20.75	35.91
SK23	3.76	74.05	3.25	1.45	0.12	16.85	0.07	7.46	43.51
SK24	3.70	85.26	0.78	1.44	0.09	5.63	0.03	7.55	88.40
SK28	9.83	5.06	27.20	4.82	0.50	65.81	0.46	23.35	37.95
SK35	8.72	82.67	2.44	1.89	0.05	7.06	0.16	8.17	43.68
SK40	10.49	11.94	23.82	4.90	0.64	57.07	0.24	25.21	44.02

W - moisture
A - ash yield
Q_s - gross calorific value
V - volatile matter
^{a} - Analytical sample
^{d} - Dry basis
^{daf} - Dry, ash free basis

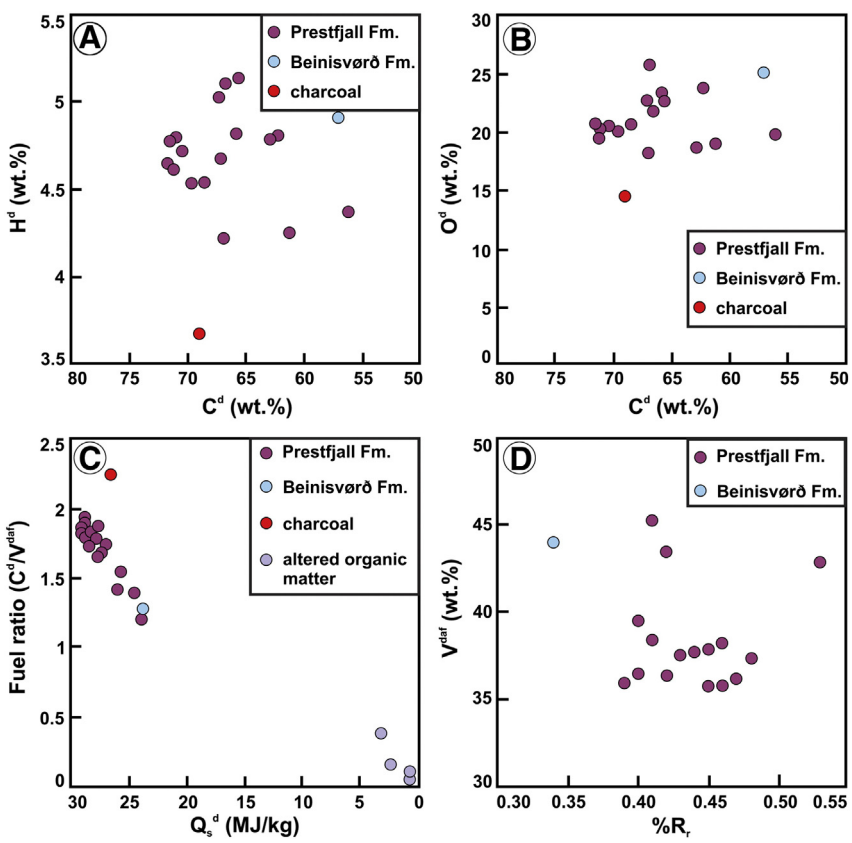

Fig. 4. Correlations between selected chemical, technological and petrographic parameters for "normal" coal, further subdivided into the Prestfjall and Beinisvørð Formations, and for "altered organic matter", further subdivided into charcoal and mineral-rich samples. A – Relationship between carbon and hydrogen content. For recognising of compositional variations in "normal" coal from both Prestfjall and Beinisvørð Formations, mineral-rich samples were not plotted; B – Relationship between carbon and oxygen content. For recognising of compositional variations in "normal" coal from both Prestfjall and Beinisvørð Formations, mineral-rich samples were not plotted; C – Modified Mott chart illustrating the relationship between fuel ratio expressed as C^d/V^{daf} and calorific value; D – Relationship between volatile matter (V^{daf}) and mean ulminite reflectance (R_r) for the studied samples from the Faroe Islands.

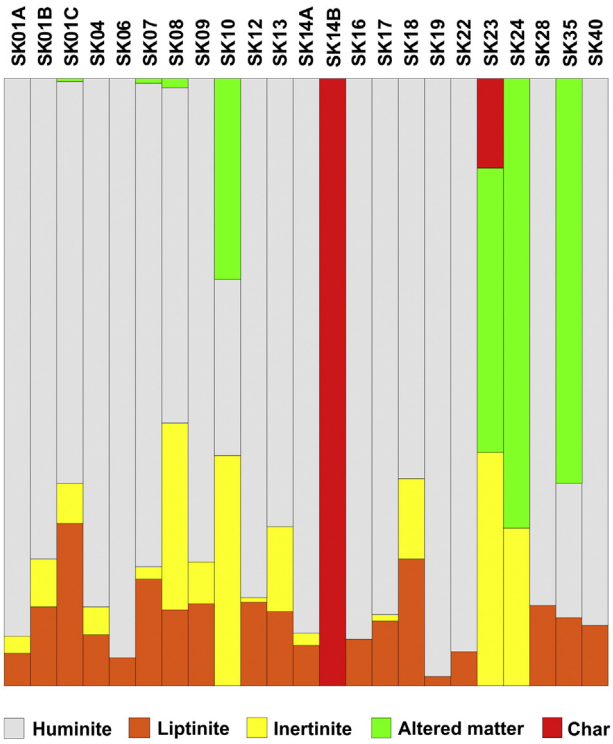

Fig. 5. Histogram based on the maceral analysis showing a ratio of macerals from the huminite, liptinite and inertinite group, altered organic paticles and char particles. For recognising of relationships within the organic matter, mineral mass was not included in this diagram.

0.04–0.09, suggesting that the coal rank of samples from the Faroe Islands is between lignite and subbituminous coal according to the ECE-UN (1998) standard. Ulminite reflectance for the group of "altered organic matter" samples varies between 0.39 and 0.83%R_r. These samples have low concentrations of unaltered organic matter, especially measurable ulminite particles. Thus, the ulminite reflectance measurements allow only tentative rank evaluations of these samples. For this reason, reflectance measurements were performed on altered and charred particles with average values ranging from 0.56% to 1.93%, suggesting that the reflectance increases along with thermal alteration of organic matter (Table 4).

4.4. Petrographic features of basaltic lava in contact with underlying tuffitic coal-bearing claystone

The volcanic rocks are very fine-grained, massive, dark-grey basalts. The absence of features such as pillow lavas or hyaloclastic breccias suggests subaerial volcanic activity (Smellie et al., 2008 and references therein). The basalts are composed of thin plagioclase laths (<100 μm) frequently associated with clinopyroxene and/or altered olivine in the form of larger glomerophyres (Fig. 9A). Plagioclase zones with higher anorthite mole fractions are selectively affected by alteration (Fig. 9A). Additionally, some samples are characterised by the occurrence of interstitial glass, tachylyte, suggesting relatively rapid cooling of the lava flow. Tachylyte shows various stages of alteration ranging from nearly opaque to orange-brown in colour (Fig. 9B). In tuffitic coal-bearing claystone from the contact of the Prestfjall and Malinstindur Formation, fragments of older basaltic volcanites altered to clay minerals were observed (Fig. 9C). Along the contact, this claystone was thermally metamorphosed to porcelanite and penetrated by a system of hydrothermal veinlets, which led to alteration of plagioclase laths (Fig. 9D).

4.5. Geochemical composition

4.5.1. Major oxides

Major element oxides compositions in all samples are represented mainly by SiO_2, Al_2O_3, and $Fe_2O_3^{tot}$. SiO_2 contents range between 0.9 and 8.6 wt.% for the majority of "normal" coal samples (Table 5). In "altered organic matter", the amount of SiO_2 reaches as high as 37.1 wt.%. "Normal" coal samples are characterized by variable amounts of Al_2O_3 that range from 0.8 to 8.4 wt.%, whereas "altered organic matter" samples show significantly elevated contents of up to 25.1 wt.%. The concentration of $Fe_2O_3^{tot}$ does not exceed 5.1 wt.% in any sample, with the exception of sample SK35 (16.1 wt.%.). CaO contents are generally below 3.5 wt.%. MnO contents (up to 2.9 wt.%) are elevated only in "altered organic matter". Additionally, the sample from the Beinisvørð Formation has a measurable concentration of P_2O_5 (0.4 wt.%), while the levels of K_2O and MgO are below their detection limits in the majority of samples.

4.5.2. Trace elements

In comparison with the worldwide average composition of low-rank coal (Ketris and Yudovich, 2009), samples from the Faroe Islands are relatively depleted in Sr (19 ppm on average), Zr (13 ppm on average) and As (2 ppm on average) and enriched in V (286 ppm on average), W (92 ppm on average), Cu (99 ppm on average) and Se (6 ppm on average). The coal sample from the older Beinisvørð Formation differs in its higher Rb, Sr, W and Ni contents (Fig. 10; Table 6). The "altered organic matter" samples show similar enrichment trends for Rb, Sr, Zr, V, Cu and especially for Cr (up to 126 ppm) and Ni (up to 291 ppm).

4.5.3. Mercury contents

The precise determination of mercury contents revealed that the majority of coal samples typically have concentrations between 22 and 210 ppb (Table 7). This places the mercury concentrations are both below and well above the worldwide average Hg content of 100 ppb Hg (Ketris and Yudovich, 2009). In contrast, "altered organic matter" has very low mercury values (<10 ppb). The sample from the older Beinisvørð Formation also yields a low Hg value of 14 ppb.

5. Discussion

5.1. Degree of coalification

The samples from the Faroe Islands classified in this work as "normal" coal have very low mean ulminite reflectance corresponding to the lignite and subbituminous stages. The samples classified as "altered organic matter" were affected by alteration related to the adjacent volcanic activity. Although these samples macroscopically resemble a detroxylitic coal, they actually correspond, in terms of their carbon content, to coaly claystones rich in altered clastic mineral component. These samples contain rare unaltered particles of ulminite with an average reflectance of 0.39–0.42%, suggesting their original low rank. The altered huminite, inertinite and char particles have reflectance values up to 1.93%, corresponding to slight thermal alteration (Table 4).

Mineralization of the coal appears to affect its quality, as shown by the correlation between increasing mineralization (ash yield) and decreasing carbon content and gross calorific value, as noted by Liu et al. (2005). This results from the release and migration of organic matter and subsequent precipitation of epigenetic minerals produced by hydrothermal fluids (Chen et al., 2014).

Samples SK40, SK01B, SK01C, SK08 and SK13 plot outside the trend followed by other studied "normal" coals in the O/C diagram (Fig. 4B). Specifically, the samples have lower oxygen percentages than might be expected for their carbon contents (e.g., Gurba and Ward, 2000). These samples also all have relatively higher mineral contents compared to other coals, but not so extremely high such as in the samples grouped into "altered organic matter".

Table 3
Result of maceral analysis and calculated facies indices.

Macerals [vol.%]	SK01A	SK01B	SK01C	SK04	SK06	SK07	SK08	SK09	SK10	SK12	SK13	SK14A
Ulminite	78.7	64.2	38.9	76.3	82.6	66.4	34.7	47	2.7	68.1	52.3	85.1
Textinite	0.3	0.8	0	0.9	1.4	1.9	0	1.3	0	6.4	0	0
Densinite	3.1	6.8	11.4	0	2.2	0	3.2	4	3.2	0	6.3	0
Corpohuminite	1.8	0.9	6.3	2.7	5.1	9.9	3.2	3.4	0.3	5.6	3.1	3.8
Attrinite	0	0	2.9	0	0	0	0	0	0	0	0	0
Huminite	83.9	72.7	59.5	79.9	91.3	78.2	41.1	55.7	6.2	80.1	61.7	88.9
Sporinite	0.7	1.8	0.7	3	0	3	2.2	3.3	0	2.1	1.6	0.9
Suberinite	0	1.2	2.9	0.4	0	0.6	1	0	0	0	1.4	0
Resinite	1.1	4.5	8.7	1.5	4.3	9.1	2	2.7	0	9.3	2.3	3.8
Liptodetrinite	2.8	4.3	3.8	2.2	0	4	4	3.4	0	1.4	4.2	1.8
Cutinite	0.3	0	8	0.5	0	0.4	0	0	0	0	0.7	0
Liptinite	4.9	11.8	24.1	7.6	4.3	17.1	9.2	9.4	0	12.8	10.2	6.5
Fusinite	0.8	1.8	1.3	0.7	0	0	7.5	0.7	0.8	0	1.5	0
Semifusinite	1.7	2.3	0.8	1.4	0	0	4.3	0.8	2.1	0.7	2.9	0
Secretinite	0	0.5	0	0	0	0	0	0	0	0	0	0
Macrinite	0	1	1.1	0.8	0	1	4.7	0.8	2.1	0	4.2	0.8
Inertodetrinite	0	1.7	2.7	1.3	0	1	6.5	2.4	3.1	0	2.5	1
Funginite	0	0	0	0	0	0	0	0	0	0	0.6	0
Inertinite	2.5	7.3	5.9	4.2	0	2	23	4.7	8.1	0.7	11.7	1.8
Clay minerals	7.1	5.9	3.1	3.5	0.8	1.1	19.1	20.1	49.2	1.8	7	1.9
Pyrite	0.3	0.4	2.2	0	0.5	0	0	0.7	0	1.4	5.9	0
Carbonates	0.2	0.9	0.6	0.5	0	0.2	2.1	1.4	11.4	0.7	0.6	0
Limonite	0	0	0	0.5	1.5	0	0	1	0	2.5	0	0
Quartz	0	0	0.5	0.6	0	0	1.1	2.7	4.8	0	0.5	0
Others	1.1	1	3.6	3.2	1.6	0.8	3.3	4.3	13.2	0	2.4	0.9
Minerals	8.7	8.2	10	8.3	4.4	2.1	25.6	30.2	78.6	6.4	16.4	2.8
Alteration [vol.%]	0	0	0.5	0	0	0.6	1.2	0	7.1	0	0	0
Char [vol.%]	0	0	0	0	0	0	0	0	0	0	0	0

MACERALS [vol.%]	SK14B	SK16	SK17	SK18	SK19	SK22	SK23	SK24	SK28	SK35	SK40
Ulminite	0	80.3	83.4	51.7	93	86	0	0	78.4	1	70.9
Textinite	0	2.3	0	1.7	0	4.3	0	0	0	0	5
Densinite	0	0	0	3.6	1.7	0	0	0	2	0	0
Corpohuminite	0	7.6	2.7	4.4	2.3	2.1	0	0	2.9	0	6.7
Attrinite	0	0	0	0	0	0	0	0	0	0	0
HUMINITE	0	90.2	86.1	61.4	97	92.4	0	0	83.3	1	82.6
Sporinite	0	0	0.8	5.3	0	0	0	0	0	0.5	0
Suberinite	0	0.7	1.1	3.6	0	0	0	0	0.5	0	0
Resinite	0	6.1	7.3	5.3	1.5	5.4	0	0	11.2	0	9
Liptodetrinite	0	0	0.8	4.3	0	0	0	0	1	0	0
Cutinite	0	0.7	0.4	0.8	0	0	0	0	0	0	0
LIPTINITE	0	7.5	10.4	19.3	1.5	5.4	0	0	12.7	0.5	9
Fusinite	0	0	0	0.9	0	0	1	2.3	0	0	0
Semifusinite	0	0	0	1.8	0	0	2.3	1	0	0	0
Secretinite	0	0	0.9	0	0	0	0	0	0	0	0
Macrinite	0	0	0	5.3	0	0	1.8	2.7	0	0	0
Inertodetrinite	0	0	0	4.3	0	0	3.2	2.6	0	0	0
Funginite	0	0	0	0	0	0	0	0	0	0	0
INERTINITE	0	0	0.9	12.3	0	0	8.3	8.9	0	0	0
Clay minerals	2.4	0.7	0	5.5	0	1.2	62.9	54.4	2	62.5	2.8
Pyrite	0	0.8	0.8	0	0	0	0.6	0	1.1	0.5	0
Carbonates	0	0	0	0	1	0	1.5	0	0.5	17.8	1
Limonite	0	0.8	0	0	0	0	0	0	0	0	0
Quartz	0	0	0	0	0	0	3.2	4.4	0	0	0
Others	3.1	0	1.8	1.5	0.5	1	10.2	7	0.4	14.7	4.6
MINERALS	5.5	2.3	2.6	7	1.5	2.2	78.4	65.8	4	95.5	8.4
ALTERATION [vol.%]	0	0	0	0	0	0	10.1	25.3	0	3	0
CHAR [vol.%]	94.5	0	0	0	0	0	3.2	0	0	0	0

The correlation between mean ulminite reflectance and volatile matter (Fig. 4D) displays a considerable amount of scatter within the studied series, especially in samples SK01B, SK01C, SK08 and SK40 with elevated volatile matter content. The observed degree of scatter is attributed to the presence of variable amounts of mineral material, rather than the coal rank. Within the studied sample set, the inorganic

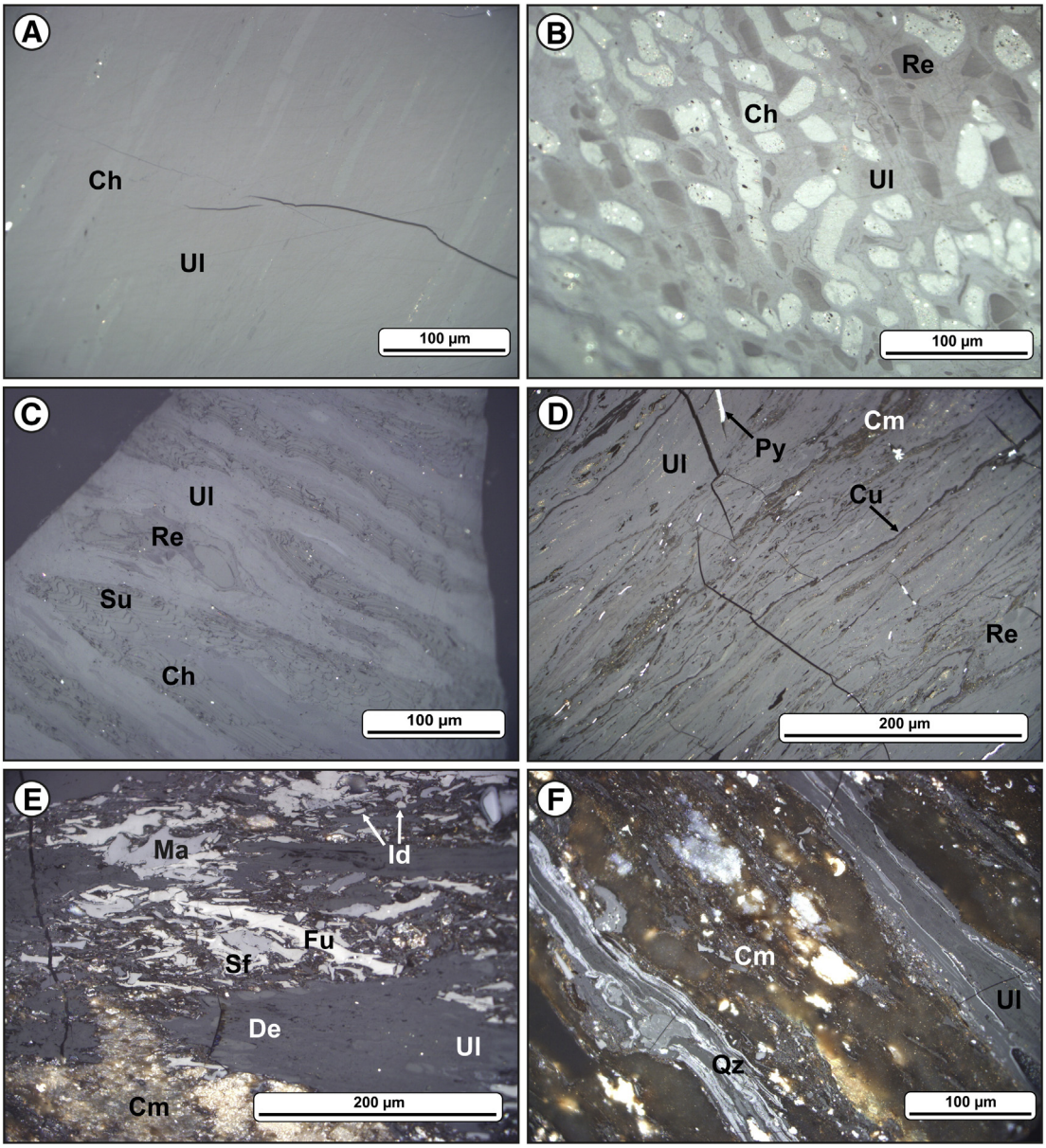

Fig. 6. Photomicrographs of macerals and mineral admixture in the "normal" coal samples. A – Ulminite (Ul) with weakly distinct corpohuminite (Ch) in sample SK14A; B – Ulminite with light bodies of corpohuminite and darker resinite (Re) in sample SK07; C – Ulminite with remnants of bark tissue forming darker suberinite (Su) filled with light corpohuminite in sample SK18; D – Humified fragments of leaves, lined by thin dark cutinite (Cu), with tiny resinite, fine-grained clay minerals (Cm) and yellowish-white pyrite (Py) filling a crack in ulminite in sample SK01C; E – Ulminite interrupted by irregular detritic position of densinite with fusinite (Fu), semifusinite (Sf), macrinite (Ma) and inertodetrinite (Id) fragments and with dispersed clay minerals that form a separate position in the lower part in sample SK08; F – Grey ulminite bands with whitish lines of quartz (Qz) separated by a thicker layer of mineral mixture dominated by clay minerals in sample SK01B.

fraction comprises variable proportions of clay minerals and carbonates. Thus, the measured volatile matter content reflects the presence of prevailing minerals rather than the coalification rank (Schobert, 2013).

5.2. Effect of post-depositional volcanic activity

Several authors have observed significant changes in coal compositions, especially an increase in thermal maturity, due to igneous intrusions or dykes penetrating coal seams (e.g., Cooper et al., 2007; Dai and Ren, 2007; Rahman and Rimmer, 2014). However, there has been no immediate contact of magma with the coal seams on the Faroe Islands. The basaltic lava flows of the Malinstindur Formation covering the coal-bearing Prestfjall Formation were deposited approximately 3–14 m distant from the studied coal seams (Rasmussen and Noe-Nygaard, 1969, 1970), with the upper sequence of volcaniclastic claystone termed the "roof clay", acting as an insulating layer that impedes contact metamorphism and coking of the coal (cf. Chen et al., 2014).

Based on the results of our combined petrological and geochemical approach, we propose two general possibilities for how the coal may have been affected by volcanic effusions: (i) by thermal alteration of limited extent leading to formation of a macroscopically visible, thin "anthracite-like" crust and (ii) by hydrothermal fluids that accompanied volcanic activity.

On the Faroe Islands it is possible to observe coals with an "anthracite-like" degree of coalification (bright, hard and lustrous). Nevertheless, both the petrographic and geochemical analyses argue against the presence of this higher quality coal lithotype. The observed macroscopic appearance of the coal is caused by the presence of a very thin "anthracite-like" surface (Fig. 3C), which may reflect slight thermal alteration, but without an increase in the mean ulminite reflectance. Aghaei et al. (2015) observed an exponential increase of the reflectance

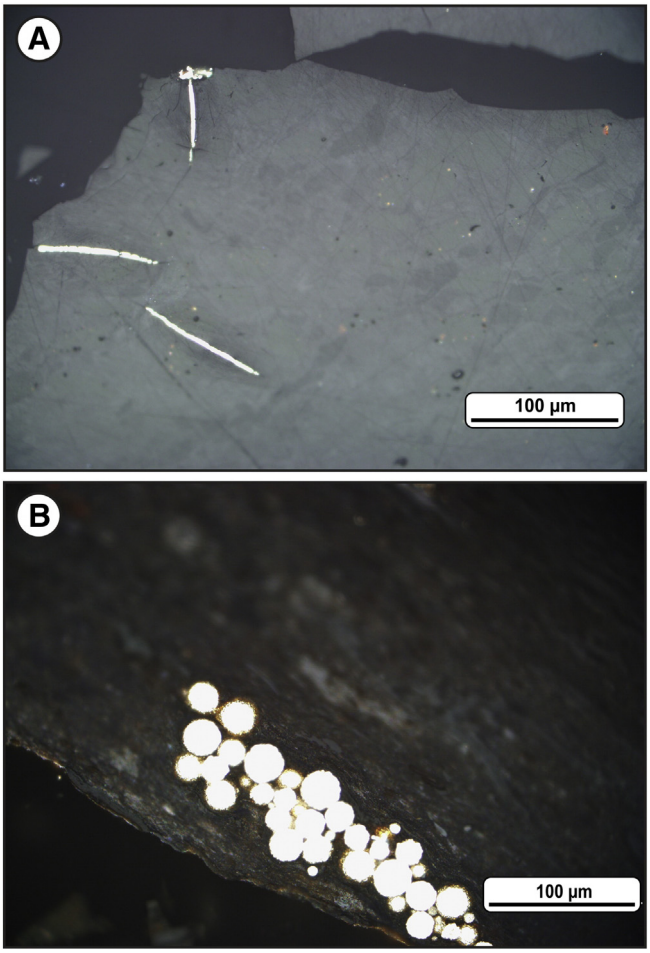

Fig. 7. Photomicrographs of pyrite occurrences in the coal. A – Epigenetic pyrite filling fractures in ulminite in sample SK19. B – Syngenetic pyrite forming a framboid cluster in sample SK09.

directly at the contact of the dyke to the coal seam. At a distance >2 m from the dyke contact, only the low initial reflectance values were recorded. The size of the contact aureole is approximately one to two times the thickness of the magmatic body (e.g., Bostick and Pawlewicz, 1984; Crelling and Dutcher, 1968; Galushkin, 1997). Considering the planar character and low viscosity of the basaltic lava, this explains why the rank of the Faroese coal is not elevated.

In contrast, the quality of the coal may have been negatively affected by accompanying hydrothermal mineralization along fractures or faults (Figs. 3A, 9D). According to Gamson et al. (1996), mineralization fills microfractures in compact bright coal of low porosity and permeability, whereas in dull coal of higher porosity and permeability, such as in the "altered organic matter", mineralization can disperse throughout the organic matrix or infill the cell lumens of corpohuminite. Additionally, "altered organic matter" contains inorganic component dominated by clay minerals (Table 3). These minerals are very likely a product of hydrothermal decomposition of plagioclase, which is visible both in basalts and in surrounding feldspar-rich tuffitic claystones (Fig. 9A, C, D).

The effect of the basaltic lava flows covering the coal-bearing volcanosedimentary sequences is also recorded in the chemical composition of the "altered organic matter" (cf. Finkelman et al., 1998). Apart from the organic components, the samples consist mainly of clay minerals and carbonates, especially siderite. Dai et al. (2012b) reported possible formation of illite from kaolinite exposed to heat from an igneous body. Dai and Ren (2007) assigned groups of elements with an enrichment trend to thermally altered coal. In accordance with their study, the studied samples of "altered organic matter" are enriched especially in Cu and Ni, Sr, Zn, Mn (specifically MnO) and less in As, indicating that basaltic lava was the source of these elements. Additionally, the enrichment in V and depletion in U in the "altered organic matter" is not consistent with their observations. The affinity with basaltic lava is clearly visible from the enrichment in Ni and Cr. These transition metals are primary characteristics for mantle-derived (basaltic) rocks (e.g., McDonough and Sun, 1995). Our unpublished analyses from overlying basalts (Malinstindur Formation) yield Ni and Cr concentrations of 78 ppm and 191 ppm, respectively. These values are relatively low compared to concentrations in primitive plateau basalts of the North Atlantic Igneous Province (cf. Hughes et al., 2015 and references therein) and point to a decomposition of primary mineral phases, i.e., olivine and Cr-rich spinel (Fig. 9A). Transition metals could be released from primary mineral phases and accumulated at nearby geochemical barriers, such as coal seams.

5.3. Quality of the exploited coal

A clear correlation between the fuel ratio and the gross calorific value (Fig. 4C) shows that the better combustion suitability and generally greater ease of ignition is attributed to the coal having fewer mineral components. Five samples, namely SK01B, SK01C, SK08, SK19 and SK40 with higher proportions of mineral matter plot in a lower position than samples with lower mineral contents. The "altered organic matter" is entirely unsuitable for combustion because of its very low fuel ratio and gross calorific value, except for the charcoal, which has by contrast the highest fuel ratio, along with an intermediate gross calorific value that is still lower than most of the studied coals.

Despite the macroscopic "anthracite-like" character of the coal from the active New Prestfjall mine (samples SK01A–C), the coal contains approximately 10 vol.% of minerals with relatively low carbon content and gross calorific value compared to samples from the abandoned coal mines in the Prestfjall Formation (Table 2). In other words, the coal from the New Prestfjall mine is less suitable for combustion compared to coals mined in the past. Øster-Mortensen (2002) described the coal exploited in the Rókhagi mine (closed in 2013) as coal of high quality, which is in line with our present study.

Coal from the Beinisvørð Formation (Mykines Island) had been extracted locally in small amounts for household use only (Rasmussen and Noe-Nygaard, 1970). This coal is of relatively low rank and quality, although it is older than the higher quality coal from the Prestfjall Formation. The low rank of the coal is indicative of very fast coalification due to the short duration of sedimentation and subsequent burial by basalts (cf. Dvořák et al., 1997). Lower coal rank was produced by mineralizing fluids that migrated along a fault and filled corpohuminite cells in the coal (Fig. 3A).

5.4. Coal geochemistry

The low sulphur contents (<1%) of the Faroese coal are primarily of organic origin, i.e., they derive from coal-forming plants (Chou, 2012) and to a lesser extent, correlate with small amounts of pyrite occurring both in epigenetic and syngenetic form as fracture fillings and framboids, respectively (Fig. 7A, B). The organic sulphur is mainly associated with vitrinite (or ulminite in low-rank coal), suggesting a positive correlation with the gelification degree (Dai et al., 2002).

Major oxides are dominated by SiO_2, Al_2O_3 and Fe_2O_3, corresponding to a mineral assemblage of clay minerals, quartz, pyrite, siderite and limonite. Limonite occurs exclusively on the surface of some samples in very small amounts. In case of its presence, it never replaces pyrite completely. Along with the microscopic appearance of pyrite (see Fig. 7A, B), this is indicative of freshness of studied samples (Littke et al., 1991). Compared to coal from the Prestfjall Formation, the "normal" coal sample from the Beinisvørð Formation is relatively enriched in trace elements, namely Rb, Sr, W and Ni. Whereas the coal seams in the Prestfjall Formation are up to 1.5 m thick, the lenses sampled in

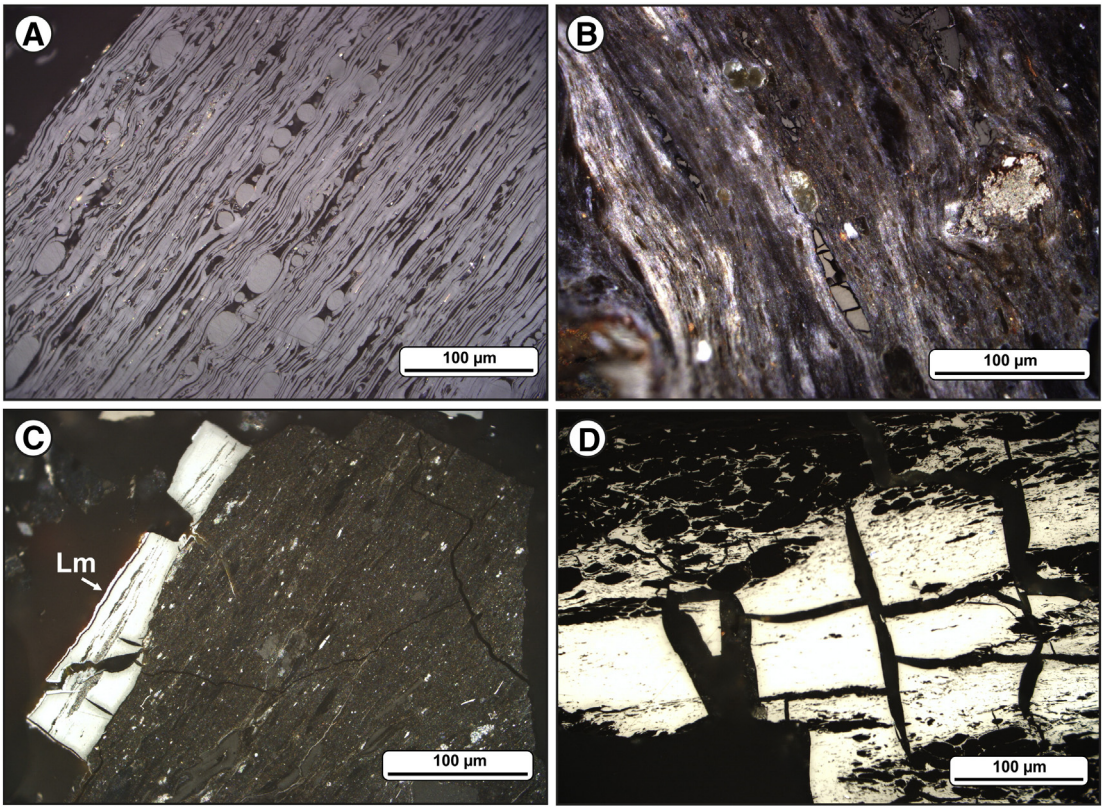

Fig. 8. Photomicrographs of "altered organic matter" samples. A – Degassed fragment of wooden tissue in sample SK14B; B – Altered fragments of coal particles in mineral matter in sample SK10. Reflectance of lighter, more altered particle with contraction fractures is 0.75%, whereas the reflectance of darker, less altered particle is 0.42%; C – Massive char particle with contraction fractures and reflectance of 1.85% that is lined by thin limonite layer (Lm), surrounded by mineral matter in sample SK23; D – Char particle with reflectance of 1.98% measured on the massive centre that is interrupted by distinct contraction fractures and rimmed by mosaic texture in sample SK23.

the Beinisvørð Formation are only a few centimetres thick. Some previous studies discuss the relationship between enrichment of certain trace elements and thickness of the coal seams (e.g., Chen et al., 2015; Eskenazy and Valceva, 2003; Li et al., 2012; Querol et al., 1992; Van Krevelen, 1963). Van Krevelen (1963) noted that thin coal layers are usually enriched in some trace elements compared to thick ones. According to Querol et al. (1992), this behaviour is related to post-depositional epigenetic percolation of diagenetic fluids through a fracture network, which was previously better developed in thinner seams than in thicker ones. Thus, the low thicknesses could explain why coal from the Beinisvørð Formation is more enriched in the trace elements listed above than coal from the Prestfjall Formation.

Table 4
Reflectance of ulminite B, altered particles and char.

Sample ID	Coal type	R_r [%]	σ	R_{alt} [%]	R_{char} [%]
SK01A	xylite	0.46	0.05	–	–
SK01B	detroxylite	0.41	0.05	–	–
SK01C	detroxylite	0.42	0.05	0.56	–
SK04	detroxylite	0.40	0.05	–	–
SK06	xylite	0.45	0.04	–	–
SK07	detroxylite	0.46	0.06	0.58	–
SK08	detroxylite	0.53	0.06	0.67	–
SK09	detroxylite	0.45	0.08	–	–
SK10	mineral-rich	0.42	0.10	0.93	–
SK12	detroxylite	0.47	0.06	–	–
SK13	detroxylite	0.44	0.08	–	–
SK14A	xylite	0.42	0.07	–	–
SK14B	charcoal	–	–	–	0.87
SK16	xylite	0.48	0.05	–	–
SK17	xylite	0.41	0.07	–	–
SK18	detroxylite	0.43	0.09	–	–
SK19	xylite	0.40	0.04	–	–
SK22	xylite	0.39	0.05	–	–
SK23	mineral-rich	–	–	0.56	1.93
SK24	mineral-rich	–	–	0.83	–
SK28	detroxylite	0.45	0.08	–	–
SK35	mineral-rich	0.39	0.05	1.35	–
SK40	xylite	0.34	0.04	–	–

5.5. Mercury speciation, behaviour and environmental impact

Trace Hg analysis revealed that mercury contents in the Faroese coal are generally low. Similar or slightly higher concentrations were also reported from Palaeozoic bituminous coals from the Czech Republic (Coufalík et al., 2011). This observation supports the idea that no correlation exists between mercury content and coal rank (Kilgroe et al., 2002).

Additionally, all studied samples are classified as low-sulphur coals (Chou, 2012). As described by Yudovich and Ketris (2005a), low-sulphur coals that are generally poor in Hg are dominated by only two Hg forms: Hg_{org} (mercury bound to humic substances) and $Hg_{sulphide}$ (commonly pyritic mercury, Hg_{pyr}). In addition to Hg and S, our samples were characterized by low As contents. The data indicate relatively low amounts of Hg_{pyr} in the coal (Kolker et al., 2006).

The CAI_{Hg} (Hg coal affinity index) is between 0.3 and 4.2 for "normal" coal samples. In comparison, "altered organic matter" samples show only limited CAI_{Hg} values of ~0.1. Values of CAI_{Hg} >1 indicate that the studied coal does not act as a geochemical barrier for the mercury, suggesting that alteration processes resulted in removal of the mercury from the affected coal seam to the surrounding sediments.

The finding that "altered organic matter" contains less mercury than "normal" coal could be related to volcanic activity. The solubility of Hg species increases with higher temperatures produced by adjacent volcanic effusions. The mercury becomes mobile and can be more easily leached from organic matter by hydrothermal fluids

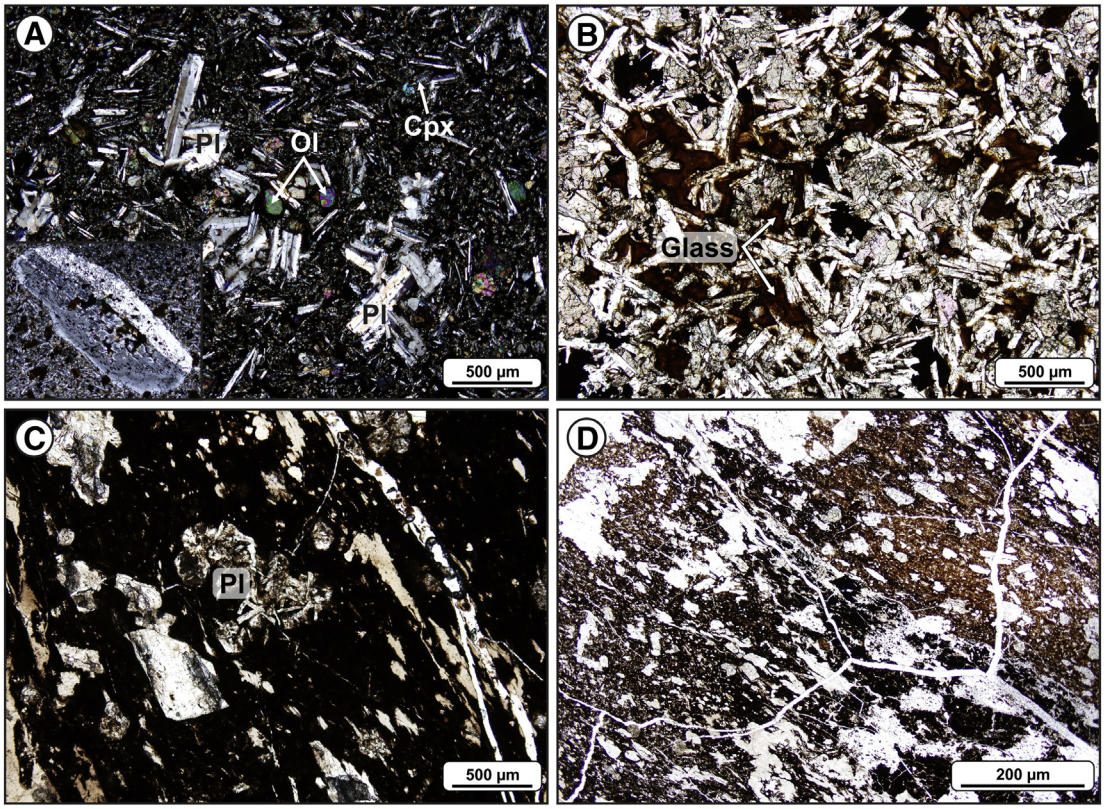

Fig. 9. Photomicrographs of the petrographic thin sections from the basalt samples (Malinstindur Formation) and underlying tuffitic coal-bearing claystone (Prestfjall Formation). A – Glomeroporphyritic texture with plagioclase (Pl), clinopyroxene (Cpx) and olivine (Ol) with altered rims; inset in the lower left corner shows selective sericitisation of plagioclase zones in detail (basalt sampled in the vicinity of SK11; crossed polars); B – Altered basaltic glass filling the interstices between the plagioclase laths (basalt sampled in the vicinity of SK01; parallel polars); C – Fragment of older basaltic volcanite showing glomeroporphyric plagioclase intergrowths altered to clay minerals (tuffitic coal-bearing claystone sampled in the vicinity of SK01; parallel polars); D – System of hydrothermal veinlets connected with subaerial volcanic activity recorded in Malinstindur Formation; the thin section contains plagioclase pseudomorphosis filled by products of its alteration (tuffitic coal-bearing claystone sampled in the vicinity of SK01; parallel polars).

(Fein and Williams-Jones, 1997; Moiseyev, 1971; Peabody and Einaudi, 1992). Finkelman et al. (1998) found that mercury content is higher in close proximity to an intrusive body due to secondary enrichment following volatilization of Hg during heat exposure and its subsequent redeposition from fluids derived from the cooling magma. No traces of mercury were recorded at a distance >50 cm from the intrusion.

In low-rank coal, such as that in the Faroese samples, the extent of mercury removal is much lower compared to bituminous coal (Kilgroe et al., 2002). Combined with the low levels of Hg in the coal, its combustion has only a limted impact on the environment.

Table 5
Contents of major oxides in the samples from the Faroe Islands (wt.%; on a whole-coal basis).

Sample ID	SiO_2	TiO_2	Al_2O_3	$Fe_2O_3^{tot}$	MnO	CaO	K_2O	P_2O_5
SK01A	1.54	BDL	1.11	0.75	0.002	1.39	0.06	BDL
SK01B	1.59	BDL	1.16	0.36	0.002	0.41	0.07	BDL
SK01C	3.95	0.29	3.11	5.05	0.009	1.11	0.04	0.03
SK04	7.57	0.38	7.10	0.82	0.001	1.69	BDL	BDL
SK06	8.59	0.88	7.22	0.85	0.013	1.24	BDL	0.04
SK07	2.36	BDL	1.74	0.38	BDL	3.51	0.04	BDL
SK08	5.86	1.03	5.59	3.27	0.011	1.44	BDL	0.18
SK09	2.15	BDL	1.70	0.47	0.013	0.90	0.06	BDL
SK10	26.25	4.13	19.91	3.60	2.877	0.03	BDL	0.06
SK12	1.92	BDL	1.71	0.66	0.003	3.09	0.04	0.04
SK13	6.98	0.61	6.39	2.12	0.004	1.49	BDL	0.05
SK14A	1.93	BDL	1.70	1.27	BDL	5.11	BDL	0.03
SK14B	4.38	BDL	2.12	0.31	BDL	0.51	0.06	0.04
SK16	2.87	BDL	2.41	0.40	BDL	2.09	0.03	0.01
SK17	2.46	BDL	2.66	0.44	BDL	1.05	0.06	0.04
SK18	8.47	0.39	8.44	1.23	0.01	1.58	BDL	0.02
SK19	0.92	BDL	0.85	0.44	BDL	0.86	0.04	0.01
SK22	3.40	0.01	3.83	0.86	0.002	2.91	0.01	0.02
SK23	37.13	2.15	25.14	4.43	0.472	0.06	BDL	0.22
SK24	1.06	BDL	1.26	0.75	BDL	1.43	0.11	0.03
SK28	2.72	0.05	3.15	0.76	0.017	2.22	0.09	0.10
SK35	30.14	2.09	12.50	16.13	0.096	1.34	0.16	0.07
SK40	7.82	0.03	2.31	1.26	0.017	2.97	0.15	0.40

BDL - below detection limit

5.6. Depositional environment of Faroese coal

5.6.1. Maceral composition

In accordance with the studies of Diessel (1992) and Teichmüller (1989), the occurrence of ulminite, corpohuminite, fusinite and semifusinite with associated resinite or suberinite point to a forest habitat, whereas the presence of densinite, liptodetrinite and inertodetrinite denote inputs of herbaceous vegetation. The strong gelification of huminite macerals reflects mostly wet conditions in a peat-forming swamp. Significant variability of the liptodetrinite and sporinite assemblages suggests unstable conditions due to a fluctuating water table (Kolcon and Sachsenhofer, 1999). The absence of alginite in coal is incompatible with marine inputs to the depositional environment of the Faroese coal. The coal plots at Apex A in the maceral-based ternary diagram of Mukhopadhyay (1989), later modified for low-rank coal by Singh et al. (2010) and is indicative of swamp vegetation with preserved cell structures that have been coalified in variably anoxic and oxic conditions (Fig. 11).

In the fusitic charcoal-rich sample SK14B, charred matter of textinite, specifically fusinite and semifusinite, predominates. It is assumed that this type of coal was derived from wood affected by local

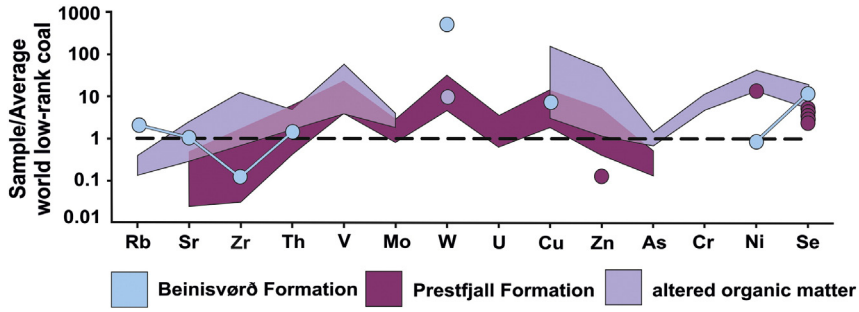

Fig. 10. Trace element contents for "normal" coal samples from both the Prestfjall and Beinisvørð Formations, and for "altered organic matter", normalized to the average worldwide low-rank coal composition (Ketris and Yudovich, 2009). Circles express individual analyses or analyses that do not fit the range for a given sample type.

wildfires, weathering or microbial activity (Cohen and Spackman, 1977; Cope and Chaloner, 1985; ICCP, 2001; Scott, 2002) or it may be formed from wood remnants affected by heat from the lava flow. The latter would explain the variable development of this sample compared to the other studied coals.

Table 6
Concentrations of trace elements in the samples from the Faroe Islands (ppm; on a whole-coal basis).

Sample ID	V	Cr	Ni	Cu	Zn	As	Se	Rb
SK01A	BDL	BDL	BDL	BDL	16	BDL	BDL	BDL
SK01B	BDL	BDL	BDL	BDL	BDL	BDL	BDL	BDL
SK01C	285	BDL	BDL	78	58	1.7	6.4	BDL
SK04	413	BDL	BDL	BDL	33	3.2	BDL	BDL
SK06	254	BDL	BDL	118	31	BDL	BDL	BDL
SK07	BDL	BDL	BDL	BDL	BDL	1.8	BDL	BDL
SK08	242	BDL	BDL	179	64	1.2	4.3	BDL
SK09	BDL	BDL	BDL	BDL	BDL	BDL	BDL	BDL
SK10	768	126	159	1736	101	6.8	6.8	1.8
SK12	BDL	BDL	BDL	33	27	1.4	BDL	BDL
SK13	97	BDL	BDL	34	15	BDL	7.0	BDL
SK14A	BDL	BDL	BDL	119	8.6	BDL	BDL	BDL
SK14B	BDL	BDL	BDL	BDL	9.1	BDL	2.8	BDL
SK16	BDL	BDL	BDL	BDL	2.7	BDL	BDL	BDL
SK17	BDL	BDL	BDL	BDL	BDL	BDL	BDL	BDL
SK18	252.51	BDL	BDL	118.65	31.02	BDL	5.16	BDL
SK19	BDL	BDL	BDL	BDL	BDL	BDL	BDL	BDL
SK22	393.36	BDL	BDL	BDL	39.7	BDL	BDL	BDL
SK23	987	89.3	291	1229	663	6.8	14.7	1.9
SK24	BDL	BDL	BDL	BDL	BDL	BDL	BDL	BDL
SK28	352	BDL	140	105	97	BDL	BDL	BDL
SK35	517	45	80	1304	128	10	5.3	12
SK40	BDL	BDL	7.4	108	BDL	BDL	9.7	18

Sample ID	Sr	Zr	Mo	W	Th	U
SK01A	9.2	4.6	BDL	6.6	3.5	BDL
SK01B	6.3	3.9	BDL	BDL	5.9	2.5
SK01C	20	39	2.1	BDL	4.0	BDL
SK04	7.1	9.1	BDL	19	BDL	BDL
SK06	7.2	15	BDL	BDL	BDL	BDL
SK07	11	6.6	6.5	10	10.7	2.8
SK08	57	51	BDL	BDL	BDL	BDL
SK09	37	3.4	BDL	BDL	6.9	4.7
SK10	223	309	6.5	BDL	12	BDL
SK12	7.9	8.4	5.0	13	15	5.3
SK13	5.6	33	BDL	BDL	BDL	BDL
SK14A	15	1.3	BDL	BDL	2.0	BDL
SK14B	4.3	9.5	5.5	20	17	8.5
SK16	9.5	1.8	BDL	BDL	3.2	BDL
SK17	8.12	BDL	BDL	BDL	1.65	BDL
SK18	15.56	36.75	BDL	BDL	BDL	BDL
SK19	3.5	3.8	BDL	BDL	6.1	2.2
SK22	5.1	3.2	BDL	31.73	BDL	BDL
SK23	93	339	5.2	BDL	11	BDL
SK24	20	4.1	BDL	BDL	4.0	2.7
SK28	8.2	3.05	BDL	27	BDL	BDL
SK35	104	165	8.8	BDL	6.4	BDL
SK40	120	4.4	BDL	606	4.8	BDL

Apart from the "altered organic matter", small amounts of detrital minerals dispersed throughout the organic matter of the "normal" coal were observed. These may result from intermittent flooding or a fluctuating lake level, as proposed for the studied area by Passey (2014).

5.6.2. Relationship between sulphur contents and the depositional environment

Coal from the Faroe Islands contains 0.03–0.99% sulphur and is therefore classified as a low-sulphur coal (Chou, 2012). Sulphur abundances <1% generally suggest low-pH conditions in the swamp (Bechtel et al., 2003). Occurrences of framboidal pyrite may be related to freshwater inputs resulting in more reducing conditions that are conductive to reducing bacteria (Strobl et al., 2014). Some authors suggest that higher proportions of the sulphur may be related to marine inputs, whereas low-sulphur coals are commonly deposited in continental environments (e.g., Chou, 2012; Dai and Ren, 2007; Markič and Sachsenhofer, 1997). However, a non-marine high-sulphur Miocene lignite with a sulphur content of up to 12.2% was reported in Turkey by Gürdal (2011) and Gürdal and Bozcu (2011), who suggested that high sulphur abundance in the lignite can be attributed to regional volcanic activity. Additionally, Dai et al. (2012a) observed an assemblage of syngenetic pyrite in non-marine medium-sulphur coal that was probably derived from sulphate-rich epithermal solutions. Considering the low sulphur contents in studied samples from the Faroe Islands, it is possible to exclude the influence of seawater during peat accumulation.

5.6.3. Comparison with results from palynological studies

Palynological studies of the Faroese coal and adjacent sediments were performed by Ellis et al. (2002) and Lund (1989) for both Suðuroy and Mykines Island. The palynoflora is dominated by *Inaperturopollenites hiatus*, *Caryapollenites circulus*, *C. veripites*, *C. triangulus*, *Laevigatosporites haardtii*, *Monocolpopollenites tranquilus*, *Momipites*, *Pityosporites* spp. and sporadically occurring *Phaseoidites stanleyii*, *Striatricolporites* sp. and *Montanapollis* spp. This tree association is typical for deposition in a warm humid climate within extensive peat swamps on overbank floodplains or small lakes margins (Wing and Hickey, 1984). No

Table 7
Mercury abundances in representative samples from studied localities.

Sample ID	Formation	Locality	Sample type	Hg [ppb]	RSD [%]	CAI_{Hg}
SK01B	Prestfjall	New Prestfjall mine	detroxylite	56	1.06	1.12
SK04	Prestfjall	Kolaminur	detroxylite	22	2.39	0.44
SK12	Prestfjall	Rókhagi	detroxylite	127	2.99	2.54
SK16	Prestfjall	Rangibotnur	xylite	35	2.05	0.7
SK22	Prestfjall	Gudmund's mine	xylite	210	1.93	4.2
SK24	Prestfjall	Kolavegurin	mineral-rich	9	0.52	0.18
SK40	Beinisvørð	Mykines	xylite	14	1.97	0.28

RSD - relative standard deviation
CAI_{Hg} - Hg coal affinity index

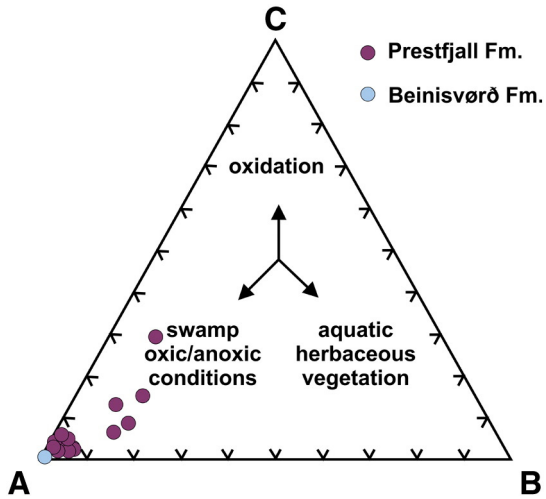

Fig. 11. ABC ternary diagram of the Faroese coal samples modified after Mukhopadhyay (1989). A – ulminite + textinite + corpohuminite + sporinite + cutinite + resinite + suberinite; B – densinite + attrinite + liptodetrinite; C – inertinite. The "altered organic matter" samples were not included in this diagram due to their irrelevance in assessment of depositional environment.

marine flora were observed within the Faroese coal. Additionally, Lund (1989) discovered the presence of fresh water algae, *Sigmopollis*, in coal from the Rókhagi mine, suggesting a lake environment. The algae were accompanied by *Polypodiaceoisporites marxheimensi*, indicating that the lake was surrounded by forest swamps. These palynological studies fully support the depositional environment (wet forest swamps in proximity to a lake) suggested in our study for the Faroese coal.

6. Conclusions

Based on a combined petrographic and geochemical approach, our study obtanis the following results:

(1) The rank of Palaeogene coal from the Faroe Islands is lignite to subbituminous. The coal is generally characterized by low sulphur contents, medium ash yields and high volatile matter contents.
(2) The maceral composition of the coal is dominated by ulminite with an average mean reflectance of 0.34–0.53%. The proportions of liptinite and inertinite vary in coal samples.
(3) The coal was derived from wood in a wet forest swamp environment in proximity to a lake with possibly fluctuating water levels.
(4) Basalt lava flows of the Malinstindur Formation overlying the coal-bearing Prestfjall Formation affected the coal to a limited degree. Thermal effects include only a thin "anthracite-like" crust, with no signs of elevated coal rank. Fluids accompanying the volcanic activity induced decomposition of primary mineral phases in basalts as well as in the surrounding volcaniclastic sediments and enriched the affected coal in mineral components. The low original rank of the coal explains the absence of typical high mean reflectance and natural coke textures throughout the coal sequence.
(5) Coal from the older Beinisvørð Formation can be distinguished from that of the Prestfjall Formation based on petrographic and geochemical criteria. The coal from the Prestfjall Formation is of higher quality and has therefore been mined in many locations on Suðuroy Island. However, only one coal mine is presently in operation and the quality of the mined coal is lower than it was in the past.
(6) Combustion of Faroese coal has a relatively low impact on the local environment due to low Hg, As and S contents.

Acknowledgements

Financial support to S.K. and R.P. was provided by the J.E. Purkyně University Internal Grant Agency FŽP IG 1/2014 and by OPVK EnviMod (CZ.1.07/2.2.00/28.0205) project. L.K. was financially supported by project No. RVO67985831 of the Institute of Geology CAS, Prague and by a BUT project No. LO1408 "AdMaS UP - Advanced Materials, Structures and Technologies", which is supported by the Ministry of Education, Youth and Sports of the Czech Republic under the "National Sustainability Programme I". The involvement of P.C. was supported by the Institute of Analytical Chemistry of the CAS under the Institutional Research Plan RVO: 68081715. We are indebted to I. Sýkorová and E. Geršlová for their excellent help with descriptions of maceral and elemental compositions. We gratefully acknowledge M. Havelcová (IRSM, CAS, Prague) for performing chemical analyses, which were covered by the Czech Science Foundation (Research Grant No. 13-18482S). Many thanks are also given to M.J. Timmerman (University of Potsdam), R.L. Romer (GFZ Potsdam) and R. Macdonald (Lancaster University) for their corrections and discussion that helped to improve the original manuscript. We sincerely thank to U.E. Árting (The Faroese Earth and Energy Directorate – Jarðfeingi) for providing maps and kind help during field exploration. We greatly appreciate an anonymous reviewer and editor-in-chief R. Littke for their constructive and helpful comments and suggestions.

References

Aghaei, H., Gurba, L.W., Ward, C.R., Hall, M., Mahmud, S.A., 2015. Effects of igneous intrusions on thermal maturity of carbonaceous fluvial sediments: a case study of the Early Cretaceous Strzelecki Group in west Gippsland, Victoria, Australia. Int. J. Coal Geol. 152, 68–77.
Amijaya, H., Littke, R., 2006. Properties of thermally metamorphosed coal from Tanjung Enim Area, South Sumatra Basin, Indonesia with special reference to the coalification path of macerals. Int. J. Coal Geol. 66, 271–295.
Bechtel, A., Gruber, W., Sachsenhofer, R.F., Gratzer, R., Lücke, A., Püttmann, W., 2003. Depositional environment of the Late Miocene Hausruck lignite (Alpine Foreland Basin): insights from petrography, organic geochemistry, and stable carbon isotopes. Int. J. Coal Geol. 53, 153–180.
Bohnhoff, M., Makris, J., 2004. Crustal structure of the southeastern Iceland-Faeroe Ridge (IFR) from wide aperture seismic data. J. Geodyn. 37, 233–252.
Bostick, N.H., Pawlewicz, M.J., 1984. Paleotemperatures based on vitrinite reflectance of shales and limestones in igneous dike aureoles in the Upper Cretaceous Pierre Shale, Walsenburg, Colorado. In: Woodward, J.G., Meissner, F.F., Clayton, J.L. (Eds.), Hydrocarbon Source Rocks of the Greater Rocky Mountain Region. Rocky Mountain Association of Geologists, Denver, pp. 387–392.
Bott, M.H.P., Sunderland, J., Smith, P.J., 1974. Evidence for continental crust beneath the Faeroe Islands. Nature 248, 202–204.
Bussio, J.P., Roberts, J.R., 2016. A large scale investigation into changes in coal quality caused by dolerite dykes in Secunda, South Africa-implications for the use of proximate analysis on a working mine. J. Afr. Earth Sci. 117, 401–409.
Casten, U., 1973. The crust beneath the Faeroe Islands. Nature 241, 83–84.
Chen, J., Liu, G., Li, H., Wu, B., 2014. Mineralogical and geochemical responses of coal to igneous intrusion in the Pansan Coal Mine of the Huainan coalfield, Anhui, China. Int. J. Coal Geol. 124, 11–35.
Chen, J., Chen, P., Yao, D., Liu, Z., Wu, Y., Liu, W., Hu, Y., 2015. Mineralogy and geochemistry of Late Permian coals from the Donglin Coal Mine in the Nantong coalfield in Chongqing, southwestern China. Int. J. Coal Geol. 149, 24–40.
Chou, C.–L., 2012. Sulfur in coals: a review of geochemistry and origins. Int. J. Coal Geol. 100, 1–13.
Cohen, A.D., Spackman, W., 1977. Phytogenic organic sediments and sedimentary environments in the Everglades mangrove complex: part II. The origin, description and classification of the peats of southern Florida. Palaeontographica 162B, 71–114.
Cooper, J.R., Crelling, J.C., Rimmer, S.M., Whittington, A.G., 2007. Coal metamorphism by igneous intrusion in the Raton Basin, CO and NM: implications for generation of volatiles. Int. J. Coal Geol. 71, 15–27.
Cope, M.J., Chaloner, W.G., 1985. Wildfire: an interaction of biological and physical processes. In: Tiffney, B.H. (Ed.), Geological Factors and the Evolution of Plants. Yale University Press, New Haven, pp. 257–277.
Coufalík, P., Červenka, R., Komárek, J., 2011. Mercury speciation in soil in vicinity of coal beds using sequential extraction. Environ. Earth Sci. 62, 421–427.
Crelling, J.C., Dutcher, R.R., 1968. A petrologic study of a thermally altered coal from the Purgatoire River Valley of Colorado. Geol. Soc. Am. Bull. 79, 1375–1386.
Czech technical standards ČSN 44 1377, 2004. Solid mineral fuels – determination of moisture. Czech office for Standards, Metrology and Testing, Prague (in Czech).
Czech technical standards ČSN ISO 1171, 2001. Solid mineral fuels – determination of ash. Czech office for Standards, Metrology and Testing, Prague (in Czech).
Czech technical standards ČSN ISO 29541, 2012r. Solid mineral fuels – determination of total carbon, hydrogen and nitrogen content – instrumental method. Czech office for Standards, Metrology and Testing, Prague (in Czech).

Dai, S., Li, W., Tang, Y., Zhang, Y., Feng, P., 2007. The sources, pathway, and preventive measures for fluorosis in Zhijin County, Guizhou, China. Appl. Geochem. 22, 1017–1024.

Dai, S., Ren, D., 2007. Effects of magmatic intrusion on mineralogy and geochemistry of coals from the Fengfeng-Handan Coalfield, Hebei, China. Energy Fuel 21, 1663–1673.

Dai, S., Ren, D., Tang, Y., Shao, L., Li, S., 2002. Distribution, isotopic variation and origin of sulfur in coals in the Wuda coalfield, Inner Mongolia, China. Int. J. Coal Geol. 51, 237–250.

Dai, S., Seredin, V.V., Ward, C.R., Jiang, J., Hower, J.C., Song, X., Jiang, Y., Wang, X., Gornostaeva, T., Li, X., Liu, H., Zhao, L., Zhao, C., 2014. Composition and modes of occurrence of minerals and elements in coal combustion products derived from high-Ge coals. Int. J. Coal Geol. 121, 79–97.

Dai, S., Wang, X., Seredin, V.V., Hower, J.C., Ward, C.R., O'Keefe, J.M., Huang, W., Li, T., Li, X., Liu, H., Xue, W., Zhao, L., 2012a. Petrology, mineralogy, and geochemistry of the Ge-rich coal from the Wulantuga Ge ore deposit, Inner Mongolia, China: new data and genetic implications. Int. J. Coal Geol. 90, 72–99.

Dai, S., Zeng, R., Sun, Y., 2006. Enrichment of arsenic, antimony, mercury, and thallium in a Late Permian anthracite from Xingren, Guizhou, Southwest China. Int. J. Coal Geol. 66, 217–226.

Dai, S., Zou, J., Jiang, Y., Ward, C.R., Wang, X., Li, T., Xue, W., Liu, S., Tian, H., Sun, X., Zhou, D., 2012b. Mineralogical and geochemical compositions of the Pennsylvanian coal in the Adaohai Mine, Daqingshan Coalfield, Inner Mongolia, China: modes of occurrence and origin of diaspore, gorceixite, and ammonian illite. Int. J. Coal Geol. 94, 250–270.

Diessel, C.F.K., 1992. Coal Formation and Sequence Stratigraphy. Springer, Berlin.

Dvořák, J., Honěk, J., Pešek, J., Valterová, P., 1997. Deep borehole evidence for a southward extension of the Early Namurian deposits near Němčičky, S. Moravia, Czech Republic: implication for rapid coalification. In: Gayer, R., Pešek, J. (Eds.), European Coal Geology and Technology. Geological Society of London Special Publications, London, pp. 179–193.

ECE-UN, 1998. International Classification of In-Seam Coals. United Nations Economic Commission for Europe, Geneva.

Ellis, D., Bell, B.R., Jolley, D.W., O'Callaghan, M., 2002. The stratigraphy, environment of eruption and age of the Faroes Lava Group, NE Atlantic Ocean. Geol. Soc. Lond. Spec. Publ. 197, 253–269.

Eskenazy, G.M., Valceva, S.P., 2003. Geochemistry of beryllium in the Mariza-east lignite deposit (Bulgaria). Int. J. Coal Geol. 55, 47–58.

Fein, J.B., Williams-Jones, A.E., 1997. The role of mercury-organic interactions in the hydrothermal transport of mercury. Econ. Geol. 92, 20–28.

Finkelman, R.B., Bostick, N.H., Dulong, F.T., Senftle, F.E., Thorpe, A.N., 1998. Influence of an igneous intrusion on the inorganic geochemistry of a bituminous coal from Pitkin County, Colorado. Int. J. Coal Geol. 36, 223–241.

Finkelman, R.B., Palmer, C.A., Krasnow, M.R., Aruscavage, P.J., Sellers, G.A., Dulong, F.T., 1990. Combustion and leaching behavior of elements in the Argonne premium coal samples. Energy Fuel 4, 755–766.

Galushkin, Y.I., 1997. Thermal effects of igneous intrusions on maturity of organic matter: a possible mechanism of intrusion. Org. Geochem. 26, 645–658.

Gamson, P., Beamish, B., Johnson, D., 1996. Coal microstructure and secondary mineralization: their effect on methane recovery. Geol. Soc. Lond. Spec. Publ. 109, 165–179.

Golab, A.N., Carr, P.F., 2004. Changes in geochemistry and mineralogy of thermally altered coal, Upper Hunter Valley, Australia. Int. J. Coal Geol. 57, 197–210.

Goodarzi, F., Cameron, A.R., 1990. Organic petrology and elemental distribution in thermally altered coals from Telkwa, British Columbia. Energy Sources 12, 315–343.

Gurba, L.W., Ward, C.R., 2000. Elemental composition of coal macerals in relation to vitrinite reflectance, Gunnedah Basin, Australia, as determined by electron microprobe analysis. Int. J. Coal Geol. 44, 127–147.

Gürdal, G., 2011. Abundances and modes of occurrence of trace elements in the Çan coals (Miocene), Çanakkale-Turkey. Int. J. Coal Geol. 87, 157–173.

Gürdal, G., Bozcu, M., 2011. Petrographic characteristics and depositional environment of Miocene Çan coals, Çanakkale-Turkey. Int. J. Coal Geol. 85, 143–160.

Hughes, H.S., McDonald, I., Kerr, A.C., 2015. Platinum-group element signatures in the North Atlantic Igneous Province: implications for mantle controls on metal budgets during continental breakup. Lithos 233, 89–110.

ICCP, 2001. The new inertinite classification (ICCP System 1994). Fuel 80, 459–471.

ISO 5069-1:1983, 1983. Brown Coals and Lignites – Principles of Sampling – Part 1: Sampling for Determination of Moisture Content and for General Analysis. International Organization for Standardization, Geneva.

ISO 7404-3:2009, 2009. Methods for the Petrographic Analysis of Coals – Part 3: Method of Determining Maceral Group Composition. International Organization for Standardization, Geneva.

Jolley, D.W., Bell, B.R., 2002. The evolution of the North Atlantic Igneous Province and the opening of the NE Atlantic rift. In: Jolley, D.W., Bell, B.R. (Eds.), The North Atlantic Igneous Province: Stratigraphy, Tectonic, Volcanic and Magmatic Processes. Geological Society of London Special Publications, London, pp. 1–13.

Ketris, M.P., Yudovich, Y.E., 2009. Estimations of Clarkes for Carbonaceous biolithes: world averages for trace element contents in black shales and coals. Int. J. Coal Geol. 78, 135–148.

Khorasani, G.K., Murchison, D.G., Raymond, A.C., 1990. Molecular disordering in natural cokes approaching dyke and sill contacts. Fuel 69, 1037–1046.

Kilgroe, J.D., Sedman, C.B., Srivastava, R.K., Ryan, J.V., Lee, C.W., Thorneloe, S.A., 2002. Control of Mercury Emissions from Coal-fired Electric Utility Boilers: Interim Report. Air Pollution Prevention and Control Division. U.S. Environmental Protection Agency, Durham.

Kisch, H.J., Taylor, G.H., 1966. Metamorphism and alteration near an intrusive-coal contact. Econ. Geol. 61, 343–361.

Kolcon, I., Sachsenhofer, R.F., 1999. Petrography, palynology and depositional environments of the early Miocene Oberdorf lignite seam (Styrian Basin, Austria). Int. J. Coal Geol. 41, 275–308.

Kolker, A., Senior, C.L., Quick, J.C., 2006. Mercury in coal and the impact of coal quality on mercury emissions from combustion systems. Appl. Geochem. 21, 1821–1836.

Kubouškova, S., Krmíček, L., Pokorný, R., 2015. Coal deposits in the Faroe Islands. Geosci. Res. Rep. for 2014. ISBN: 978-80-7075-884-7, pp. 115–120 (in Czech with English abstract).

Kwiecińska, B., Petersen, H.I., 2004. Graphite, semi-graphite, natural coke, and natural char classification – ICCP system. Int. J. Coal Geol. 57, 99–116.

Laier, T., Nytoft, H.P., Jørgensen, O., Isaksen, G.H., 1997. Hydrocarbon traces in the Tertiary basalts of the Faeroe Islands. Mar. Pet. Geol. 14, 257–266.

Li, J., Zhuang, X., Querol, X., Font, O., Moreno, N., Zhou, J., Lei, G., 2012. High quality of Jurassic coals in the Southern and Eastern Junggar Coalfields, Xinjiang, NW China: geochemical and mineralogical characteristics. Int. J. Coal Geol. 99, 1–15.

Littke, R., Klussmann, U., Krooss, B., Leythaeuser, D., 1991. Quantification of loss of calcite, pyrite, and organic matter due to weathering of Toarcian black shales and effects on kerogen and bitumen characteristics. Geochim. Cosmochim. Acta 55, 3369–3378.

Liu, G., Zheng, L., Gao, L., Zhang, H., Peng, Z., 2005. The characterization of coal quality from the Jining coalfield. Energy 30, 1903–1914.

Lund, J., 1989. A late Paleocene non-marine microflora from the interbasaltic coals of the Faeroe Islands, North Atlantic. Bull. Geol. Soc. Den. 37, 181–203.

Markič, M., Sachsenhofer, R.F., 1997. Petrographic composition and depositional environments of the Pliocene Velenje lignite seam (Slovenia). Int. J. Coal Geol. 33, 229–254.

Mastalerz, M., Drobniak, A., Schimmelmann, A., 2009. Changes in optical properties, chemistry, and micropore and mesopore characteristics of bituminous coal at the contact with dikes in the Illinois Basin. Int. J. Coal Geol. 77, 310–319.

McDonough, W.F., Sun, S.S., 1995. The composition of the Earth. Chem. Geol. 120, 223–253.

Merritt, R.D., 1985. Review of coking phenomena in relation to an occurrence of prismatically fractured natural coke from the Castle Mountain mine, Matanuska coal field, Alaska. Int. J. Coal Geol. 4, 281–298.

Moiseyev, A.N., 1971. A non-magmatic source for mercury ore deposits? Econ. Geol. 66, 591–601.

Mukherjee, A.B., Zevenhoven, R., Bhattacharya, P., Sajwan, K.S., Kikuchi, R., 2008. Mercury flow via coal and coal utilization by-products: a global perspective. Resour. Conserv. Recycl. 52, 571–591.

Mukhopadhyay, P.K., 1989. Organic Petrography and Organic Geochemistry of Texas Tertiary Coals in Relation to Depositional Environment and Hydrocarbon Generation. Bureau of Economic Geology. University of Texas, Austin 978-9991387178.

Noe-Nygaard, A., Rasmussen, J., 1968. Petrology of a 3,000 metre sequence of basaltic lavas in the Faeroe Islands. Lithos 1, 286–304.

Øster-Mortensen, J., 2002. De sidste kulminearbejdere. Ilustrated 2, 34–37.

Parra, M., Delmont, P., Dumon, J.C., Ferragne, A., Pons, J.C., 1987. Mineralogy and origin of Tertiary interbasaltic clays from the Faeroe Islands, northeastern Atlantic. Clay Miner. 22, 63–82.

Passey, S.R., 2014. The habit and origin of siderite spherules in the Eocene coal-bearing Prestfjall Formation, Faroe Islands. Int. J. Coal Geol. 122, 76–90.

Passey, S.R., Jolley, D.W., 2009. A revised lithostratigraphic nomenclature for the Palaeogene Faroe Islands Basalt group, NE Atlantic Ocean. Earth Env. Sci. T. R. So. 99, 127–158.

Passey, S.R., Varming, T., 2010. Surface interpolation within a continental flood basalt province: an example from the Palaeogene Faroe Islands Basalt Group. J. Struct. Geol. 32, 709–723.

Peabody, C.E., Einaudi, M.T., 1992. Origin of petroleum and mercury in the Culver-Baer cinnabar deposit, Mayacmas district, California. Econ. Geol. 87, 1078–1103.

Poissant, L., Zhang, H.H., Canário, J., Constant, P., 2008. Critical review of mercury fates and contamination in the arctic tundra ecosystem. Sci. Total Environ. 400, 173–211.

Pokorný, R., Krmíček, L., Árting, U.E., 2015. The first evidence of trace fossils and pseudofossils in the continental interlava volcaniclastic sediments on the Faroe Islands. Bull. Geol. Soc. Den. 63, 45–57.

Querol, X., Turiel, J.F., Soler, A.L., Duran, M.E., 1992. Trace elements in high-S subbituminous coals from the Teruel Mining District, northeast Spain. Appl. Geochem. 7, 547–561.

Rahman, M.W., Rimmer, S.M., 2014. Effects of rapid thermal alteration on coal: geochemical and petrographic signatures in the Springfield (No. 5) Coal, Illinois Basin. Int. J. Coal Geol. 131, 214–226.

Rasmussen, J., Noe-Nygaard, A., 1969. Beskrivelse til geologisk kort over Færøerne. C. A. Reitzels Forlag, København (in Danish).

Rasmussen, J., Noe-Nygaard, A., 1970. Geology of the Faeroe Islands (Pre-quaternary). C. A. Reitzels Forlag, København.

Richardson, K.R., Smallwood, J.R., White, R.S., Snyder, D.B., Maguire, P.K.H., 1998. Crustal structure beneath the Faroe Islands and the Faroe-Iceland ridge. Tectonophysics 300, 159–180.

Rudnick, R.L., Gao, S., 2014. Composition of the continental crust. In: Holland, H., Turekian, K. (Eds.), Treatise on Geochemistry 4, second ed. Elsevier, Amsterdam, pp. 1–51.

Saunders, A.D., Fitton, J.G., Kerr, A.C., Norry, M.J., Kent, R.W., 1997. The North Atlantic Igneous Province. In: Mahoney, J.J., Coffin, M.F. (Eds.), Large Igneous Provinces: Continental, Oceanic, and Planetary Flood Volcanism. American Geophysical Union, Washington D. C, pp. 45–93.

Schobert, H., 2013. Chemistry of Fossil Fuels and Biofuels. Cambridge University Press, Cambridge.

Scott, A.C., 2002. Coal petrology and the origin of coal macerals: a way ahead? Int. J. Coal Geol. 50, 119–134.

Shotyk, W., Goodsite, M.E., Roos-Barraclough, F., Givelet, N., Le Roux, G., Weiss, D., Cheburkin, A.K., Knudsen, K., Heinemeier, J., van Der Knaap, W.O., Norton, S.A., Lohse, C., 2005. Accumulation rates and predominant atmospheric sources of natural and anthropogenic Hg and Pb on the Faroe Islands. Geochim. Cosmochim. Acta 69, 1–17.

Singh, A.K., Sharma, M., Singh, M.P., 2008. Genesis of natural cokes: some Indian examples. Int. J. Coal Geol. 75, 40–48.

Singh, A.K., Singh, M.P., Sharma, M., Srivastava, S.K., 2007. Microstructures and microtextures of natural cokes: a case study of heat-affected coking coals from the Jharia coalfield, India. Int. J. Coal Geol. 71, 153–175.

Singh, P.K., Singh, M.P., Singh, A.K., Arora, M., 2010. Petrographic characteristics of coal from the Lati Formation, Tarakan basin, East Kalimantan, Indonesia. Int. J. Coal Geol. 81, 109–116.

Smellie, J.L., Johnson, J.S., McIntosh, W.C., Esser, R., Gudmundsson, M.T., Hambrey, M.J., De Vries, B.V.W., 2008. Six million years of glacial history recorded in volcanic lithofacies of the James Ross Island Volcanic Group, Antarctic Peninsula. Palaeogeogr. Palaeoclimatol. Palaeoecol. 260, 122–148.

Stokes, A.H., 1874. Notes on the coal seam and geology on Suderøe. Trans. Chester. Derby. Inst. Min. Engrs. 11, 320–341.

Storey, M., Duncan, R.A., Tegner, C., 2007. Timing and duration of volcanism in the North Atlantic Igneous Province: implications for geodynamics and links to the Iceland hotspot. Chem. Geol. 241, 264–281.

Strobl, S.A., Sachsenhofer, R.F., Bechtel, A., Meng, Q., 2014. Paleoenvironment of the Eocene coal seam in the Fushun Basin (NE China): implications from petrography and organic geochemistry. Int. J. Coal Geol. 134, 24–37.

Suchý, V., Sýkorová, I., Stejskal, M., Šafanda, J., Machovič, V., Novotná, M., 2002. Dispersed organic matter from Silurian shales of the Barrandian basin, Czech Republic: optical properties, chemical composition and thermal maturity. Int. J. Coal Geol. 53, 1–25.

Swaine, D.J., Goodarzi, F., 1995. Environmental Aspects of Trace Elements in Coal. Kluwer Academic Publishers, Amsterdam.

Taylor, G.H., Teichmüller, M., Davis, A., Diessel, C.F.K., Littke, R., Robert, P., 1998. Organic Petrology. Gebrüder Borntraeger, Berlin.

Teichmüller, M., 1989. The genesis of coal from the viewpoint of coal petrology. Int. J. Coal Geol. 12, 1–87.

Van Krevelen, D.W., 1963. Geochemistry of Coal. In: Breger, I.A. (Ed.), Organic Geochemistry. Pergamon Press, Oxford, pp. 183–247.

Waagstein, R., Guise, P., Rex, D., 2002. K/Ar and $^{39}Ar/^{40}Ar$ whole-rock dating of zeolite facies metamorphosed flood basalts: the upper Paleocene basalts of the Faroe Islands, NE Atlantic. In: Jolley, D.W., Bell, B.R. (Eds.), The North Atlantic Igneous Province: Stratigraphy, Tectonic, Volcanic and Magmatic Processes. Geological Society of London Special Publications, London, pp. 219–252.

Wang, L., Cheng, L.B., Cheng, Y.P., Yin, G.Z., Cai, C.C., Xu, C., Jin, K., 2014. Thermal effects of magmatic sills on coal seam metamorphism and gas occurrence. Bull. Volcanol. 76, 1–16.

Ward, C.R., Warbrooke, P.R., Roberts, F.I., 1989. Geochemical and mineralogical changes in a coal seam due to contact metamorphism, Sydney Basin, New South Wales, Australia. Int. J. Coal Geol. 11, 105–125.

Whitney, D.L., Evans, B.W., 2010. Abbreviations for names of rock-forming minerals. Am. Mineral. 95, 185–187.

Wing, S.L., Hickey, L.J., 1984. The *Platycarya perplex* and the evolution of the Juglandaceae. Am. J. Bot. 71, 388–411.

Xu, W., Wang, H., Zhu, T., Kuang, J., Jing, P., 2013. Mercury removal from coal combustion flue gas by modified fly ash. J. Environ. Sci. 25, 393–398.

Yao, Y., Liu, D., 2012. Effects of igneous intrusions on coal petrology, pore-fracture and coalbed methane characteristics in Hongyang, Handan and Huaibei coalfields, North China. Int. J. Coal Geol. 96, 72–81.

Yudovich, Y.E., Ketris, M.P., 2005a. Mercury in coal: a review: Part 1. Geochemistry. Int. J. Coal Geol. 62, 107–134.

Yudovich, Y.E., Ketris, M.P., 2005b. Mercury in coal: a review: Part 2. Coal use and environmental problems. Int. J. Coal Geol. 62, 135–165.

Zhang, J., Ren, D., Zhu, Y., Chou, C.L., Zeng, R., Zheng, B., 2004. Mineral matter and potentially hazardous trace elements in coals from Qianxi Fault Depression Area in southwestern Guizhou, China. Int. J. Coal Geol. 57, 49–61.